VIBRATION SUPPRESSION OF A ROTATIONALLY PERIODIC STRUCTURE USING AN ADAPTIVE/PPF CONTROL LAW

THESIS

Mark J. Keller, Captain, USAF

AFIT/GAE/ENY/01M-05

DEPARTMENT OF THE AIR FORCE

AIR UNIVERSITY

AIR FORCE INSTITUTE OF TECHNOLOGY

Wright-Patterson Air Force Base, Ohio

20010523 023

The views expressed in this thesis are those of the author and do not reflect the official policy or position of the United States Air Force, Department of Defense, or the United States Government.

VIBRATION SUPPRESSION OF A ROTATIONALLY PERIODIC STRUCTURE USING AN ADAPTIVE/PPF CONTROL LAW

THESIS

Presented to the Faculty

Department of Aeronautics and Astronautics

Graduate School of Engineering and Management

Air Force Institute of Technology

Air University

Air Education and Training Command

In Partial Fulfillment of the Requirements for the

Degree of Master of Science in Aeronautical Engineering

Mark J. Keller, B.S.

Captain, USAF

March 2001

VIBRATION SUPPRESSION OF A ROTATIONALLY PERIODIC STRUCTURE USING AN ADAPTIVE/PPF CONTROL LAW

Mark J. Keller, B.S.

Captain, USAF

Approved:
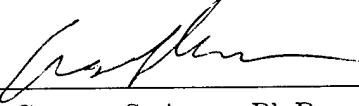
Maj Gregory S. Agnes, Ph.D.
Chairman
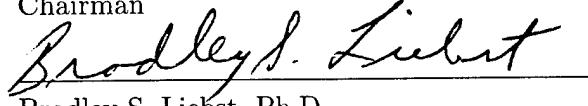
7 Mar 01
Date

Bradley S. Liebst, Ph.D.
Member
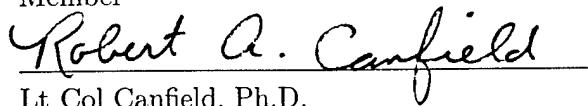
7 MAR 01
Date

Lt Col Canfield, Ph.D.
Member

7 mar 01
Date

Acknowledgements

First and foremost, I would like to thank my family for always being there when I needed them. They have always believed in me. Their love, strength, and guidance have sustained me through many difficult times.

I would also like to extend my sincerest appreciation to Major Greg Agnes, Ph.D. The research topic presented herein was his idea, but I tried to make it my own. He guided me along the way, and yet he let me find my own path. His help, and patience, made this thesis possible. The most important thing I learned here at AFIT was about the trials and tribulations of research. There is a satisfaction all its own in doing something no one else has ever done before. Even when it doesn't work the way you wanted it to, you still learn something.

Next, I would like to thank Dr. Liebst, Lt Col Jacques, Lt Col Canfield, and the other fine professors here at AFIT for their hard work and dedication. They made the work here not only challenging, but also interesting. I learned a lot from them. Well, at least enough to know that I have a lot more to learn.

You can't make it through this place by yourself, so I would also like to thank Mike, Dan, Geno, and the rest of the guys from GAE-01M. Your help and friendship kept me sane through all the long days.

Finally, I would like to thank my friends (especially Lance, Chris, Susie, Claudia, and Deanna) for constantly reminding me that.there was life outside of AFIT. You were always there when I needed to blow off steam, get away from it all, or just talk to someone. Thank you.

Mark J. Keller

iv

Table of Contents

List of Figures

xi

List of Abbreviations

AFIT/GAE/ENY/01M-05

Abstract

For a compressor disk, effective vibration suppression requires broadband control, and the elimination of inter-blade coupling forces. Previous researchers achieved this using an active/passive piezoelectric shunt network. Unfortunately, optimal tuning of the shunt requires prior knowledge of the coupling strength, which is not well defined. This thesis uses an adaptive parameter estimator to eliminate the inter-blade coupling forces. In addition, the passive shunt is replaced with an analogous positive position feedback method. The resulting control law was used on a simulated four and eight bladed system. While substantial reductions in system response were achieved for the Adaptive/PPF control technique, the parameter estimates did not always converge to the correct solution. Similar reductions in the response were achieved using PPF control by itself.

VIBRATION SUPPRESSION OF A ROTATIONALLY PERIODIC STRUCTURE USING AN ADAPTIVE/PPF CONTROL LAW

I. Introduction

1.1 Background

The jet turbine engine is one of the most maintenance intensive systems on an aircraft. The compressor of a typical engine contains numerous bladed-disk assemblies rotating at high RPM, alternated with fixed stators. These bladed-disks are constructed of nearly identical blades machined to great precision, and positioned symmetrically around a hub.

As the blades rotate behind the stators, they experience a periodic wake from the inlet air flow. The aeroelastic and aeroacoustic loads between the compressor blades and the stators are largely undetermined [17]. It is known, however, that the forcing occurs at integer multiples of the bladed-disk's rotational frequency, or engine order [5]. If the engine order frequency coincides with a natural frequency of the bladed-disk, resonance occurs and the compressor blades experience high stress/strain conditions. Repeated exposure to this dynamic loading causes high cycle fatigue (HCF) [7].

HCF accelerates the wear and deterioration of the compressor blades. Numerous man-hours are expended tearing down engines to inspect the blades for fatigue damage. In the worst cases, HCF can cause a separation of a compressor blade from its hub, resulting in a catastrophic failure of the engine. In fact, HCF was identified as the primary unforeseen engine failure mode from 1989 to 1994 [19]. Suppression of the vibrations leading to HCF would significantly reduce the life-cycle cost of an aircraft engine.
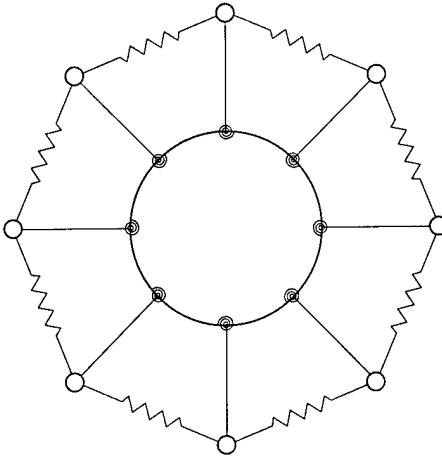
Figure 1.1   Bladed-disk Model

1.2   Rotationally Periodic Structures

Compressor disks belong to a class of structure know as rotationally periodic structures (RPS). A simple model of the bladed-disk system is shown in Figure 1.1. Cyclic symmetry is a convenient assumption when analyzing an RPS, since they consist of spatially repetitive substructures; thus all substructures are geometrically and dynamically similar [16]. For a compressor disk, this implies that: the blades are identical, they are uniformly spaced, and the hub is symmetric. If these conditions are met, then the system is said to be tuned.

An RPS possesses several modal families or bands, which correspond to a specific cantilever beam bending mode; there are as many linear modes within a band as there are substructures [5]. An important feature of a tuned RPS is that in a given mode, all of the substructures have the same vibration amplitude and differ only in phase [18]. These vibration modes, known as global or extended modes, allow the equations of motion to be decoupled [5]. Thus, analysis of a representative substructure is only required, instead of the whole structure.

Unfortunately, real blades have material and manufacturing imperfections. The system is said to be mistuned when these defects cause mass, stiffness, and damping variances [15]. Mistuning breaks down the rotationally periodic nature of the compressor disk,

changing global modes into local modes. In a tuned system, the vibration energy is spread equally amongst all the blades. Mode localization, however, concentrates the energy in several blades, or even a single blade. This results in some blades having a higher steady state amplitude than in a perfectly tuned system [4]. More importantly, mode localization is amplified by weak or variable inter-blade coupling, be it aerodynamic or structural [20]. A variation in blade natural frequency of less than 2% can cause amplitude increases of over 100% [15]. Consequently, the HCF problem in bladed-disk assemblies is severely aggravated by mistuning effects.

1.3 Piezoelectric Vibration Absorbers

Engineers have used mechanical vibration absorbers (MVAs), or tuned mass dampers, to control vibrating structures for over a century. Basically, a single degree of freedom (DOF) mass-spring system is added to the structure, and tuned to its resonance frequency. When properly tuned, the MVA reduces the response of the system to a narrow band harmonic excitation near the tuning frequency [3]. If a damper is added to the absorber, response to broadband excitation is reduced as well.

The close tolerances of a jet engine make the use of MVAs impractical. Fortunately, piezoelectric elements provide an alternative that is small, light weight, and can be bonded directly to the structure. Piezoelectric materials transform strain energy into electrical energy, and vice versa, so they can be used as both sensors and actuators. Forward created a piezoelectric vibration absorber (PVA) using a piezoelectric element and a passive resonant electrical circuit, or shunt [9]. He also demonstrated that it is analogous to an MVA. The piezoelectric element behaves as a capacitor which is comparable to the spring in an MVA. The shunt is comprised of an inductor (comparable to the mass), and a resistor (comparable to the damper). As the structure vibrates, the piezoelectric element transforms a portion of the strain energy into electrical energy. Tuning the piezoelectric shunt near a structural mode dissipates the electrical energy in the resistor, similar to a tuned mass damper [3].

Hagood and von Flotow developed an analytical solution for the optimal inductance and resistance tuning parameters of a single mode shunt. Their results closely parallel those

for an MVA [11]. The inductance adjusts the shunt natural frequency, while the resistance changes the response amplitude over some frequency range [14]. Later, Hollkamp added more electrical branches onto the shunt to increase the number of electrical resonances, and thereby achieved multi-mode vibration suppression. Unfortunately, each individual branch of the shunt cannot be treated as a separate single mode shunt. Tuning one electrical resonance to suppress a particular mode, detunes the rest of the circuit [12]. Hollkamp determined the shunt parameters by a numerical optimization technique.

The passive piezoelectric shunts discussed above only effect structural response at resonance, and are therefore narrowband devices. While this is sufficient for some problems, passive shunts cannot provide the broadband response control required in many applications [2]. For broadband control, active feedback is necessary. Fortunately, piezoelectric elements can also serve as actuators for feedback control.

A hybrid active/passive piezoelectric shunt network has been suggested by both Agnes [2] and Wang, et al [18]. Wang and Tang studied a system similar to the one shown in Figure 1.1, with a PVA attached to each blade. They analytically derived the optimal tuning parameters. Unfortunately, the equations depend on the coupling strength, a quantity not well defined.

1.4 Active Vibration Control

Flexible structures are distributed parameter systems with many vibratory modes. All physical systems possess some degree of internal damping which normally increases with frequency. Since the bandwidth of any practical controller is finite, there will be modes that are beyond its bandwidth, or that are unmodelled within its bandwidth. The uncontrolled modes within the bandwidth of the closed loop system result in the well known problem of observation spillover. This can destabilize the residual dynamics of the system, especially at higher frequencies where the dynamics of the structure are least well known [8].

In the absence of actuator dynamics, collocated direct velocity feedback is unconditionally stable in the presence of observation spillover [10]. Actuator dynamics, however,

must be included in any real system, or instabilities may occur. Caughey and Goh designed a stable velocity feedback controller including actuator dynamics. Unfortunately, they showed that the stability is highly dependent on the natural damping of the structure [10]. Since damping models are not well known, this is not a practical vibration control method.

The technique of positive position feedback (PPF) was developed by Caughey along with Goh, and later Fanson, as an alternative to direct velocity feedback [10], [8]. PPF is not affected by spillover, nor is it destabilized by actuator dynamics. While PPF is not unconditionally stable, Caughey, et al, showed that the stability criteria is static and unaffected by the natural damping of the structure. PPF only requires generalized displacement measurements, making the use of strain based sensors, such as piezoelectric elements, very practical [8]. In fact, if the proper parameters are chosen, the PPF equations are analogous to those of the tuned mechanical or piezoelectric vibration absorbers.

As stated previously, the analysis of a tuned RPS simplifies to that of a single representative substructure. To take advantage of this property for a bladed-disk, one needs to take into account the largely unknown inter-blade coupling forces and mistuning affects. Ertur, et al, developed an adaptive vibration control technique based on Lyapunov theory. Their method cancels unknown bounded disturbances while compensating for uncertainties [6]. Jarosh used this control technique on a 5 DOF rocket model [13]. He showed that it significantly reduced the response compared to a purely passive and purely active controller.

1.5 Thesis Overview

The main drawback of Wang and Tang's piezoelectric shunt network, is that a priori knowledge of the coupling forces is required for optimal tuning. The objective of this research was to replace their piezoelectric vibration absorber with PPF control, while using Ertur's adaptive control technique to cancel out the unknown inter-blade coupling and damping.

The individual theories are more fully explored in the next chapter. Wang and Tang's equations for an RPS with multiple piezoelectric shunts are presented. The PPF equations of motion and the associated stability criteria are developed for a single DOF system. Ertur's adaptive control scheme is also developed and studied. Then, in Chapter 3, the adaptive and PPF control strategies are combined into a single control law. This new technique is used to regulate the response of a single DOF in a 4 DOF model. In the fourth chapter, Adaptive/PPF control is expanded to control all the DOFs of the model. The technique is also applied to the model of an eight bladed-disk previously developed by Duffield [5]. Finally, significant findings, conclusions, and recommendations for further research are presented in Chapter 5.

II. Development of Individual Theories

2.1 Hybrid Active/Passive Piezoelectric Shunt Network

2.1.1 Background.

As a rotationally periodic structure (RPS) vibrates, a high strain area normally occurs on all of its substructures [18]; accordingly, each requires a PVA. As discussed in Chapter 1, passive piezoelectric shunts are narrowband devices. Active control is required for broadband suppression. Agnes and Wang, et al, have both suggested a hybrid active/passive piezoelectric shunt network [2], [18]. In this setup, the vibration energy of the structure is partially transformed into electrical energy and passively dissipated in the shunt circuit. In addition, an active control voltage is supplied to the circuit to drive the piezoelectric element, and thereby further suppress vibrations.

Construction and application of the system is simplified if identical piezoelectric patches and shunts are used on every substructure. The problem becomes how to set the shunt resistance (R) and inductance (L) parameters. Since an RPS is a multi-DOF system, Hagood and von Flotow's optimal tuning procedure does not directly apply [11]. The mechanical coupling between the substructures splits the otherwise repeated substructure frequency into a group of frequencies [18]. Wang and Tang showed that the mechanical coupling can be offset, and optimal tuning achieved, by combining active and passive control.

2.1.2 Equations of Motion.

Wang and Tang derived the equations of motion (EOM) for an RPS using an active/passive shunt network [18]. They used a tuned RPS consisting of N identical cantilevered beams arranged symmetrically around a circular hub, with coupling springs between adjacent blades. The individual blades are damped, but there are no dampers between blades. An identical piezoelectric patch and shunt circuit is attached to each beam. Applying Hamilton's principle to this system,

$$\int_{t_0}^{t_1} (\delta T - \delta U_b - \delta U_p + \delta W_v) dt = 0 \tag{2.1}$$

where T is the kinetic energy of the whole system, U_b is the potential energy of the beams and coupling springs, U_p is the elastic and electrical energy of the piezoelectric patches, and δW_v is the virtual work term.

First, the kinetic and potential energy of the substructure are expressed in terms of the dominant mode of vibration, $\Phi(x)$. The transverse displacement of the jth beam is approximated as

$$w_j(x,t) \approx \Phi(x)q_j(t) \tag{2.2}$$

Expressions for T and U_b are then obtained from elementary beam theory,

$$T = \frac{1}{2}\sum_{j=1}^{N} m\dot{q}_j^2 \tag{2.3}$$

$$U_b = \frac{1}{2}\sum_{j=1}^{N} k_b q_j^2 + \frac{1}{2}\sum_{j=1}^{N} k_c(q_{j+1} - q_j)^2 \tag{2.4}$$

where k_b and k_c are the equivalent beam and coupling stiffness, respectively.

Using the constitutive equations for a typical piezoelectric material, the variation of the elastic and electrical energy of the patches is

$$U_p = \sum_{j=1}^{N}(k_p q_j \delta q_j + k_2 Q_j \delta q_j + k_2 q_j \delta Q_j + k_1 Q_j \delta Q_j) \tag{2.5}$$

where k_p is the equivalent piezoelectric patch stiffness, k_1 is the inverse of the capacitance of the patch, k_2 is the generalized electro-mechanical coupling coefficient, and Q_j is the charge of the jth piezoelectric patch.

If the active voltage input to the jth circuit is V_{aj}, then the voltage across the piezoelectric patch is related to the external circuit by

$$V_j = -L\ddot{Q}_j - R\dot{Q}_j + V_{aj} \tag{2.6}$$

where R and L are the resistance and inductance of the shunt. Note that for a purely passive shunt, $V_{aj} = 0$. Thus, the virtual work term is

$$\delta W_v = \sum_{j=1}^{N} \left(V_j \delta Q_j + f_j \delta q_j - \dot{q}_j \, d \, \delta q_j \right) \tag{2.7}$$

where f_j is the generalized external force on the jth beam, and d is the equivalent beam damping.

Substituting Equations 2.3 through 2.7 into Equation 2.1, and letting $k = k_b + k_p$, Wang and Tang found the discretized EOMs for a substructure to be

$$m\ddot{q}_j + d\,\dot{q}_j + (k + 2k_c)\,q_j - k_c q_{j-1} - k_c q_{j+1} = -k_2 Q_j + f_j \tag{2.8}$$

$$L\ddot{Q}_j + R\dot{Q}_j + k_1 Q_j = -k_2 q_j + V_{aj} \tag{2.9}$$

The EOMs for the whole structure in matrix form are

$$M\ddot{X} + D\dot{X} + KX = GX + F \tag{2.10}$$

where the generalized displacement vector is $X = [q_1, Q_1, ..., q_N, Q_N]^T$; the generalized force vector is $F = [f_1, V_{a1}, ..., f_N, V_{aN}]^T$, consisting of the external disturbances and active voltage input. The generalized mass (M), damping (D), stiffness (K), and gain (G) matrices are

$$M = \begin{bmatrix} m & & & & 0 \\ & L & & & \\ & & \ddots & & \\ & & & m & \\ 0 & & & & L \end{bmatrix} \qquad D = \begin{bmatrix} d & & & & 0 \\ & R & & & \\ & & \ddots & & \\ & & & d & \\ 0 & & & & R \end{bmatrix} \tag{2.11}$$

$$K = \begin{bmatrix} \chi_m & \chi_c & 0 & \cdots & 0 & \chi_c^T \\ \chi_c^T & \chi_m & \chi_c & \ddots & \vdots & 0 \\ 0 & \chi_c^T & \ddots & \ddots & 0 & \vdots \\ \vdots & \ddots & \ddots & \ddots & \chi_c & 0 \\ 0 & \cdots & 0 & \chi_c^T & \chi_m & \chi_c \\ \chi_c & 0 & \cdots & 0 & \chi_c^T & \chi_m \end{bmatrix} \qquad G = \begin{bmatrix} \chi_g & & 0 \\ & \ddots & \\ 0 & & \chi_g \end{bmatrix} \qquad (2.12)$$

with $\quad \chi_m = \begin{bmatrix} k + 2k_c & 0 \\ 0 & k_1 \end{bmatrix}$, $\quad \chi_c = \begin{bmatrix} -k_c & 0 \\ 0 & 0 \end{bmatrix}$, $\quad$ and $\quad \chi_g = \begin{bmatrix} 0 & -k_2 \\ -k_2 & 0 \end{bmatrix}$

Note that M, D, K, and G are $2N \times 2N$.

2.1.3 Purely Passive Control.

In a purely passive control design, there is no active voltage input. Using the properties of an RPS, and neglecting all structural damping, Wang and Tang transformed the matrix EOMs, Equation 2.10, into N independent 2×2 matrices. Then, following Hagood and von Flotow's approach, they analytically determined the optimal tuning parameters for an arbitrary spatial harmonic excitation [18]. The optimal inductance and resistance they found are

$$L^* = \frac{mk_1}{k + 2k_c \left[1 - \cos\left(\frac{2\pi}{N}(i-1)\right)\right]} \qquad R^* = \frac{\left(\sqrt{2mk_1}\right)k_2}{k + 2k_c \left[1 - \cos\left(\frac{2\pi}{N}(i-1)\right)\right]} \qquad (2.13)$$

Note that these two equations depend explicitly on i, which is the mode of the external disturbance. Thus, using these tuning parameters, identical shunts will only provide optimal vibration suppression if the external disturbance is purely the ith spatial Fourier harmonic [18]. Also, prior knowledge of the coupling strength, k_c, is required to calculate these optimal tuning parameters.

2.1.4 Active/Passive Control.

To suppress all harmonics optimally, Wang and Tang used charge feedback with the following active voltage control

$$V_{aj} = V_{aj}^{(1)} + V_{aj}^{(2)} \qquad (2.14)$$

with

$$V_{aj}^{(1)} = \frac{k_1 k_c}{k} \left(2Q_j - Q_{j-1} - Q_{j+1}\right) \tag{2.15}$$

and if N is even,

$$V_{aj}^{(2)} = r_0 \dot{Q}_j + \sum_{i=1}^{(N-1)/2} \left[r_i \left(\dot{Q}_{j+i} + \dot{Q}_{j+N-i}\right)\right] + r_{N/2}\dot{Q}_{j+N/2} \tag{2.16}$$

or if N is odd,

$$V_{aj}^{(2)} = r_0 \dot{Q}_j + \sum_{i=1}^{(N-1)/2} \left[r_i \left(\dot{Q}_{j+i} + \dot{Q}_{j+N-i}\right)\right] \tag{2.17}$$

Note that r_j is the current feedback gain.

Using this active voltage control, the optimal tuning parameters they found are

$$L^* = \frac{mk_1}{k} \qquad\qquad R^* = \frac{\left(\sqrt{2mk_1}\right)k_2}{k} \tag{2.18}$$

Neither of the tuning parameters depend on i; they are optimal for all spatial harmonics. It may also appear that the optimal tuning parameters no longer depend on k_c. While the active control has cancelled out the mechanical coupling effects, prior knowledge of that coupling was required to determine the active control voltage.

2.1.5 Results.

Wang and Tang ran numerical simulations with a purely passive, purely active, and an active/passive hybrid controller. As expected, the purely passive controller was only optimal for one spatial harmonic, and mistuned for all others. The hybrid controller actively retuned the shunt network and significantly outperformed the passive controller. It also required much less control effort than the purely active controller [18].

This hybrid controller combines the best of both worlds. The active component delivers high performance broadband vibration suppression, while the passive shunt provides

a stable, fail-safe, easily constructed vibration absorber. At least in theory. Inductors normally operate in the range of milli-Henries, but the PVAs needed to suppress vibrations in a compressor disk would require inductors on the order of kilo-Henries [1]. The only alternative is to actively synthesize the inductors using op-amps, which negates the benefits of a passive system. Another important disadvantage of this technique is that it requires prior knowledge of the coupling strength, a quantity which is not well defined [17].

2.2 Positive Position Feedback

2.2.1 Background.
Multi-DOF systems, such as an RPS, have numerous vibratory modes. Many of these modes are not targeted for control, or lie outside the finite bandwidth of the vibration controller. This leads to the well known phenomenon of observation spillover, which can destabilize the residual dynamics of the closed loop system [8]. Caughey along with Goh, and later Fanson, developed positive position feedback (PPF) because it is not affected by observation spillover, nor is it destabilized by actuator dynamics [10], [8].

The technique of PPF is introduced by considering a second-order scalar system subjected to second-order actuator dynamics

$$\text{structure} \qquad \ddot{x} + 2\zeta\omega\dot{x} + \omega^2 x = \mu\omega^2\eta \qquad (2.19)$$

$$\text{actuator} \qquad \ddot{\eta} + 2\zeta_f\omega_f\dot{\eta} + \omega_f^2\eta = \omega_f^2 x \qquad (2.20)$$

where x and η are the system and actuator states respectively, ζ and ζ_f are the system and actuator damping ratios ($0 < ... < 1$), ω and ω_f are the system and actuator frequencies (> 0), and μ is the PPF gain (> 0). Caughey and Fanson derived the following theorem and proof regarding this system [8]:

Theorem

The combined structure and actuator dynamics of Equations 2.19 and 2.20 are Lyapunov Asymptotically Stable (LAS) if and only if $\mu < 1$.

Proof

To make the equations symmetric, define the following transformation for η

$$\eta = \left(\frac{\omega_f}{\omega\mu^{1/2}}\right)\psi \tag{2.21}$$

Substituting Equation 2.21 into Equations 2.19 and 2.20, and multiplying Equation 2.20 by $\left(\frac{\omega_f}{\omega\mu^{1/2}}\right)^{-1}$, gives the following system of equations in matrix form

$$\left\{\begin{array}{c} \ddot{x} \\ \ddot{\psi} \end{array}\right\} + \underbrace{\left[\begin{array}{cc} 2\zeta\omega & 0 \\ 0 & 2\zeta_f\omega_f \end{array}\right]}_{L}\left\{\begin{array}{c} \dot{x} \\ \dot{\psi} \end{array}\right\} + \underbrace{\left[\begin{array}{cc} \omega^2 & -\omega\omega_f\mu^{1/2} \\ -\omega\omega_f\mu^{1/2} & \omega_f^2 \end{array}\right]}_{N}\left\{\begin{array}{c} x \\ \psi \end{array}\right\} = 0 \tag{2.22}$$

L is positive definite $(L > 0)$, because it is diagonal, and ζ, ζ_f, ω, and ω_f are all > 0. It is a known result that for $L > 0$, Equation 2.22 is LAS if and only if $N > 0$. So, for any nonzero y_1 and y_2, if $N > 0$, then

$$\left[\begin{array}{cc} y_1 & y_2 \end{array}\right]\left[\begin{array}{cc} \omega^2 & B \\ B & \omega_f^2 \end{array}\right]\left[\begin{array}{c} y_1 \\ y_2 \end{array}\right] > 0 \tag{2.23}$$

where $B = -\omega\omega_f\mu^{1/2}$. Expanding the above

$$\omega^2 y_1^2 + 2By_1y_2 + \omega_f^2 y_2^2 > 0 \tag{2.24}$$

Adding and subtracting $\left(\frac{B}{\omega_f}\right)^2 y_1^2$ to this gives us

$$\omega^2 y_1^2 + 2By_1y_2 + \omega_f^2 y_2^2 + \left(\frac{B}{\omega_f}\right)^2 y_1^2 - \left(\frac{B}{\omega_f}\right)^2 y_1^2 > 0 \tag{2.25}$$

After collecting terms

$$\left[\omega^2 - \left(\frac{B}{\omega_f}\right)^2\right] y_1^2 + \left[\left(\frac{B}{\omega_f}\right)^2 y_1^2 + 2By_1y_2 + \omega_f^2 y_2^2\right] > 0 \tag{2.26}$$
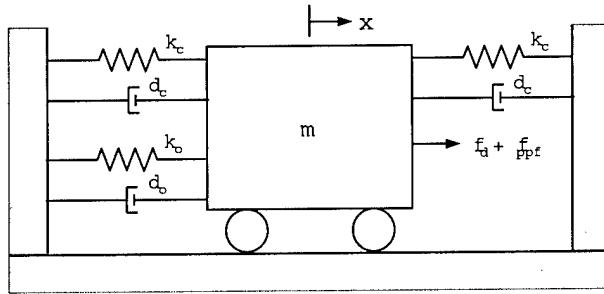
Figure 2.1   Single DOF System

which reduces to

$$\left[\omega^2 - \left(\frac{B}{\omega_f}\right)^2\right] y_1^2 + \underbrace{\left[\left(\frac{B}{\omega_f}\right) y_1 + \omega_f y_2\right]^2}_{>0} > 0 \qquad (2.27)$$

The second term in the above expression is always positive. Since the whole expression must be positive, the first term must be positive for any nonzero y_1, so

$$\omega^2 - \left(\frac{B}{\omega_f}\right)^2 > 0 \qquad (2.28)$$

$$\omega^2 - \left(\frac{\omega\omega_f\mu^{1/2}}{\omega_f}\right)^2 > 0 \qquad (2.29)$$

$$\omega^2 - \omega^2\mu > 0 \qquad (2.30)$$

Therefore, $\mu < 1$ (2.31)

2.2.2   Equations of Motion for Single Cart System.   To understand the use and application of PPF, the single DOF system shown in Figure 2.1 was studied. This system is analogous to a single blade of a compressor disk, with the two adjacent blades fixed. The blade has mass m. Its structural stiffness and damping are represented by k_0 and d_0. The inter-blade coupling forces are represented by the stiffness and damping parameters, k_c and d_c. The EOM for this single cart system is simply

$$mx\ddot{} + (d_0 + 2d_c)\dot{x} + (k_0 + 2k_c)x = f_d \tag{2.32}$$

$$\ddot{x} + \left(\frac{d_0 + 2d_c}{m}\right)\dot{x} + \left(\frac{k_0 + 2k_c}{m}\right)x = \frac{f_d}{m} \tag{2.33}$$

$$\ddot{x} + 2\zeta_n\omega_n\dot{x} + \omega_n^2 x = \tag{2.34}$$

where

$$\omega_n = \sqrt{\frac{k_0 + 2k_c}{m}} \tag{2.35}$$

is the natural frequency of the structure, ζ_n is the structural damping ratio, and f_d is the external disturbance.

Adding a PPF actuator to the system results in the combined EOMs

$$\ddot{x} + 2\zeta_n\omega_n\dot{x} + \omega_n^2 x = \mu\omega_n^2\eta + \frac{f_d}{m} \tag{2.36}$$

$$\ddot{\eta} + 2\zeta_f\omega_f\dot{\eta} + \omega_f^2\eta = \omega_f^2 x \tag{2.37}$$

The first term on the right hand side of Equation 2.36 is the PPF force provided by the actuator, f_{ppf}, divided by the mass of the cart, or

$$\frac{f_{ppf}}{m} = \mu\omega_n^2\eta \tag{2.38}$$

Thus,

$$f_{ppf} = m\mu\omega_n^2\eta = \mu(k_0 + 2k_c)\eta \tag{2.39}$$

Therefore, as you increase the PPF gain, μ, the control effort of the actuator also increases.

2.2.3 Simulation.
To numerically solve for the system response, Equations 2.36 and 2.37 are first put into state-space form

$$\left\{ \begin{array}{c} \dot{x} \\ \ddot{x} \end{array} \right\} = \left[\begin{array}{cc} 0 & 1 \\ -\omega_n^2 & -2\zeta_n\omega_n \end{array} \right] \left\{ \begin{array}{c} x \\ \dot{x} \end{array} \right\} + \left\{ \begin{array}{c} 0 \\ 1 \end{array} \right\} \left(\mu\omega_n^2\eta + \frac{f_d}{m} \right) \qquad (2.40)$$

$$\left\{ \begin{array}{c} \dot{\eta} \\ \ddot{\eta} \end{array} \right\} = \left[\begin{array}{cc} 0 & 1 \\ -\omega_f^2 & -2\zeta_f\omega_f \end{array} \right] \left\{ \begin{array}{c} \eta \\ \dot{\eta} \end{array} \right\} + \left\{ \begin{array}{c} 0 \\ 1 \end{array} \right\} \omega_f^2 x \qquad (2.41)$$

The system is modelled using SIMULINK^{TM} (see Figure A.1 on p. A-1) and the response evaluated. For simulation purposes, an external disturbance of

$$f_d = 10\sin(\omega_d t) \qquad (2.42)$$

was used, where ω_d is the disturbance frequency. The system parameters are set such that $m = 1$ Kg, $k_0 = 100$ N/m, $k_c = 5$ N/m, and $\zeta_n = 0.01$. Using Equation 2.35, $\omega_n = 10.488$ rad/sec.

The simulation outputs the displacement of the cart as a function of time at discrete intervals, $x_i = x(t_i)$. Responses due to different PPF parameter settings are evaluated by comparing the Root Mean Square (RMS) of the displacements over a range of disturbance frequencies. Herein, $0 < \omega_d < 20$ rad/sec, with a step size of 0.02. The RMS of a signal is calculated by

$$x_{rms} = \sqrt{\frac{\sum_{i=1}^{N} x_i^2}{N}} \qquad (2.43)$$

where N is the number of samples from t_1 to $t_N = t_f$.

2.2.4 PPF Parameter Selection.
Similar to a PVA, the desired response is achieved by properly tuning the PPF system. The tuning parameters are the actuator frequency (ω_f), the damping ratio (ζ_f), and the feedback gain (μ). The question becomes how to optimally tune these parameters. An analytical solution was not found in the literature.

2-10

Instead, a numerical technique was used to iteratively determine the parameters. Setting ζ_f and ω_f to typical values, μ was varied. Comparing the RMS plots, the μ that minimized the response was chosen. Fixing μ at this value and holding ω_f at the original value, ζ_f was varied. Once again the ζ_f that minimized the RMS plot was selected. Finally, with μ and ζ_f fixed, ω_f was varied, and again the value that resulted in the best performance was chosen. Using these three values as a starting point, the process was repeated several times, until the results more or less converged. While not necessarily providing parameter values that yield a globally minimum response, it is sufficient for the work here.

2.2.4.1 Selection of PPF Gain.

The MATLAB^{TM} code used to run the simulation is given in Appendix A.1.1, beginning on p. A-1. Using the system values given in Section 2.2.3, and the process just described, the RMS curves as μ varied from 0 to 1, with a step size of 0.1, are plotted in Figure 2.2. For the sake of clarity, not all response curves are displayed. As expected, when the system is uncontrolled, $\mu = 0$, the response spikes at resonance (i.e. $\omega_d = \omega_n$). At the other extreme, when $\mu = 1$, the response blows up at low frequencies.

Looking closer at the plot, Figure 2.3, as the gain is increased, the response at resonance decreases. However, as you push down on the middle of the response curve, the sides bulge up. In other words, the response increases at lower frequencies, and to a lesser extent also at higher frequencies. The goal is to improve the performance at resonance without degrading it elsewhere. To that end, the response curve should be as flat as possible at low frequencies through resonance, and then roll off at high frequencies. Therefore, $\mu = 0.4$ is selected as the PPF gain, which is the curve marked with an " $*$ " in Figure 2.3.

2.2.4.2 Selection of Actuator Damping Ratio.

The MATLAB^{TM} code used to run this simulation is given in Appendix A.1.2, beginning on p. A-2. Since the structure is lightly damped, $\zeta_n = 0.01$, one of the purposes of the PPF actuator is to add damping to the system. The damping ratio, ζ_f, was varied from 0 to 1, with a step size of 0.1. The RMS plots are shown in Figure 2.4. When the actuator provides no additional
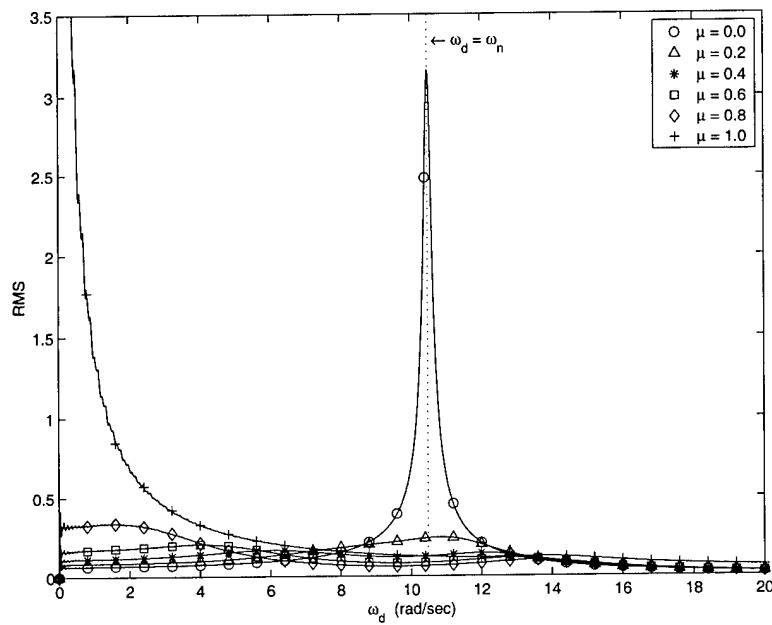
Figure 2.2   RMS of Displacement for the Single Cart System as μ varies $(\omega_f = \omega_n, \zeta_f = 0.4)$
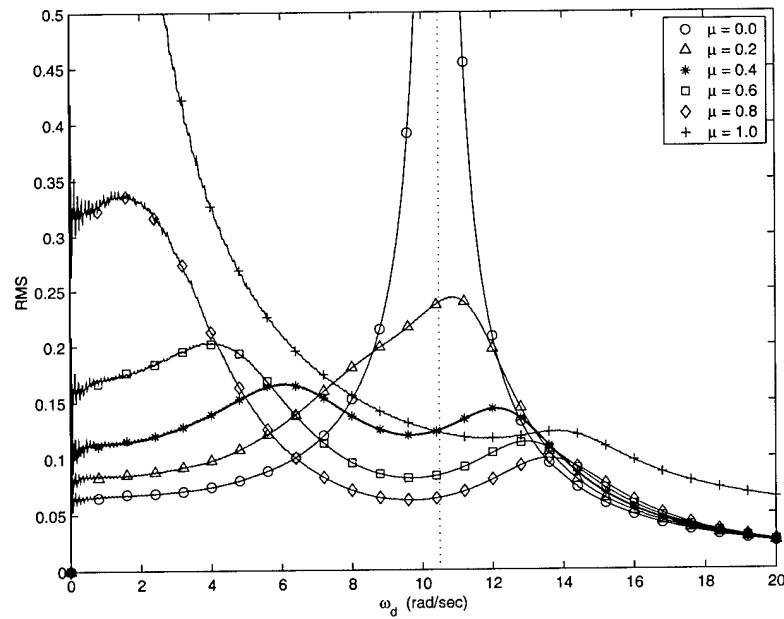
Figure 2.3   A Closer Look at the RMS of Displacement for the Single Cart System as μ varies $(\omega_f = \omega_n, \zeta_f = 0.4)$
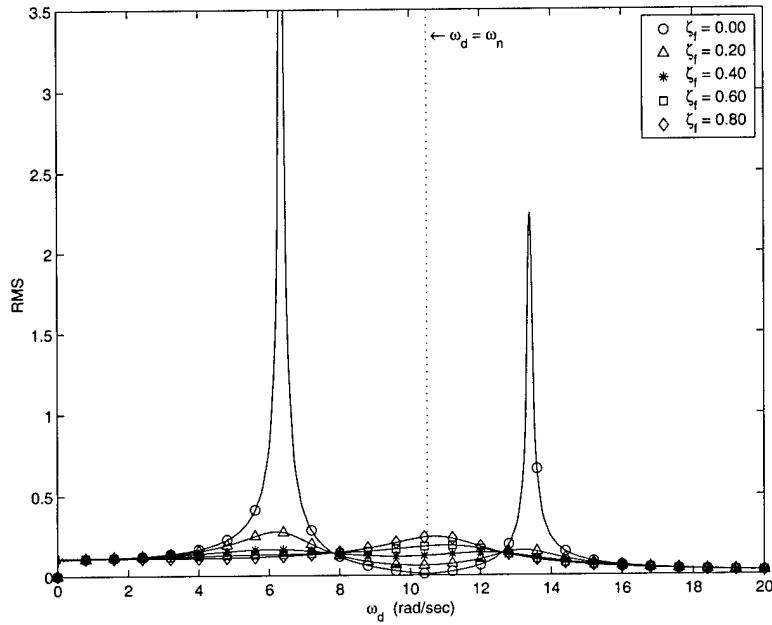
Figure 2.4 RMS of Displacement for the Single Cart System as ζ_f varies $(\omega_f = \omega_n, \mu = 0.4)$

damping, $\zeta_f = 0$, the response spikes on both sides of the resonance frequency. This is typical for lightly damped systems.

Taking a closer look at the plot, Figure 2.5, as the damping is increased, the amplitude of these two peaks decreases, but the response at resonance increases. Once again, the goal was to minimize the response over the whole range of frequencies. Thus, $\zeta_f = 0.4$ was chosen as the actuator damping ratio; the " $*$ " curve again.

2.2.4.3 Selection of Actuator Frequency.

The MATLAB^{TM} code used to run this simulation is given in Appendix A.1.3, beginning on p. A-4. Intuitively, it is expected that the actuator should be at least as fast as, if not faster than, the natural frequency of the structure controlled. The actuator frequency, ω_f, is varied from 0 to 20, with a step size of 1. The RMS plots are shown in Figure 2.6. When the system is uncontrolled, $\omega_f = 0$, the maximum amplitude is at the resonant frequency. As ω_f is increased, the peak occurs at a higher disturbance frequency, ω_d, and its amplitude is reduced.
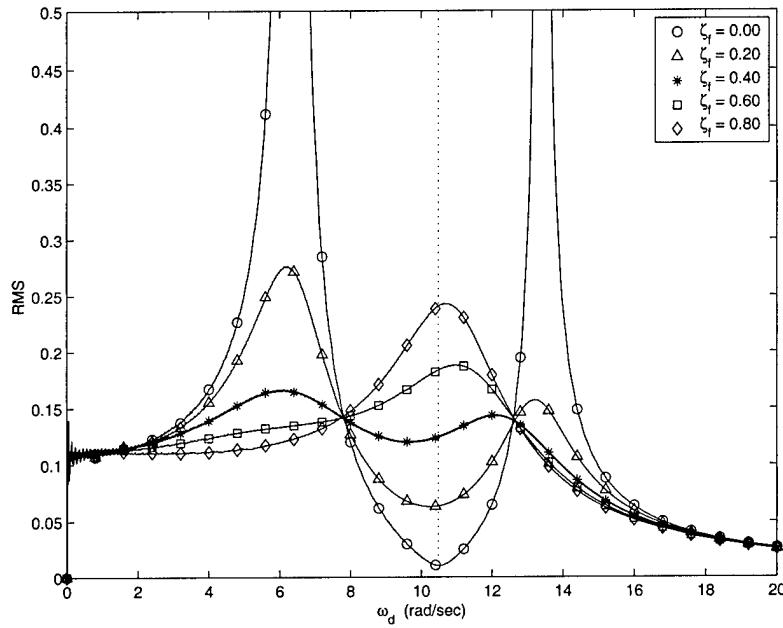
Figure 2.5   A Closer Look at the RMS of Displacement for the Single Cart System as ζ_f varies ($\omega_f = \omega_n, \mu = 0.4$)

Taking a closer look at the plot, Figure 2.7, while the amplitude is decreased above the resonant frequency, it is also increased below resonance. Since the goal again is to minimize response throughout, $\omega_f = 10.488 = \omega_n$ was selected; the " $*$ " curve once more.

2.3   Adaptive Vibration Control

2.3.1   Background.   To take full advantage of the benefits of positive position feedback in an RPS, like a compressor disk, the largely unknown inter-blade coupling forces must be dealt with. Ertur, et al, developed an adaptive vibration control strategy based on Lyapunov theory. This regulation controller cancels unknown bounded disturbances, while eliminating parametric uncertainties, such as the coupling stiffness and damping parameters [6].

2-14
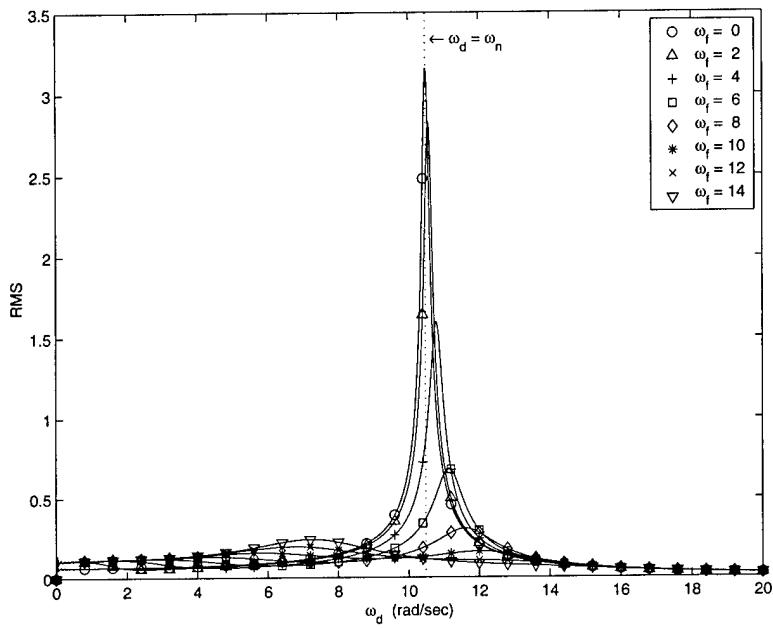
Figure 2.6   RMS of Displacement for the Single Cart System as ω_f varies $(\mu = 0.4, \zeta_f = 0.4)$
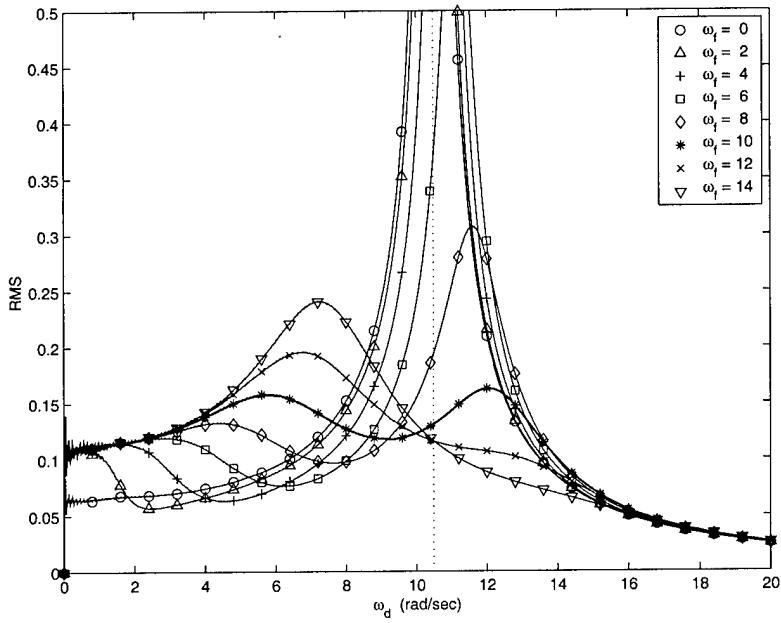
Figure 2.7   A Closer Look at the RMS of Displacement for the Single Cart System as ω_f varies $(\mu = 0.4, \zeta_f = 0.4)$

The equations of motion for a discrete flexible structure are

$$M\ddot{q} + D\dot{q} + Kq = f \tag{2.44}$$

where q represents the physical coordinates of the system, f is the forces on the system, and M, D, and K are the system mass, damping, and stiffness matrices respectively.

The controlled and uncontrolled coordinates of the system, q_c and q_u respectively, are now defined as subsets of q. Equation 2.44 is then rearranged and partitioned as follows

$$\begin{bmatrix} M_c & 0 \\ 0 & M_u \end{bmatrix} \begin{Bmatrix} \ddot{q}_c \\ \ddot{q}_u \end{Bmatrix} + \begin{bmatrix} D_c & D_{cu} \\ D_{uc} & D_u \end{bmatrix} \begin{Bmatrix} \dot{q}_c \\ \dot{q}_u \end{Bmatrix} + \begin{bmatrix} K_c & K_{cu} \\ K_{uc} & K_u \end{bmatrix} \begin{Bmatrix} q_c \\ q_u \end{Bmatrix} = \begin{Bmatrix} f_c \\ f_u \end{Bmatrix} \tag{2.45}$$

Note that in Ertur's development of this theory, f_c only takes into account the applied control forces on q_c. He does not explicitly deal with disturbances applied to the controlled coordinates.

Equation 2.45 is divided into the equations of motion for the controlled coordinates

$$M_c\ddot{q}_c + D_c\dot{q}_c + K_cq_c = f_c - D_{cu}\dot{q}_u - K_{cu}q_u \tag{2.46}$$

and for the uncontrolled coordinates

$$M_u\ddot{q}_u + D_u\dot{q}_u + K_uq_u = f_u - D_{uc}\dot{q}_c - K_{uc}q_c \tag{2.47}$$

To regulate the controlled coordinates, Equation 2.46 is rewritten as

$$M_c\ddot{q}_c + D_c\dot{q}_c + K_cq_c = f_c - D_{cu}\dot{q}_u - K_{cu}q_u = f_c - Y_r\Phi_r \tag{2.48}$$

where Y_r is a regression matrix based on q_u and $\dot{q}_u$, and Φ_r is an unknown parameter vector containing the elements of D_{cu} and K_{cu}.

Ertur suggests the following control law:

$$f_c = Y_r \hat{\Phi}_r - D_f \dot{q}_c - K_f q_c \qquad (2.49)$$

where D_f and K_f are loosely referred to as the controller damping and stiffness matrices.

The adaptation law for the parameter estimates, $\hat{\Phi}_r$, is

$$\dot{\hat{\Phi}}_r = -\Gamma_r \Upsilon^T P X_c \qquad (2.50)$$

where $X_c = \begin{bmatrix} q_c & \dot{q}_c \end{bmatrix}^T$; Γ_r is a symmetric, positive definite, gain matrix $\left(\Gamma_r = \Gamma_r^T > 0\right)$, and $\Upsilon^T = \begin{bmatrix} 0 & \left(M_c^{-1} Y_r\right)^T \end{bmatrix}$. P is found from the Lyapunov equation,

$$A_c^T P + P A_c = -Q \qquad (2.51)$$

with $P = P^T > 0$, $Q = Q^T > 0$, and

$$A_c = \begin{bmatrix} 0 & I \\ -M_c^{-1}\left(K_c + K_f\right) & -M_c^{-1}\left(D_c + D_f\right) \end{bmatrix} \qquad (2.52)$$

Equations 2.49 and 2.50 guarantee asymptotic stability of the controlled states, X_c, and boundedness of the uncontrolled coordinates, q_u, under the following assumptions:

(A1) $M_c = M_c^T > 0$

(A2) f_u is bounded

(A3) The roots, λ, of $|\lambda^2 M_u + \lambda D_u + K_u| = 0$, have negative real parts

(A4) D_f and K_f are selected so that the roots, λ, of $|\lambda^2 M_c + \lambda \left(D_f + D_c\right) + \left(K_f + K_c\right)| = 0$, have negative real parts

For the proof, see Ertur [6]. Note that there is no guarantee of convergence for the parameter estimates. Assumptions A3 and A4 are equivalent to saying that A_c, Equation 2.52,
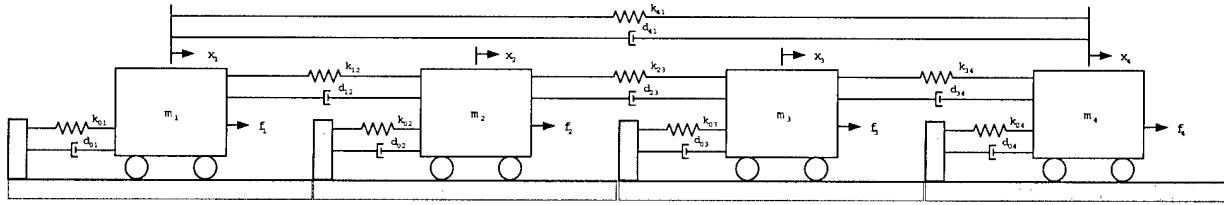
Figure 2.8   Cyclic 4 DOF System

and A_u are negative definite; where

$$A_u = \begin{bmatrix} 0 & I \\ -M_u^{-1}K_u & -M_u^{-1}D_u \end{bmatrix}$$

(2.53)

2.3.2   Equations of Motion for a Four Cart System.   The 4 DOF
cyclic system shown in Figure 2.8 is studied to better understand the application of this
adaptive control law. The system is drawn linearly, but it is analogous to the rotary
periodic structure of a compressor disk. The blades, or carts, have mass m_i, and their
structural stiffness and damping are represented by k_{0i} and d_{0i}. The inter-blade coupling
forces are expressed in terms of k_{ij} and d_{ij}, where $i, j = 1...4$; by convention m_i is the left
cart, and m_j is the right cart. A simpler chain system is obtained by cutting the spring
and damper between carts 1 and 4. The external control and disturbance forces on each
of the carts are represented by f_i. The EOMs for this system are

$$M\ddot{\underline{x}} + D\dot{\underline{x}} + K\underline{x} = \underline{f}$$

(2.54)

where

$$M = \begin{bmatrix} m_1 & 0 & 0 & 0 \\ 0 & m_2 & 0 & 0 \\ 0 & 0 & m_3 & 0 \\ 0 & 0 & 0 & m_4 \end{bmatrix} \qquad \underline{x} = \begin{Bmatrix} x_1 \\ x_2 \\ x_3 \\ x_4 \end{Bmatrix} \qquad \underline{f} = \begin{Bmatrix} f_1 \\ f_2 \\ f_3 \\ f_4 \end{Bmatrix}$$

(2.55)

2-18

$$
D = \begin{bmatrix}
d_{01} + d_{41} + d_{12} & -d_{12} & 0 & -d_{41} \\
-d_{12} & d_{02} + d_{12} + d_{23} & -d_{23} & 0 \\
0 & -d_{23} & d_{03} + d_{23} + d_{34} & -d_{34} \\
-d_{41} & 0 & -d_{34} & d_{04} + d_{34} + d_{41}
\end{bmatrix}
\tag{2.56}
$$

$$
K = \begin{bmatrix}
k_{01} + k_{41} + k_{12} & -k_{12} & 0 & -k_{41} \\
-k_{12} & k_{02} + k_{12} + k_{23} & -k_{23} & 0 \\
0 & -k_{23} & k_{03} + k_{23} + k_{34} & -k_{34} \\
-k_{41} & 0 & -k_{34} & k_{04} + k_{34} + k_{41}
\end{bmatrix}
\tag{2.57}
$$

The objective of this example is to regulate the position of cart 2, which means that $q_c = x_2$ and $q_u = \begin{bmatrix} x_1 & x_3 & x_4 \end{bmatrix}^T$. Thus, rearranging Equation 2.54, yields

$$
\left[\begin{array}{c|ccc}
m_2 & 0 & 0 & 0 \\
\hline
0 & m_1 & 0 & 0 \\
0 & 0 & m_3 & 0 \\
0 & 0 & 0 & m_4
\end{array} \right]
\begin{Bmatrix} \ddot{x}_2 \\ \hline \ddot{x}_1 \\ \ddot{x}_3 \\ \ddot{x}_4 \end{Bmatrix}
\tag{2.58}
$$

$$
+ \left[\begin{array}{c|ccc}
d_{02} + d_{12} + d_{23} & -d_{12} & -d_{23} & 0 \\
\hline
-d_{12} & d_{01} + d_{41} + d_{12} & 0 & -d_{41} \\
-d_{23} & 0 & d_{03} + d_{23} + d_{34} & -d_{34} \\
0 & -d_{41} & -d_{34} & d_{04} + d_{34} + d_{41}
\end{array} \right]
\begin{Bmatrix} \dot{x}_2 \\ \hline \dot{x}_1 \\ \dot{x}_3 \\ \dot{x}_4 \end{Bmatrix}
$$

$$
+ \left[\begin{array}{c|ccc}
k_{02} + k_{12} + k_{23} & -k_{12} & -k_{23} & 0 \\
\hline
-k_{12} & k_{01} + k_{41} + k_{12} & 0 & -k_{41} \\
-k_{23} & 0 & k_{03} + k_{23} + k_{34} & -k_{34} \\
0 & -k_{41} & -k_{34} & k_{04} + k_{34} + k_{41}
\end{array} \right]
\begin{Bmatrix} x_2 \\ \hline x_1 \\ x_3 \\ x_4 \end{Bmatrix}
=
\begin{Bmatrix} f_2 \\ \hline f_1 \\ f_3 \\ f_4 \end{Bmatrix}
$$

Comparing the above with Equation 2.45, repeated below,

$$\begin{bmatrix} M_c & 0 \\ 0 & M_u \end{bmatrix} \left\{ \begin{array}{c} \ddot{q}_c \\ \ddot{q}_u \end{array} \right\} + \begin{bmatrix} D_c & D_{cu} \\ D_{uc} & D_u \end{bmatrix} \left\{ \begin{array}{c} \dot{q}_c \\ \dot{q}_u \end{array} \right\} + \begin{bmatrix} K_c & K_{cu} \\ K_{uc} & K_u \end{bmatrix} \left\{ \begin{array}{c} q_c \\ q_u \end{array} \right\} = \left\{ \begin{array}{c} f_c \\ f_u \end{array} \right\}$$

results in

$$M_c = m_2 \qquad (2.59) \qquad\qquad K_c = k_{02} + k_{12} + k_{23} \qquad (2.63)$$

$$f_c = f_2 \qquad (2.60) \qquad\qquad D_c = d_{02} + d_{12} + d_{23} \qquad (2.64)$$

$$q_c = x_2 \qquad (2.61) \qquad\qquad K_{cu} = \begin{bmatrix} -k_{12} & -k_{23} & 0 \end{bmatrix} \qquad (2.65)$$

$$q_u = \begin{bmatrix} x_1 & x_3 & x_4 \end{bmatrix}^T \qquad (2.62) \qquad\qquad D_{cu} = \begin{bmatrix} -d_{12} & -d_{23} & 0 \end{bmatrix} \qquad (2.66)$$

After making these substitutions into Equation 2.48, the controlled coordinate EOM becomes

$$\begin{aligned} M_c \ddot{q}_c + D_c \dot{q}_c + K_c q_c &= f_c - K_{cu} q_u - D_{cu} \dot{q}_u \\ &= f_c - \begin{bmatrix} -k_{12} & -k_{23} & 0 \end{bmatrix} q_u - \begin{bmatrix} -d_{12} & -d_{23} & 0 \end{bmatrix} \dot{q}_u \\ &= f_c - (-k_{12} x_1 - k_{23} x_3 - d_{12} \dot{x}_1 - d_{23} \dot{x}_3) \\ &= f_c - Y_r \Phi_r \qquad\qquad\qquad (2.67) \end{aligned}$$

where the regression matrix is $Y_r = \begin{bmatrix} x_1 & x_3 & \dot{x}_1 & \dot{x}_3 \end{bmatrix}$, and the unknown parameter vector is $\Phi_r = -\begin{bmatrix} k_{12} & k_{23} & d_{12} & d_{23} \end{bmatrix}^T$. The control force is now found from Equation 2.49

$$\begin{aligned} f_c &= Y_r \hat{\Phi}_r - K_f q_c - D_f \dot{q}_c \\ &= (-\hat{k}_{12} x_1 - \hat{k}_{23} x_3 - \hat{d}_{12} \dot{x}_1 - \hat{d}_{23} \dot{x}_3) - K_f x_2 - D_f \dot{x}_2 \qquad (2.68) \end{aligned}$$

K_f and D_f must meet the requirements of assumption A4, p. 2-17, and are chosen to give the desired performance. They are defined in terms of an actuator with damping ratio, ζ_f, and frequency, ω_f, so that $K_f = \omega_f^2 M_c$ and $D_f = 2\zeta_f \omega_f M_c$.

The adaptation law for the parameter estimates is given by Equation 2.50

$$\dot{\hat{\Phi}}_r = -\Gamma_r \Upsilon^T P X_c$$

where for the 4 DOF system

$$\Gamma_r = \begin{bmatrix} \gamma_1 & & & 0 \\ & \gamma_2 & & \\ & & \gamma_3 & \\ 0 & & & \gamma_4 \end{bmatrix} > 0 \qquad (2.69)$$

$$\Upsilon^T = \begin{bmatrix} 0 & (M_c^{-1} Y_r)^T \end{bmatrix} = \left(\frac{1}{m_2}\right) \begin{bmatrix} 0 & x_1 \\ 0 & x_3 \\ 0 & \dot{x}_1 \\ 0 & \dot{x}_3 \end{bmatrix} \qquad (2.70)$$

$$X_c = \left\{ \begin{array}{c} q_c \\ \dot{q}_c \end{array} \right\} = \left\{ \begin{array}{c} x_2 \\ \dot{x}_2 \end{array} \right\} \qquad (2.71)$$

To simplify the Lyapunov equation, Equation 2.51, Q is assumed diagonal, and selected so that $X_c^T Q X_c$ results in an energy term. Thus,

$$\begin{bmatrix} x_2 & \dot{x}_2 \end{bmatrix} \begin{bmatrix} Q_{11} & 0 \\ 0 & Q_{22} \end{bmatrix} \begin{bmatrix} x_2 \\ \dot{x}_2 \end{bmatrix} = Q_{11} x_2^2 + Q_{22} \dot{x}_2^2 \qquad (2.72)$$

The first term in the above expression is the spring potential energy associated with cart 2, and the second term is the kinetic energy. After normalizing, Q is

$$Q = \begin{bmatrix} 1 & 0 \\ 0 & \frac{m_2}{k_{02}+k_{12}+k_{23}} \end{bmatrix} = \begin{bmatrix} 1 & 0 \\ 0 & \omega_{n2}^{-2} \end{bmatrix} = Q^T > 0 \qquad (2.73)$$

It may appear that Q depends on coupling strength between carts. However, unlike Wang and Tang's technique, exact knowledge of k_{12} and k_{23} is not required. The lower diagonal term is the inverse of the square of the natural frequency of cart 2 when the adjacent carts are fixed. This value can be found experimentally.

With the Q defined above, and A_c from Equation 2.52, the Lyapunov equation is solved for P, which in generic terms is

$$P = \begin{bmatrix} p_{11} & p_{21} \\ p_{21} & p_{22} \end{bmatrix} \qquad (2.74)$$

Therefore, substituting Equations 2.69 through 2.74 into Equation 2.50, and performing some matrix algebra, the adaptive parameter estimate law for the 4 DOF system becomes

$$\dot{\hat{\Phi}}_r = -\left(\frac{1}{m_2}\right) \begin{bmatrix} \gamma_1 & & & 0 \\ & \gamma_2 & & \\ & & \gamma_3 & \\ 0 & & & \gamma_4 \end{bmatrix} \begin{Bmatrix} x_1 \\ x_3 \\ \dot{x}_1 \\ \dot{x}_3 \end{Bmatrix} \begin{bmatrix} p_{21} & p_{22} \end{bmatrix} \begin{Bmatrix} x_2 \\ \dot{x}_2 \end{Bmatrix} = - \begin{Bmatrix} \dot{\hat{k}}_{12} \\ \dot{\hat{k}}_{23} \\ \dot{\hat{d}}_{12} \\ \dot{\hat{d}}_{23} \end{Bmatrix} \qquad (2.75)$$

The only variables left unassigned in the above equation are the gains $(\gamma_1, \ldots, \gamma_4)$. The gains allow for adjustments in the parameter estimation process. Unfortunately, Ertur gives no assistance in determining these values. Since there is no analytical solution for the gains, they are found through experimentation.

2.3.3 Simulation.
To model the 4 DOF system in SIMULINK^{TM} the EOMs are put into state-space form, so Equation 2.54 becomes

$$\left\{ \begin{array}{c} \dot{x} \\ \ddot{x} \end{array} \right\} = \left[\begin{array}{cc} [0]_{4\times4} & [I]_{4\times4} \\ -M^{-1}K & -M^{-1}D \end{array} \right] \left\{ \begin{array}{c} x \\ \dot{x} \end{array} \right\} + \left[\begin{array}{c} [0]_{4\times4} \\ -M^{-1} \end{array} \right] f \qquad (2.76)$$

In this simulation, the system is tuned. This means that all of the carts have identical: mass, $m_i = 1$ Kg; stiffness, $k_{0i} = 100$ N/m; and coupling, $k_{ij} = k_c = 5$ N/m, where $i, j = 1...4$. Using these values, the mass and stiffness matrices, M and K respectively, are found from Equations 2.55 and 2.57. Also, assuming a structural damping ratio of $\zeta_n = 0.01$, the damping matrix, D, is calculated from

$$D = \Psi \left[2\zeta_n \left(\Psi^T K \Psi \right)^{\frac{1}{2}} \right] \Psi^T \qquad \Psi^T D \Psi = \left[\begin{array}{ccc} 2\zeta_n\omega_{n1} & & 0 \\ & \ddots & \\ 0 & & 2\zeta_n\omega_{n4} \end{array} \right] \qquad (2.77)$$

where Ψ is the system mass normalized modal matrix.

An external disturbance of $f_d = 10\sin(\omega_d t)$, is applied to cart 3 only. The disturbance frequency was set equal to the lowest natural frequency of the system, $\omega_d = \omega_n$.

As previously stated, the controller stiffness and damping are defined as $K_f = \omega_f^2 M_c$ and $D_f = 2\zeta_f\omega_f M_c$, respectively. The controller frequency was also set equal to the lowest natural frequency of the system, $\omega_f = \omega_n$. A relatively high damping ratio of $\zeta_f = 0.7$ was used.

The stability of the system is guaranteed if assumptions A1 through A4, p. 2-17, are satisfied. For this system, $M_c = M_c^T = m_2 > 0$, so A1 is met. Since the disturbance is sinusoidal, and therefore bounded, A2 is also fulfilled. Lastly, A3 and A4 are satisfied if A_c, Equation 2.52, and A_u, Equation 2.53, are negative definite; these are checked numerically by the simulation.

2.3.4 Results.
The SIMULINK^{TM} model of the 4 DOF system with adaptive control only on cart 2 is shown in Figures A.2 and A.3, on p. A-6. The MATLAB^{TM} code
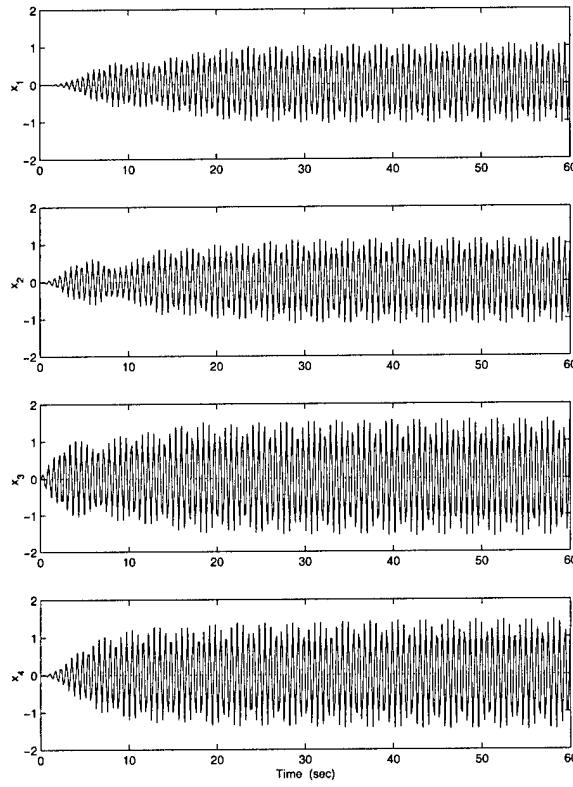
Figure 2.9   Displacements (m) for the Uncontrolled Chain System

used to run the chain system simulation is given in Appendix A.2.1, beginning on p. A-7. The MATLAB^{TM} code used to run the cyclic system simulation is given in Appendix A.2.2, beginning on p. A-9.

2.3.4.1   Chain System.   The first model studied was a 4 DOF chain system. In this setup, the spring and damper between carts 1 and 4 are cut (i.e. $k_{41} = d_{41} = 0$). This means that while the disturbance can move sequentially through the carts, it cannot wrap around the ends. Keep in mind that adaptive control is only employed on cart 2, and the disturbance is only applied to cart 3. A plot of the uncontrolled response of the system is shown in Figure 2.9. All cart displacements have a maximum amplitude of roughly 1 to 1.5 meters.
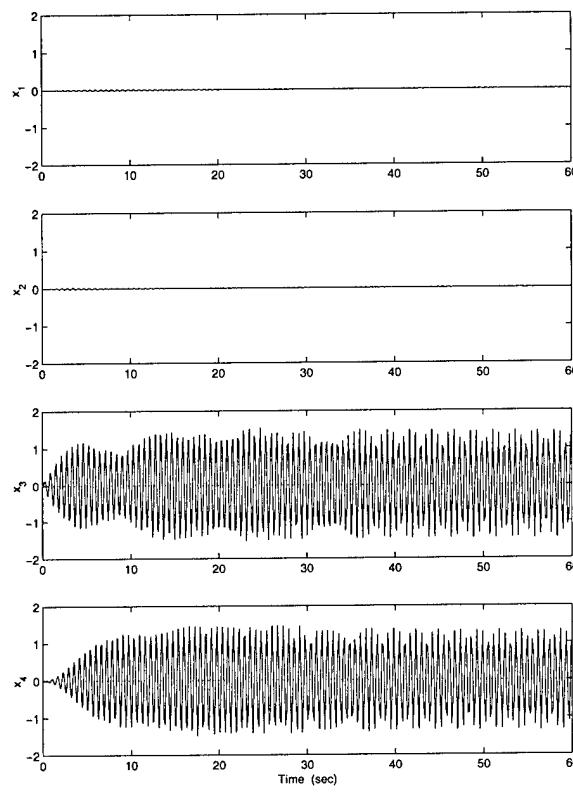
Figure 2.10   Displacements (m) for Chain System: Adaptive Control, $\Gamma_r = 10^4 \, \mathrm{I}$
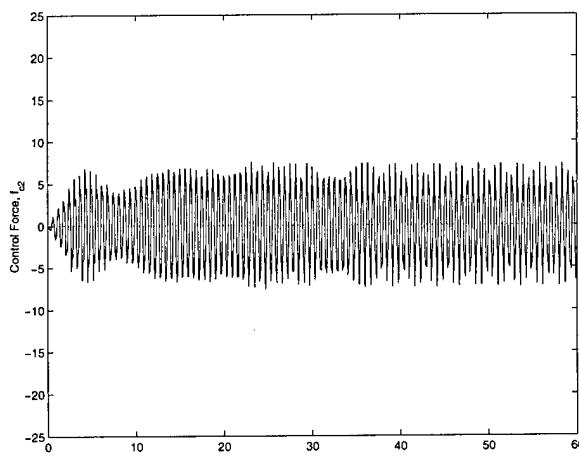
Figure 2.11   Control Force (N) for Chain System: Adaptive Control, $\Gamma_r = 10^4 \, \mathrm{I}$
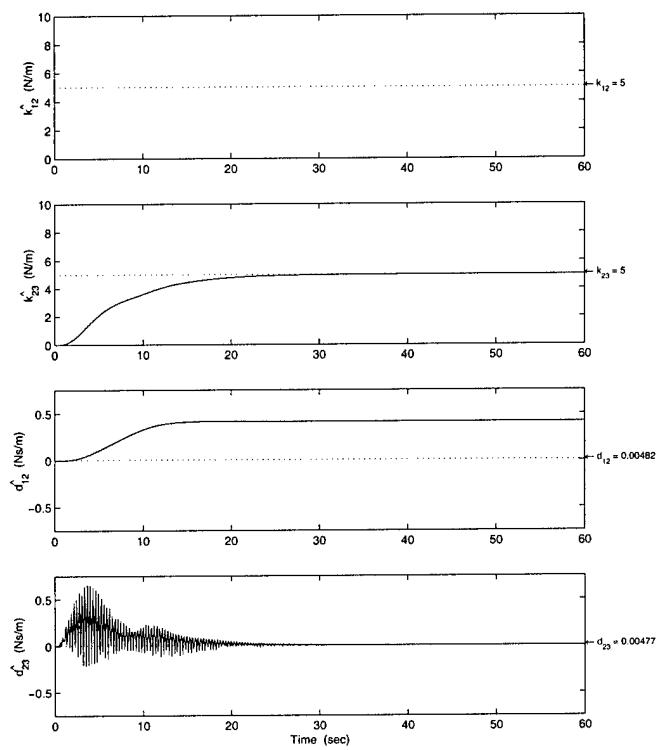
Figure 2.12   Parameter Estimates for Chain System: Adaptive Control, $\Gamma_r = 10^4\,\mathrm{I}$

The selection of gains is required to implement the adaptive control technique. Initially, $\Gamma_r = I$ was picked. The magnitude of Γ_r was increased by a factor of 10 until the parameter estimates converged; this occurred at $\Gamma_r = 10^4\,I$. As shown in Figure 2.10, with adaptive control turned on, the response of cart 2 is negligible. There is also the added benefit that cart 1 is completely isolated from the disturbance, so its response is negligible as well. The responses of carts 3 and 4 remain largely unchanged. The control force, shown in Figure 2.11, is sinusoidal in nature with roughly the same frequency as the disturbance and a slightly lower amplitude. The parameter estimates are shown in Figure 2.12. Note that in parameter estimate plots, $\hat{k}_{ij}$ and $\hat{d}_{ij}$ are the estimated values of k_{ij} and d_{ij} respectively. It is interesting that even though the response in cart 2 is completely suppressed, not all of the parameter estimates have converged to their correct values. The estimator determined that $\hat{k}_{12}$ is identically zero, and produced a high estimate for $\hat{d}_{12}$.

Referring back to the parameter estimate law, Equation 2.75, $\hat{k}_{12}$ and $\hat{d}_{12}$ depend on γ_1 and γ_3 respectively. It is reasonable to assume, that adjusting these values will effect the estimates. Varying γ_1 did not effect $\hat{k}_{12}$ at all. However, setting $\gamma_3 = 0.01 \times 10^4$, caused $\hat{d}_{12}$ to converge to the correct value. The displacement, control force, and parameter estimate plots for this new Γ_r are shown in Figures 2.13 through 2.15. All responses are similar to those for the previous Γ_r, except now $\hat{d}_{12}$ immediately converges.

There is still a problem with the parameter estimate for k_{12}. Examining the estimation law, Equation 2.75 again, $\hat{k}_{12}$ is directly related to the displacement of cart 1. The response of cart 1 is basically zero from the start of the simulation. This may cause problems for the estimator. The simulation was rerun with adaptive control turned off for the first ten seconds. This allowed cart 1 to build up a response before the estimator started. The results are shown in Figures 2.16 through 2.18. All of the parameter estimates now converge to the correct values. The response of carts 1 and 2 are still completely suppressed.

2.3.4.2 Cyclic System.

The next model studied was a 4 DOF cyclic system. A plot of the uncontrolled response of the system is shown in Figure 2.19. There
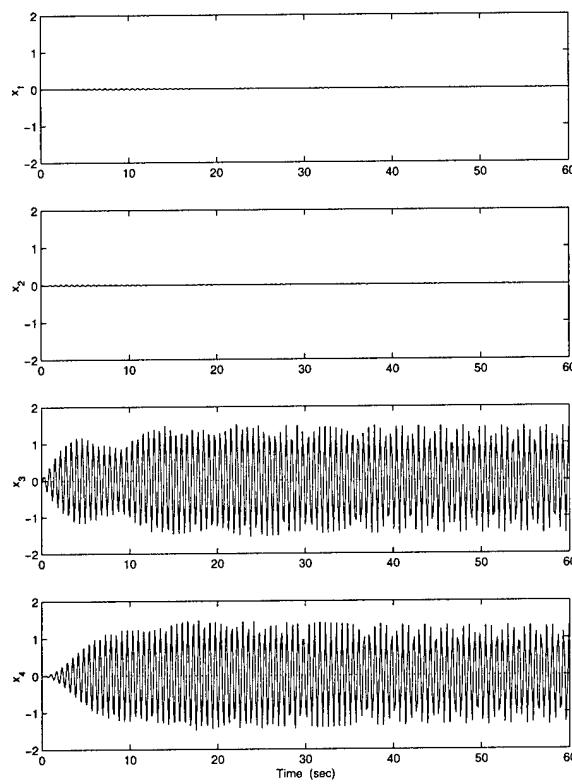
Figure 2.13 Displacements (m) for Chain System: Adaptive Control, $\Gamma_r = 10^4 \times \text{diag}(1, 1, 0.01, 1)$
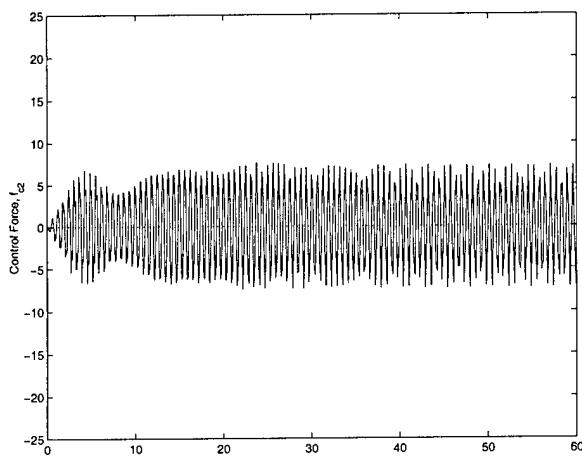
Figure 2.14   Control   Force   (N)   for   Chain   System: Adaptive   Control, $\Gamma_r = 10^4 \times \text{diag}(1,1,0.01,1)$
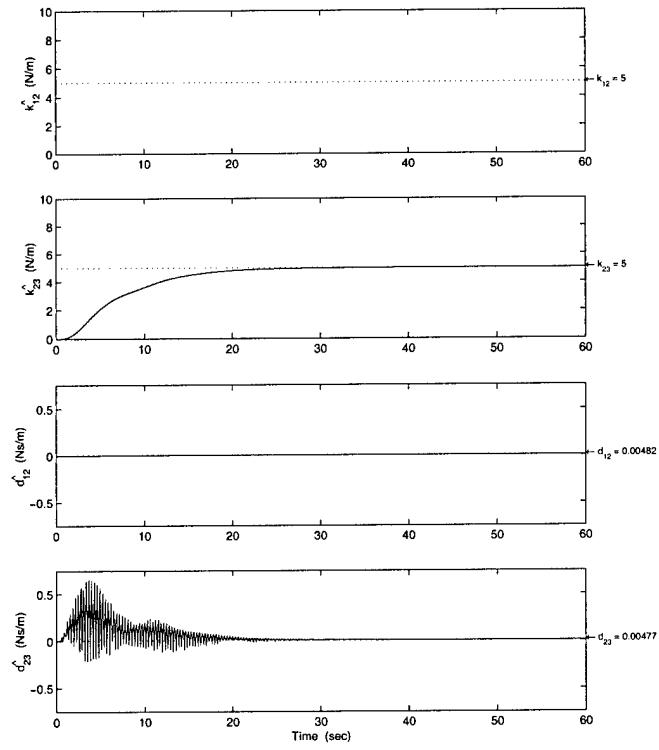
Figure 2.15   Parameter   Estimates   for   Chain   System: Adaptive   Control, $\Gamma_r = 10^4 \times \text{diag}(1,1,0.01,1)$

2-29
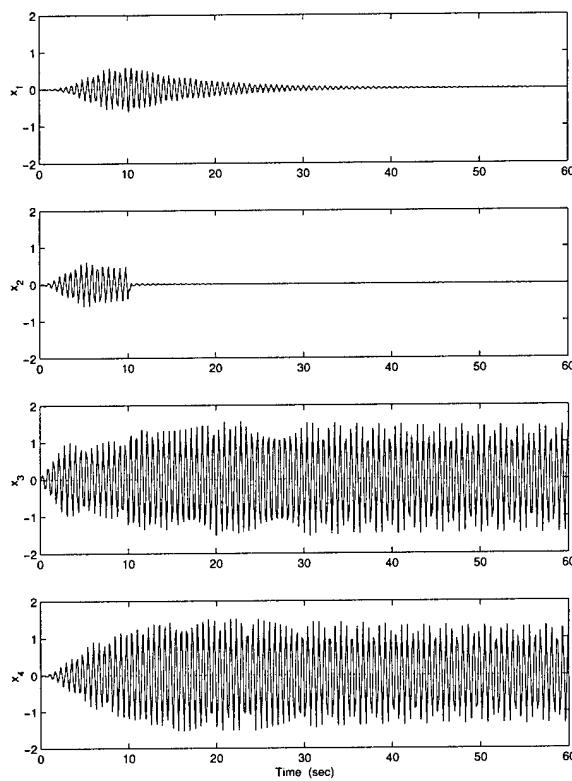
Figure 2.16   Displacements (m) for Chain System: Adaptive Control turned on at $t = 10$ sec, $\Gamma_r = 10^4 \times \mathrm{diag}(6, 1, 0.00045, 1)$
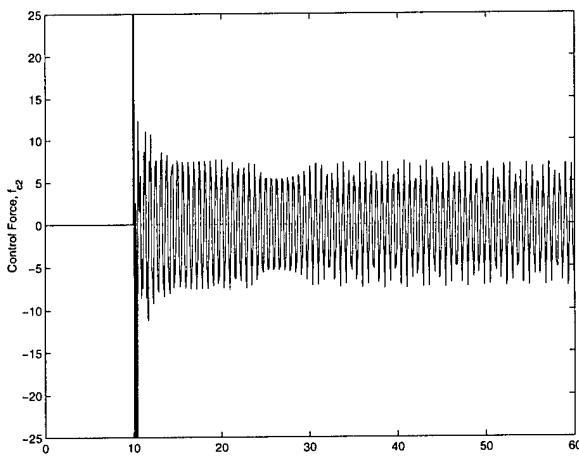
Figure 2.17   Control Force (N) for Chain System: Adaptive Control turned on at $t = 10$ sec, $\Gamma_r = 10^4 \times \text{diag}(6, 1, 0.00045, 1)$
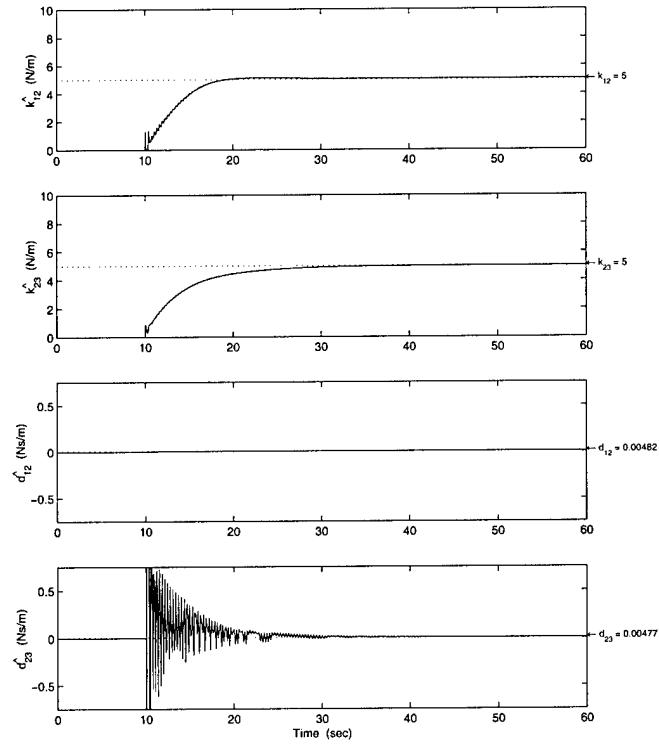
Figure 2.18   Parameter Estimates for Chain System: Adaptive Control turned on at $t = 10$ sec, $\Gamma_r = 10^4 \times \text{diag}(6, 1, 0.00045, 1)$
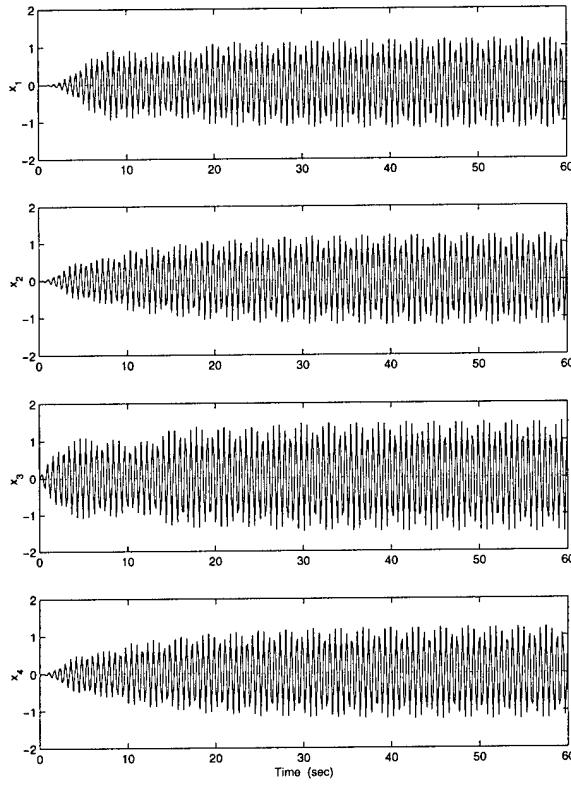
Figure 2.19   Displacements (m) for the Uncontrolled Cyclic System

are no tangible differences between the uncontrolled response of the cyclic system and the chain system, Figure 2.9.

As with the chain system, the gain matrix for adaptive control, Γ_r, was selected through a trial and error process. The gains used for the chain system did not produce acceptable results for the cyclic system. A value of $\Gamma_r = 10^2 \times \text{diag}(1000, 100, 1, 1)$ was finally settled on. The displacements for the cyclic system are shown in Figure 2.20. The response of cart 2 is again completely suppressed. However, since this is a cyclic system, cart 1 is not isolated from the disturbance. Its response is substantially reduced, but no longer negligible. The adaptive control also appears to have more of an effect on the whole system. The responses of both carts 3 and 4 are noticeably lower than in the chain system, Figure 2.10. Now that cart 2 is influenced by all of the other carts, the controller also has
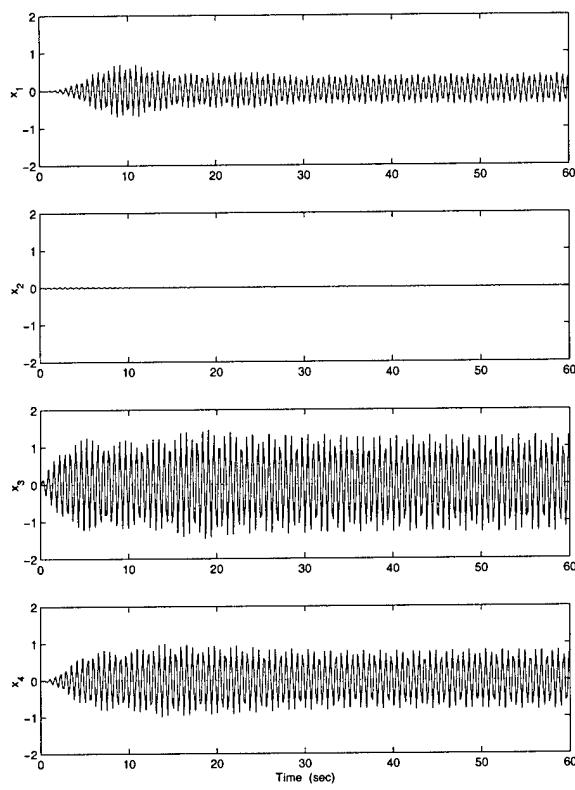
Figure 2.20   Displacements   (m)   for   Cyclic   System: Adaptive   Control,
$\Gamma_r = 10^2 \times \text{diag}(1000, 100, 1, 1)$
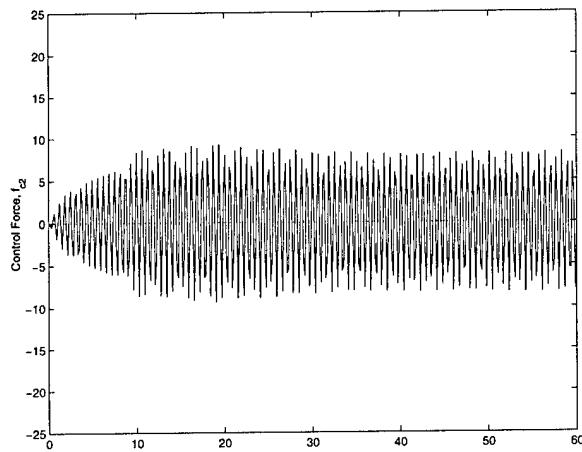
Figure 2.21   Control   Force   (N)   for   Cyclic   System: Adaptive   Control,
$\Gamma_r = 10^2 \times \text{diag}(1000, 100, 1, 1)$
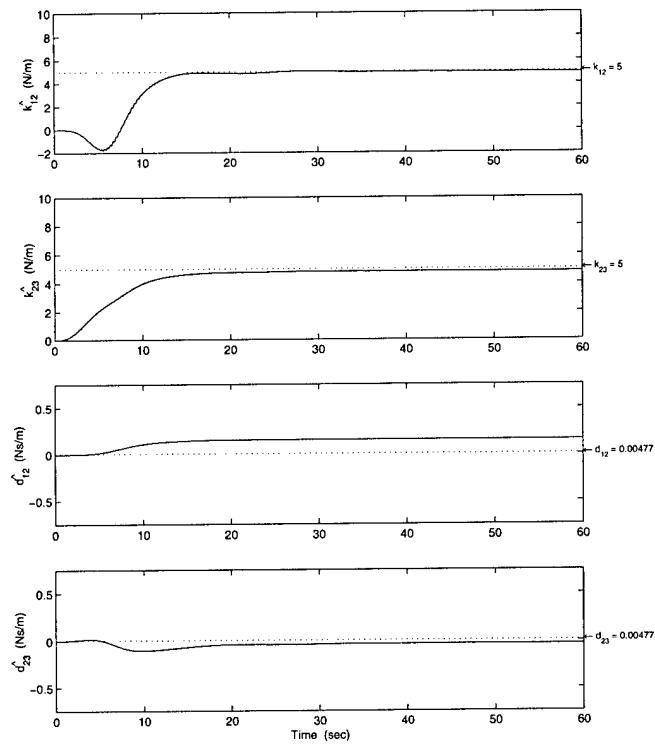
Figure 2.22   Parameter   Estimates   for   Cyclic   System: Adaptive   Control,
$\Gamma_r = 10^2 \times \text{diag}(1000, 100, 1, 1)$
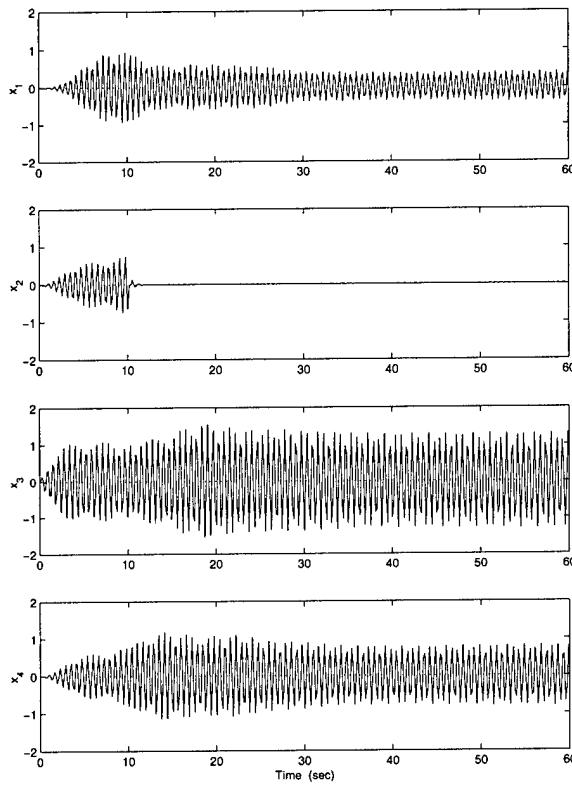
Figure 2.23   Displacements (m) for Cyclic System: Adaptive Control turned on at $t = 10$ sec, $\Gamma_r = 10^3 \times \mathrm{diag}(100, 100, 1, 1)$

to do more work. This shows up in a slightly higher control force, Figure 2.21, than in the chain system, Figure 2.11.

The parameter estimates, Figure 2.22, all converge quickly to the correct values, although there are some minor offsets in the damping parameters. Unlike the chain system, there is no problem with the estimate for k_{12}. In the cyclic system, vibration energy can be transferred from cart 4 to cart 1, which gives cart 1 a discernible response. As was seen in the chain system, when cart 1 was allowed to first build up a response before adaptive control was started, the estimate for k_{12} converged quickly to the correct value.

For comparison purposes, the cyclic system was also run with a delayed start of adaptive control. The results are shown in Figures 2.23 through Figure 2.25. At steady-
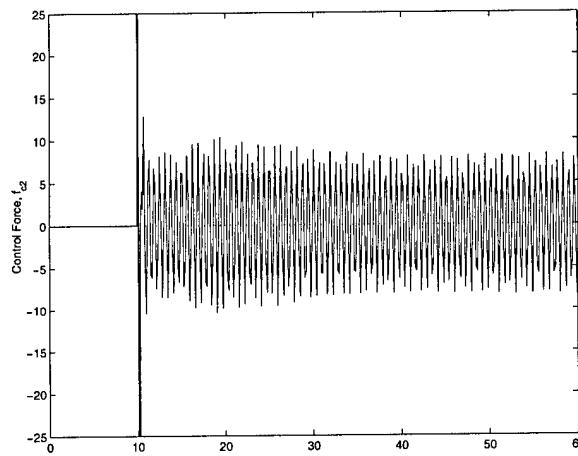
Figure 2.24   Control Force (N) for Cyclic System: Adaptive Control turned on at $t = 10$ sec, $\Gamma_r = 10^3 \times \text{diag}(100, 100, 1, 1)$
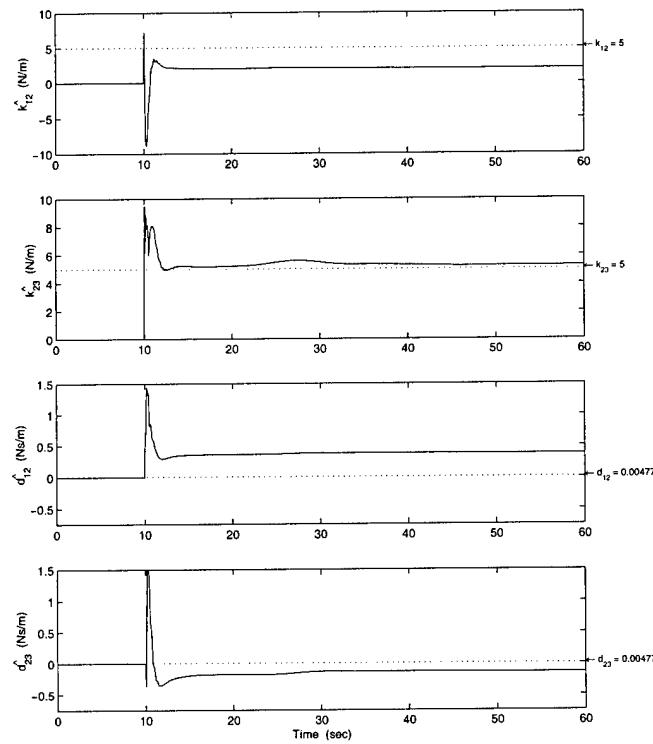
Figure 2.25   Parameter Estimates for Cyclic System: Adaptive Control turned on at $t = 10$ sec, $\Gamma_r = 10^3 \times \text{diag}(100, 100, 1, 1)$

state, the maximum amplitudes of the displacements are similar to when control was started immediately. The magnitude of the control force is slightly higher, most likely because the controller had to overcome a greater initial amount of vibration energy when turned on. Unexpectedly though, the parameter estimates are noticeably worse. The offset in the damping parameters is larger, although not alarmingly so. More importantly, though, the estimate for k_{12} is considerably off, and even starts out negative.

2.3.4.3 Summary.

It appears quite evident, at least for the stiffness parameters, that the estimator requires a minimum level of input to work properly. This was clearly demonstrated by the estimates of k_{12}, the stiffness of the spring between carts 1 and 2. In the chain system, when cart 1 was isolated from the disturbance, and thus had zero response, the estimator could not estimate k_{12}. However, when cart 1 was allowed to build up a response before the estimator started, the result converged to the correct value quickly. This was also the case in the cyclic system.

If the other inputs to the estimation law are at acceptable levels, then the individual gains ($\gamma_1, \ldots, \gamma_4$) allow for some adjustments in the convergence of the parameter estimates. The relative scaling of the gains will raise or lower the value of convergence. That is of course if you are in the neighborhood of a feasible solution. There are some combinations of the gains which will cause the estimates to converge to significantly incorrect values. It is important to note that even if this happens, the response of the system may be substantially reduced.

Finally, it should be pointed out, that the actual values of the estimated parameters are unknown in a real system. That is in fact why they are estimated. This raises the question, should the gains be set to drive the estimates to uncertain parameter values, or should the deciding factor merely be system performance.

2.4 Synopsis

This chapter introduced three individual theories. First, a hybrid active/passive piezoelectric vibration absorber developed by Wang and Tang [18] was studied. The EOMs were derived and the optimal tuning parameters found. While providing superior perfor-

mance to a purely active or purely passive system, it requires a priori knowledge of the coupling strength, which is not well defined.

Next, the active control theory of positive position feedback (PPF) was presented and the stability requirements explained. The EOMs were then developed for a single DOF system. This system was simulated, and the optimal tuning parameters were found.

Finally, an adaptive parameter estimation and control technique suggested by Ertur, et al, was explored. Their method cancels unknown bounded disturbances while compensating for uncertainties [6]. The EOMs were developed for a 4 DOF system. The response of the system to a simulated sinusoidal disturbance were presented and discussed.

In the following chapter, Ertur's adaptive control and PPF are combined into a single control methodology for a 4 DOF system. The adaptive parameter estimator eliminates the coupling forces, and then the vibrations are suppressed by PPF.

III. Combined Adaptive/PPF Control for a Single Degree of Freedom

3.1 Motivation

In a compressor disk, effective vibration suppression requires broadband control effort, and elimination of the inter-blade coupling forces. Wang and Tang's hybrid active/passive piezoelectric shunt network achieved this with greater performance than a purely active or purely passive system. The active component delivered high performance broadband vibration suppression, while the passive shunt provided a stable, fail-safe, easily constructed vibration absorber. Unfortunately, optimal tuning of the passive shunt requires prior knowledge of the coupling strength, a quantity not well defined. Also, for typical applications it is necessary to actively synthesize inductors for the passive shunt network. This negates any benefits of a passive system, and complicates implementation.

Since the shunt network is no longer truly passive, replacing it with a simpler, purely active system is desirable. The PVA is analogous to an MVA, but this is an impractical solution for a compressor disk. The PPF method discussed in Section 2.2 is also analogous to an MVA and provides active vibration suppression that is guaranteed stable. The question is whether or not PPF is equivalent to a PVA. To answer this, consider again the N-DOF cyclic system used by Wang and Tang, see Section 2.1.2. This time, however, N identical PPF actuators are used instead of PVAs. The EOMs are

$$m_1\ddot{x}_1 + d\,\dot{x}_1 + (k + 2k_c)\,x_1 - k_c\,(x_N + x_2) = \mu\omega_{n_1}^2 m_1\eta_1 + f_{d1}$$

$$\ddot{\eta}_1 + 2\zeta_f\omega_f\dot{\eta}_1 + \omega_f^2\eta_1 = \omega_f^2 x_1$$

$$\vdots \qquad\qquad (3.1)$$

$$m_N\ddot{x}_N + d\,\dot{x}_N + (k + 2k_c)\,x_N - k_c\,(x_{N-1} + x_1) = \mu\omega_{n_N}^2 m_N\eta_N + f_{dN}$$

$$\ddot{\eta}_N + 2\zeta_f\omega_f\dot{\eta}_N + \omega_f^2\eta_N = \omega_f^2 x_N$$

where $\omega_{n_i}^2 = \frac{k+2k_c}{m_i}$. In matrix form, these equations become

$$M\ddot{X} + D\dot{X} + KX = GX + F \qquad (3.2)$$

where $X = [x_1, \eta_1, ..., x_N, \eta_N]^T$ is the generalized displacement vector; $F = [f_{d1}, 0, ..., f_{dN}, 0]^T$ is the generalized force vector consisting of the external disturbances. The generalized mass (M), damping (D), gain (G), and stiffness (K) matrices are

$$M = \begin{bmatrix} m_1 & & & & 0 \\ & 1 & & & \\ & & \ddots & & \\ & & & m_N & \\ 0 & & & & 1 \end{bmatrix} \qquad D = \begin{bmatrix} d_1 & & & & 0 \\ & 2\zeta_f\omega_f & & & \\ & & \ddots & & \\ & & & d_N & \\ 0 & & & & 2\zeta_f\omega_f \end{bmatrix} \qquad (3.3)$$

$$K = \begin{bmatrix} \chi_m & \chi_c & 0 & \cdots & 0 & \chi_c^T \\ \chi_c^T & \chi_m & \chi_c & \ddots & \vdots & 0 \\ 0 & \chi_c^T & \ddots & \ddots & 0 & \vdots \\ \vdots & \ddots & \ddots & \ddots & \chi_c & 0 \\ 0 & \cdots & 0 & \chi_c^T & \chi_m & \chi_c \\ \chi_c & 0 & \cdots & 0 & \chi_c^T & \chi_m \end{bmatrix} \qquad G = \begin{bmatrix} \chi_{g1} & & 0 \\ & \ddots & \\ 0 & & \chi_{gN} \end{bmatrix} \qquad (3.4)$$

with $\quad \chi_m = \begin{bmatrix} k + 2k_c & 0 \\ 0 & \omega_f^2 \end{bmatrix}, \quad \chi_c = \begin{bmatrix} -k_c & 0 \\ 0 & 0 \end{bmatrix}, \quad$ and $\quad \chi_{gi} = \begin{bmatrix} 0 & \mu\omega_{n_i}^2 m_i \\ \omega_f^2 & 0 \end{bmatrix}$

Note that M, D, K, and G are $2N \times 2N$. The PPF equations of motion, Equation 3.2, are nearly identical to those derived by Wang and Tang for a PVA, Equation 2.10. The only significant difference in the two methods lies in the force vectors. Wang and Tang used an active voltage control in the shunt equations to cancel the mechanical coupling effects. PPF does not have an active input force. Therefore, to eliminate the coupling effects, PPF will be augmented with Ertur's adaptive control technique, Section 2.3.
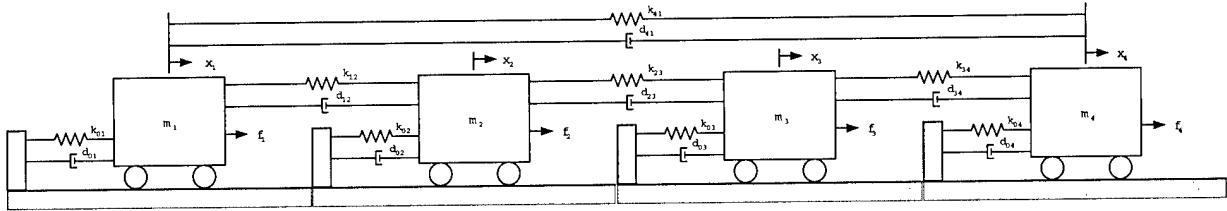
Figure 3.1   Cyclic 4 DOF System

3.2   Development

3.2.1   Equations of Motion for a Four Cart System.   To begin

with, the Adaptive/PPF control law is developed for vibration suppression of a single substructure in an RPS. The 4 DOF cyclic system, studied in Section 2.3.2, and shown again in Figure 3.1, is used here as well. The system is drawn linearly, but it is analogous to the rotary periodic structure of a compressor disk. The blades, or carts, have mass m_i, and their structural stiffness and damping are represented by k_{0i} and d_{0i}. The inter-blade coupling forces are expressed in terms of k_{ij} and d_{ij}, where $i, j = 1...4$; by convention m_i is the left cart, and m_j is the right cart. The external control and disturbance forces on each cart are represented by f_i. It was established, see Equation 2.54, that the EOMs for this system are

$$M\underline{\ddot{x}} + D\underline{\dot{x}} + K\underline{x} = \underline{f} \tag{3.5}$$

where the matrices and vectors are defined in Equations 2.55 through 2.57. A PPF actuator is now added to cart 2 of this system, with the following form

$$\ddot{\eta}_2 + 2\zeta_f \omega_f \dot{\eta}_2 + \omega_f^2 \eta_2 = h_2 \tag{3.6}$$

Note that there is only one PPF actuator in this example; the subscript 2 merely signifies that it is on cart 2.

As before, the objective of this example is to regulate the position of cart 2, thus x_2 and η_2 are the controlled coordinates in the adaptive control technique. This means that $q_c = \begin{bmatrix} x_2 & \eta_2 \end{bmatrix}^T$ and $q_u = \begin{bmatrix} x_1 & x_3 & x_4 \end{bmatrix}^T$. So augmenting Equation 3.5 with Equa-

tion 3.6, and rearranging into the controlled/uncontrolled partitioned form, yields

$$
\begin{bmatrix}
m_2 & 0 & 0 & 0 & 0 \\
0 & 1 & 0 & 0 & 0 \\
\hline
0 & 0 & m_1 & 0 & 0 \\
0 & 0 & 0 & m_3 & 0 \\
0 & 0 & 0 & 0 & m_4
\end{bmatrix}
\left\{
\begin{array}{c}
\ddot{x}_2 \\
\ddot{\eta}_2 \\
\hline
\ddot{x}_1 \\
\ddot{x}_3 \\
\ddot{x}_4
\end{array}
\right\}
+
\tag{3.7}
$$

$$
\begin{bmatrix}
d_{02}+d_{12}+d_{23} & 0 & -d_{12} & -d_{23} & 0 \\
0 & 2\zeta_f\omega_f & 0 & 0 & 0 \\
\hline
-d_{12} & 0 & d_{01}+d_{41}+d_{12} & 0 & -d_{41} \\
-d_{23} & 0 & 0 & d_{03}+d_{23}+d_{34} & -d_{34} \\
0 & 0 & -d_{41} & -d_{34} & d_{04}+d_{34}+d_{41}
\end{bmatrix}
\left\{
\begin{array}{c}
\dot{x}_2 \\
\dot{\eta}_2 \\
\hline
\dot{x}_1 \\
\dot{x}_3 \\
\dot{x}_4
\end{array}
\right\}
+
$$

$$
\begin{bmatrix}
k_{02}+k_{12}+k_{23} & 0 & -k_{12} & -k_{23} & 0 \\
0 & \omega_f^2 & 0 & 0 & 0 \\
\hline
-k_{12} & 0 & k_{01}+k_{41}+k_{12} & 0 & -k_{41} \\
-k_{23} & 0 & 0 & k_{03}+k_{23}+k_{34} & -k_{34} \\
0 & 0 & -k_{41} & -k_{34} & k_{04}+k_{34}+k_{41}
\end{bmatrix}
\left\{
\begin{array}{c}
x_2 \\
\eta_2 \\
\hline
x_1 \\
x_3 \\
x_4
\end{array}
\right\}
=
\left\{
\begin{array}{c}
f_2 \\
h_2 \\
\hline
f_1 \\
f_3 \\
f_4
\end{array}
\right\}
$$

It is obvious from the above and Equation 2.58 that the uncontrolled part of the system remains unchanged. Comparing Equation 3.7 to Equation 2.45, results in

$$
M_c = \begin{bmatrix} m_2 & 0 \\ 0 & 1 \end{bmatrix}
\tag{3.8}
\qquad
f_c = \left\{ \begin{array}{c} f_2 \\ h_2 \end{array} \right\}
\tag{3.11}
$$

$$
D_c = \begin{bmatrix} d_{02}+d_{12}+d_{23} & 0 \\ 0 & 2\zeta_f\omega_f \end{bmatrix}
\tag{3.9}
\qquad
D_{cu} = \begin{bmatrix} -d_{12} & -d_{23} & 0 \\ 0 & 0 & 0 \end{bmatrix}
\tag{3.12}
$$

$$
K_c = \begin{bmatrix} k_{02}+k_{12}+k_{23} & 0 \\ 0 & \omega_f^2 \end{bmatrix}
\tag{3.10}
\qquad
K_{cu} = \begin{bmatrix} -k_{12} & -k_{23} & 0 \\ 0 & 0 & 0 \end{bmatrix}
\tag{3.13}
$$

The controlled coordinate EOMs, the top half of Equation 3.7, are

$$M_c \ddot{q}_c + D_c \dot{q}_c + K_c q_c = f_c - K_{cu} q_u - D_{cu} \dot{q}_u \tag{3.14}$$

Thus, substituting Equations 3.12 and 3.13 into Equation 3.14 and performing some matrix algebra, the controlled coordinate EOMs become

$$M_c \ddot{q}_c + D_c \dot{q}_c + K_c q_c = f_c - \begin{bmatrix} -k_{12} x_1 - k_{23} x_3 - d_{12} \dot{x}_1 - d_{23} \dot{x}_3 \\ 0 \end{bmatrix} \tag{3.15}$$

Recall that for adaptive control, the controlled coordinate EOMs are rewritten as

$$M_c \ddot{q}_c + D_c \dot{q}_c + K_c q_c = f_c - Y_r \Phi_r \tag{3.16}$$

Therefore, comparing Equations 3.15 and 3.16, the regression matrix, Y_r, and unknown parameter vector, Φ_r, are

$$Y_r = \begin{bmatrix} x_1 & x_3 & \dot{x}_1 & \dot{x}_3 \\ 0 & 0 & 0 & 0 \end{bmatrix} \tag{3.17} \qquad \Phi_r = - \begin{Bmatrix} k_{12} \\ k_{23} \\ d_{12} \\ d_{23} \end{Bmatrix} \tag{3.18}$$

Note that the parameter vector, Φ_r, is the same as before. The adaptive control law is still estimating the stiffness and damping coupling parameters between cart 2 and the adjacent carts.

3.2.2 Adaptive/PPF Control Law.   Ertur suggested the following control law:

$$f_c = Y_r \hat{\Phi}_r - D_f \dot{q}_c - K_f q_c \tag{3.19}$$

The generic controller damping and stiffness matrices, D_f and K_f respectively, are now replaced by PPF. Only the displacement states, q_c, are used for PPF, so letting $D_f = 0$ and $K_{ppf} = -K_f$ in Equation 3.19, the new Adaptive/PPF control law becomes

$$f_c = Y_r \hat{\Phi}_r + K_{ppf} \, q_c \tag{3.20}$$

Substituting Equations 3.8 through 3.10, and Equation 3.20 into Equation 3.16, gives

$$\begin{bmatrix} m_2 & 0 \\ 0 & 1 \end{bmatrix} \left\{ \begin{array}{c} \ddot{x}_2 \\ \ddot{\eta}_2 \end{array} \right\} + \begin{bmatrix} d_{02} + d_{12} + d_{23} & 0 \\ 0 & 2\zeta_f \omega_f \end{bmatrix} \left\{ \begin{array}{c} \dot{x}_2 \\ \dot{\eta}_2 \end{array} \right\}$$

$$+ \begin{bmatrix} k_{02} + k_{12} + k_{23} & 0 \\ 0 & \omega_f^2 \end{bmatrix} \left\{ \begin{array}{c} x_2 \\ \eta_2 \end{array} \right\} = K_{ppf} \left\{ \begin{array}{c} x_2 \\ \eta_2 \end{array} \right\} + Y_r \left(\hat{\Phi}_r - \Phi_r \right) \tag{3.21}$$

If the adaptive parameter estimator works properly, the coupling forces are cancelled (i.e. $\hat{\Phi}_r - \Phi_r \to 0$), and Equation 3.21 reduces to PPF only. Comparing Equation 3.21 to the standard PPF formulation, Equations 2.19 and 2.20, it is obvious that

$$K_{ppf} = \begin{bmatrix} 0 & \mu m_2 \omega_{n2}^2 \\ \omega_f^2 & 0 \end{bmatrix} \qquad \text{with} \qquad \omega_{n2}^2 = \frac{(k_{02} + k_{12} + k_{23})}{m_2} \tag{3.22}$$

It may appear that K_{ppf} depends on coupling strength between carts. However, unlike Wang and Tang's technique, exact knowledge of k_{12} and k_{23} is not required. The natural frequency of cart 2 when the adjacent carts are fixed, ω_{n2}, can be found experimentally.

3.2.3 *Adaptive Parameter Estimation.*   As in the purely adaptive case, the parameter estimates, $\hat{\Phi}_r$, are found from the adaptation law

$$\dot{\hat{\Phi}}_r = -\Gamma_r \Upsilon^T P X_c \tag{3.23}$$

where as before

$$\Gamma_r = \begin{bmatrix} \gamma_1 & & & 0 \\ & \gamma_2 & & \\ & & \gamma_3 & \\ 0 & & & \gamma_4 \end{bmatrix} > 0 \tag{3.24}$$

Now, however,

$$X_c = \left\{ \begin{array}{c} q_c \\ \dot{q}_c \end{array} \right\} = \begin{bmatrix} x_2 & \eta_2 & \dot{x}_2 & \dot{\eta}_2 \end{bmatrix}^T \tag{3.25}$$

and using Equations 3.8 and 3.17

$$\Upsilon^T = \begin{bmatrix} 0 & (M_c^{-1}Y_r)^T \end{bmatrix} = \left(\frac{1}{m_2}\right) \begin{bmatrix} 0 & 0 & x_1 & 0 \\ 0 & 0 & x_3 & 0 \\ 0 & 0 & \dot{x}_1 & 0 \\ 0 & 0 & \dot{x}_3 & 0 \end{bmatrix} \tag{3.26}$$

P is still found from the Lyapunov equation, Equation 2.51, but the definition of A_c is changed for PPF. Substituting $D_f = 0$ and $K_{ppf} = -K_f$ into Equation 2.52 gives

$$A_c = \begin{bmatrix} [0]_{2\times2} & [I]_{2\times2} \\ -M_c^{-1}(K_c - K_{ppf}) & -M_c^{-1}D_c \end{bmatrix} \tag{3.27}$$

As before, Q is assumed diagonal, and chosen so that $X_c^T Q X_c$ results in an energy term. Thus,

$$\begin{bmatrix} x_2 & \eta_2 & \dot{x}_2 & \dot{\eta}_2 \end{bmatrix} \begin{bmatrix} Q_{11} & 0 & 0 & 0 \\ 0 & Q_{22} & 0 & 0 \\ 0 & 0 & Q_{33} & 0 \\ 0 & 0 & 0 & Q_{44} \end{bmatrix} \left\{ \begin{array}{c} x_2 \\ \eta_2 \\ \dot{x}_2 \\ \dot{\eta}_2 \end{array} \right\} = Q_{11}x_2^2 + Q_{22}\eta_2^2 + Q_{33}\dot{x}_2^2 + Q_{44}\dot{\eta}_2^2$$

$$\tag{3.28}$$

The first term in the above expression is the spring potential energy for cart 2, and the third term is the kinetic energy. The second and fourth terms are the pseudo spring potential and kinetic energy associated with the PPF actuator. After normalizing, Q is

$$Q = \begin{bmatrix} 1 & 0 & 0 & 0 \\ 0 & \dfrac{\omega_f^2}{m_2 \omega_{n2}^2} & 0 & 0 \\ 0 & 0 & \dfrac{1}{\omega_{n2}^2} & 0 \\ 0 & 0 & 0 & \dfrac{1}{m_2 \omega_{n2}^2} \end{bmatrix} = Q^T > 0 \tag{3.29}$$

where ω_{n2}^2 is defined in Equation 3.22.

With the Q defined above, and A_c from Equation 3.27, the Lyapunov equation is solved for P, which in generic terms is

$$P = \begin{bmatrix} p_{11} & p_{21} & p_{31} & p_{41} \\ p_{21} & p_{22} & p_{32} & p_{42} \\ p_{31} & p_{32} & p_{33} & p_{43} \\ p_{41} & p_{42} & p_{43} & p_{44} \end{bmatrix} \tag{3.30}$$

Therefore, substituting Equations 3.24 through 3.26 and Equation 3.30 into Equation 3.23, and performing some matrix algebra, the adaptive parameter estimate law for the 4 DOF system becomes

$$\dot{\hat{\Phi}}_r = -\left(\frac{1}{m_2}\right) \begin{bmatrix} \gamma_1 & & & 0 \\ & \gamma_2 & & \\ & & \gamma_3 & \\ 0 & & & \gamma_4 \end{bmatrix} \begin{Bmatrix} x_1 \\ x_3 \\ \dot{x}_1 \\ \dot{x}_3 \end{Bmatrix} \begin{bmatrix} p_{31} & p_{32} & p_{33} & p_{34} \end{bmatrix} \begin{Bmatrix} x_2 \\ \eta_2 \\ \dot{x}_2 \\ \dot{\eta}_2 \end{Bmatrix} = -\begin{Bmatrix} \dot{\hat{k}}_{12} \\ \dot{\hat{k}}_{23} \\ \dot{\hat{d}}_{12} \\ \dot{\hat{d}}_{23} \end{Bmatrix} \tag{3.31}$$

3.2.4 Stability.

Ertur proved the stability of the controlled states and boundedness of the uncontrolled coordinates given four assumptions, see Section 2.3.1. These guarantees also hold for the new Adaptive/PPF control method presented here, under the following five assumptions:

(A1) $M_c = M_c^T > 0$

(A2) f_u is bounded

(A3) The roots, λ, of $|\lambda^2 M_u + \lambda D_u + K_u| = 0$, have negative real parts

(A4') K_{ppf} is selected so that the roots, λ, of $|\lambda^2 M_c + \lambda D_c + (K_c - K_{ppf})| = 0$, have negative real parts

(A5') $0 < \mu < 1$

The first three conditions are identical to Ertur's. The fourth is obtained from his A4 by setting $D_f = 0$ and $K_{ppf} = -K_f$. The fifth condition is a statement of the stability requirement for PPF, see Section 2.2. Assumptions A3 and A4' are equivalent to saying that A_c, Equation 3.27, and A_u, Equation 2.53, are negative definite.

3.3 Simulation

To model the 4 DOF system in SIMULINK^{TM} the EOMs are put into state-space form, so Equations 3.5 and 3.6 become

$$\left\{ \begin{array}{c} \dot{x} \\ \ddot{x} \end{array} \right\} = \left[\begin{array}{cc} [0]_{4\times4} & [I]_{4\times4} \\ -M^{-1}K & -M^{-1}D \end{array} \right] \left\{ \begin{array}{c} x \\ \dot{x} \end{array} \right\} + \left[\begin{array}{c} [0]_{4\times4} \\ -M^{-1} \end{array} \right] \underline{f} \qquad (3.32)$$

$$\left\{ \begin{array}{c} \dot{\eta}_2 \\ \ddot{\eta}_2 \end{array} \right\} = \left[\begin{array}{cc} 0 & 1 \\ -\omega_f^2 & -2\zeta_f\omega_f \end{array} \right] \left\{ \begin{array}{c} \eta_2 \\ \dot{\eta}_2 \end{array} \right\} + \left\{ \begin{array}{c} 0 \\ 1 \end{array} \right\} h_2 \qquad (3.33)$$

In this simulation, the tuned cyclic system is used. This means that all of the carts have identical: mass, $m_i = 1$ Kg; stiffness, $k_{0i} = 100$ N/m; and coupling, $k_{ij} = k_c = 5$ N/m, where $i, j = 1...4$. Using these values, the mass and stiffness matrices, M and K respectively, are found from Equations 2.55 and 2.57. Also, assuming a structural damping ratio of $\zeta_n = 0.01$, the damping matrix, D, is calculated from Equation 2.77.

Similar to a PVA, the desired response is achieved by properly tuning the PPF actuator. The tuning parameters are the actuator frequency (ω_f), the damping ratio (ζ_f),

and the feedback gain (μ). These are set using the values determined in Sections 2.2.4.1 through 2.2.4.3: $\mu = 0.4$, $\zeta_f = 0.4$, and $\omega_f = \omega_n$.

The stability of the system is guaranteed if assumptions A1 through A5′, on p. 3-9, are satisfied. For M_c as defined in Equation 3.8, A1 is met. Since the disturbance is sinusoidal, and therefore bounded, A2 is also met. A3 and A4′ are satisfied if A_c, Equation 3.27, and A_u, Equation 2.53, are negative definite; these are checked numerically by the simulation. Lastly, since $\mu = 0.4$, A5′ is fulfilled.

3.3.1 Sinusoidal Disturbance.

Two separate disturbances are used in this simulation. First, an external disturbance of $f_d = 10 \sin(\omega_d t)$, is applied to cart 3 only. The disturbance frequency was set equal to the lowest natural frequency of the system, $\omega_d = \omega_n$.

3.3.2 Cyclic Disturbance.

The second disturbance simulates the periodic forcing a compressor disk experiences as it rotates behind fixed stator blades in a turbine engine. A generic harmonic excitation that differs only in phase from blade to blade, is modelled as

$$f_d = Ae^{j\omega_d t} \begin{Bmatrix} 1 \\ e^{j\phi_1} \\ \vdots \\ e^{j\phi_{N-1}} \end{Bmatrix} \qquad \phi_i = \frac{2\pi E_o(i-1)}{N} \qquad i = 1,\ldots,N \qquad (3.34)$$

where A is the amplitude, ω_d is the frequency, ϕ_i is the inter-blade phase angle, and E_o is the engine order of the disturbance.

For the 4 DOF system, assuming the same amplitude and frequency as the sinusoidal disturbance ($A = 10$, $\omega_d = \omega_n$), and $E_o = 1$, Equation 3.34 reduces to

$$f_{di} = 10 \cos(\omega_d t + \phi_i) \qquad \phi_i = \frac{\pi(i-1)}{2} \qquad i = 1,\ldots,4 \qquad (3.35)$$

3.4 Results

The SIMULINK^{TM} model of the 4 DOF system with Adaptive/PPF control only on cart 2 is shown in Figures A.4 and A.5, on p. A-12. The MATLAB^{TM} code used to run the cyclic system simulation is given in Appendix A.3.1, beginning on p. A-13. The MATLAB^{TM} code used to find the system RMS responses is given in Appendix A.3.2, beginning on p. A-15.

3.4.1 For a Sinusoidal Disturbance.
The first model studied was the 4 DOF cyclic system experiencing a sinusoidal disturbance applied to cart 3 only. Keep in mind that when Adaptive/PPF control is active, it is only employed on cart 2. When not controlled, this system is identical the one used in Section 2.3.4.2; a plot of the uncontrolled response is shown in Figure 2.19, on p. 2-32. All cart displacements have a maximum amplitude of roughly 1 to 1.5 meters.

As with the purely adaptive technique, Γ_r was initially set equal to the identity matrix. It was increased by a factor of 10 until achieving satisfactory responses and near convergence for the parameter estimates. The individual gains, $(\gamma_1, \ldots, \gamma_4)$, were then adjusted to improve convergence. Finally, a value of $\Gamma_r = 10^1 \times diag(100, 20, 0.01, 1)$ was selected. This is an order of magnitude lower than in the purely adaptive simulations.

As you can see in Figure 3.2, the response of cart 2 is completely suppressed almost immediately. The response of carts 1 and cart 4 are also substantially reduced. The control forces are shown in Figure 3.3. The adaptive control is sinusoidal in nature; it starts out low and ramps up to a steady-state amplitude roughly the same as the disturbance. The adaptive control reaches steady state when the all parameter estimates converge to their exact values, see Figure 3.4.

It is obvious from Figure 3.3, that the adaptive control has to work continuously to eliminate the coupling effects. The PPF control, on the other hand, works at the beginning and then ramps off quickly. The adaptive control isolates cart 2 from the disturbance so that once the PPF control suppresses the response, it has no more work to do.
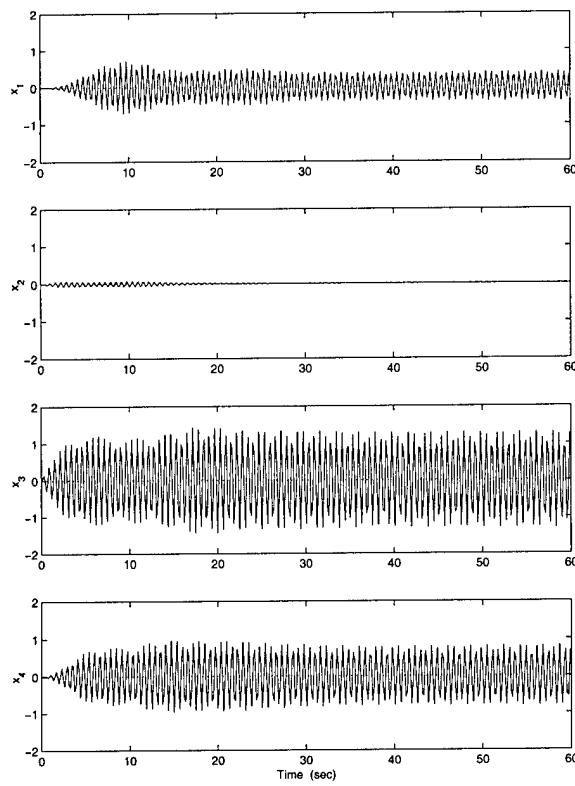
Figure 3.2   Displacements (m) for Cyclic System: Adaptation / PPF Both On, Sinusoidal Disturbance, $\Gamma_r = 10^1 \times diag(100, 20, 0.01, 1)$
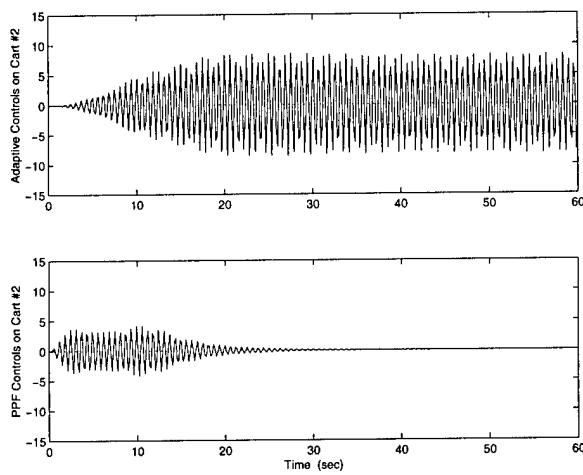
Figure 3.3   Control Forces (N) for Cyclic System: Adaptation / PPF Both On, Sinusoidal Disturbance, $\Gamma_r = 10^1 \times diag(100, 20, 0.01, 1)$
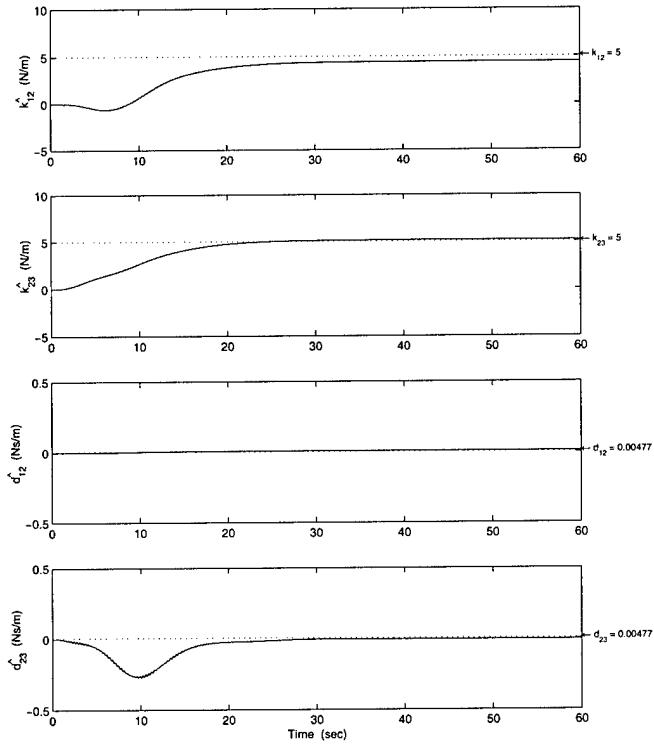
Figure 3.4   Parameter Estimates for Cyclic System: Adaptation / PPF Both On, Sinusoidal Disturbance, $\Gamma_r = 10^1 \times diag(100, 20, 0.01, 1)$

3-13
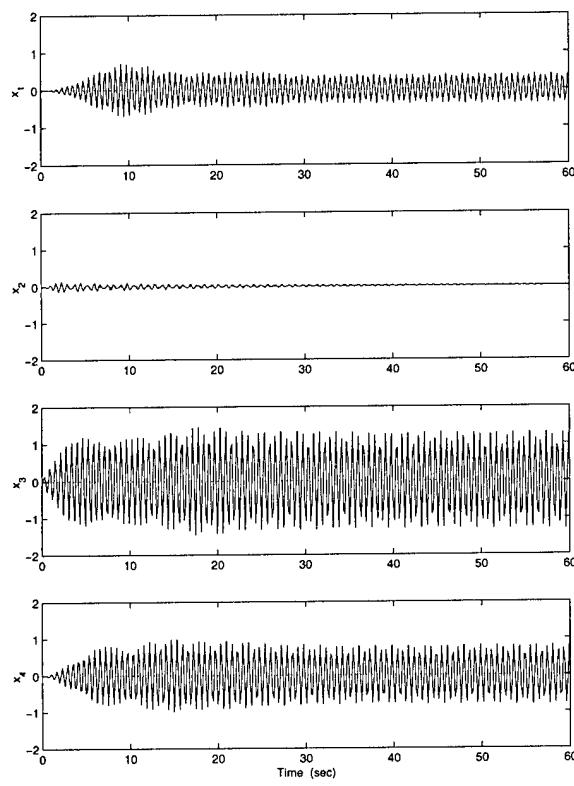
Figure 3.5   Displacements (m) for Cyclic System: Adaptation on / PPF off, Sinusoidal Disturbance, $\Gamma_r = 10^1 \times diag(100, 20, 0.01, 1)$
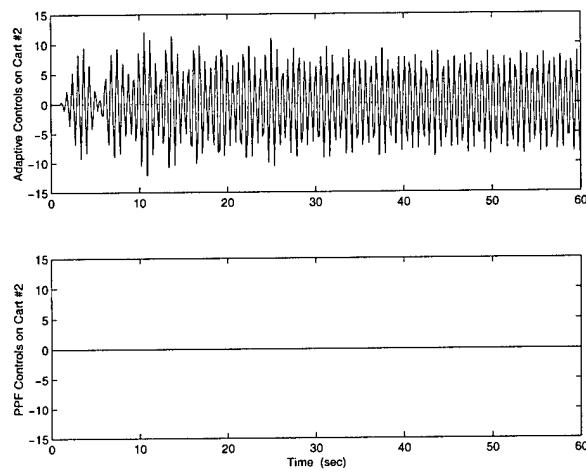
Figure 3.6   Control Forces (N) for Cyclic System: Adaptation on / PPF off, Sinusoidal
Disturbance, $\Gamma_r = 10^1 \times diag(100, 20, 0.01, 1)$
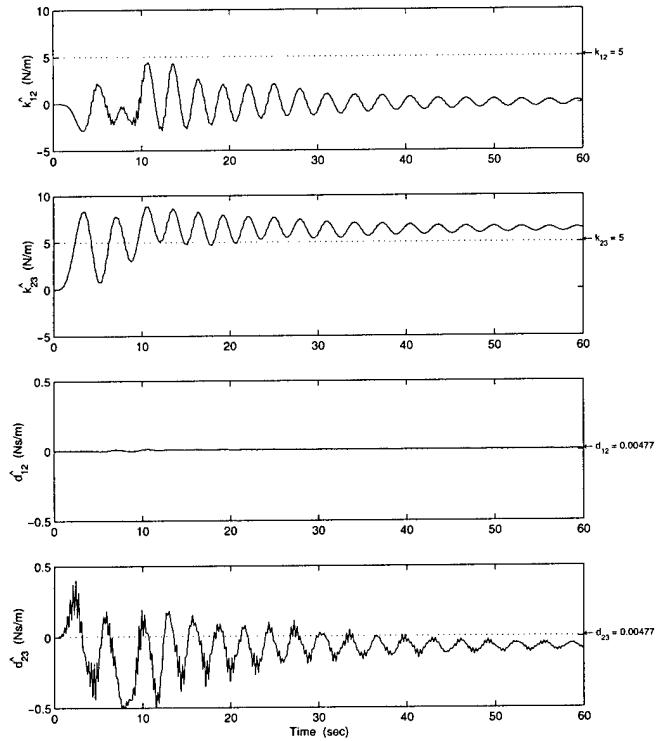
Figure 3.7   Parameter Estimates for Cyclic System: Adaptation on / PPF off, Sinusoidal
Disturbance, $\Gamma_r = 10^1 \times diag(100, 20, 0.01, 1)$
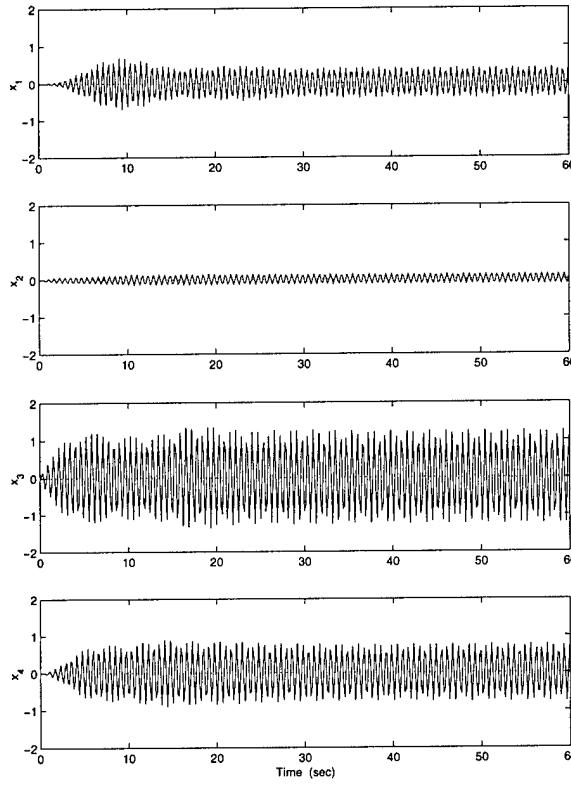
Figure 3.8   Displacements (m) for Cyclic System: Adaptation off / PPF on, Sinusoidal
Disturbance, $\Gamma_r = 10^1 \times diag(100, 20, 0.01, 1)$

Next, the simulation was rerun with PPF control turned off. This was done by setting the output of the PPF control force to zero; K_{ppf} was still used in calculations for the parameter estimator. The displacement, control forces, and parameter estimates are shown in Figures 3.5 through 3.7. As you can plainly see, the steady-state displacements are nearly identical to when both adaptive and PPF control are used, Figure 3.2, although cart 2 does takes slightly longer to converge. The parameter estimates also take longer to converge, and do not achieve their exact values.

Finally, PPF control was turned on, and adaptive control turned off. As before, this was done by setting the force output of the adaptive estimator to zero. As shown in Figure 3.8, the displacements of carts 1, 3, and 4 are once again identical to the fully
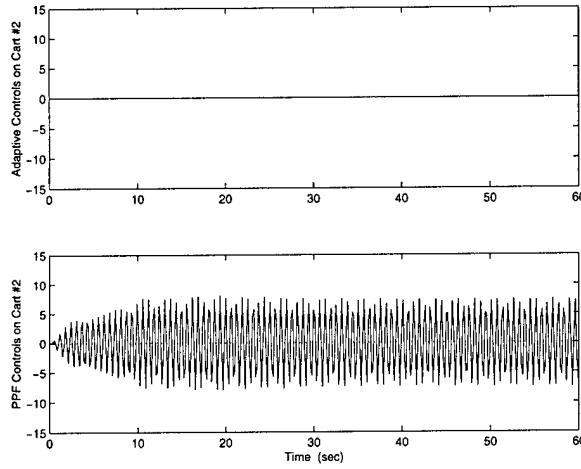
Figure 3.9   Control Forces (N) for Cyclic System: Adaptation off / PPF on, $\Gamma_r = 10^1 \times diag(100, 20, 0.01, 1)$

controlled and adaptive only cases. The response of cart 2 is substantially reduced, but since it is no longer isolated from the coupling effects by adaptive control, there is a steady-state amplitude. It is also observed from Figure 3.9, that unlike the fully controlled case, the PPF force now has to operate continuously to suppress the response.

There are three control configurations: Adaptive/PPF, Adaptive-Only, and PPF-Only. The effectiveness of these three options are compared using the RMS of the response for cart 2. The RMS of x_2 is calculated from Equation 2.43, over the frequency range $0 < \omega_d < 20$ rad/sec. The results are shown in Figure 3.10. Note that the responses are normalized by the maximum RMS for the uncontrolled system. As you can see, all three options substantially reduce the response at resonance. However, the Adaptive/PPF and Adaptive only control perform the best.

3.4.2   For a Cyclic Disturbance.

The 4 DOF cyclic system was next subjected to the cyclic disturbance described in Section 3.3.2. Adaptive/PPF control is still employed only on cart 2. The uncontrolled response of the system is shown in Figure 3.11. All cart displacements achieve a steady-state amplitude of roughly 1 meter.

Using the same process as described for the sinusoidal disturbance, a value of $\Gamma_r = 10^1 \times diag(1, 100, 1, 1)$ was selected. The displacements for the system are shown in Fig-
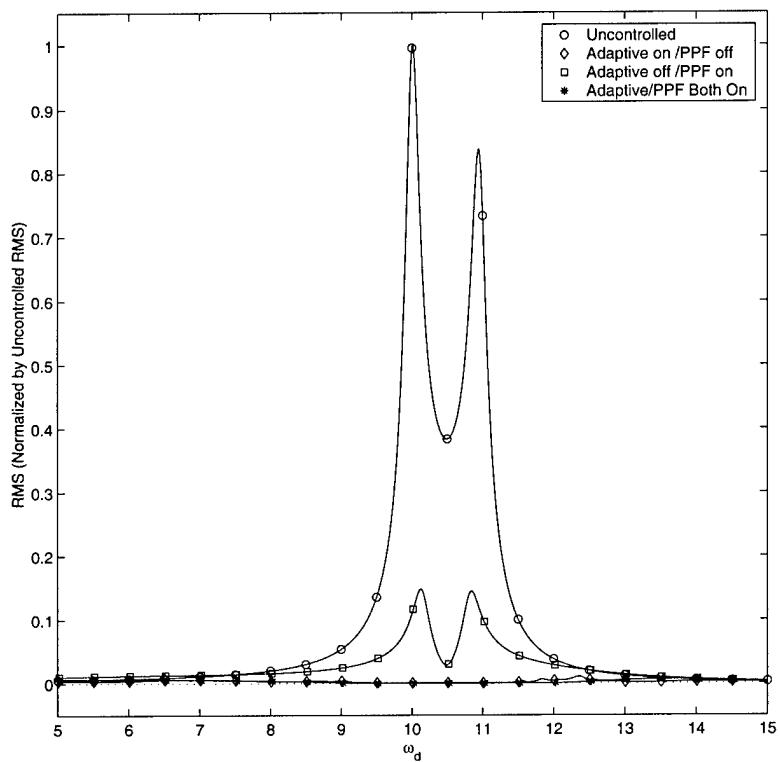
Figure 3.10   RMS of Cart 2 Displacement for Sinusoidal Disturbance
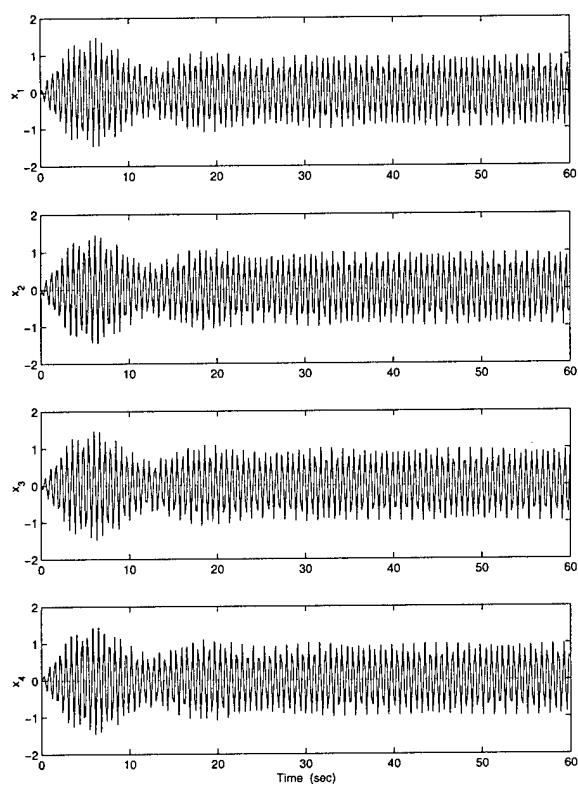
Figure 3.11   Displacements (m) for Cyclic System: Uncontrolled, Cyclic Disturbance
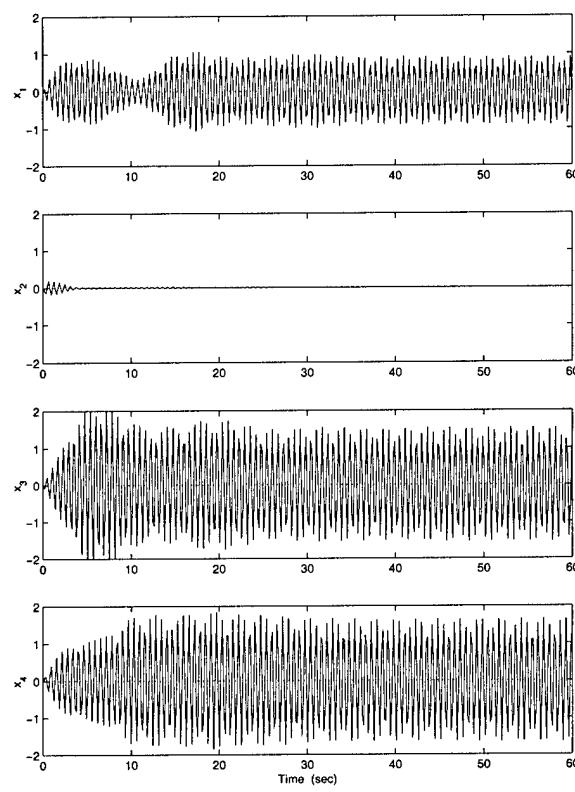
Figure 3.12   Displacements (m) for Cyclic System: Adaptation / PPF Both On, Cyclic Disturbance, $\Gamma_r = 10^1 \times diag(1, 100, 1, 1)$
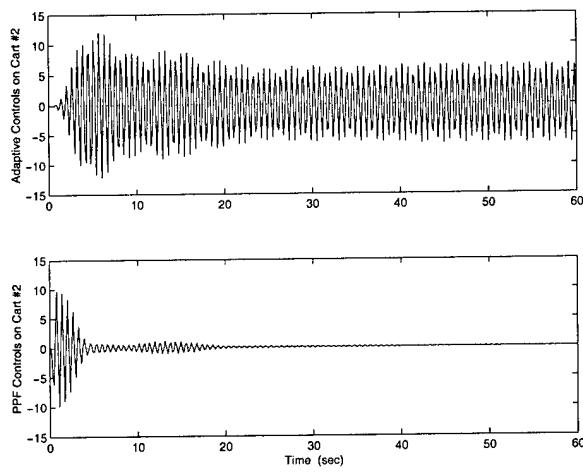
Figure 3.13   Control Forces (N) for Cyclic System: Adaptation / PPF Both On, Cyclic
Disturbance, $\Gamma_r = 10^1 \times diag(1, 100, 1, 1)$
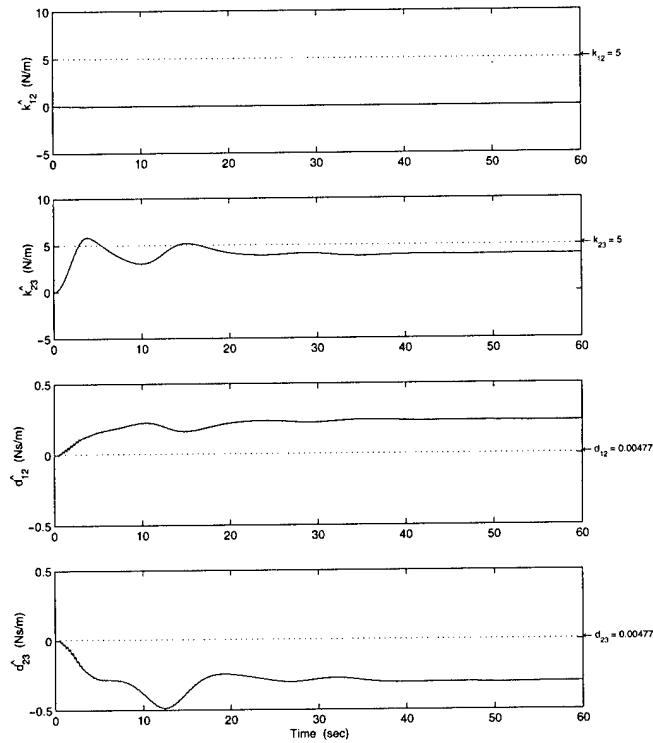
Figure 3.14   Parameter Estimates for Cyclic System: Adaptation / PPF Both On, Cyclic
Disturbance, $\Gamma_r = 10^1 \times diag(1, 100, 1, 1)$

ure 3.12. As with the sinusoidal disturbance, the response of cart 2 is almost immediately suppressed. It is interesting that while the response of cart 1 remains largely unchanged from the uncontrolled case, the responses of carts 3 and 4 actually increase. Once again, the control forces plot, Figure 3.13, shows that adaptive control works continuously to cancel the coupling effects. The PPF control, however, works only in the early stages. With cart 2 isolated by adaptive control, PPF is only necessary until the response is suppressed.

The parameter estimates are shown in Figure 3.14. It is immediately obvious, that while all parameters converge quickly, they do not converge to the correct values. The offset in $\hat{k}_{23}$ is negligible, but the estimator determined that $\hat{k}_{12}$ is identically zero. The estimates for d_{12} and d_{23} are also incorrect, but of greater concern is that $\hat{d}_{23}$ converges to a negative value.

The simulation was run again with PPF control turned off. The displacements, control forces, and parameter estimates are shown in Figures 3.15 through 3.17. The response of cart 2 is still completely suppressed, although it does take longer to converge than in the fully controlled case. Again, the response of cart 1 remains largely unchanged from the uncontrolled case, while the responses of carts 3 and 4 increase. The adaptive control force is substantially higher in the beginning, but eventually reaches the same steady-state amplitude as the fully controlled case. The parameter estimates take much longer to converge, and still do not achieve the correct values.

Finally, PPF control was turned on, and adaptive control turned off. The displacements are shown in Figure 3.18. The response of cart 2 is substantially reduced, but since it is no longer isolated from the coupling effects by adaptive control, there is a steady-state amplitude. Once again, the response of cart 1 remains largely unchanged from the uncontrolled case, while the responses of carts 3 and 4 increase. It is also observed from Figure 3.19, that unlike the fully controlled case, the PPF force now has to operate continuously to suppress the response. The steady-state amplitude of the PPF-Only control force is approximately the same as for the adaptive only case, Figure 3.16.

As before, the effectiveness of the three control configurations are compared using the RMS of the response for cart 2. As you can see in Figure 3.20, all three options
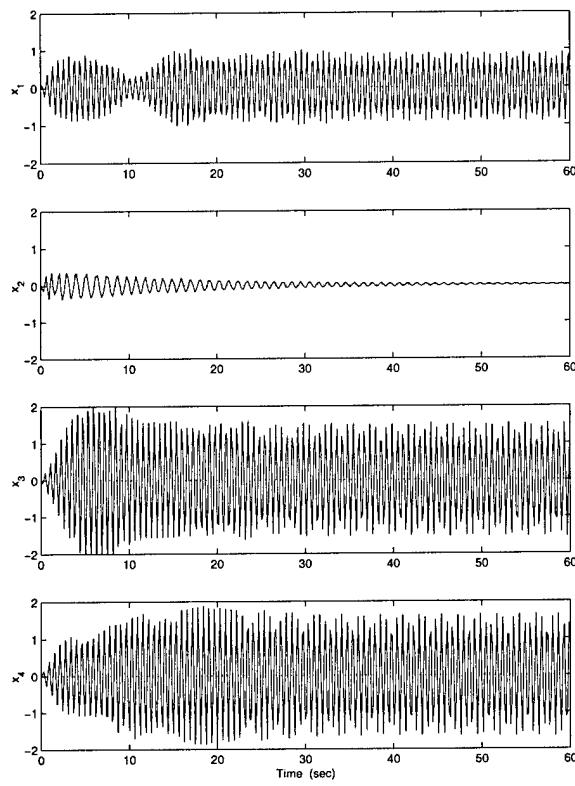
Figure 3.15   Displacements (m) for Cyclic System: Adaptation on / PPF off, Cyclic Disturbance, $\Gamma_r = 10^1 \times diag(1, 100, 1, 1)$
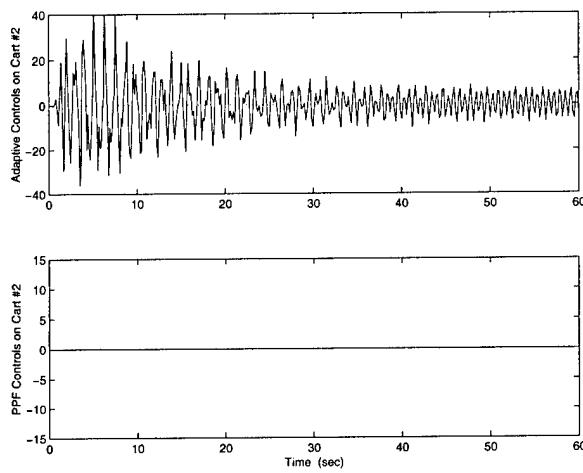
Figure 3.16   Control Forces (N) for Cyclic System: Adaptation on / PPF off, Cyclic Disturbance, $\Gamma_r = 10^1 \times diag(1, 100, 1, 1)$
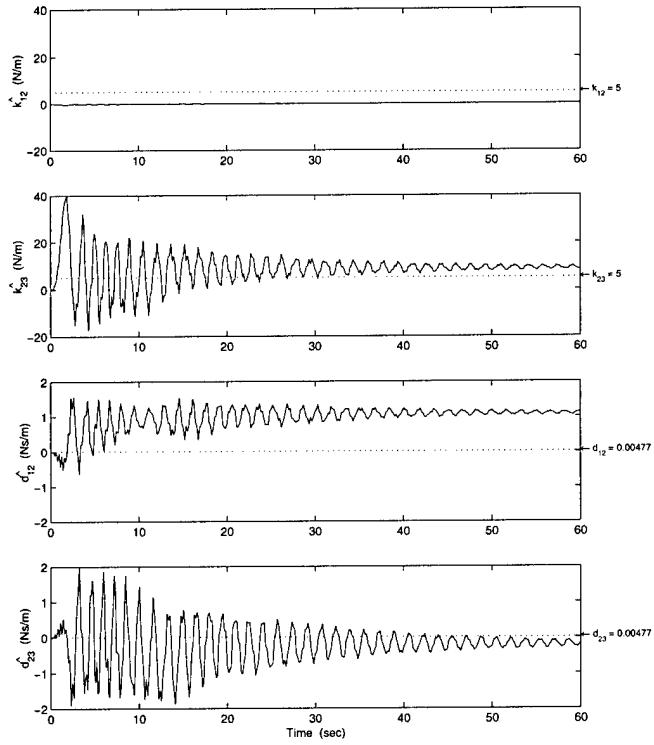
Figure 3.17   Parameter Estimates for Cyclic System: Adaptation on / PPF off, Cyclic Disturbance, $\Gamma_r = 10^1 \times diag(1, 100, 1, 1)$
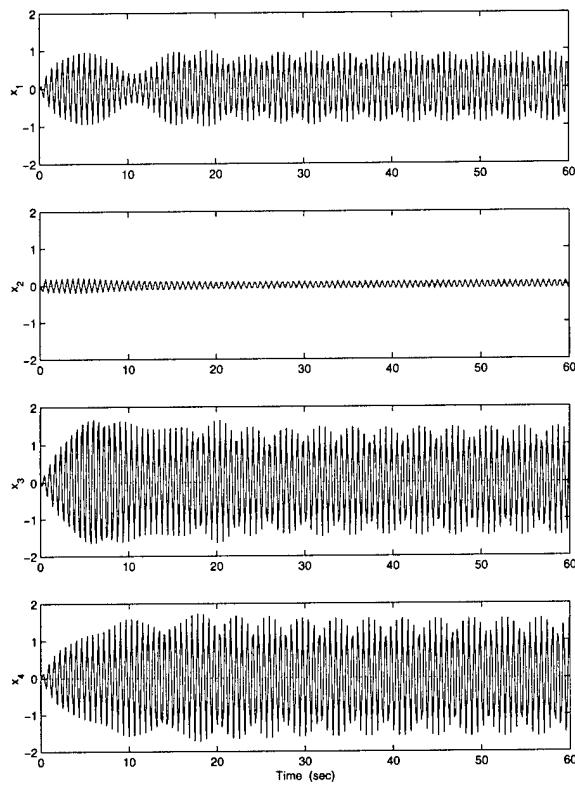
Figure 3.18   Displacements (m) for Cyclic System: Adaptation off / PPF on, Cyclic
Disturbance, $\Gamma_r = 10^1 \times diag(1, 100, 1, 1)$
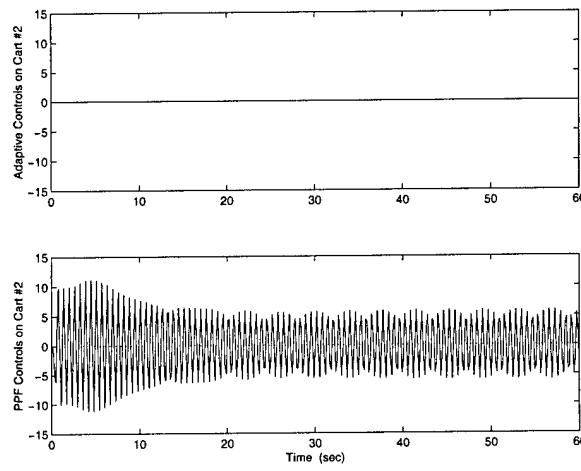
Figure 3.19   Control Forces (N) for Cyclic System: Adaptation off / PPF on, Cyclic Disturbance, $\Gamma_r = 10^1 \times diag(1, 100, 1, 1)$
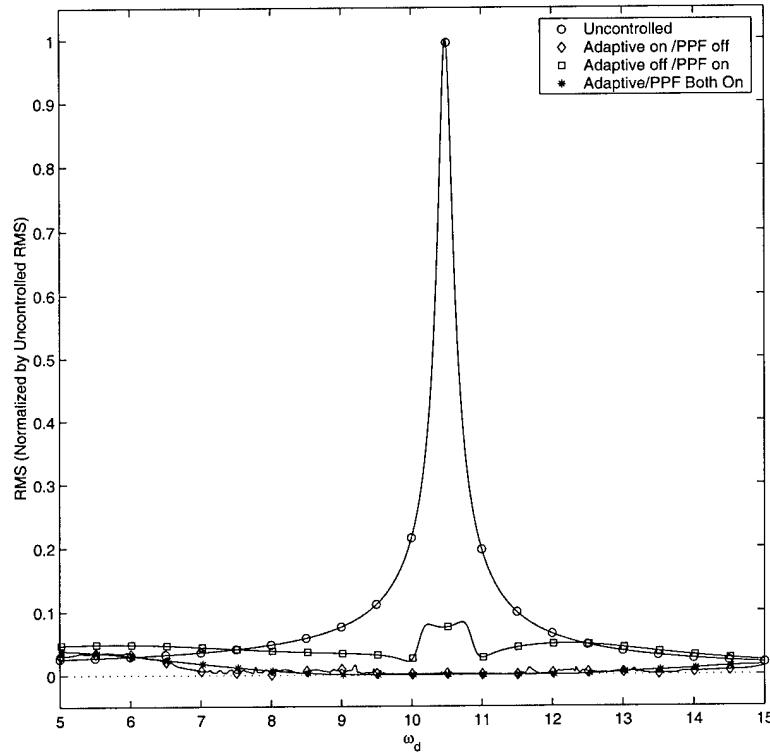

Figure 3.20   RMS of Cart 2 Displacement for Cyclic Disturbance

substantially reduce the response at resonance. However, once again, the Adaptive/PPF and Adaptive-Only control perform the best.

3.4.3 Summary.

The new Adaptive/PPF control law completely suppressed the response of cart 2 for both disturbances. For the sinusoidal disturbance on cart 3 only, the responses of carts 1 and 4 were substantially reduced. For the cyclic disturbance, on the other hand, the response of cart 1 remained largely unchanged, while carts 3 and 4 actually increased. Turning off PPF control only significantly effected the response of cart 2, causing it to take longer to converge. When PPF was turned on, and adaptive control turned off, cart 2 was no longer isolated from the coupling, and its response had a steady-state amplitude. The other responses remained largely unaffected. Comparing the RMS of displacement for cart 2, all three control configurations substantially reduced the response. However, the Adaptive/PPF and Adaptive-Only control performed the best.

The parameter estimator for the Adaptive/PPF control worked flawlessly for the sinusoidal disturbance. Unfortunately, there were problems when the cyclic disturbance was used. The estimates failed to converge to the correct values, and one of the damping estimates even converged to a negative number. There are two possible causes for these problems. First, recall that in the development of the adaptive estimator, there is no guarantee that the parameter estimates will converge. In fact, there is no guarantee that there is a unique solution to the estimation law. In this case, the estimator may have a found a solution where the estimates do not converge to the actual values, but still produce a control force that results in good performance. The second possible cause is that there is a disturbance applied to cart 2. Even though all of the stability requirements were met, Ertur's adaptive control technique was not developed with a disturbance applied directly to the controlled coordinate.

Finally, as with the purely adaptive system in Chapter 2, the gains $(\gamma_1, \ldots, \gamma_4)$ allow for some adjustments in the convergence of the parameter estimates if you are in the neighborhood of a feasible solution. However, there are some combinations of the gains which will cause the estimates to converge to significantly incorrect values. Once

again, it is important to note that even if this happens, the response of the system may be substantially reduced.

3.5   Synopsis

In this chapter, Ertur's adaptive control technique and PPF were combined into a single control methodology for a one DOF of a multi-DOF system. The adaptive parameter estimator eliminated the coupling forces, and then the vibrations were suppressed by PPF. This technique was used to control a single cart of the 4 cart system. The simulated system was subjected to both a sinusoidal disturbance on a single cart, and a harmonic disturbance that cycles through all of the carts. Response plots were presented and discussed.

In the following chapter, the Adaptive/PPF control technique is expanded to control all 4 DOFs of the system. In addition, the system is mistuned, so that the coupling springs are no longer identical. Finally, an eight bladed model is also studied.

IV. Combined Adaptive/PPF Control for Multiple Degrees of Freedom

4.1 Development for 4 DOF System

4.1.1 Equations of Motion.
In Chapter 3 it was demonstrated that Adaptive/PPF control significantly reduces the response of a single substructure in an RPS. In this chapter, the control theory is expanded to include all of the substructures in the RPS. The 4 DOF cyclic system studied in Chapters 2 and 3 is used again here, see Figure 3.1 on p. 3-3. Recall that the carts have mass m_i, and their structural stiffness and damping are represented by k_{0i} and d_{0i}. The inter-blade coupling forces are expressed in terms of k_{ij} and d_{ij}, where $i, j = 1...4$. The external control and disturbance forces on each cart are represented by f_i. As before, the EOMs are

$$
M \left\{ \begin{array}{c} \ddot{x}_1 \\ \ddot{x}_2 \\ \ddot{x}_3 \\ \ddot{x}_4 \end{array} \right\} + D \left\{ \begin{array}{c} \dot{x}_1 \\ \dot{x}_2 \\ \dot{x}_3 \\ \dot{x}_4 \end{array} \right\} + K \left\{ \begin{array}{c} x_1 \\ x_2 \\ x_3 \\ x_4 \end{array} \right\} = \left\{ \begin{array}{c} f_1 \\ f_2 \\ f_3 \\ f_4 \end{array} \right\} \tag{4.1}
$$

where the mass, damping, and stiffness matrices (M, D, and K respectively) are defined in Equations 2.55 through 2.57. Using identical PPF actuators on each cart, with a damping ratio of ζ_f and a frequency of ω_f, results in the following additional equations

$$
\left\{ \begin{array}{c} \ddot{\eta}_1 \\ \ddot{\eta}_2 \\ \ddot{\eta}_3 \\ \ddot{\eta}_4 \end{array} \right\} + 2\zeta_f \omega_f \left\{ \begin{array}{c} \dot{\eta}_1 \\ \dot{\eta}_2 \\ \dot{\eta}_3 \\ \dot{\eta}_4 \end{array} \right\} + \omega_f^2 \left\{ \begin{array}{c} \eta_1 \\ \eta_2 \\ \eta_3 \\ \eta_4 \end{array} \right\} = \left\{ \begin{array}{c} h_1 \\ h_2 \\ h_3 \\ h_4 \end{array} \right\} \tag{4.2}
$$

Before, vibrations were only suppressed in a single cart. The objective now is to regulate all of them. The Adaptive/PPF control theory is applied to each cart individually, with the controlled coordinates equal to the displacement and actuator states for that

cart. The procedure is essentially the same as in Section 3.2.1. Beginning with cart 1, this means that $q_{c1} = \begin{bmatrix} x_1 & \eta_1 \end{bmatrix}^T$ and $q_{u1} = \begin{bmatrix} x_2 & \eta_2 & x_3 & \eta_3 & x_4 & \eta_4 \end{bmatrix}^T$. Thus, combining Equations 4.1 and 4.2, and rearranging into the controlled/uncontrolled partitioned form yields

$$
\begin{bmatrix}
m_1 & 0 & & & & & & & 0 \\
0 & 1 & & & & & & & \\
\hline
 & & m_2 & & & & & & \\
 & & & 1 & & & & & \\
 & & & & m_3 & & & & \\
 & & & & & 1 & & & \\
 & & & & & & m_4 & & \\
0 & & & & & & & & 1
\end{bmatrix}
\begin{Bmatrix}
\ddot{x}_1 \\
\ddot{\eta}_1 \\
\ddot{x}_2 \\
\ddot{\eta}_2 \\
\ddot{x}_3 \\
\ddot{\eta}_3 \\
\ddot{x}_4 \\
\ddot{\eta}_4
\end{Bmatrix}
+
$$ (4.3)

$$
\begin{bmatrix}
d_{01}+d_{41}+d_{12} & 0 & -d_{12} & 0 & 0 & 0 & -d_{41} & 0 \\
0 & 2\zeta_f\omega_f & 0 & 0 & 0 & 0 & 0 & 0 \\
\hline
-d_{12} & 0 & & & & & & \\
0 & 0 & & & & & & \\
0 & 0 & & & D_{u1} & & & \\
0 & 0 & & & & & & \\
-d_{41} & 0 & & & & & & \\
0 & 0 & & & & & &
\end{bmatrix}
\begin{Bmatrix}
\dot{x}_1 \\
\dot{\eta}_1 \\
\dot{x}_2 \\
\dot{\eta}_2 \\
\dot{x}_3 \\
\dot{\eta}_3 \\
\dot{x}_4 \\
\dot{\eta}_4
\end{Bmatrix}
+
$$

$$
\begin{bmatrix}
k_{01}+k_{41}+k_{12} & 0 & -k_{12} & 0 & 0 & 0 & -k_{41} & 0 \\
0 & 2\zeta_f\omega_f & 0 & 0 & 0 & 0 & 0 & 0 \\
\hline
-k_{12} & 0 & & & & & & \\
0 & 0 & & & & & & \\
0 & 0 & & & K_{u1} & & & \\
0 & 0 & & & & & & \\
-k_{41} & 0 & & & & & & \\
0 & 0 & & & & & &
\end{bmatrix}
\begin{Bmatrix}
x_1 \\
\eta_1 \\
x_2 \\
\eta_2 \\
x_3 \\
\eta_3 \\
x_4 \\
\eta_4
\end{Bmatrix}
=
\begin{Bmatrix}
f_1 \\
h_1 \\
f_2 \\
h_2 \\
f_3 \\
h_3 \\
f_4 \\
h_4
\end{Bmatrix}
$$

Comparing the above to the standard form,

$$\begin{bmatrix} M_{c1} & 0 \\ 0 & M_{u1} \end{bmatrix} \begin{Bmatrix} \ddot{q}_{c1} \\ \ddot{q}_{u1} \end{Bmatrix} + \begin{bmatrix} D_{c1} & D_{cu1} \\ D_{uc1} & D_{u1} \end{bmatrix} \begin{Bmatrix} \dot{q}_{c1} \\ \dot{q}_{u1} \end{Bmatrix} + \begin{bmatrix} K_{c1} & K_{cu1} \\ K_{uc1} & K_{u1} \end{bmatrix} \begin{Bmatrix} q_{c1} \\ q_{u1} \end{Bmatrix} = \begin{Bmatrix} f_{c1} \\ f_{u1} \end{Bmatrix}$$

(4.4)

results in

$$M_{c1} = \begin{bmatrix} m_1 & 0 \\ 0 & 1 \end{bmatrix} \qquad (4.5) \qquad f_{c1} = \begin{Bmatrix} f_1 \\ h_1 \end{Bmatrix} \qquad (4.8)$$

$$D_{c1} = \begin{bmatrix} d_{01} + d_{41} + d_{12} & 0 \\ 0 & 2\zeta_f \omega_f \end{bmatrix} \qquad (4.6) \qquad D_{cu1} = \begin{bmatrix} -d_{12} & 0 & 0 & 0 & -d_{41} & 0 \\ 0 & 0 & 0 & 0 & 0 & 0 \end{bmatrix} \qquad (4.9)$$

$$K_{c1} = \begin{bmatrix} k_{01} + k_{41} + k_{12} & 0 \\ 0 & \omega_f^2 \end{bmatrix} \qquad (4.7) \qquad K_{cu1} = \begin{bmatrix} -k_{12} & 0 & 0 & 0 & -k_{41} & 0 \\ 0 & 0 & 0 & 0 & 0 & 0 \end{bmatrix} \qquad (4.10)$$

The controlled coordinate EOMs, the top half of Equation 4.4, are

$$M_{c1}\ddot{q}_{c1} + D_{c1}\dot{q}_{c1} + K_{c1}q_{c1} = f_{c1} - K_{cu1}q_{u1} - D_{cu1}\dot{q}_{u1}$$

(4.11)

Thus, substituting Equations 4.9 and 4.10 into Equation 4.11 and performing some matrix algebra, the controlled coordinate EOMs become

$$M_{c1}\ddot{q}_{c1} + D_{c1}\dot{q}_{c1} + K_{c1}q_{c1} = f_{c1} - \begin{bmatrix} -k_{12}x_2 - k_{41}x_4 - d_{12}\dot{x}_2 - d_{41}\dot{x}_4 \\ 0 \end{bmatrix}$$

(4.12)

Recall that for adaptive control, the controlled coordinate EOMs are rewritten as

$$M_c\ddot{q}_c + D_c\dot{q}_c + K_cq_c = f_c - Y_r\Phi_r$$

(4.13)

Therefore, comparing Equations 4.12 and 4.13, for cart 1 the regression matrix, Y_{r1}, and unknown parameter vector, Φ_{r1}, are

$$Y_{r1} = \begin{bmatrix} x_2 & x_4 & \dot{x}_2 & \dot{x}_4 \\ 0 & 0 & 0 & 0 \end{bmatrix} \quad (4.14) \qquad \Phi_{r1} = -\begin{bmatrix} k_{12} & k_{41} & d_{12} & d_{41} \end{bmatrix}^T \quad (4.15)$$

In general, the controlled coordinate EOMs for each cart of the 4 DOF cyclic system are given as

$$M_{ci}\ddot{q}_{ci} + D_{ci}\dot{q}_{ci} + K_{ci}q_{ci} = f_{ci} - Y_{ri}\Phi_{ri} \qquad\qquad i = 1, \ldots, 4 \qquad (4.16)$$

where

$$q_{ci} = \left\{ \begin{array}{c} x_i \\ \eta_i \end{array} \right\} \quad (4.17) \qquad f_{ci} = \left\{ \begin{array}{c} f_i \\ h_i \end{array} \right\} \quad (4.18) \qquad M_{ci} = \begin{bmatrix} m_i & 0 \\ 0 & 1 \end{bmatrix} \quad (4.19)$$

$$D_{ci} = \begin{bmatrix} d_{0i} + d_{(i-1),i} + d_{i,(i+1)} & 0 \\ 0 & 2\zeta_f\omega_f \end{bmatrix} \quad (4.20) \qquad K_{ci} = \begin{bmatrix} k_{0i} + k_{(i-1),i} + k_{i,(i+1)} & 0 \\ 0 & \omega_f^2 \end{bmatrix} \quad (4.21)$$

Note that for the 4 DOF cyclic system, cart 1 connects to cart 4. So for $i = 1$, $i - 1 \equiv 4$, and for $i = 4$, $i + 1 \equiv 1$.

Therefore, applying the same procedure as before, the regression matrices and unknown parameter vectors for carts 2, 3, and 4 are

$$Y_{r2} = \begin{bmatrix} x_1 & x_3 & \dot{x}_1 & \dot{x}_3 \\ 0 & 0 & 0 & 0 \end{bmatrix} \quad (4.22) \qquad \Phi_{r2} = -\begin{bmatrix} k_{12} & k_{23} & d_{12} & d_{23} \end{bmatrix}^T \quad (4.23)$$

$$Y_{r3} = \begin{bmatrix} x_2 & x_4 & \dot{x}_2 & \dot{x}_4 \\ 0 & 0 & 0 & 0 \end{bmatrix} \quad (4.24) \qquad \Phi_{r3} = -\begin{bmatrix} k_{23} & k_{34} & d_{23} & d_{34} \end{bmatrix}^T \quad (4.25)$$

$$Y_{r4} = \begin{bmatrix} x_1 & x_3 & \dot{x}_1 & \dot{x}_3 \\ 0 & 0 & 0 & 0 \end{bmatrix} \qquad (4.26) \qquad \Phi_{r4} = -\begin{bmatrix} k_{41} & k_{34} & d_{41} & d_{34} \end{bmatrix}^T \qquad (4.27)$$

4.1.2 Adaptive/PPF Control Law.

The control law developed for controlling a single cart in Section 3.2.2 still applies here, but now there is a control force for each cart. Note that identical PPF actuators are assumed, so the same gain, μ, is used for each one. Thus, the general form of the control law is

$$f_{ci} = Y_{ri}\hat{\Phi}_{ri} + K_{ppf_i} q_{ci} \qquad\qquad i = 1, \ldots, 4 \qquad (4.28)$$

where

$$K_{ppf_i} = \begin{bmatrix} 0 & \mu m_i \omega_{ni}^2 \\ \omega_f^2 & 0 \end{bmatrix} \qquad \text{with} \qquad \omega_{ni}^2 = \frac{k_{0i} + k_{(i-1),i} + k_{i,(i+1)}}{m_i} \qquad (4.29)$$

4.1.3 Adaptive Parameter Estimation.

As with the control law, the estimator law is identical to the one developed for a single cart in Section 3.2.3. In general,

$$\dot{\hat{\Phi}}_{ri} = -\Gamma_{ri} \Upsilon_i^T P_i X_{ci} \qquad (4.30)$$

where

$$\Gamma_{ri} = \begin{bmatrix} \gamma_1 & & & 0 \\ & \gamma_2 & & \\ & & \gamma_3 & \\ 0 & & & \gamma_4 \end{bmatrix}_i > 0, \quad X_{ci} = \left\{ \begin{array}{c} q_{ci} \\ \dot{q}_{ci} \end{array} \right\}, \quad \Upsilon_i^T = \begin{bmatrix} 0 & \left(M_{ci}^{-1} Y_{ri} \right)^T \end{bmatrix} \quad (4.31)$$

The individual P_i matrices are solutions to the Lyapunov equation, $A_{ci}^T P_i + P_i A_{ci} = -Q_i$, with $P_i = P_i^T > 0$, $Q_i = Q_i^T > 0$, and where

$$A_{ci} = \begin{bmatrix} [0]_{2\times2} & [I]_{2\times2} \\ -M_{ci}^{-1}\left(K_{ci} - K_{ppf_i}\right) & -M_{ci}^{-1} D_{ci} \end{bmatrix} \tag{4.32}$$

The Q_i matrices are defined in a similar manner to the Q developed for controlling a single cart, Equation 3.29. In general this is

$$Q_i = \begin{bmatrix} 1 & 0 & 0 & 0 \\ 0 & \frac{\omega_f^2}{m_i \omega_{ni}^2} & 0 & 0 \\ 0 & 0 & \frac{1}{\omega_{ni}^2} & 0 \\ 0 & 0 & 0 & \frac{1}{m_i \omega_{ni}^2} \end{bmatrix} = Q^T > 0 \tag{4.33}$$

where ω_{ni}^2 is defined in Equation 4.29. Thus, using the above result, along with substituting Equations 4.19 through 4.21 and 4.29 into 4.32, the Lyapunov equation is solved for P_i.

The adaptive estimate law is then found by substituting the solution for P_i, as well as Equations 4.17, 4.19, and 4.31, into Equation 4.30. After simplification, this yields

$$\dot{\Phi}_{ri} = -\left(\frac{1}{m_i}\right) \begin{bmatrix} \gamma_1 & & & 0 \\ & \gamma_2 & & \\ & & \gamma_3 & \\ 0 & & & \gamma_4 \end{bmatrix}_i Y_{ri}^T \begin{bmatrix} [p_{31} & p_{32} & p_{33} & p_{34}]_i \\ 0 & 0 & 0 & 0 \end{bmatrix} \begin{Bmatrix} x_i \\ \eta_i \\ \dot{x}_i \\ \dot{\eta}_i \end{Bmatrix}, \quad i = 1, \ldots, 4 \tag{4.34}$$

where Y_{ri} and Φ_{ri} are defined in Equations 4.14, 4.15, and 4.22 through 4.27.

4.1.4 Stability.

In Section 3.2.4, stability requirements were developed for Adaptive/PPF control. It was demonstrated that the 4 DOF system is stable when only one of the four carts is controlled. This is now extended to controlling all of them. Stability is guaranteed, as long as the following five assumptions are satisfied (for $i = 1, \ldots, 4$):

(A1) $M_{ci} = M_{ci}^T > 0$

4-6

(A2) f_{ui} is bounded

(A3) The roots, λ, of $|\lambda^2 M_{ui} + \lambda D_{ui} + K_{ui}| = 0$, have negative real parts

(A4′) The roots, λ, of $|\lambda^2 M_{ci} + \lambda D_c + (K_{ci} - K_{ppf_i})| = 0$, have negative real parts

(A5′) $0 < \mu < 1$

The mass matrix, M, is positive definite and diagonal, which means that all of the M_c submatrices are symmetric and positive definite; the first condition is therefore satisfied. The unknown forces, f_{ui}, are comprised of the external cyclic disturbance and the control forces on the other carts. Since both of these are individually bounded, f_{ui} is bounded, and the second condition is met. The PPF gain is $\mu = 0.4$, which satisfies assumption A5′.

To determine if assumptions A3 and A4′ are met, the system is looked at as a whole, see Equation 4.4. Assumption A4′ requires that the controlled portion of the system is stable. This is equivalent to saying that A_{c1}, as defined in Equation 4.32, is negative definite (< 0). However, assumption A3 also requires that the uncontrolled part of the system is stable when uncoupled from the controlled part. In other words, it requires that the following is also stable

$$M_{u1}\ddot{q}_{u1} + D_{u1}\dot{q}_{u1} + K_{u1}q_{u1} = f_{u1} \qquad (4.35)$$

But this can be rewritten as

$$\begin{bmatrix} M_{c2} & \\ & \tilde{M}_{u2} \end{bmatrix} \begin{Bmatrix} \ddot{q}_{c2} \\ \ddot{q}_{u2} \end{Bmatrix} + \begin{bmatrix} D_{c2} & \tilde{D}_{cu2} \\ \tilde{D}_{uc2} & \tilde{D}_{u2} \end{bmatrix} \begin{Bmatrix} \dot{q}_{c2} \\ \dot{q}_{u2} \end{Bmatrix} + \begin{bmatrix} K_{c2} & \tilde{K}_{cu2} \\ \tilde{K}_{uc2} & \tilde{K}_{u2} \end{bmatrix} \begin{Bmatrix} q_{c2} \\ \tilde{q}_{u2} \end{Bmatrix} = \begin{Bmatrix} f_{c2} \\ \tilde{f}_{u2} \end{Bmatrix}$$
$$(4.36)$$

Note that the tilde above matrices signifies that the coupling terms to the previous carts are removed. Reapplying assumptions A3 and A4′, this new system is stable if the controlled and uncontrolled parts are independently stable. The controlled portion is stable if $A_{c2} < 0$.

Again, the uncontrolled part is rewritten as

$$
\begin{bmatrix} M_{c3} & \\ & \tilde{M}_{u3} \end{bmatrix} \begin{Bmatrix} \ddot{q}_{c3} \\ \ddot{\tilde{q}}_{u3} \end{Bmatrix} + \begin{bmatrix} D_{c3} & \tilde{D}_{cu3} \\ \tilde{D}_{uc3} & \tilde{D}_{u3} \end{bmatrix} \begin{Bmatrix} \dot{q}_{c3} \\ \dot{\tilde{q}}_{u3} \end{Bmatrix} + \begin{bmatrix} K_{c3} & \tilde{K}_{cu3} \\ \tilde{K}_{uc3} & \tilde{K}_{u3} \end{bmatrix} \begin{Bmatrix} q_{c3} \\ \tilde{q}_{u3} \end{Bmatrix} = \begin{Bmatrix} f_{c3} \\ \tilde{f}_{u3} \end{Bmatrix}
$$

$$(4.37)$$

Once again, which system is stable if $A_{c3} < 0$, and the following system is stable

$$
M_{c4}\ddot{q}_{c4} + D_{c4}\dot{q}_{c4} + K_{c4}q_{u4} = f_{c4} \tag{4.38}
$$

Finally, this system is stable for $A_{c4} < 0$. Therefore, A3 and A4′ reduce to the requirement that $A_{ci} < 0$ for all $i = 1, \ldots, 4$. This is checked during the simulation.

4.1.5 Simulation.
The 4 cart system is now simulated with Adaptive/PPF control on all of the carts. Both tuned and mistuned systems are studied. To model the 4 DOF system in SIMULINK^{TM} the structure and actuator EOMs, Equations 4.1 and 4.2 respectively, are first put into state-space form:

$$
\begin{Bmatrix} \dot{x} \\ \ddot{x} \end{Bmatrix} = \begin{bmatrix} [0]_{4\times4} & [I]_{4\times4} \\ -M^{-1}K & -M^{-1}D \end{bmatrix} \begin{Bmatrix} x \\ \dot{x} \end{Bmatrix} + \begin{bmatrix} [0]_{4\times4} \\ -M^{-1} \end{bmatrix} \underline{f} \tag{4.39}
$$

$$
\begin{Bmatrix} \dot{\eta} \\ \ddot{\eta} \end{Bmatrix} = \begin{bmatrix} [0]_{4\times4} & [I]_{4\times4} \\ -\omega_f^2 [I]_{4\times4} & -2\zeta_f\omega_f [I]_{4\times4} \end{bmatrix} \begin{Bmatrix} \eta \\ \dot{\eta} \end{Bmatrix} + \begin{bmatrix} [0]_{4\times4} \\ [I]_{4\times4} \end{bmatrix} \underline{h} \tag{4.40}
$$

The PPF tuning parameters are set using the values determined in Sections 2.2.4.1 through 2.2.4.3: $\mu = 0.4$, $\zeta_f = 0.4$, and $\omega_f = \omega_n$.

The gain matrices for the adaptive estimators, Γ_{ri}, can be set independently for each individual cart. However, for ease of set-up and analysis, it is assumed that they are all identical. The matrix was determined experimentally in a manner similar to that used in Chapter 3. The value finally chosen was $\Gamma_r = 10^2 I$.

For these simulations, the system is only subjected to the cyclic disturbance, developed in Section 3.3.2. The disturbance frequency is still equal to the lowest natural

frequency of the system, $\omega_d = \omega_n$. This time, however, the engine order, E_o, of the disturbance is varied to study its effect. Thus, the disturbance force is given by

$$f_{di} = 10\cos\left(\omega_d t + \phi_i\right) \qquad \phi_i = \frac{\pi E_o(i-1)}{2} \qquad i = 1,\ldots,4 \qquad (4.41)$$

4.1.5.1 Tuned System. As in previous simulations, for the tuned system, all of the carts have identical: mass, $m_i = 1$ Kg; stiffness, $k_{0i} = 100$ N/m; and coupling, $k_{ij} = k_c = 5$ N/m, where $i, j = 1...4$. Using these values, the mass and stiffness matrices, M and K respectively, are found from Equations 2.55 and 2.57. Also, assuming a structural damping ratio of $\zeta_n = 0.002$, the damping matrix, D, is calculated from Equation 2.77. The damping is lower than in previous simulations, so it is easier to compare the results with those found by Duffield in his research [5].

4.1.5.2 Mistuned System. Up until now, all of the systems studied have been perfectly tuned. This means that all of the carts are identical and experience the same coupling and damping forces. Unfortunately, this is an idealization, since all real systems have material and manufacturing imperfections. The system is said to be mistuned when these defects cause mass, stiffness, and damping variances [15]. To study the effects of mistuning, the structural stiffness of each cart, k_{0i}, was varied. This also changes the damping, since it is calculated as a function of the stiffness. Castanier and Pierre showed that the maximum amplitude magnification factor of a compressor bladed-disk with various random mistuning strengths peaked at a standard deviation of $\sigma \approx 0.01$ [4]. A random mistuning pattern was created using this σ as a goal, and such that the mean was near zero: $\Delta k_{01} = -0.014017$, $\Delta k_{02} = 0.002013$, $\Delta k_{03} = 0.012155$, and $\Delta k_{04} = -0.000299$ N/m. These values result in a $\sigma = 0.011$, and a mean $= 0.00004$. The individual cart stiffness parameters are then calculated by $k_{0i} = k_0(1 + \Delta k_{0i})$, where $k_0 = 100$ N/m is the nominal stiffness. All of the carts are still assumed to have identical: mass, $m_i = 1$ Kg; and coupling, $k_{ij} = k_c = 5$ N/m, where $i, j = 1...4$. The mass, damping, and stiffness matrices (M, D, and K respectively) are then calculated as in the tuned system.

4.1.6   Results.   The SIMULINK^{TM} model of the 4 DOF cyclic system with Adaptive/PPF control on all carts is shown in Figures A.6 and A.7, beginning on p. A-17. The MATLAB^{TM} code used to run the simulation is given in Appendix A.4.1, beginning on p. A-19. The MATLAB^{TM} code used to find the system RMS responses is given in Appendix A.4.2, beginning on p. A-22.

4.1.6.1   For the Tuned System, with $E_o = 1$.   The first model studied was the tuned system subjected to a cyclic disturbance, with $E_o = 1$. A plot of the uncontrolled response is shown in Figure 4.1. All cart displacements achieve a steady-state amplitude of roughly 1 meter.

The response of the system with all carts controlled is shown in Figure 4.2. As you can see, the steady state amplitudes of the displacements are all identical and substantially reduced. The responses are not completely suppressed as they were for the single control system, Figure 3.12. It is also quite obvious that the control system looses tracking, causing brief pulses of increased amplitude at regular intervals. However, the maximum amplitude is still considerably less than the uncontrolled response of the system.

The adaptive and PPF control forces are presented in Figures 4.3 and 4.4. They too exhibit the same pulsing at the same intervals as the displacement plots. This is expected since the actuators have to work harder to bring the system back under control. The "steady-state" amplitude of the adaptive forces is approximately double that of the single control system, Figure 3.13. The initial amplitude of the PPF forces is equivalent to the initial amplitude for the single control system. However, now the PPF forces do not die out as they did before.

The stiffness and damping parameter estimates are shown in Figures 4.5 and 4.6. Recall that k and d are the actual parameters, whereas $\hat{k}$ and $\hat{d}$ are the estimates. There are two plots for each parameter, because now there are two estimators that calculate them, one on either side of the spring or damper. The estimates take nearly 30 times as long to converge as in the single control system, Figure 3.14. After they do converge, they immediately loose convergence, and then reacquire. This gives the plots a distinctive
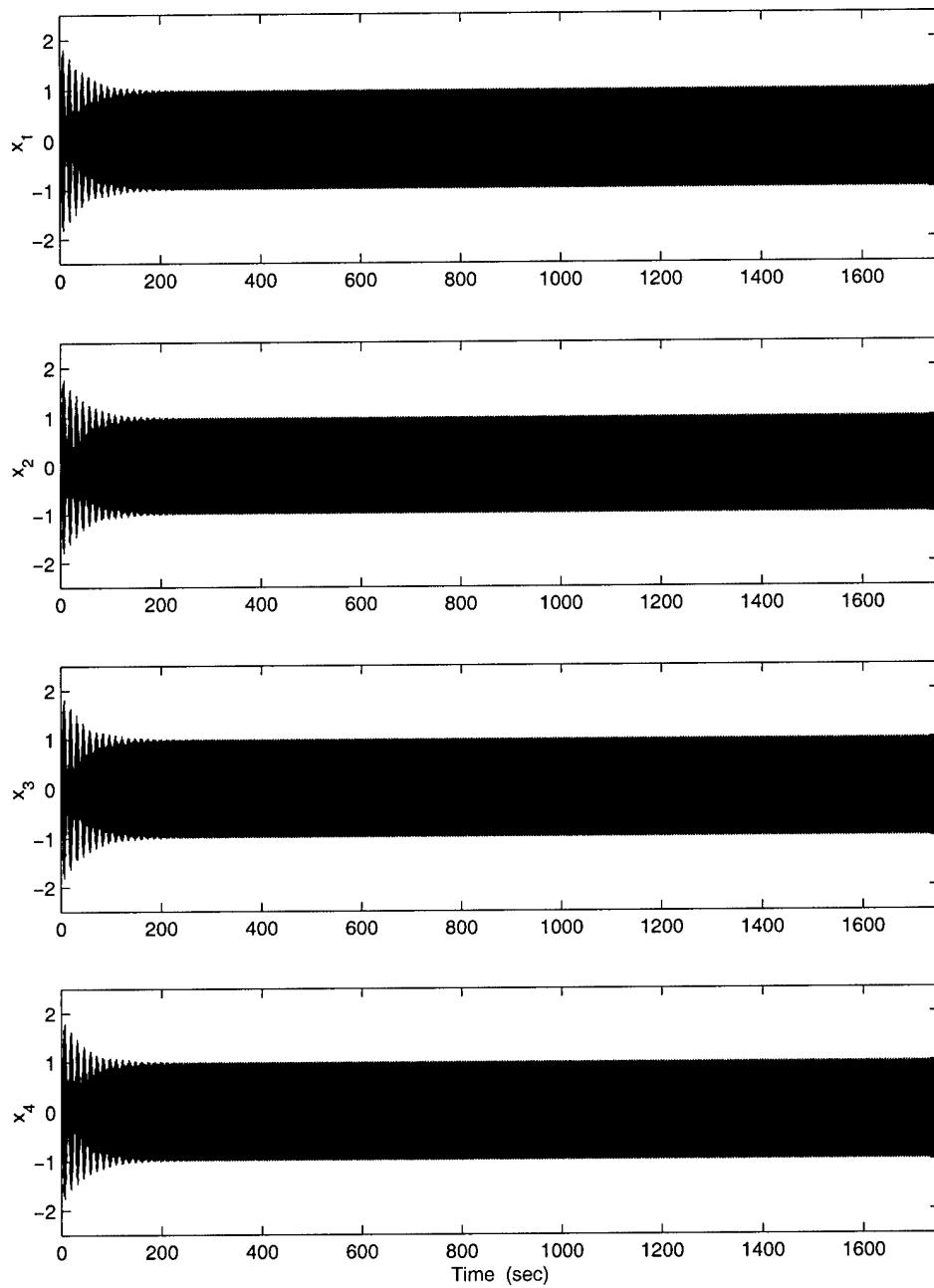
Figure 4.1   Displacements (m) for the Tuned Cyclic System: Uncontrolled, Cyclic Disturbance, $E_o = 1$, $\Gamma_r = 10^2\,\mathrm{I}$

sawtooth pattern. The point where the estimates loose convergence coincides with the pulsing exhibited in the displacement and force plots.

Of greater concern is that the two estimators for each parameter are finding equal and opposite values. It is demonstrated in later plots that this is not just a sign error. The stiffness parameters are converging to the correct value, but the estimators to the right of the spring find a negative answer. For the damping parameter the left estimator finds the negative solution. The damping estimates are also significantly off from their correct values; much greater error than in any of the single control cases.

Next, the simulation was run with PPF control turned off. As you can plainly see in Figure 4.7, the response of the even carts is completely suppressed, while it remains largely unchanged from the uncontrolled values for the odd carts. None of the response plots exhibit the pulsing that was seen in the full Adaptive/PPF case. The adaptive forces, Figure 4.8, for the even carts reach a steady-state amplitude comparable to the full control case. The controllers for the odd carts appear to work in the beginning, and then the force drops off to zero.

The parameter estimates are shown in Figures 4.9 and 4.10. It is noted that all of the parameter estimates from the odd carts diverge from the correct values, albeit very slowly for the damping. This is most likely the reason that the response of the odd carts is not effected.

Finally, the simulation was run with PPF control on, and adaptive control off. The responses of all of the carts are substantially reduced and identical, Figure 4.11. They are also on par with the response of the single cart controlled by PPF-Only, Figure 3.18. However, the amplitudes of the PPF forces, Figure 4.12, are slightly greater than for the single control case, Figure 3.19.

The three control configurations (Adaptive/PPF, Adaptive-Only, and PPF-Only) along with the uncontrolled system are compared using the maximum RMS of the cart displacements. The RMS for each cart is calculated over a frequency range of $0 < \omega_d < 20$ rad/sec. The maximum RMS for each configuration is the maximum RMS out of all the carts at every ω_d. The results are shown in Figure 4.13. Note that the responses are

4-12
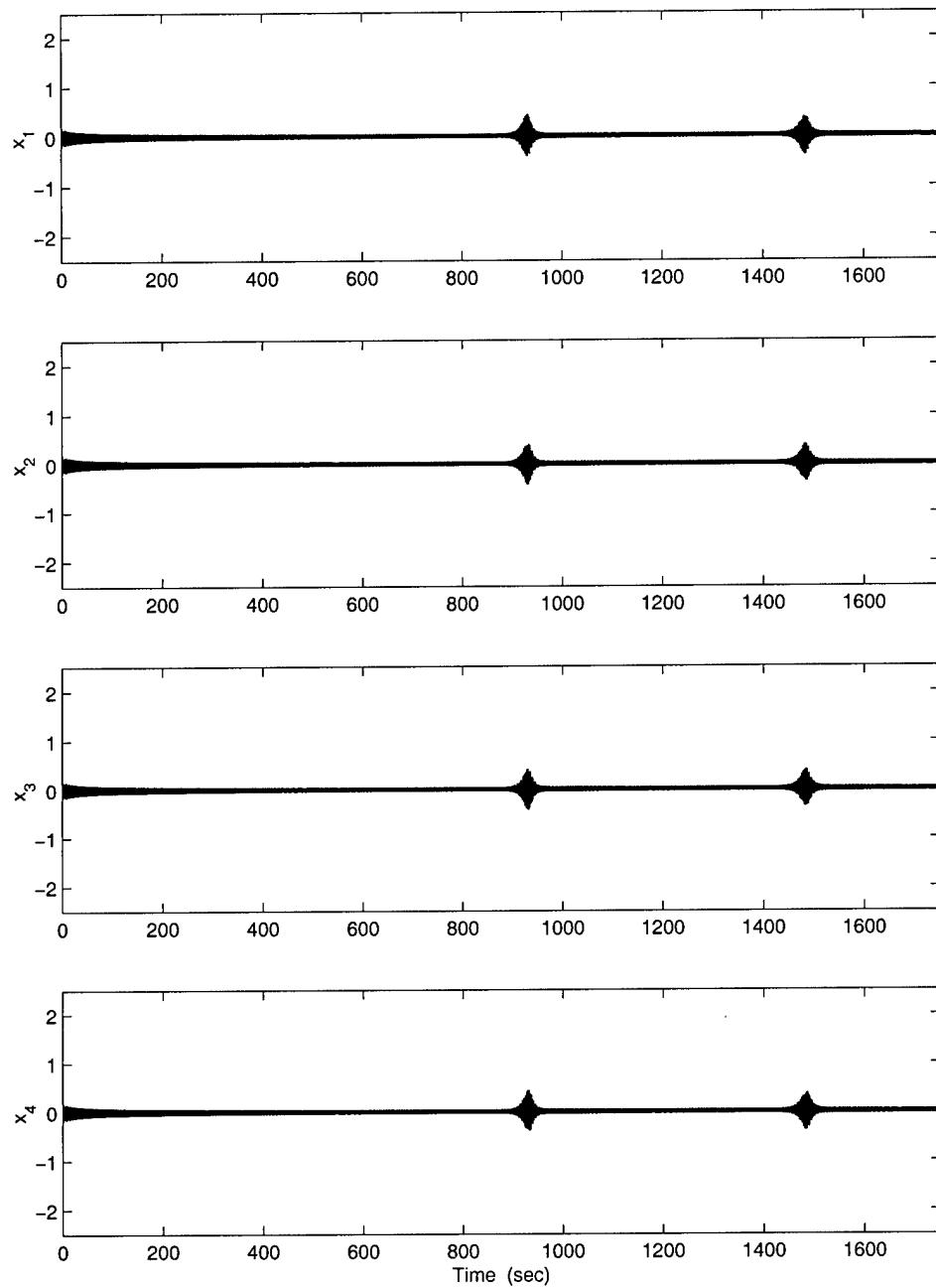
Figure 4.2   Displacements (m) for the Tuned Cyclic System: Adaptation/PPF Both on, Cyclic Disturbance, $E_o = 1$, $\Gamma_r = 10^2\,\mathrm{I}$
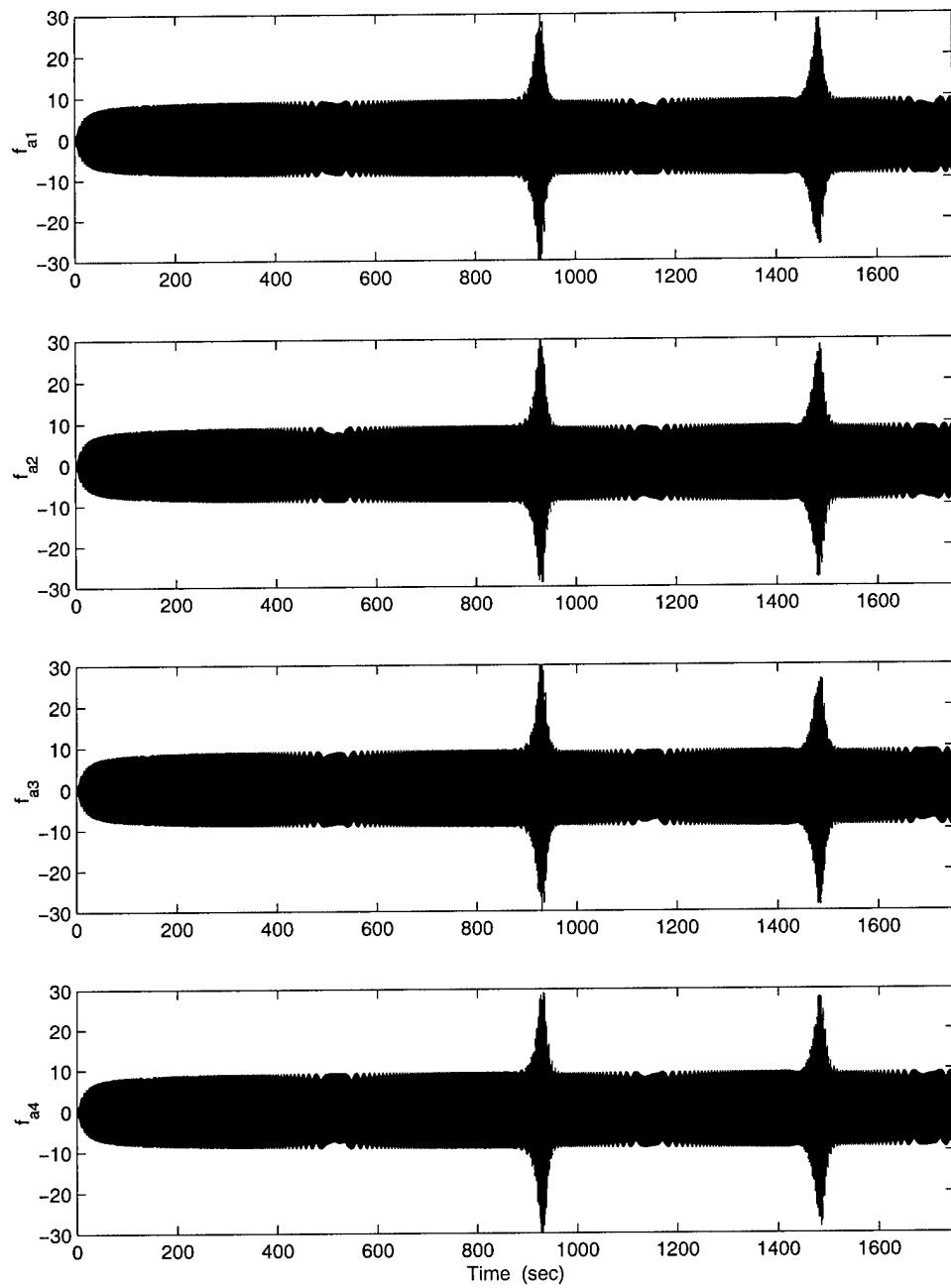
Figure 4.3   Adaptive Forces (N) for the Tuned Cyclic System: Adaptation/PPF Both on, Cyclic Disturbance, $E_o = 1$, $\Gamma_r = 10^2 \, \mathrm{I}$
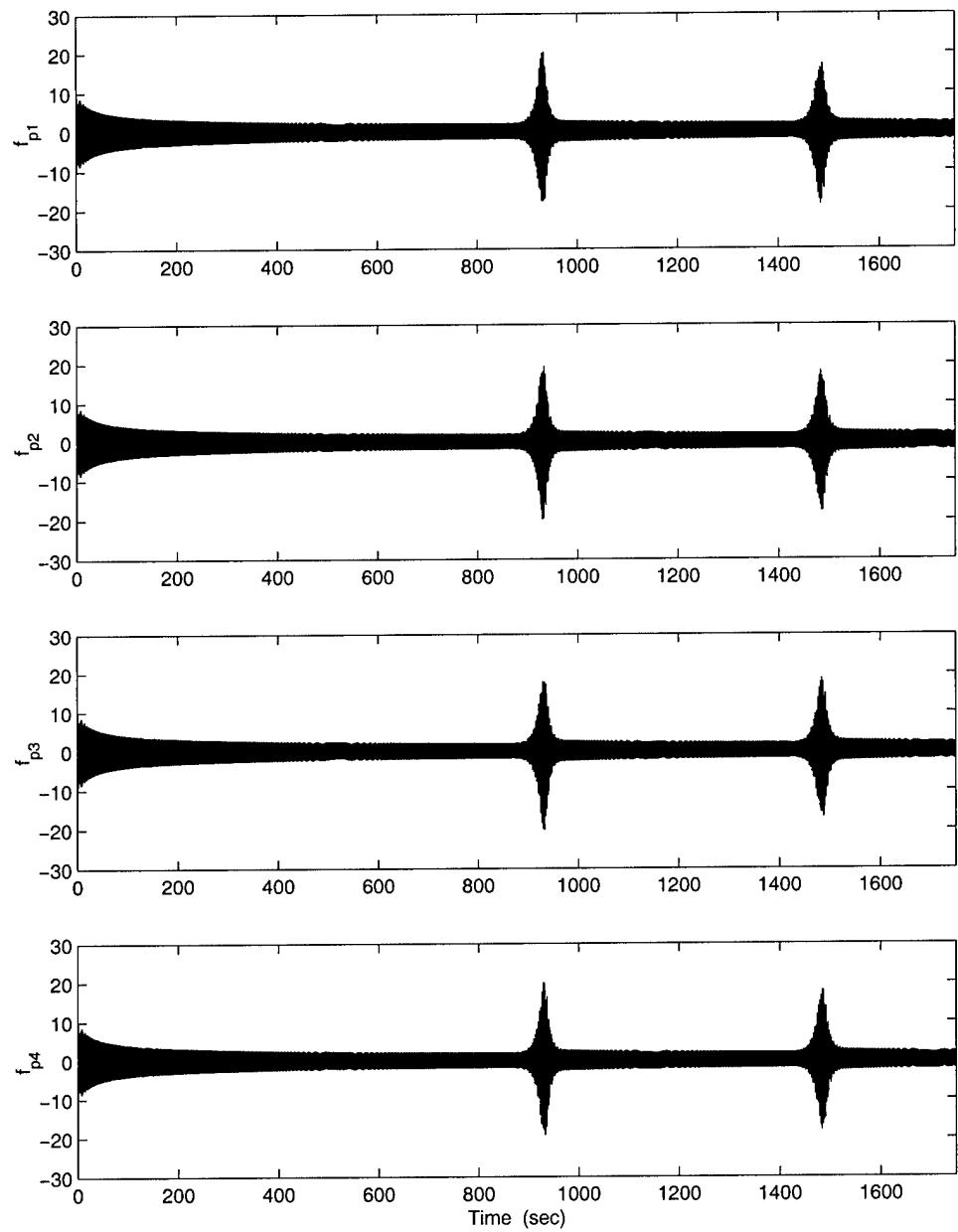
Figure 4.4   PPF Forces (N) for the Tuned Cyclic System: Adaptation/PPF Both on, Cyclic Disturbance, $E_o = 1$, $\Gamma_r = 10^2\,\mathrm{I}$
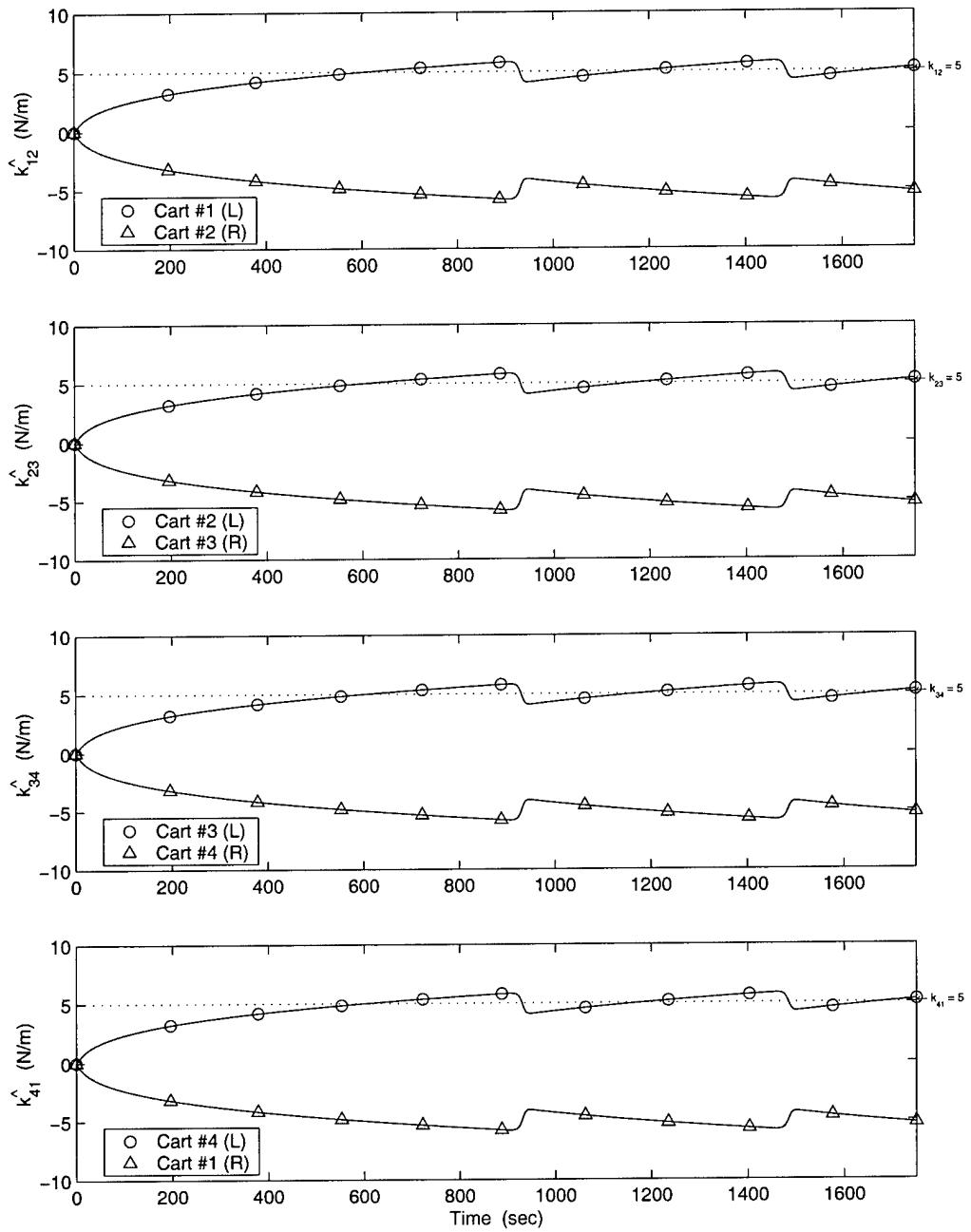
Figure 4.5   Stiffness Parameter Estimates for the Tuned Cyclic System: Adaptation/PPF Both on, Cyclic Disturbance, $E_o = 1$, $\Gamma_r = 10^2\,\mathrm{I}$
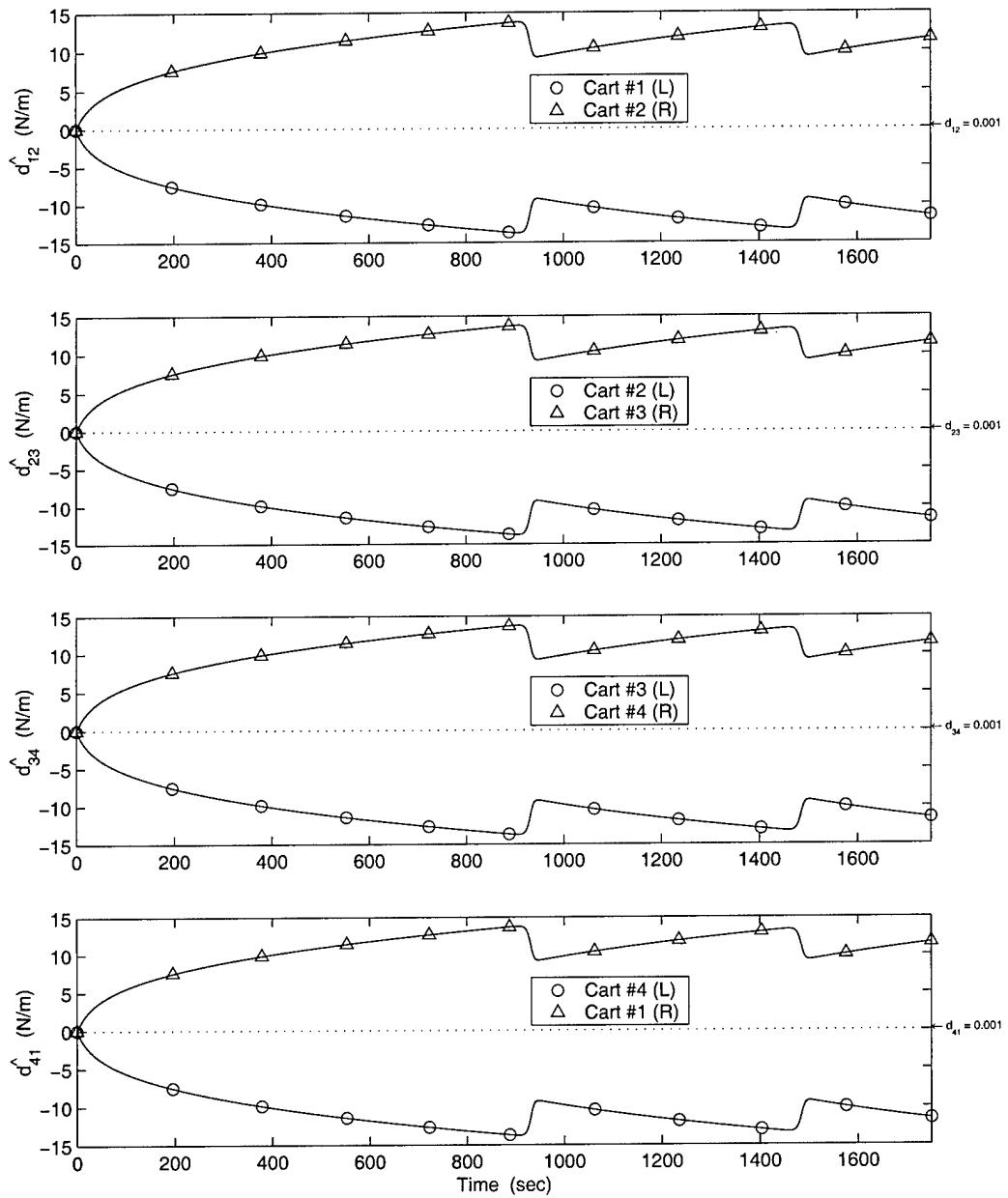
Figure 4.6   Damping Parameter Estimates for the Tuned Cyclic System: Adaptation/PPF Both on, Cyclic Disturbance, $E_o = 1$, $\Gamma_r = 10^2\,\mathrm{I}$
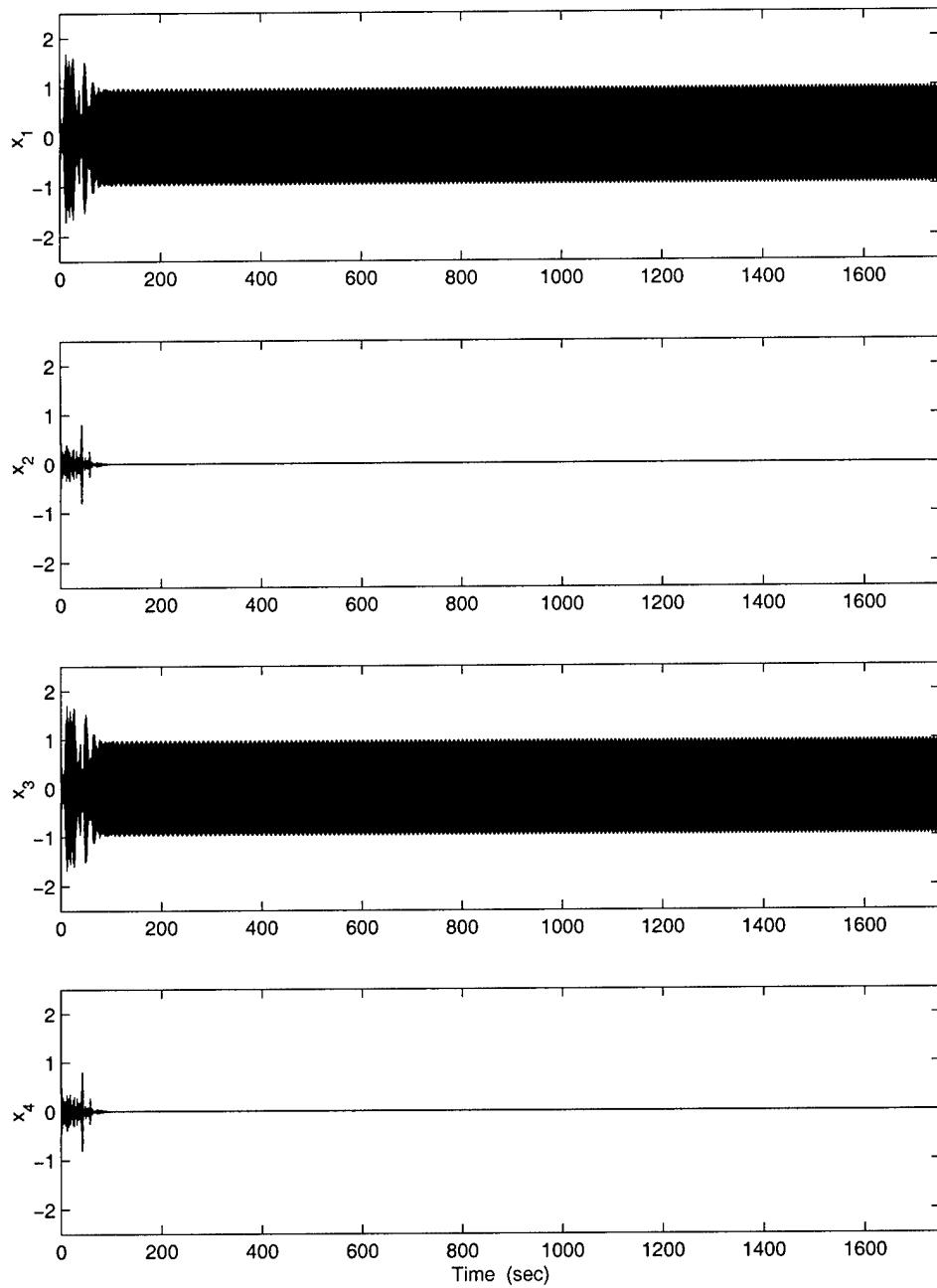
Figure 4.7   Displacements (m) for the Tuned Cyclic System: Adaptation on / PPF off, Cyclic Disturbance, $E_o = 1$, $\Gamma_r = 10^2\,\mathrm{I}$
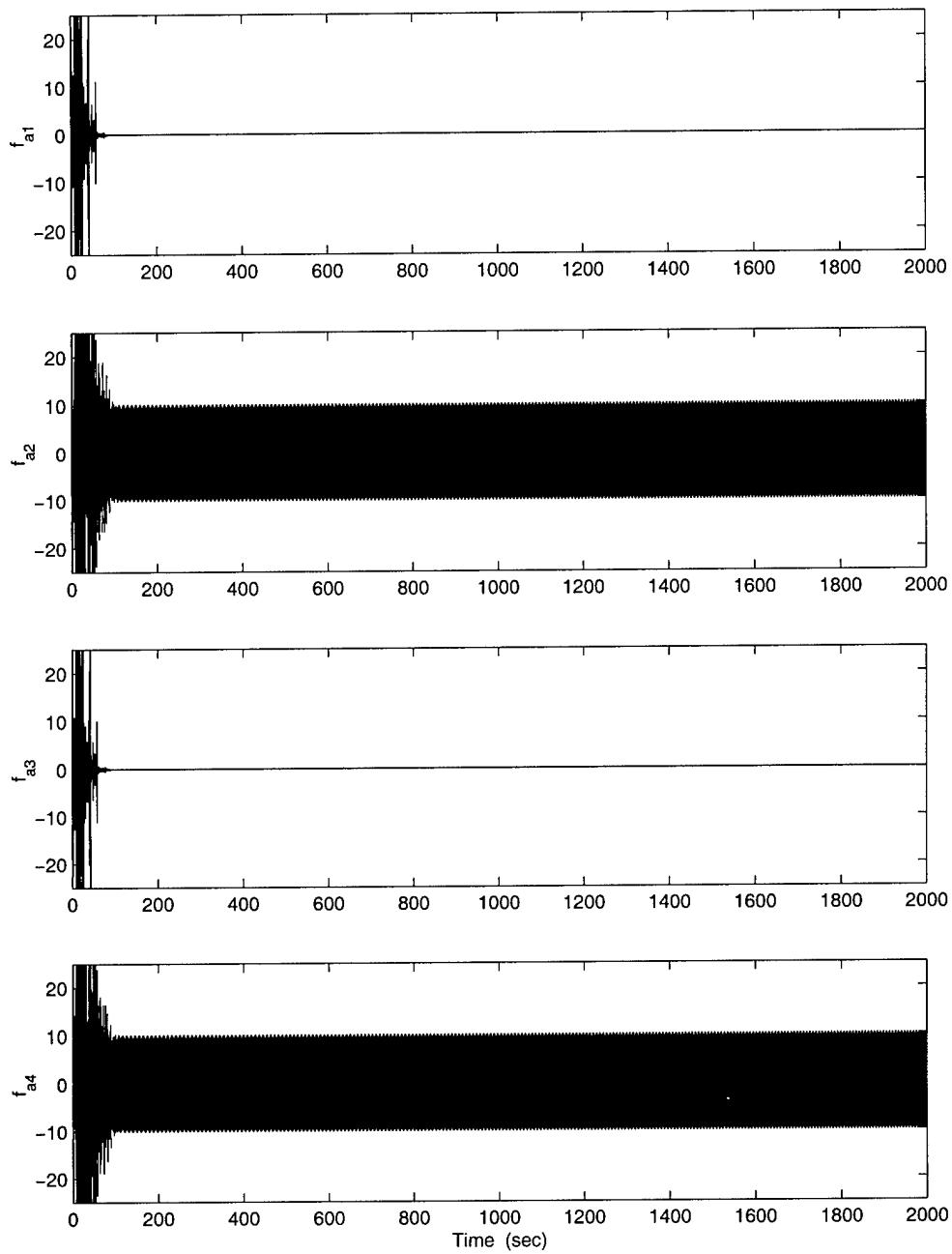
Figure 4.8   Adaptive Forces (N) for the Tuned Cyclic System: Adaptation on / PPF off, Cyclic Disturbance, $E_o = 1$, $\Gamma_r = 10^2\,\mathrm{I}$
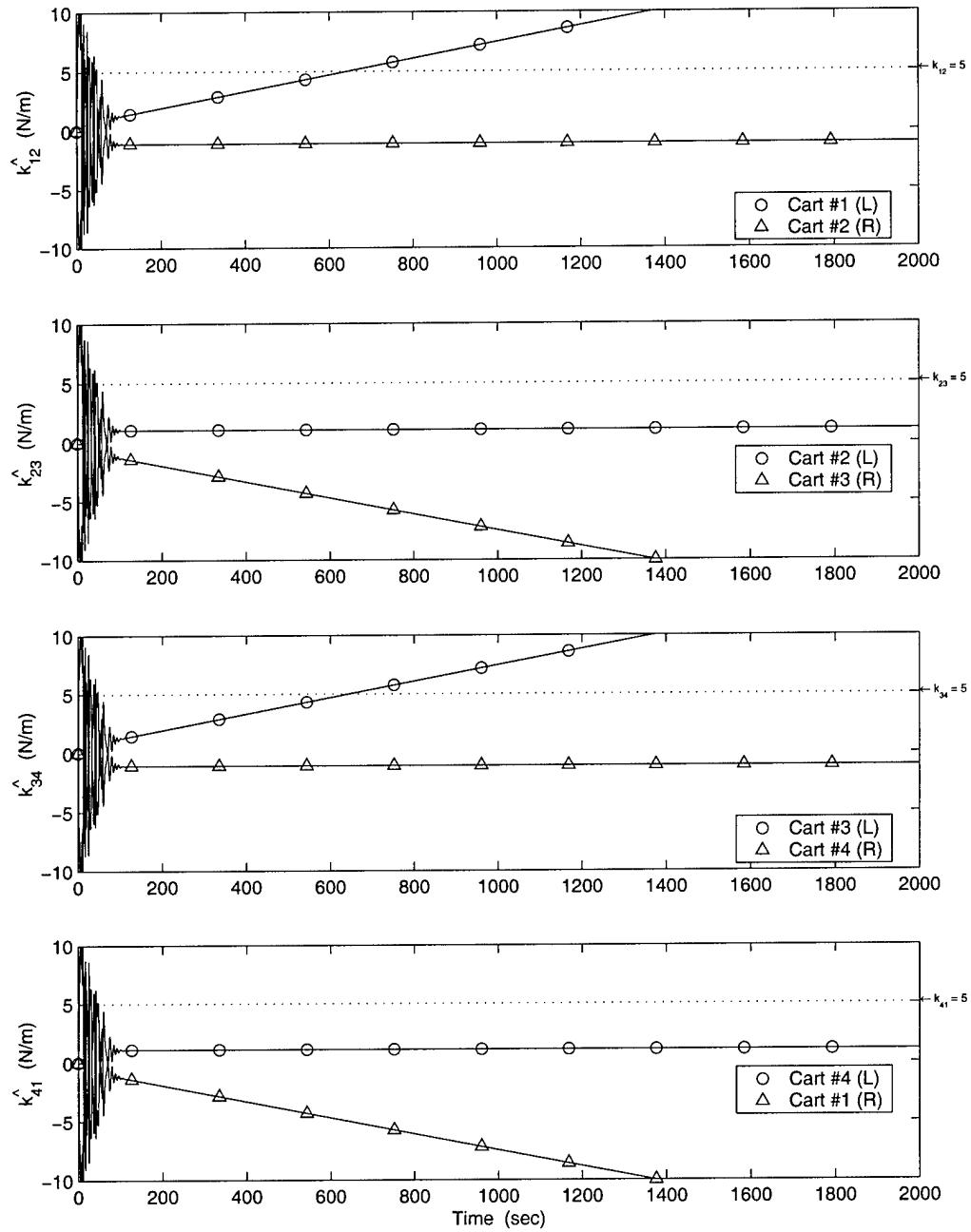
Figure 4.9   Stiffness Parameter Estimates for the Tuned Cyclic System: Adaptation on
/ PPF off, Cyclic Disturbance, $E_o = 1$, $\Gamma_r = 10^2\,\mathrm{I}$
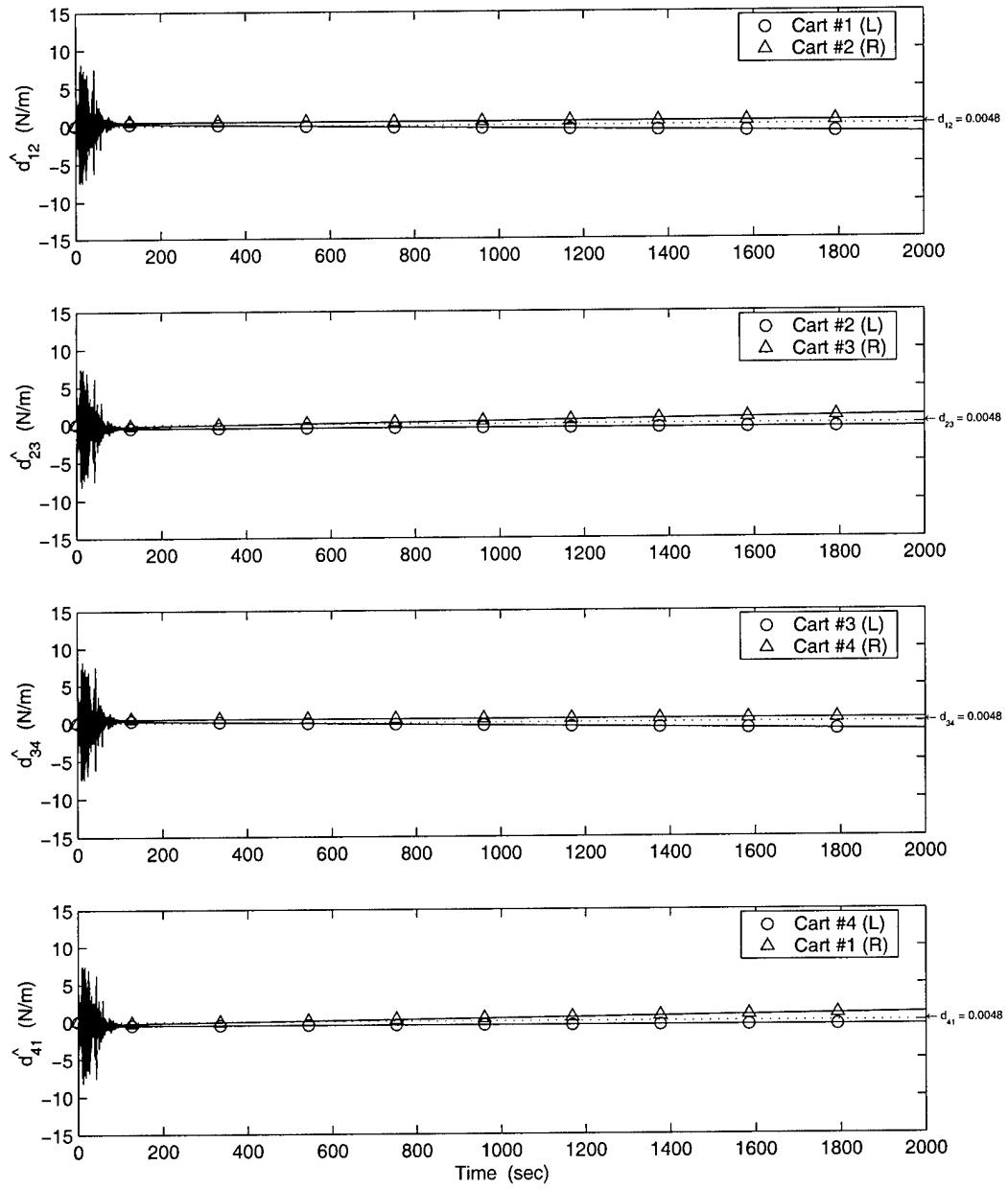
Figure 4.10   Damping Parameter Estimates for the Tuned Cyclic System: Adaptation on / PPF off, Cyclic Disturbance, $E_o = 1$, $\Gamma_r = 10^2 I$
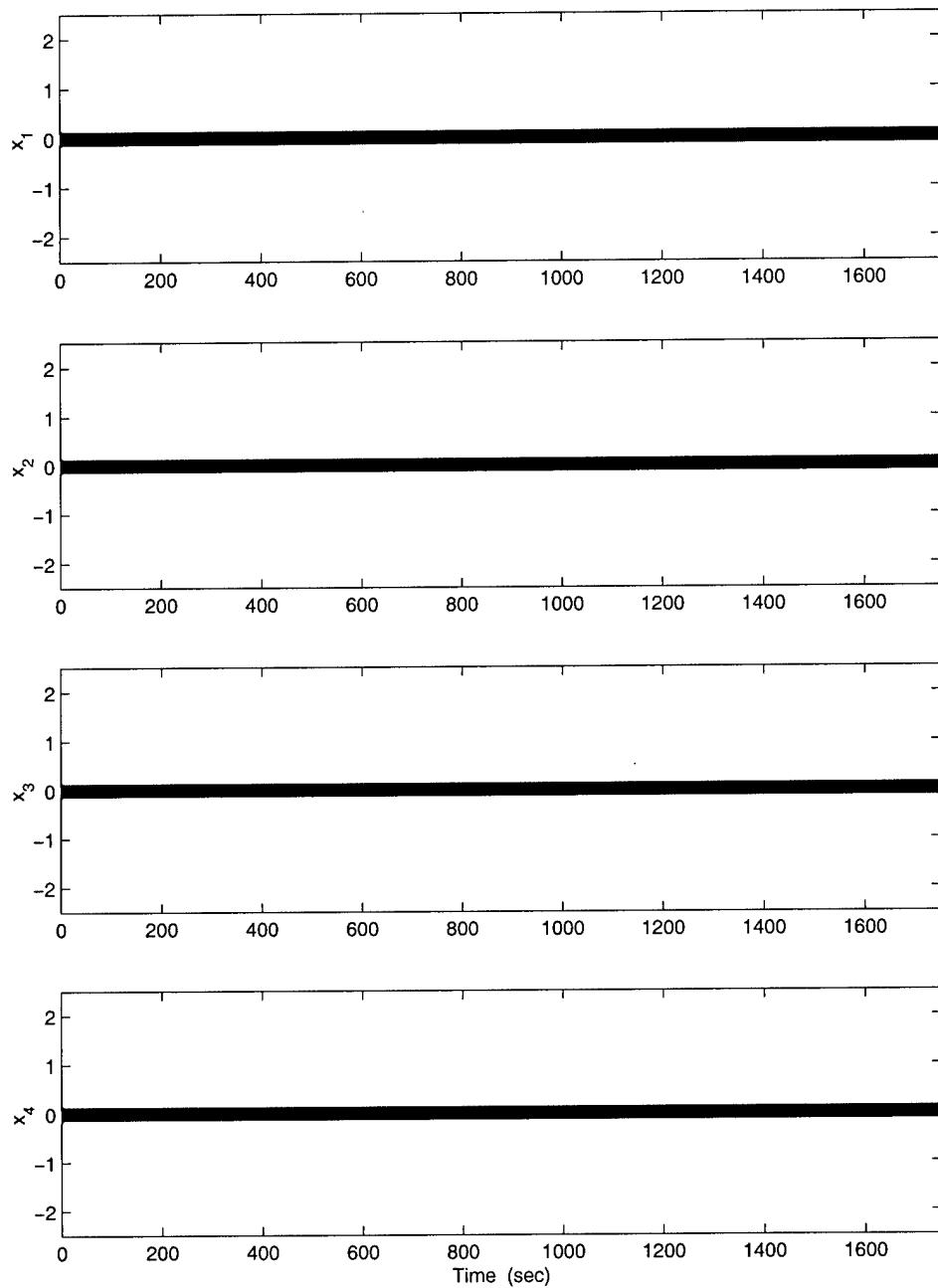
Figure 4.11   Displacements (m) for the Tuned Cyclic System: Adaptation off / PPF on,
Cyclic Disturbance, $E_o = 1$, $\Gamma_r = 10^2\,\mathrm{I}$
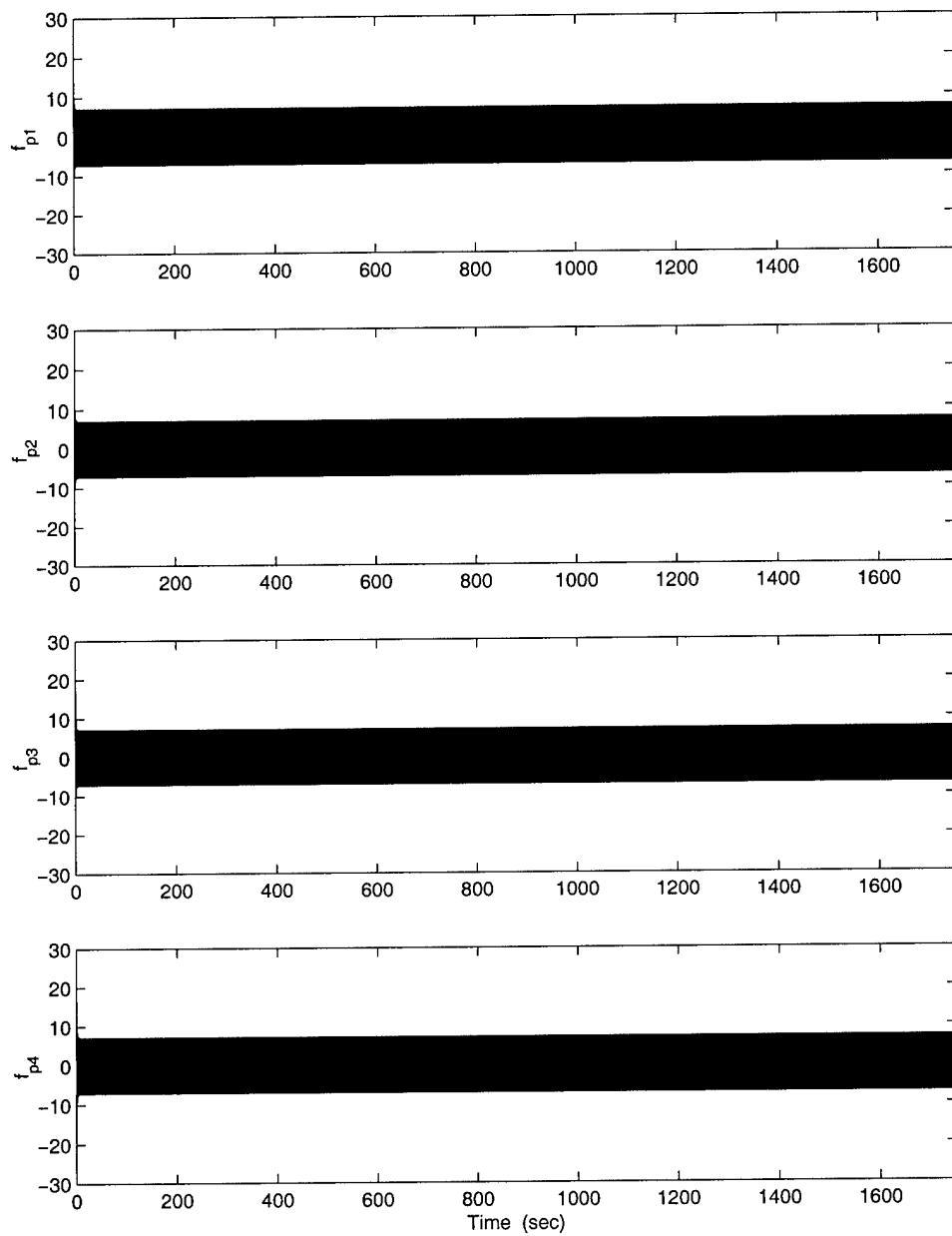
Figure 4.12 PPF Forces (N) for the Tuned Cyclic System: Adaptation off / PPF on, Cyclic Disturbance, $E_o = 1$, $\Gamma_r = 10^2\,\mathrm{I}$
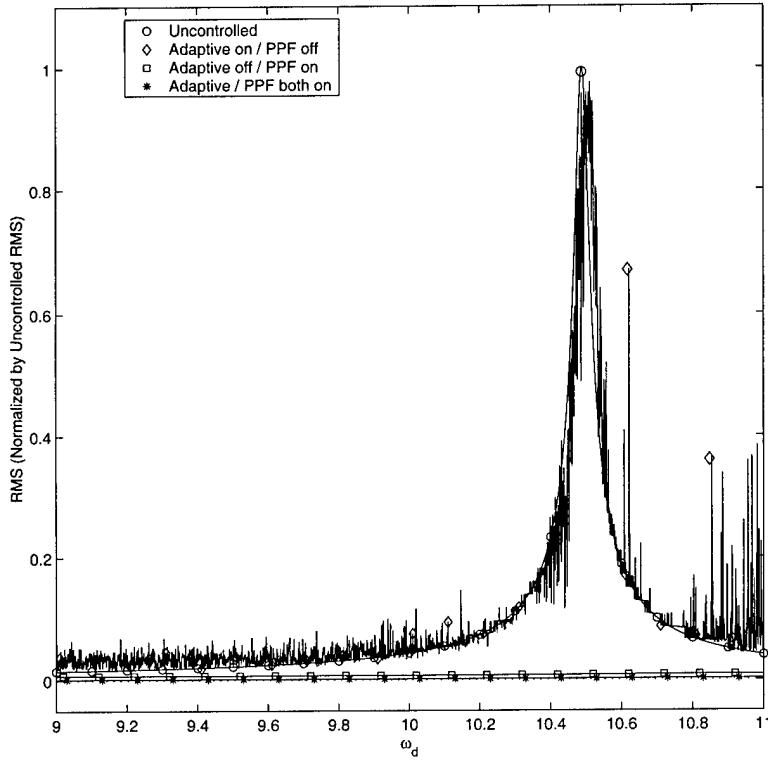
Figure 4.13   Maximum RMS of Displacements for the Tuned Cyclic System: Cyclic Disturbance, $E_o = 1$

normalized by the maximum RMS for the uncontrolled system. All configurations appear to perform well at the lower frequencies. It is immediately obvious, however, that the Adaptive-Only control produces very poor results; at best, the response no better than the uncontrolled system. The Adaptive/PPF and PPF-Only controls perform equally well, resulting in a near zero response.

4.1.6.2   For the Tuned System, Varying E_o.   The tuned system with full Adaptive/PPF control is used again here. This time however, the effects of varying the engine order of the disturbance are studied. First, the simulation was run with $E_o = 3$. The displacement, force, and parameter estimate plots were nearly identical to those for $E_o = 1$, see Figures 4.2 through 4.6. The only difference was in the parameter estimates. As with $E_o = 1$, the two estimators for each parameter found equal and opposite answers. However,

for $E_o = 3$, the left estimator found the negative solution for the stiffness parameters and the positive solution for the damping parameters. This is the reverse of $E_o = 1$.

Next, the simulation was run again with $E_o = 4$. The uncontrolled response, Figure 4.14, is approximately 20 times greater than the response for $E_o = 1$. When Adaptive/PPF control is turned on, the response of all four carts is substantially reduced, Figure 4.15. Unlike $E_o = 1$, there is no pulsing, or loss of convergence, in the displacement or force plots, Figures 4.16 and 4.17. The adaptive force amplitudes for $E_o = 4$ are roughly equivalent to those for $E_o = 1$, but the PPF forces have nearly doubled in magnitude. The parameter estimates are shown in Figures 4.18 and 4.19. As you can see, the two estimators for each parameter find the same solution in this case. However, the stiffness parameters diverge from the correct values.

Finally, the simulation was run with $E_o = 12$. The response of the system was identical to the response for $E_o = 4$. It is not surprising that these two engine orders produce similar responses. When the forcing phase angle coincides with a system mode, the mode is excited. Therefore, engine orders with similar forcing phase angles should produce similar responses. Referring to Equation 4.41, the nominal phase angle for $E_o = 4$ is 2π, and for $E_o = 12$ it is 6π, which are equivalent. Duffield demonstrated this property experimentally using an 8 bladed disk [5]. This is also most likely the reason that $E_o = 1$ and $E_o = 3$ are producing equivalent responses, but the parameter estimates are reversed. The nominal phase angles for these two cases are $\frac{\pi}{2}$ and $\frac{3\pi}{2}$ respectively. These are similar, but opposite in phase.

The maximum RMS of the cart displacements for $E_o = 1, 3, \& 4$ are shown in Figure 4.20. Note that the range on the RMS axis is 0 to 0.01. The RMS response is significantly reduced for all engine orders when compared to the normalized uncontrolled peak value of 1, see Figure 4.13. Note that the curves for $E_o = 1 \& 3$ are nearly identical.

4.1.6.3 For the Mistuned System, $E_o = 1$.   The effects of mistuning on the cyclic system are now studied. The uncontrolled response of the mistuned system is shown in Figure 4.21. It is immediately obvious that the steady-state amplitudes of the
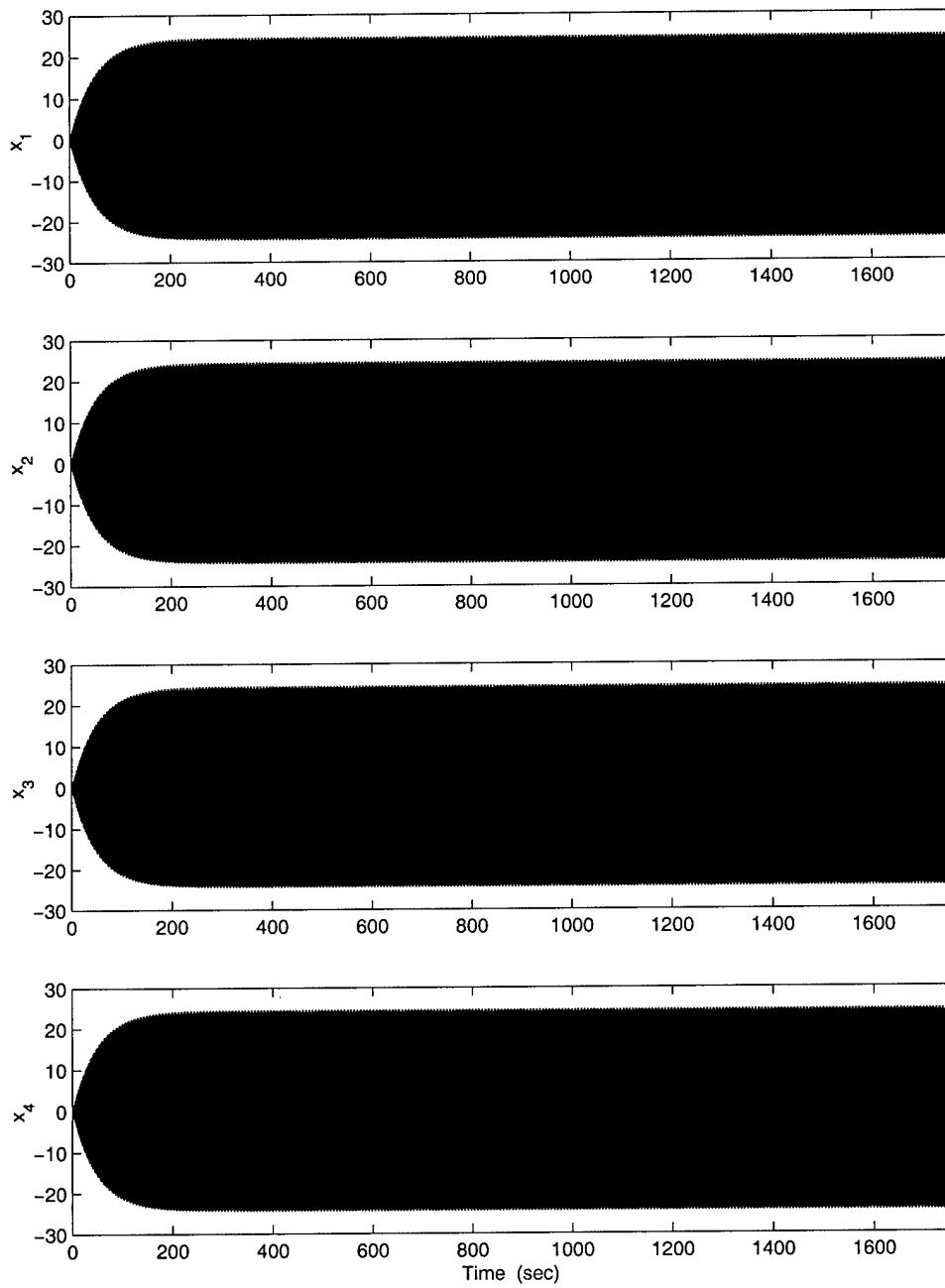
Figure 4.14   Displacements (m) for the Tuned Cyclic System: Uncontrolled, Cyclic Disturbance, $E_o = 4$, $\Gamma_r = 10^2\,\mathrm{I}$
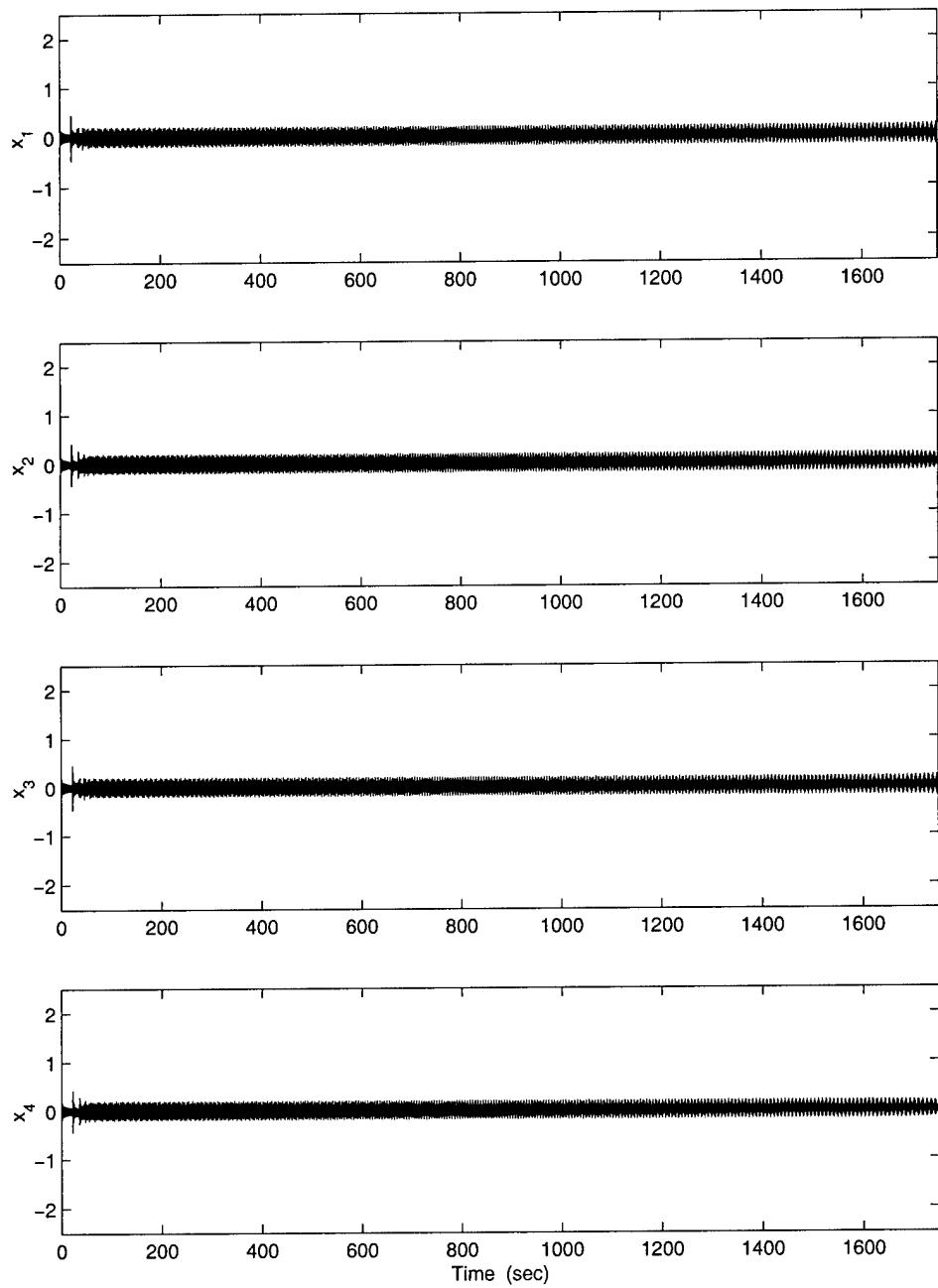
Figure 4.15   Displacements (m) for the Tuned Cyclic System: Adaptation/PPF Both on, Cyclic Disturbance, $E_o = 4$, $\Gamma_r = 10^2\,\mathrm{I}$
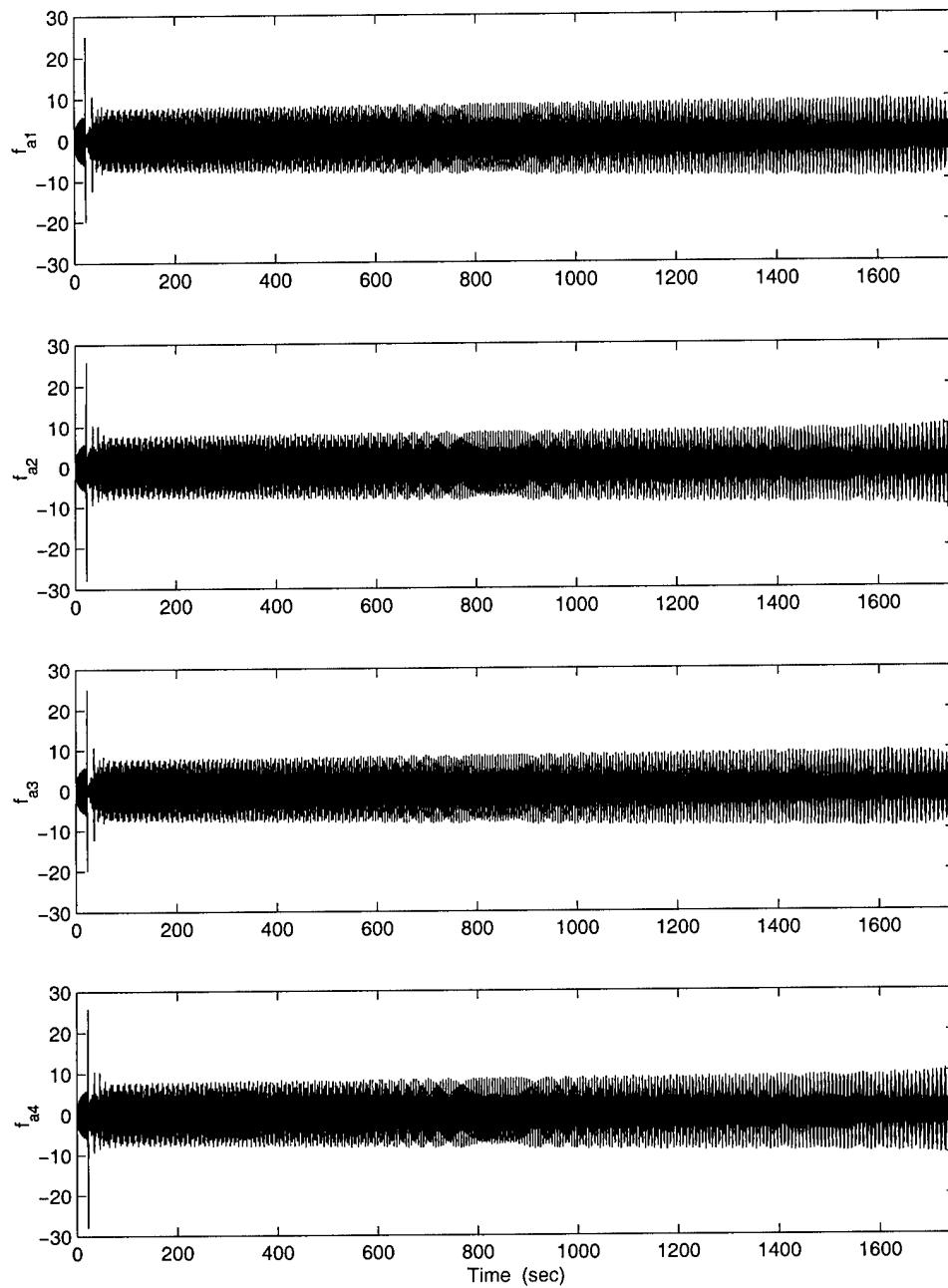
Figure 4.16   Adaptive Forces (N) for the Tuned Cyclic System: Adaptation/PPF Both
on, Cyclic Disturbance, $E_o = 4$, $\Gamma_r = 10^2 \, I$
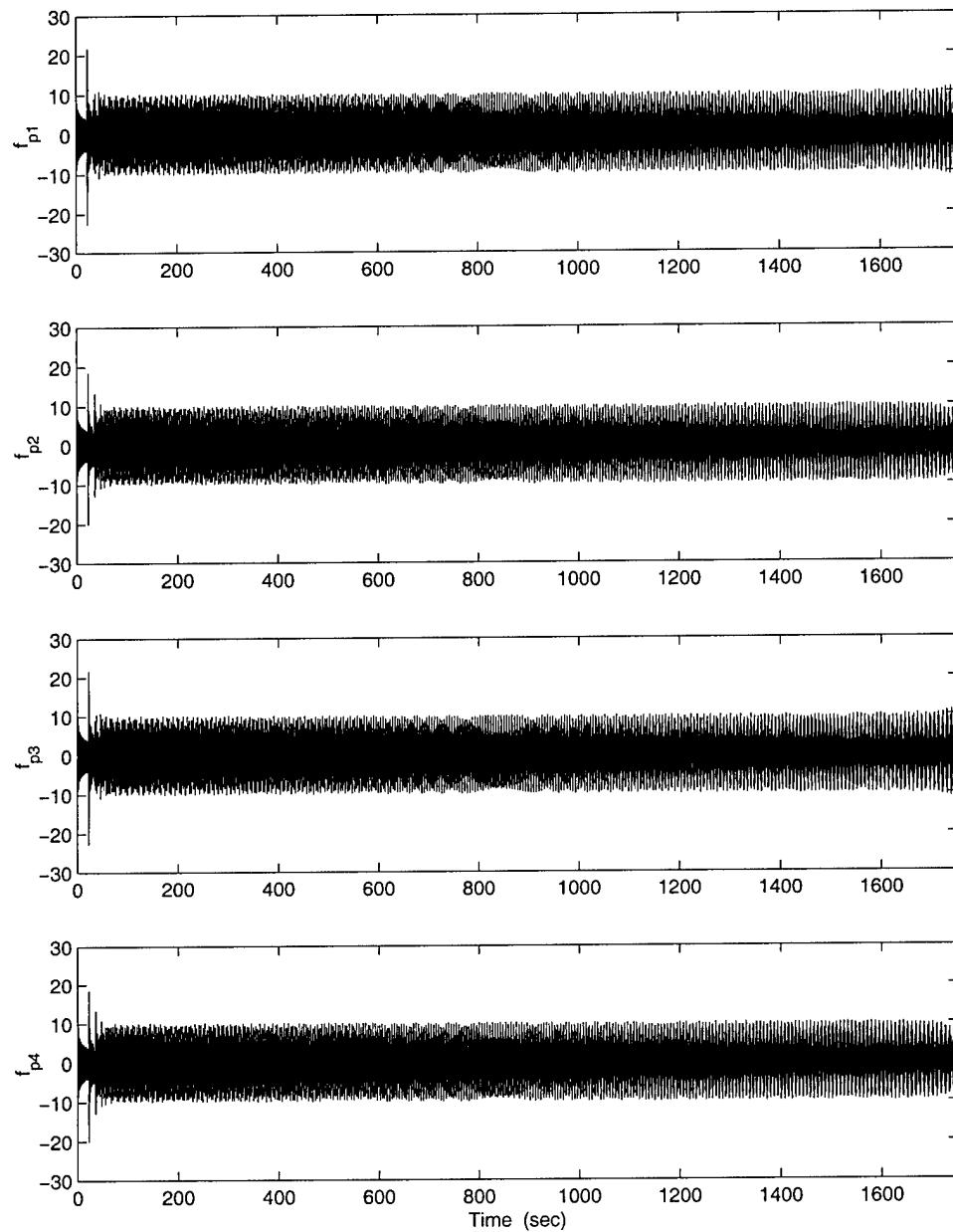
Figure 4.17   PPF Forces (N) for the Tuned Cyclic System: Adaptation/PPF Both on, Cyclic Disturbance, $E_o = 4$, $\Gamma_r = 10^2 I$
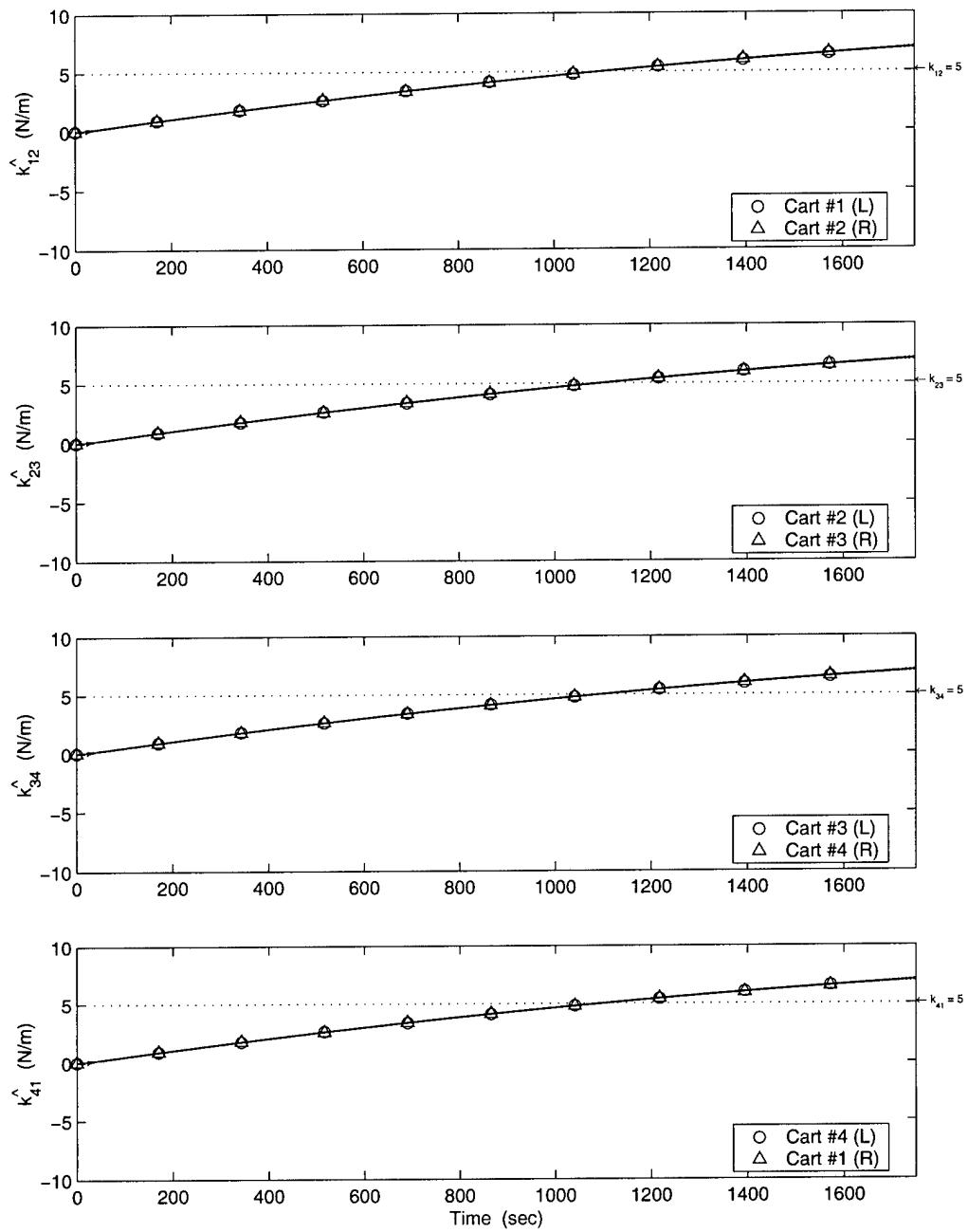
Figure 4.18   Stiffness Parameter Estimates for the Tuned Cyclic System: Adaptation/PPF Both on, Cyclic Disturbance, $E_o = 4$, $\Gamma_r = 10^2\,\mathrm{I}$
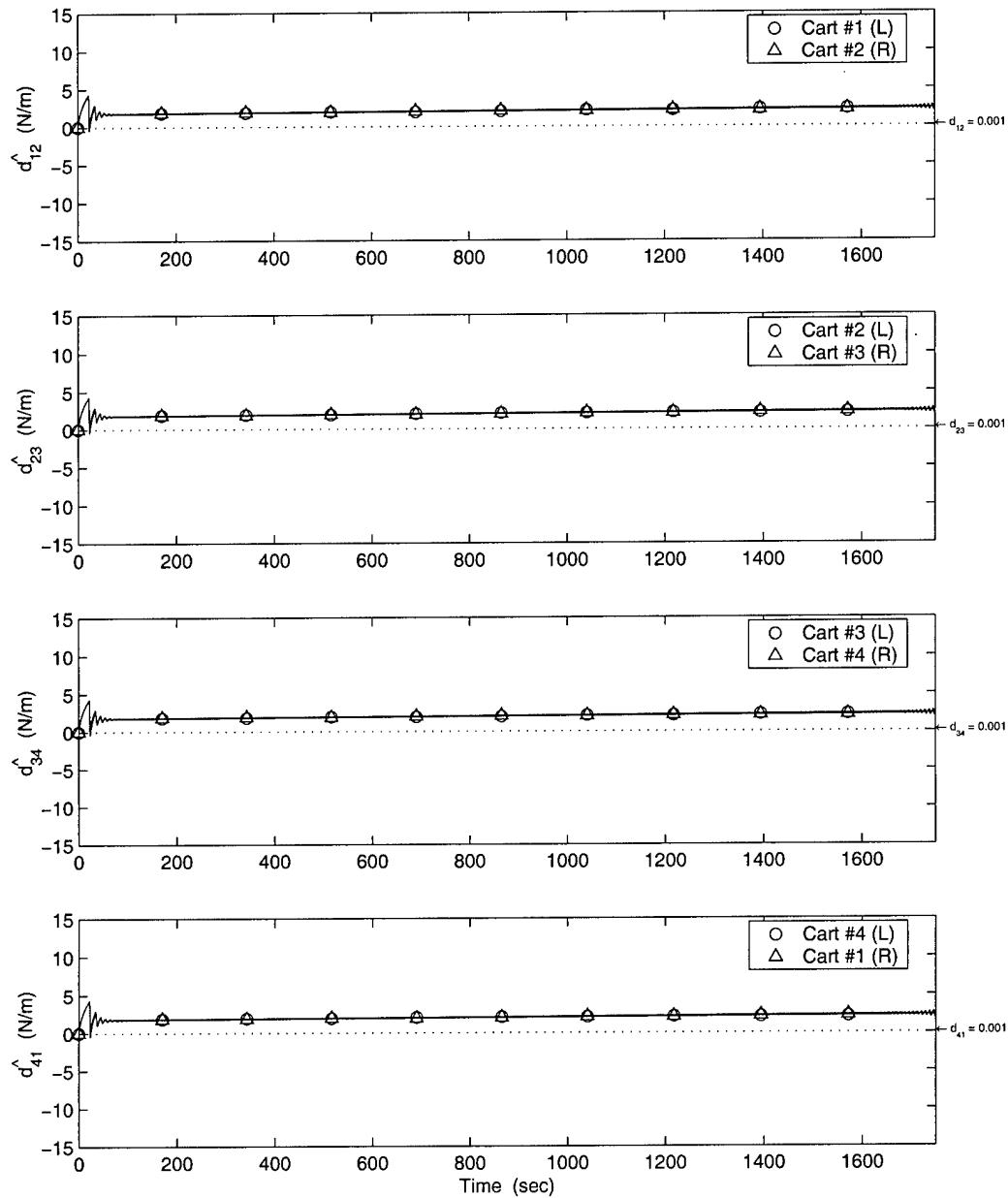
Figure 4.19   Damping Parameter Estimates for the Tuned Cyclic System: Adaptation/PPF Both on, Cyclic Disturbance, $E_o = 4$, $\Gamma_r = 10^2\,I$
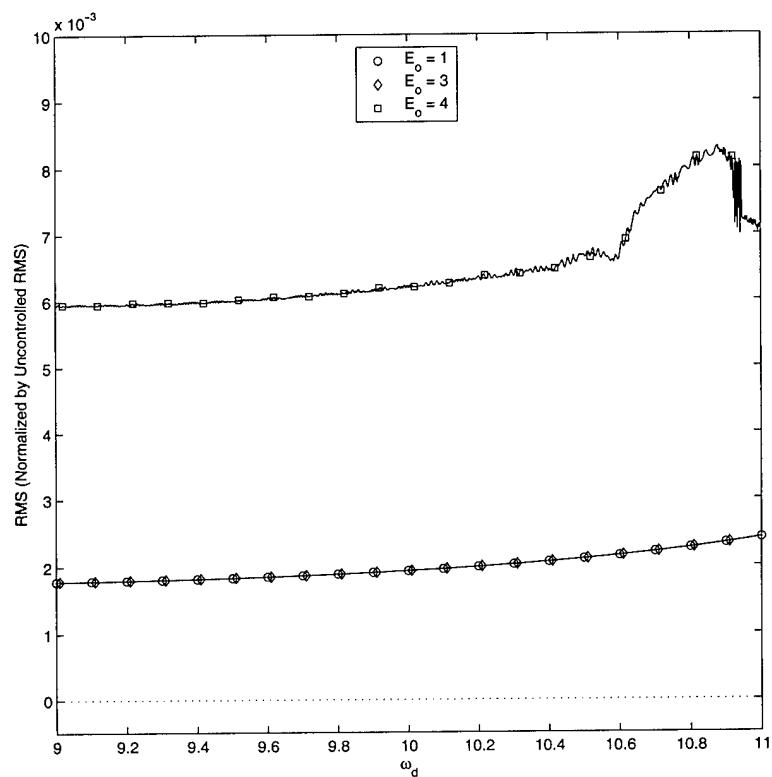
Figure 4.20   Maximum RMS of Displacements for the Tuned Cyclic System: Adaptation/PPF Both on, Cyclic Disturbance, $E_o = 1, 3,$ & 4

individual carts are no longer equal, like they were for the tuned system. This demonstrates the effect of mode localization brought on by the mistuning.

When Adaptive/PPF control is turned on, it nullifies the effects of mode localization so that all of the carts have the same "steady-state" amplitudes. The displacements, control forces, and parameter estimates for Adaptive/PPF control of the mistuned system are shown in Figures 4.22 through 4.26. When compared to the tuned system, Figures 4.2 through 4.6, it is noted that the responses are nearly identical. The only major differences are that the pulses, or periods of lost convergence, initially occur at a later time and at a slightly longer interval than in the tuned system. This is an interesting result, since it means that there are longer periods of good performance for the mistuned system when compared to the tuned system.

The maximum displacement RMS values for the three control configurations (Adaptive/PPF, Adaptive-Only, and PPF-Only) are plotted in Figure 4.27. These plots are similar to the tuned results. Adaptive-Only control is still for the most part no better than the uncontrolled system, except at resonance. As with the tuned case, the Adaptive/PPF and PPF-Only controls perform equally well, resulting in a near zero response.

Finally, the maximum RMS values for $E_o = 1 \& 4$, both tuned and mistuned, with Adaptive/PPF control are shown in Figure 4.28. Note that the range on the RMS axis is 0 to 0.01, and the normalized uncontrolled peak is 1. It is quite obvious from this plot, that for a given E_o, the tuned and mistuned systems behaved similarly when using Adaptive/PPF control.

4.1.6.4 *Summary.*

The 4 DOF system was first studied with Adaptive/PPF control on each cart, and subjected to a cyclic disturbance with $E_o = 1$. Although the responses were substantially reduced, they were not completely suppressed like they were for the single control system in Chapter 3. There are also regular periods when the controller seems to loose tracking, and the response pulses to a higher amplitude, which is still lower than the uncontrolled system.

These pulses correspond to when the parameter estimates loose convergence and then reacquire. This creates a distinctive sawtooth pattern in the estimate plots. The stiffness
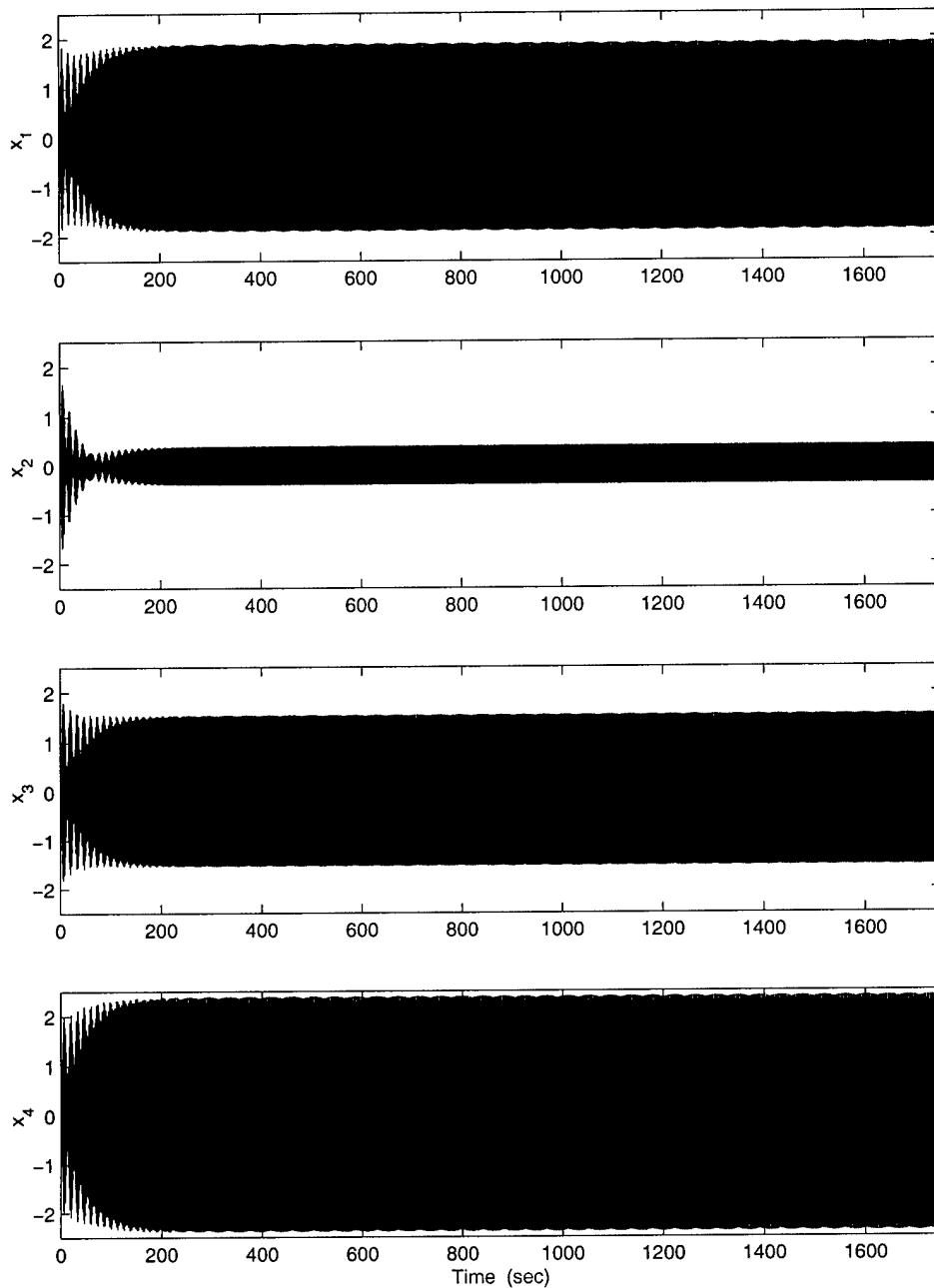
Figure 4.21   Displacements (m) for the Mistuned Cyclic System: Uncontrolled, Cyclic
Disturbance, $E_o = 1$, $\Gamma_r = 10^2\,\mathrm{I}$
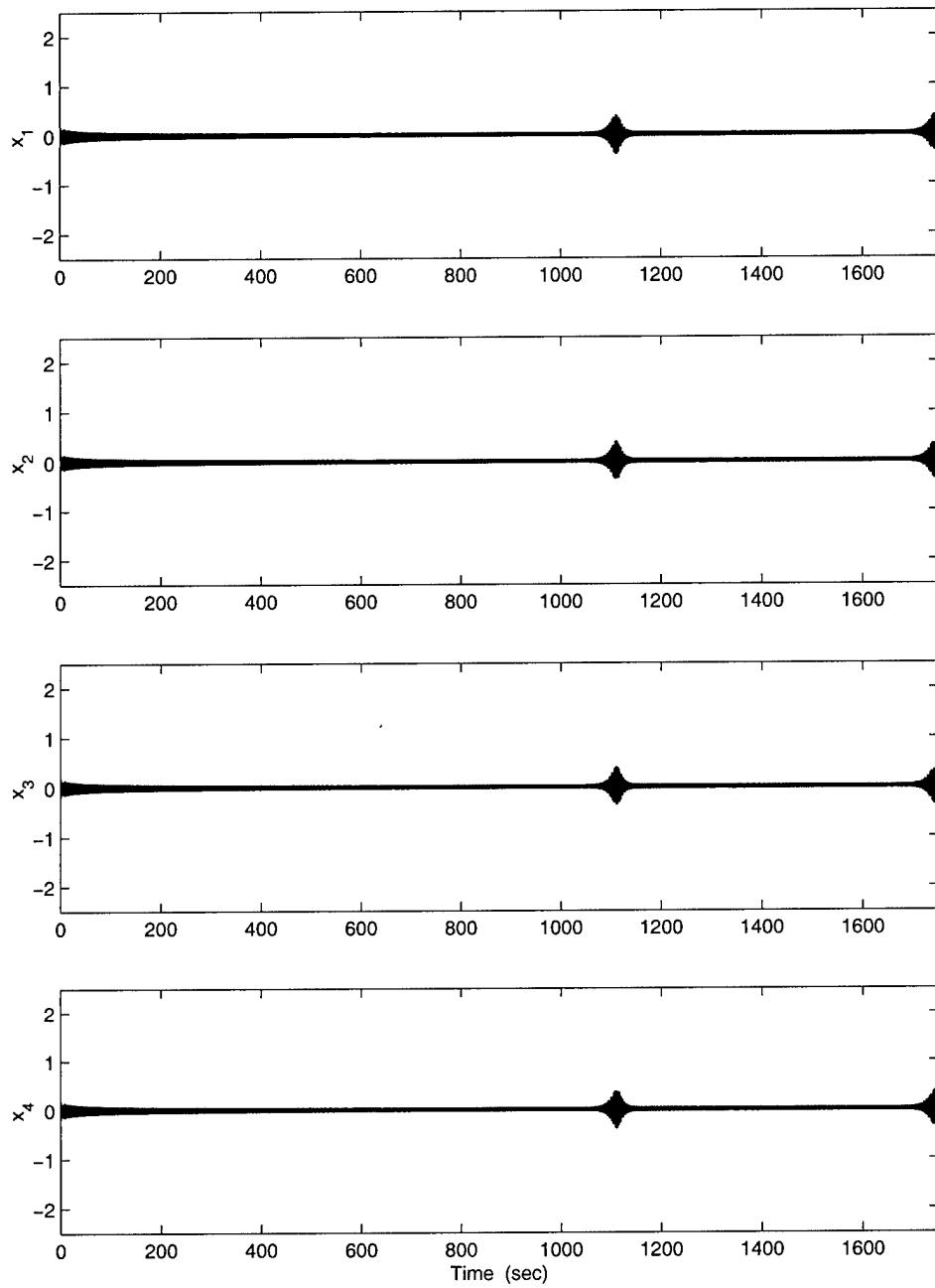
Figure 4.22   Displacements (m) for the Mistuned Cyclic System: Adaptation/PPF Both on, Cyclic Disturbance, $E_o = 1$, $\Gamma_r = 10^2 \, \mathrm{I}$
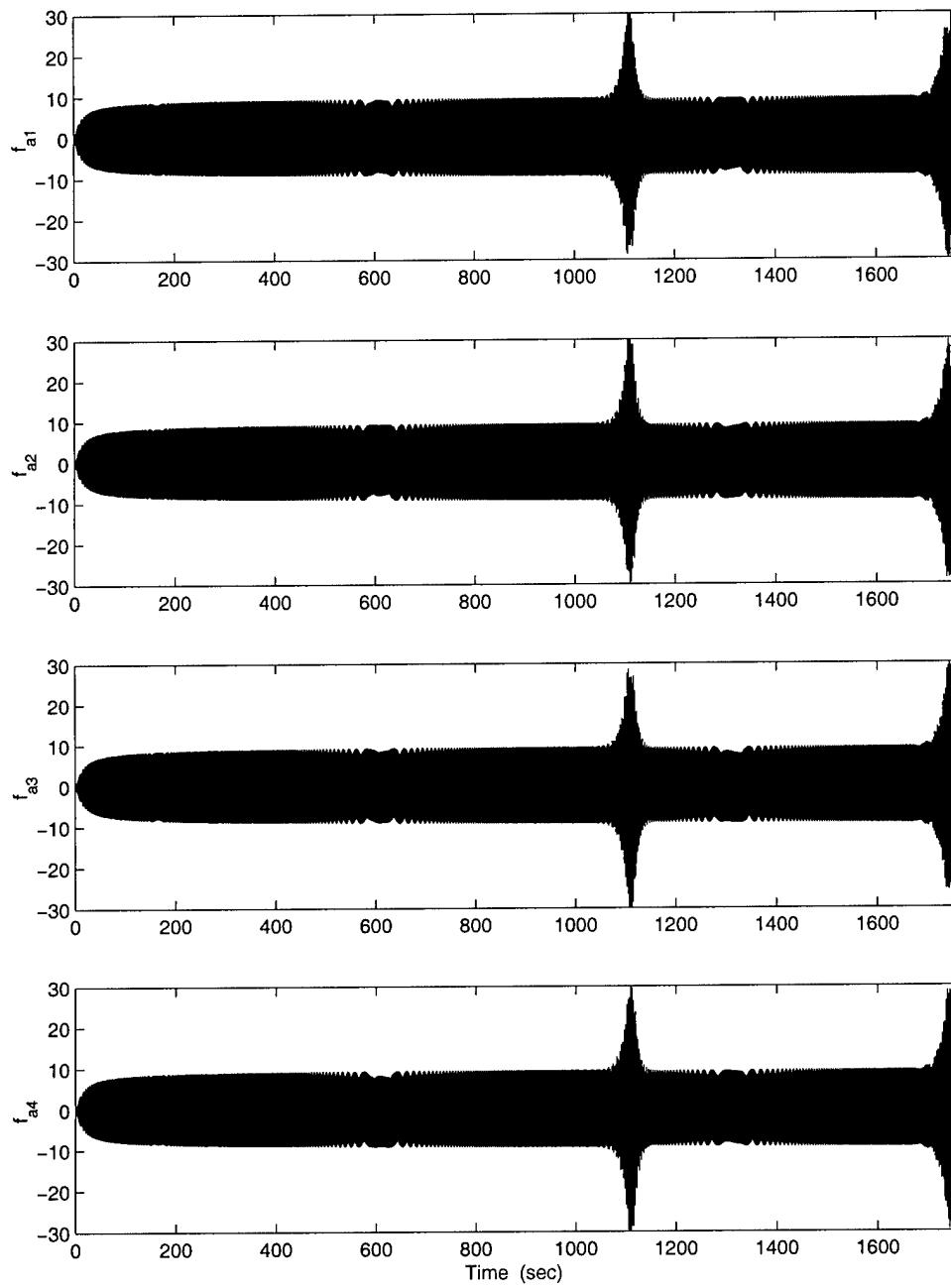
Figure 4.23   Adaptive Forces (N) for the Mistuned Cyclic System: Adaptation/PPF Both on, Cyclic Disturbance, $E_o = 1$, $\Gamma_r = 10^2\,\mathrm{I}$
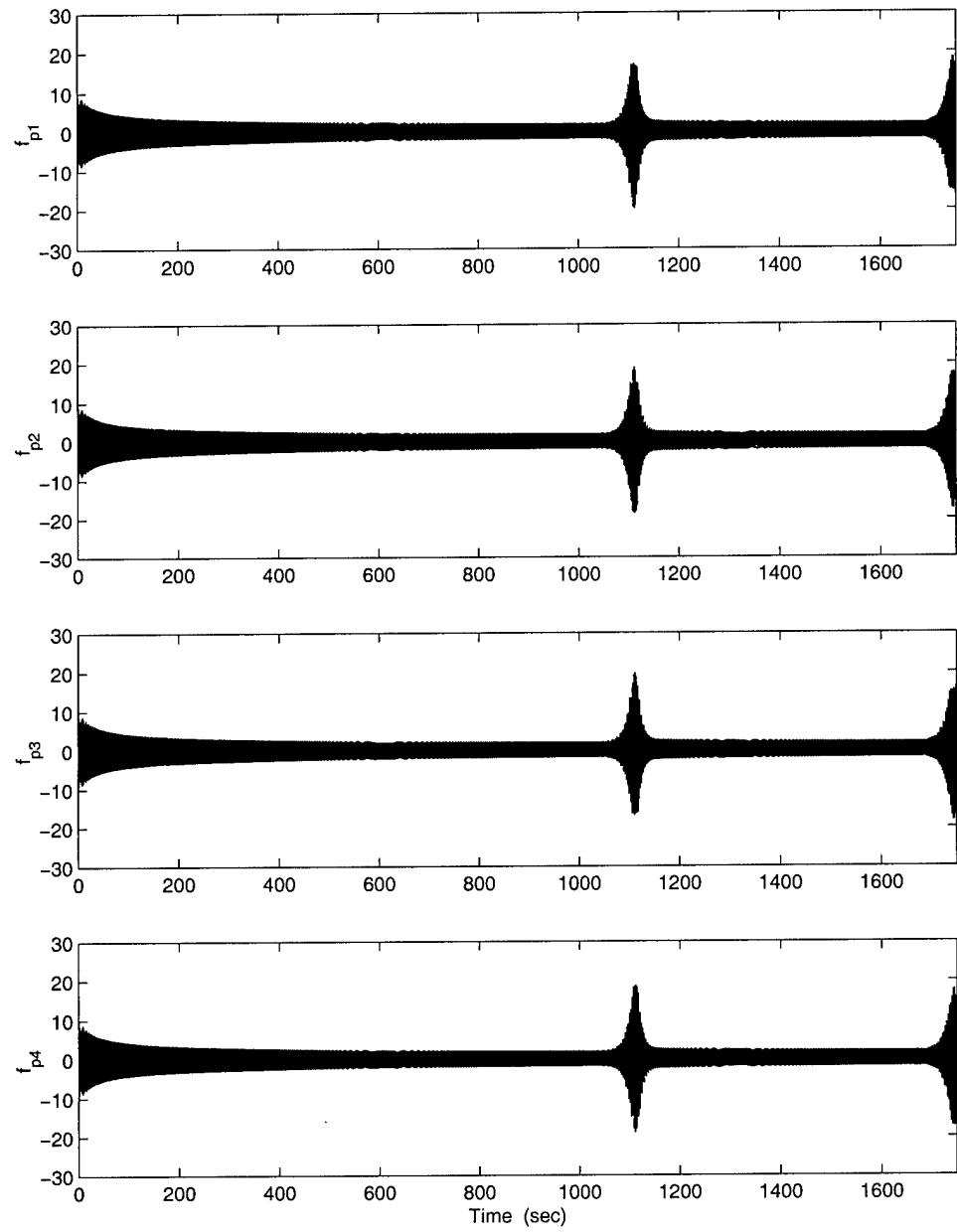
Figure 4.24   PPF Forces (N) for the Mistuned Cyclic System: Adaptation/PPF Both
on, Cyclic Disturbance, $E_o = 1$, $\Gamma_r = 10^2 \mathrm{I}$
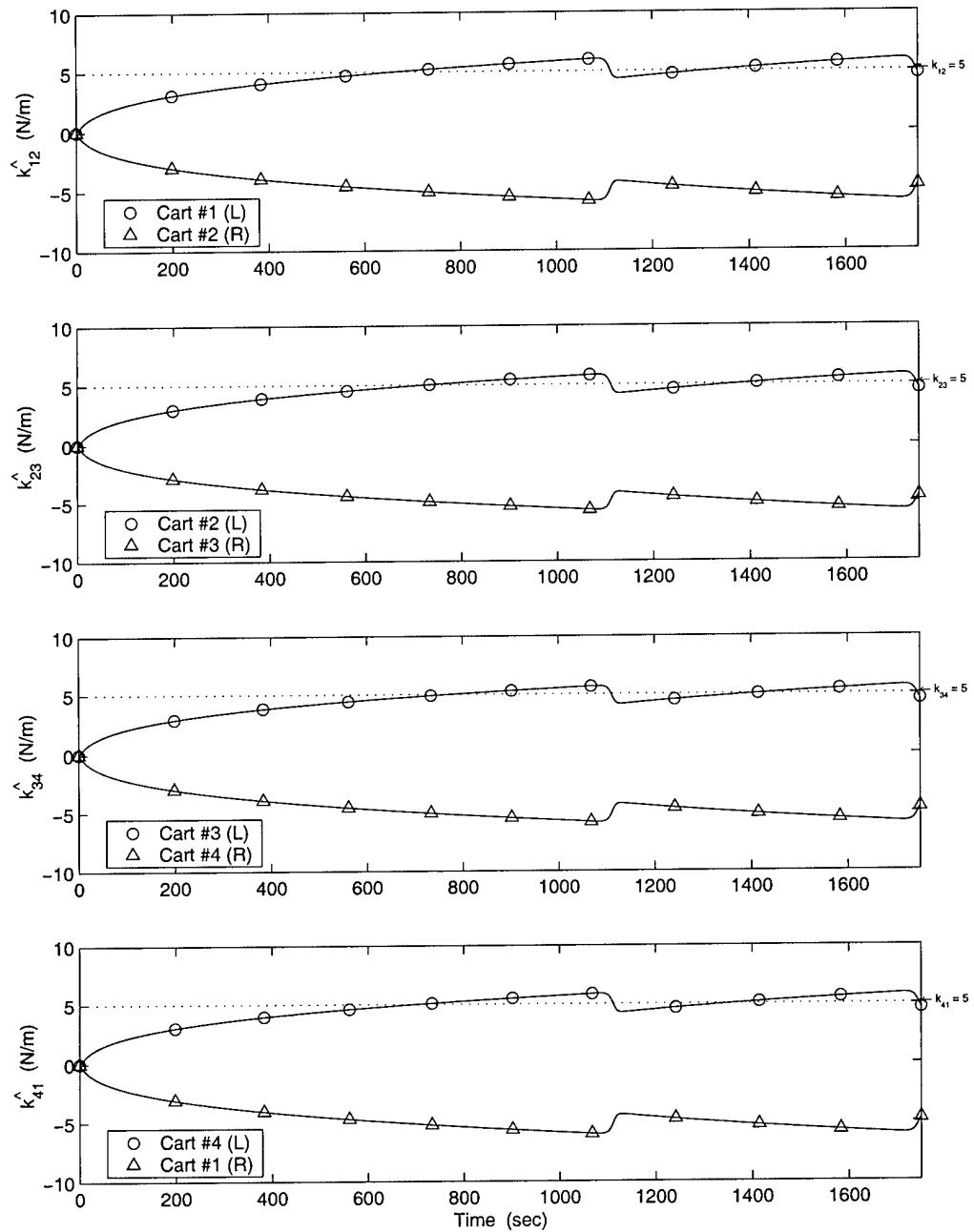
Figure 4.25   Stiffness Parameter Estimates for the Mistuned Cyclic System: Adaptation/PPF Both on, Cyclic Disturbance, $E_o = 1$, $\Gamma_r = 10^2\,I$
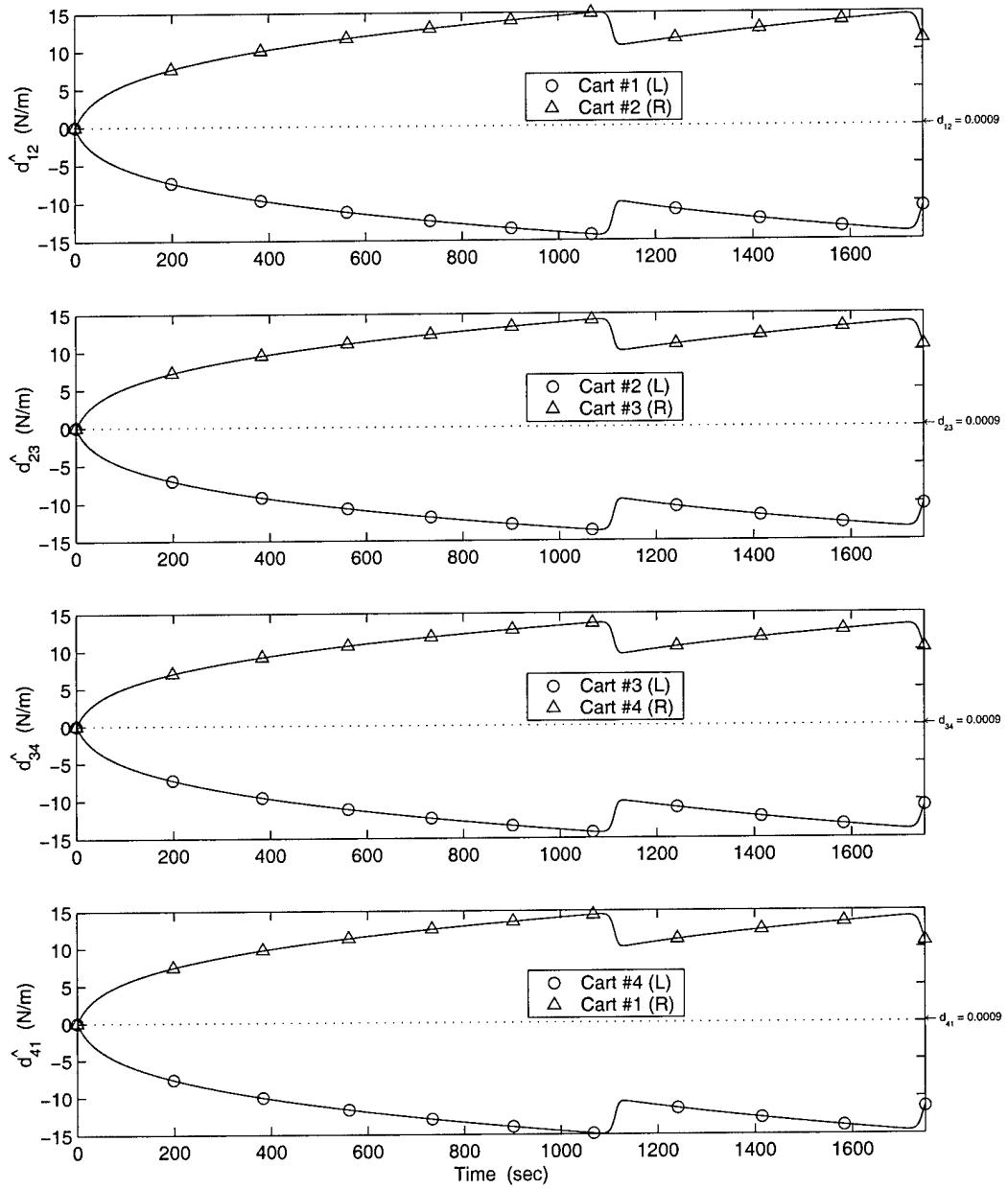
Figure 4.26 Damping Parameter Estimates for the Mistuned Cyclic System: Adaptation/PPF Both on, Cyclic Disturbance, $E_o = 1$, $\Gamma_r = 10^2\,I$
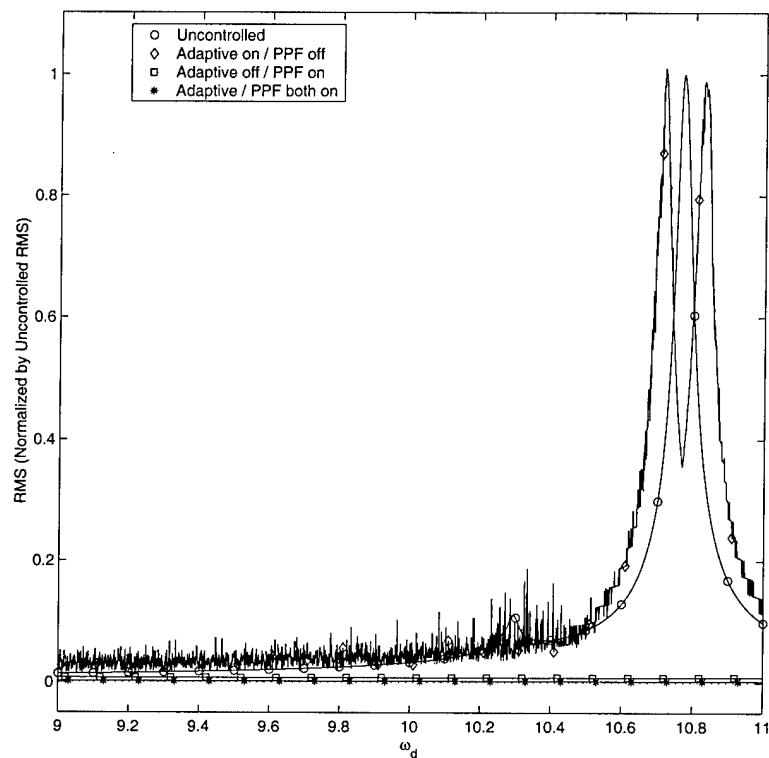
Figure 4.27   Maximum RMS of Displacements for the Mistuned Cyclic System: Cyclic Disturbance, $E_o = 1$
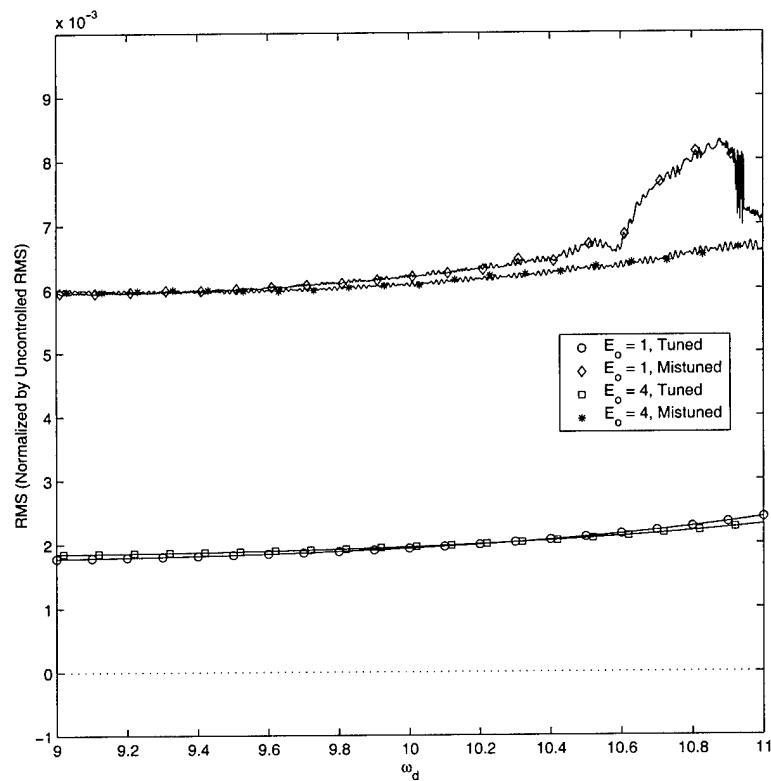
Figure 4.28   Comparison of Maximum RMS of Displacements for the Tuned & Mistuned
Cyclic Systems: Adaptation/PPF Both on, Cyclic Disturbance, $E_o = 1 \& 4$

estimates are converging to the correct values, but the damping estimates are significantly greater than the actual values. More disconcerting, however, is that the two estimators for each parameter are finding equal and opposite solutions. The left estimators found a positive solution for the stiffness parameters, and a negative answer for the damping parameters. It appears that the estimators are working against each other. Also, recall that the adaptive technique does not guarantee that the estimates will converge, or that there is even a unique solution. While the solutions for the parameter estimates are not correct, they still provide acceptable response reduction.

Comparing the maximum RMS plots of three control configurations (Adaptive/PPF, Adaptive-Only, and PPF-Only), it is evident that the Adaptive/PPF and PPF-Only controls perform equally well, resulting in a near zero response. When Adaptive-Only control is used, it produces very poor results, and at best is no better than the uncontrolled system. This is quite different from the single control case. Recall for the single control system, Adaptive/PPF control and Adaptive-Only control provided nearly identical reduction in the response. When adaptive control was used on a single cart, it was able to isolate it from the others, and completely suppressed the response. It appears now, however, that the adaptive estimators on each cart work against each other.

Next, the simulation was rerun with $E_o = 3$ for the cyclic disturbance, and the responses were nearly identical to those for $E_o = 1$. The only difference was in the parameter estimates. As with $E_o = 1$, the two estimators for each parameter found equal and opposite answers, but the signs were reversed. When the simulation was run with $E_o = 4$, the steady state response was slightly greater than for $E_o = 1$ or 3, but there was no pulsing, or loss of convergence. This is most likely because the two estimators for each parameter find the same solution in this case. Unfortunately, the parameters diverge from the correct values. Responses identical to those for $E_o = 4$, were also found when the simulation was run with $E_o = 12$.

It is not surprising that identical responses occur when $E_o = 4$ & 12; engine orders with similar forcing phase angles should produce similar responses. The nominal phase angle for $E_o = 4$ is 2π, and for $E_o = 12$ it is 6π, which are equivalent. This is also most likely the reason that $E_o = 1$ and $E_o = 3$ are producing equivalent responses, but the
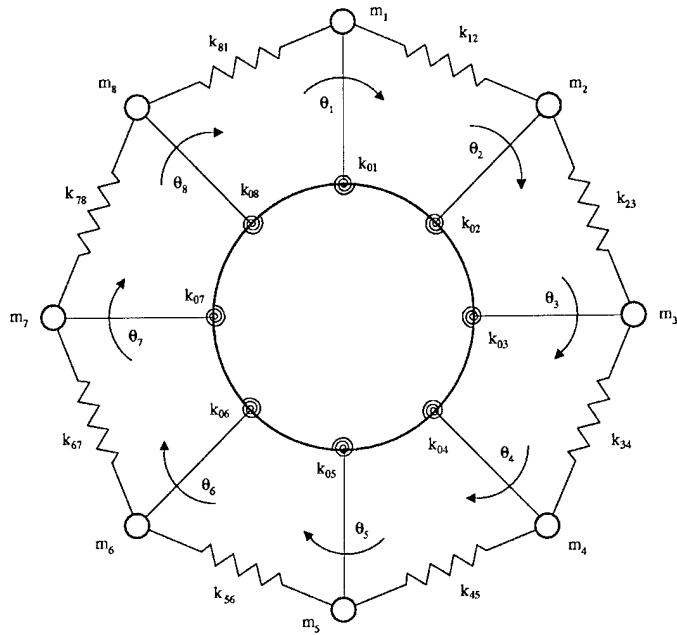
Figure 4.29   Model of an 8 Blade Compressor Disk

parameter estimates are reversed. The nominal phase angles for these two cases are $\frac{\pi}{2}$ and $\frac{3\pi}{2}$ respectively. These are similar, but opposite in phase.

Finally, mistuning effects on the system were studied for a cyclic disturbance with $E_o = 1$. The simulation demonstrated the occurrence of mode localization; some of the carts had higher steady-state amplitudes than the others. When Adaptive/PPF control was turned on, the effects of mode localization were nullified, and all carts had identical responses. The periods of lost convergence still occur like they did for the tuned system. Interestingly, though, the initial pulse occurs at a later time, and the pulses occur at longer intervals. RMS plots were generated for tuned and mistuned systems with $E_o = 1 \& 4$. With Adaptive/PPF control, the tuned and mistuned systems behaved similarly, for a given engine order.

4.2 Development for an 8 Blade Compressor Disk Model

4.2.1 Equations of Motion.

Finally, a model of an 8 blade compressor disk is studied. As you can see in Figure 4.29, the blades are represented by a point mass, m_i, a distance L away from the hub. As with the 4 DOF model, the structural stiffness is represented by k_{0i}, and the inter-blade coupling forces are expressed in terms of k_{ij}, where $i, j = 1...8$, and by convention m_i is the left blade. The external control and disturbance force on each blade is represented by f_i. Duffield [5] showed that the undamped EOMs are

$$
\begin{aligned}
m_1 L^2 \ddot{\theta}_1 &- \left[\cos\left(\frac{\pi}{8}\right) L^2 k_{12}\right]\theta_2 &&+ \left[\cos\left(\frac{\pi}{8}\right) L^2 (k_{81} + k_{12}) + k_{01}\right]\theta_1 &&- \left[\cos\left(\frac{\pi}{8}\right) L^2 k_{81}\right]\theta_8 &&= f_1 \\
m_2 L^2 \ddot{\theta}_2 &- \left[\cos\left(\frac{\pi}{8}\right) L^2 k_{12}\right]\theta_1 &&+ \left[\cos\left(\frac{\pi}{8}\right) L^2 (k_{12} + k_{23}) + k_{02}\right]\theta_2 &&- \left[\cos\left(\frac{\pi}{8}\right) L^2 k_{23}\right]\theta_3 &&= f_2 \\
m_3 L^2 \ddot{\theta}_3 &- \left[\cos\left(\frac{\pi}{8}\right) L^2 k_{23}\right]\theta_2 &&+ \left[\cos\left(\frac{\pi}{8}\right) L^2 (k_{23} + k_{34}) + k_{03}\right]\theta_3 &&- \left[\cos\left(\frac{\pi}{8}\right) L^2 k_{34}\right]\theta_4 &&= f_3 \\
m_4 L^2 \ddot{\theta}_4 &- \left[\cos\left(\frac{\pi}{8}\right) L^2 k_{34}\right]\theta_3 &&+ \left[\cos\left(\frac{\pi}{8}\right) L^2 (k_{34} + k_{45}) + k_{04}\right]\theta_4 &&- \left[\cos\left(\frac{\pi}{8}\right) L^2 k_{45}\right]\theta_5 &&= f_4 \\
m_5 L^2 \ddot{\theta}_5 &- \left[\cos\left(\frac{\pi}{8}\right) L^2 k_{45}\right]\theta_4 &&+ \left[\cos\left(\frac{\pi}{8}\right) L^2 (k_{45} + k_{56}) + k_{05}\right]\theta_5 &&- \left[\cos\left(\frac{\pi}{8}\right) L^2 k_{56}\right]\theta_6 &&= f_5 \\
m_6 L^2 \ddot{\theta}_6 &- \left[\cos\left(\frac{\pi}{8}\right) L^2 k_{56}\right]\theta_5 &&+ \left[\cos\left(\frac{\pi}{8}\right) L^2 (k_{56} + k_{67}) + k_{06}\right]\theta_6 &&- \left[\cos\left(\frac{\pi}{8}\right) L^2 k_{67}\right]\theta_7 &&= f_6 \\
m_7 L^2 \ddot{\theta}_7 &- \left[\cos\left(\frac{\pi}{8}\right) L^2 k_{67}\right]\theta_6 &&+ \left[\cos\left(\frac{\pi}{8}\right) L^2 (k_{67} + k_{78}) + k_{07}\right]\theta_7 &&- \left[\cos\left(\frac{\pi}{8}\right) L^2 k_{78}\right]\theta_8 &&= f_7 \\
m_8 L^2 \ddot{\theta}_8 &- \left[\cos\left(\frac{\pi}{8}\right) L^2 k_{81}\right]\theta_1 &&+ \left[\cos\left(\frac{\pi}{8}\right) L^2 (k_{78} + k_{87}) + k_{08}\right]\theta_8 &&- \left[\cos\left(\frac{\pi}{8}\right) L^2 k_{78}\right]\theta_7 &&= f_8
\end{aligned}
$$

$$(4.42)$$

In matrix form, with damping added, the EOMs become

$$
M\underline{\ddot{\theta}} + D\underline{\dot{\theta}} + K\underline{\theta} = \underline{f}
\tag{4.43}
$$

The elements of the mass and stiffness matrices, M and K, are taken from Equation 4.42, and the damping matrix, D, is found from Equation 2.77.

As in the 4 DOF system, using identical PPF actuators on each cart, with a damping ratio of ζ_f and a frequency of ω_f, results in the following additional equations

$$
\left\{ \begin{array}{c} \ddot{\eta}_1 \\ \vdots \\ \ddot{\eta}_8 \end{array} \right\} + 2\zeta_f \omega_f \left\{ \begin{array}{c} \dot{\eta}_1 \\ \vdots \\ \dot{\eta}_8 \end{array} \right\} + \omega_f^2 \left\{ \begin{array}{c} \eta_1 \\ \vdots \\ \eta_8 \end{array} \right\} = \left\{ \begin{array}{c} h_1 \\ \vdots \\ h_8 \end{array} \right\}
\tag{4.44}
$$

Recall (see Section 4.1.1) that in general, the controlled coordinate EOMs for each substructure of an RPS are given as

$$M_{ci}\ddot{q}_{ci} + D_{ci}\dot{q}_{ci} + K_{ci}q_{ci} = f_{ci} - Y_{ri}\Phi_{ri} \qquad i = 1, \ldots, N \qquad (4.45)$$

where M_{ci}, D_{ci}, K_{ci}, q_{ci}, and f_{ci} are defined in Equations 4.17 through 4.21. The regression and unknown parameter matrices are

$$Y_{ri} = \begin{bmatrix} x_{(i-1)} & x_{(i+1)} & \dot{x}_{(i-1)} & \dot{x}_{(i+1)} \\ 0 & 0 & 0 & 0 \end{bmatrix} \quad \Phi_{ri} = - \begin{bmatrix} k_{(i-1),i} & k_{i,(i+1)} & d_{(i-1),i} & d_{i,(i+1)} \end{bmatrix}^T$$

$$(4.46)$$

Note for the 8 blade system that $N = 8$, and cart 1 connects to cart 8. So for $i = 1$, $i - 1 \equiv 8$, and for $i = 8$, $i + 1 \equiv 1$.

4.2.2 Adaptive/PPF Control.

The Adaptive/PPF control theory was previously developed for a generic RPS with cyclic coupling. The control forces and parameter estimates are calculated from Equations 4.28 and 4.34 respectively, with $i = 1, \ldots, 8$.

4.2.3 Stability.

As with the 4 DOF system, stability is guaranteed, as long as the five assumptions listed in Section 4.1.4 are satisfied for $i = 1, \ldots, 8$. The mass matrix, M, is positive definite and diagonal, which means that all of the M_c submatrices are symmetric and positive definite; the first condition is therefore satisfied. The unknown forces, f_{ui}, are comprised of the external cyclic disturbance and the control forces on the other carts. Since both of these are individually bounded, f_{ui} is bounded, and the second condition is met. It was shown in Section 4.1.4, that assumptions A3 and A4' reduce to the requirement that $A_{ci} < 0$ for all $i = 1, \ldots, 8$; this is checked during the simulation. Finally, the PPF gain is $\mu = 0.4$, which satisfies assumption A5'.

4.2.4 Simulation.

The 8 blade system is simulated with Adaptive/PPF control on all of the blades. Both tuned and mistuned systems are studied. To model this 8 DOF system in SIMULINK^{TM} the structure and actuator EOMs, Equations 4.43

and 4.44 respectively, are put into state-space form:

$$\left\{ \begin{array}{c} \dot{\underline{\theta}} \\ \ddot{\underline{\theta}} \end{array} \right\} = \left[\begin{array}{cc} [0]_{8 \times 8} & [I]_{8 \times 8} \\ -M^{-1}K & -M^{-1}D \end{array} \right] \left\{ \begin{array}{c} \underline{\theta} \\ \dot{\underline{\theta}} \end{array} \right\} + \left[\begin{array}{c} [0]_{8 \times 8} \\ -M^{-1} \end{array} \right] \underline{f} \qquad (4.47)$$

$$\left\{ \begin{array}{c} \dot{\underline{\eta}} \\ \ddot{\underline{\eta}} \end{array} \right\} = \left[\begin{array}{cc} [0]_{8 \times 8} & [I]_{8 \times 8} \\ -\omega_f^2 [I]_{8 \times 8} & -2\zeta_f \omega_f [I]_{8 \times 8} \end{array} \right] \left\{ \begin{array}{c} \underline{\eta} \\ \dot{\underline{\eta}} \end{array} \right\} + \left[\begin{array}{c} [0]_{8 \times 8} \\ [I]_{8 \times 8} \end{array} \right] \underline{h} \qquad (4.48)$$

The PPF tuning parameters are set using the same values as for the 4 DOF system: $\mu = 0.4$, $\zeta_f = 0.4$, and $\omega_f = \omega_n$. The gain matrices for the adaptive estimators, Γ_{ri}, are assumed identical for each blade. The same values were used as for the 4 DOF system, $\Gamma_r = 10^2 I$.

The system is subjected to the cyclic disturbance, developed in Section 3.3.2, with $E_o = 3$. The disturbance frequency is still equal to the lowest natural frequency of the system, $\omega_d = \omega_n$. Thus, from Equation 3.34, the disturbance force is given by

$$f_{di} = 10 \cos{(\omega_d t + \phi_i)} \qquad \phi_i = \frac{3\pi(i-1)}{4} \qquad i = 1, \ldots, 8 \qquad (4.49)$$

4.2.4.1   Tuned System.   As in previous simulations, for the tuned system, all of the carts have identical: blade length, $L = 1$ m; mass, $m_i = 1$ Kg; stiffness, $k_{0i} = 100$ N/m; and coupling, $k_{ij} = k_c = 5$ N/m, where $i, j = 1...8$. Also, a structural damping ratio of $\zeta_n = 0.002$ is assumed.

4.2.4.2   Mistuned System.   The mistuning pattern used for the simulation is the same as the one used by Duffield [5]: $\Delta k_{01} = 0.01227$, $\Delta k_{02} = 0.0003$, $\Delta k_{03} = -0.0003$, $\Delta k_{04} = -0.0038$, $\Delta k_{05} = -0.0117$, $\Delta k_{06} = -0.0012$, $\Delta k_{07} = -0.007$, and $\Delta k_{08} = 0.0126$. These values result in a $\sigma = 0.0086$, and a mean = 0.0001. The individual cart stiffness parameters are then calculated by $k_{0i} = k_0(1 + \Delta k_{0i})$, where $k_0 = 100$ N/m is the nominal stiffness. The rest of the parameters remain unchanged from the tuned system.

4.2.5 Results. The SIMULINK^{TM} model of the 8 blade system with Adaptive/PPF control on all carts is shown in Figure A.8 on p. A-25. The MATLAB^{TM} code used to run the simulation is given in Appendix A.5.1, beginning on p. A-26. The MATLAB^{TM} code used to find the system RMS responses is given in Appendix A.5.2, beginning on p. A-29.

The uncontrolled response of the 8 blade system is shown in Figure 4.30. The steady state response is nearly half that of the 4 DOF system, Figure 4.1. The response of the system with Adaptive/PPF control turned on is shown in Figures 4.31 through 4.35. Note that plots are only shown for blades 1 through 4, in order to reduce the number of graphs presented. The plots for blades 5 through 8 are very similar, if not identical, to the first four blades.

It is immediately obvious that the controller still looses tracking, causing the displacement response to pulse in amplitude at regular intervals. This occurs initially much sooner than the 4 DOF system, and at shorter intervals. As before, the pulses occur when the parameter estimates loose convergence, and then reacquire. Also, the two estimators for each parameter still find equal and opposite solutions.

The maximum RMS responses for the tuned and mistuned systems, with $E_o = 3$, are shown in Figure 4.36; note that the plots are normalized by the mistuned response. As you can plainly see, the response of the mistuned system is everywhere greater than the tuned system; there is approximately a 20% increase in the maximum blade amplitude. It is also noted that the mistuned system has several distinct peaks due to mode localization.

Next, the three control configurations (Adaptive/PPF, Adaptive-Only, and PPF-Only) along with the uncontrolled system are compared using the maximum RMS of the blade displacements. The results are shown in Figure 4.37 for the tuned system, and in Figure 4.38 for the mistuned system. Note that each plot is normalized by the maximum RMS for its uncontrolled case. As you can see, in both the tuned and mistuned systems, the Adaptive-Only control produces poorer results than the uncontrolled system at all frequencies. It is also noted that the Adaptive/PPF and PPF-Only controls perform
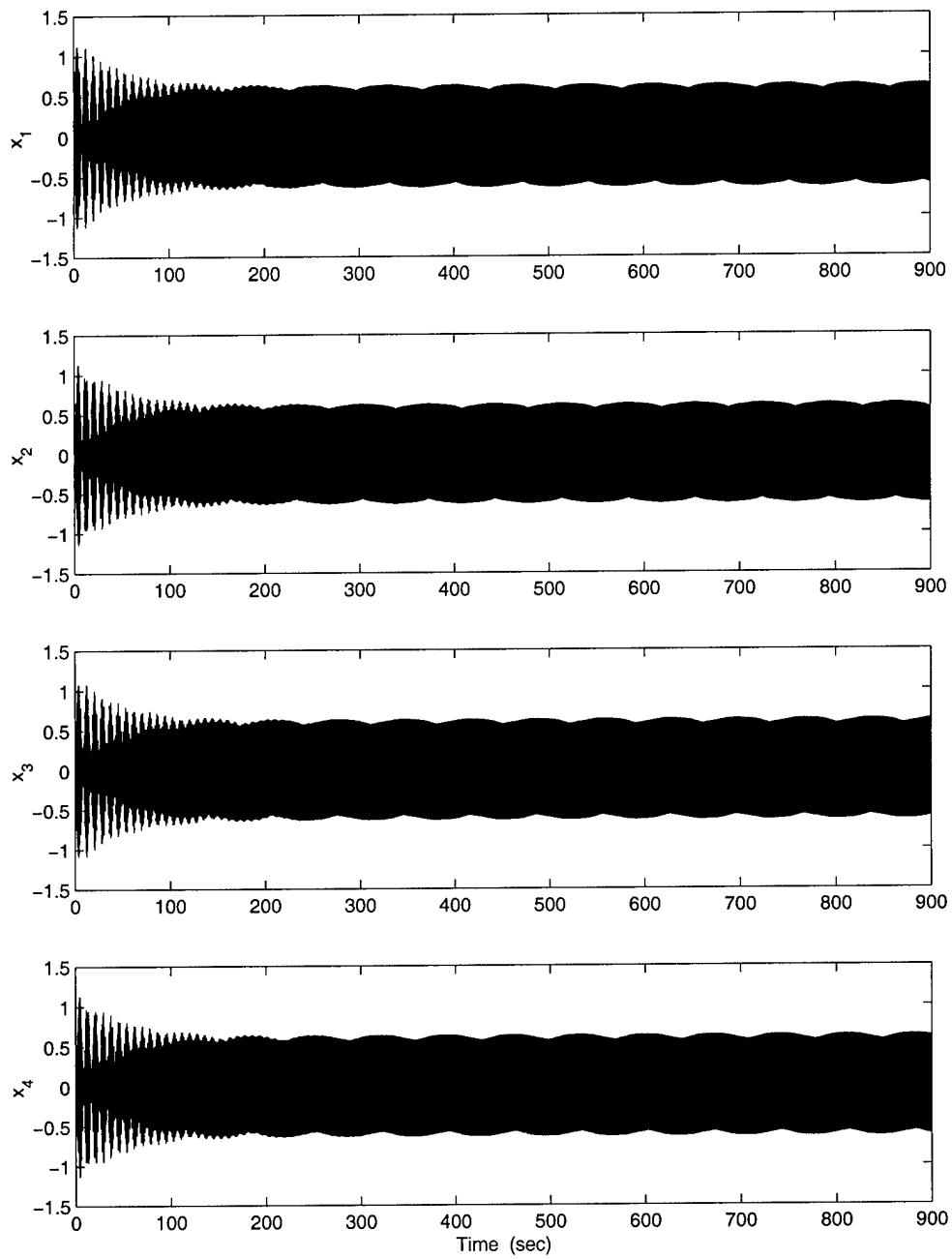
Figure 4.30   Displacements (m) for the Tuned 8 Blade System: Uncontrolled, Cyclic Disturbance, $E_o = 3$, $\Gamma_r = 10^2\,\mathrm{I}$
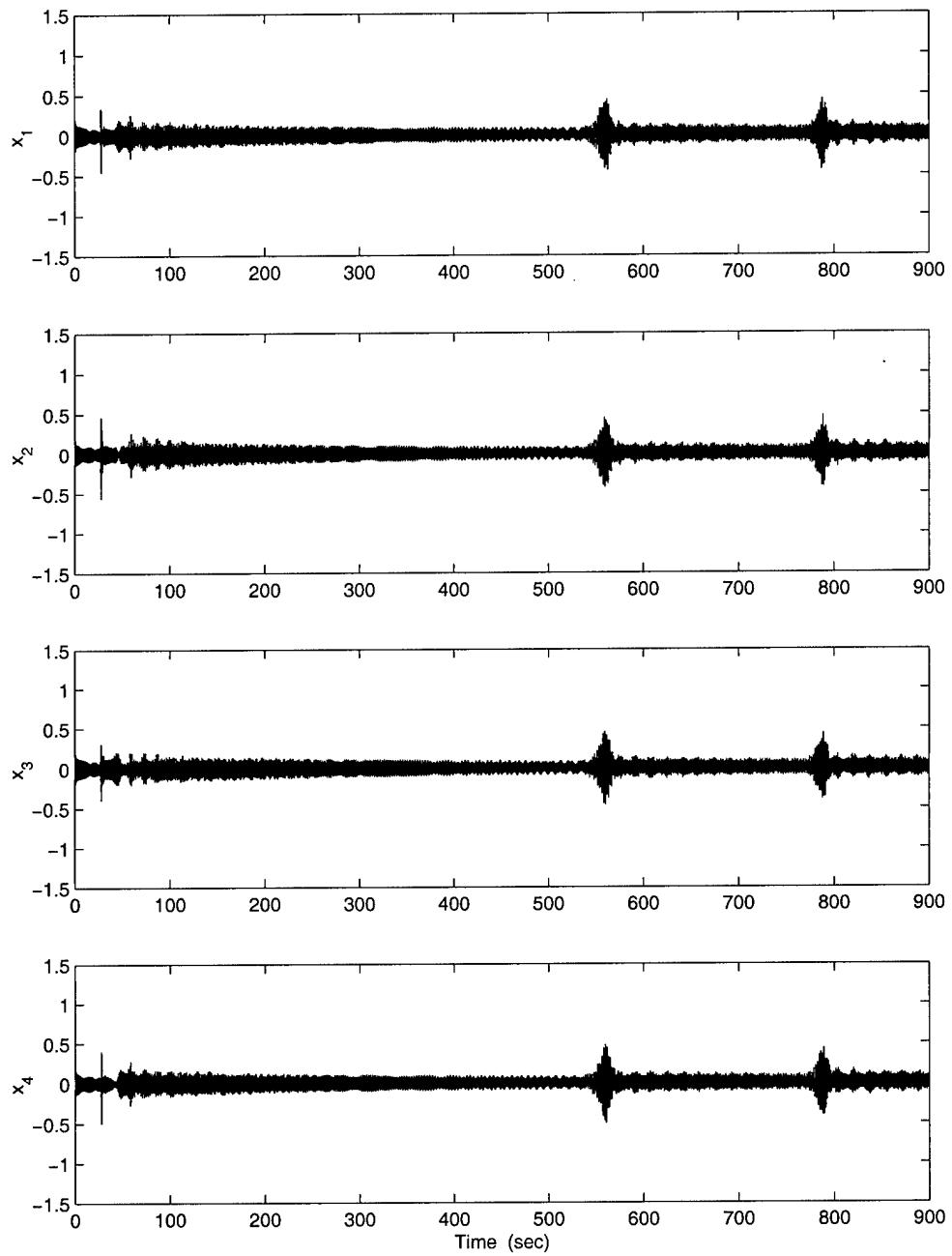
Figure 4.31   Displacements (m) for the Tuned 8 Blade System: Adaptation/PPF Both on, Cyclic Disturbance, $E_o = 3$, $\Gamma_r = 10^2\,\mathrm{I}$
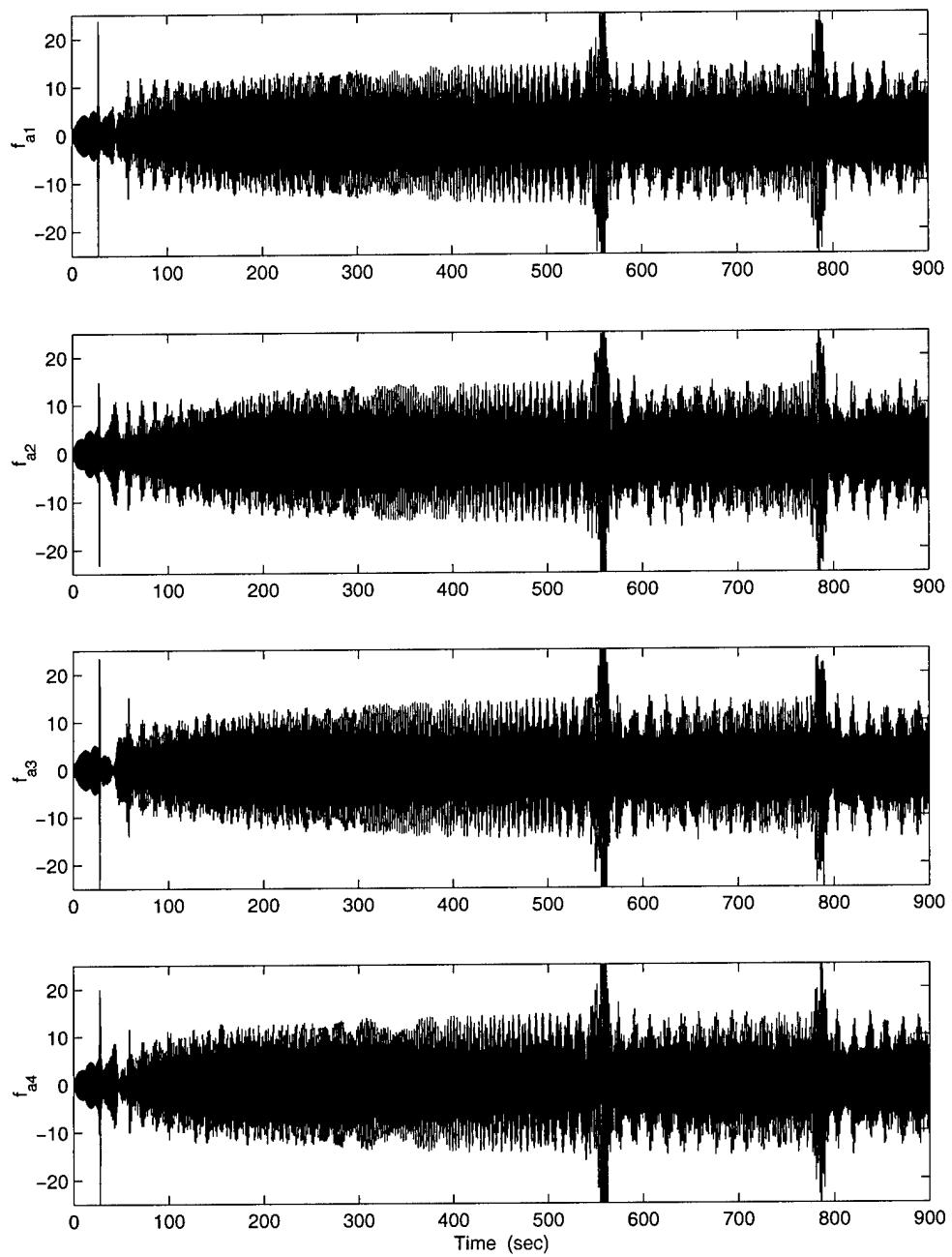
Figure 4.32   Adaptive Forces (N) for the Tuned 8 Blade System: Adaptation/PPF Both on, Cyclic Disturbance, $E_o = 3$, $\Gamma_r = 10^2 \, \mathrm{I}$
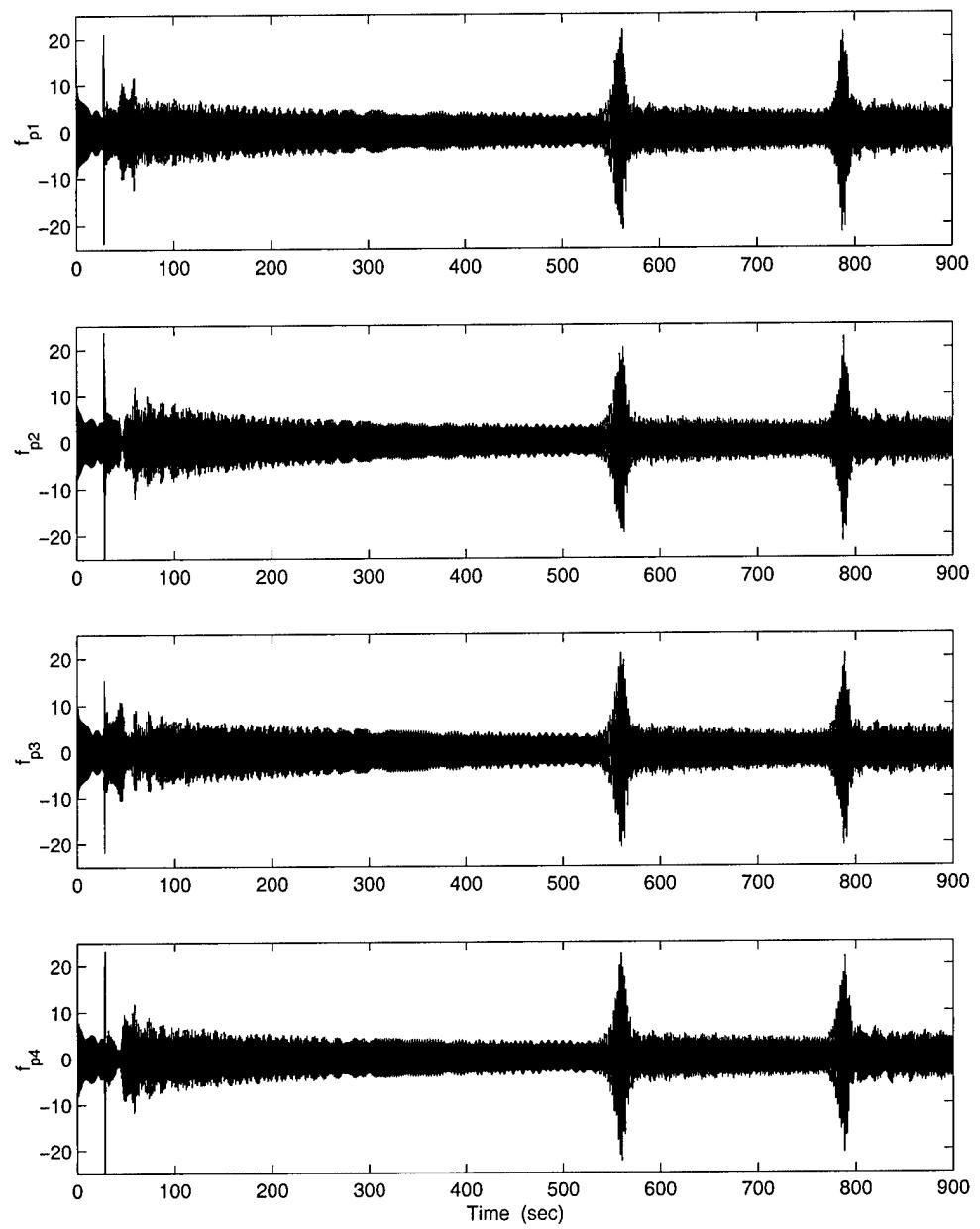
Figure 4.33   PPF Forces (N) for the Tuned 8 Blade System: Adaptation/PPF Both on, Cyclic Disturbance, $E_o = 3$, $\Gamma_r = 10^2\,\mathrm{I}$
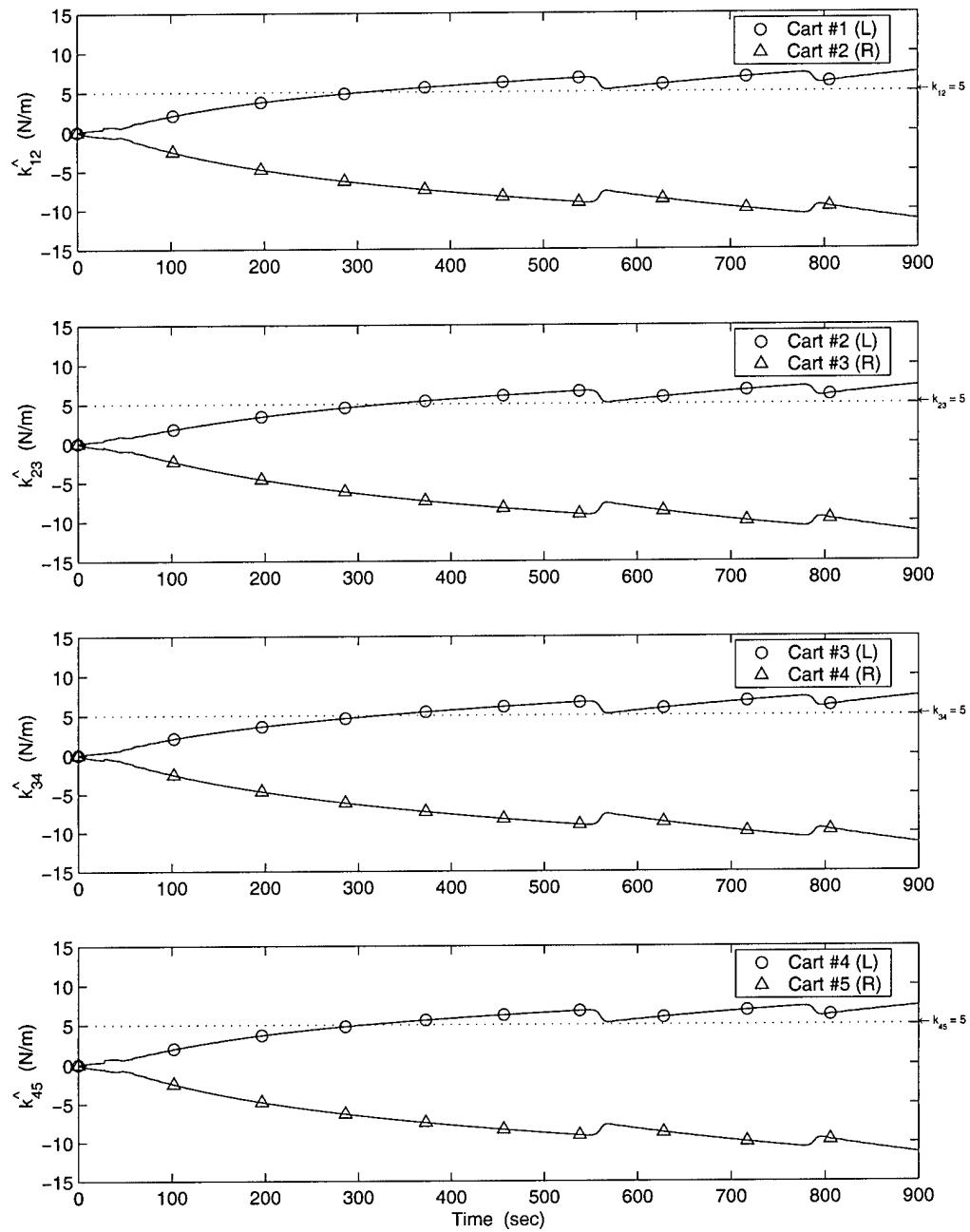
Figure 4.34   Stiffness Parameter Estimates for the Tuned 8 Blade System: Adaptation/PPF Both on, Cyclic Disturbance, $E_o = 3$, $\Gamma_r = 10^2\,I$
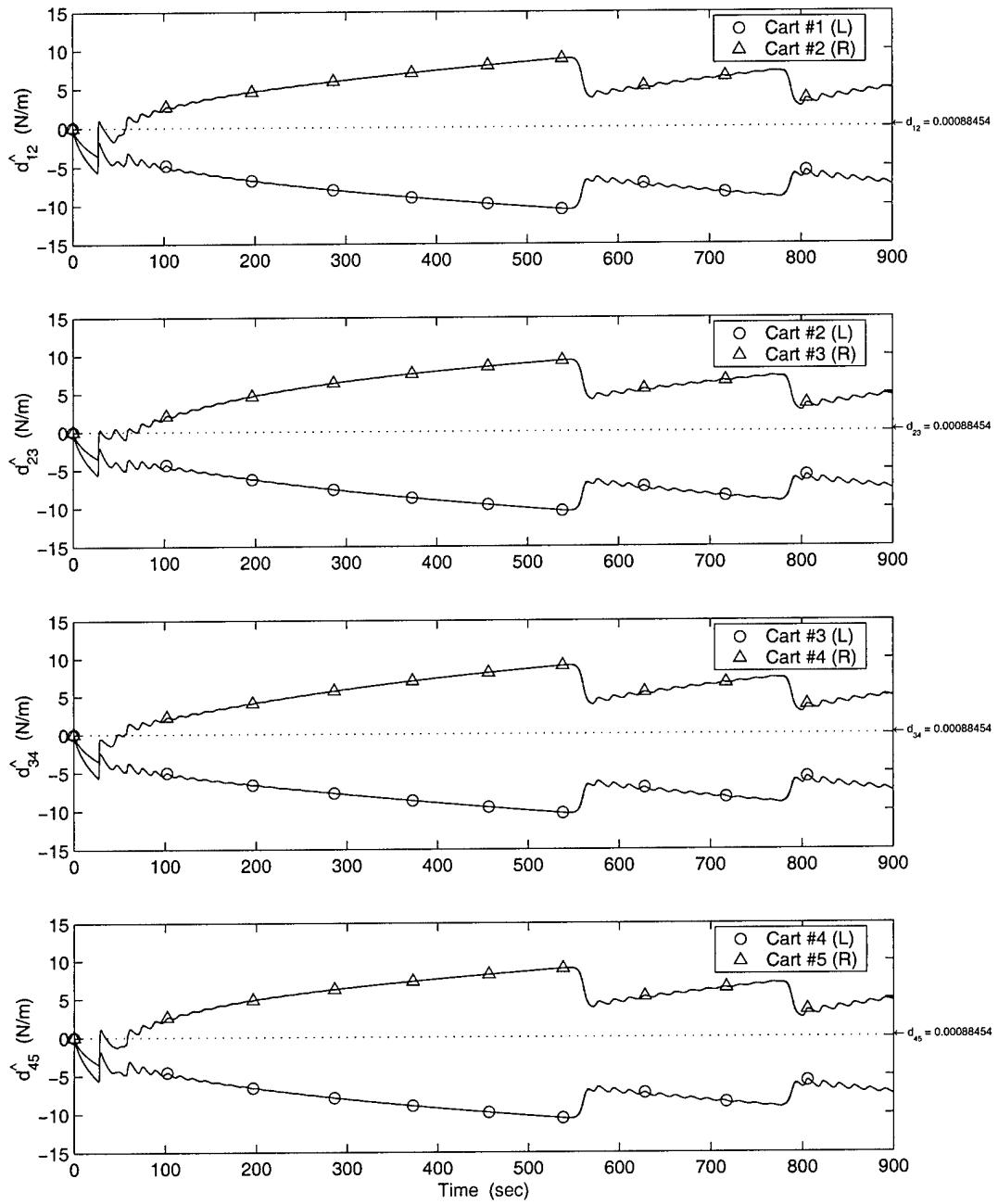
Figure 4.35   Damping Parameter Estimates for the Tuned 8 Blade System: Adaptation/PPF Both on, Cyclic Disturbance, $E_o = 3$, $\Gamma_r = 10^2\,\mathrm{I}$
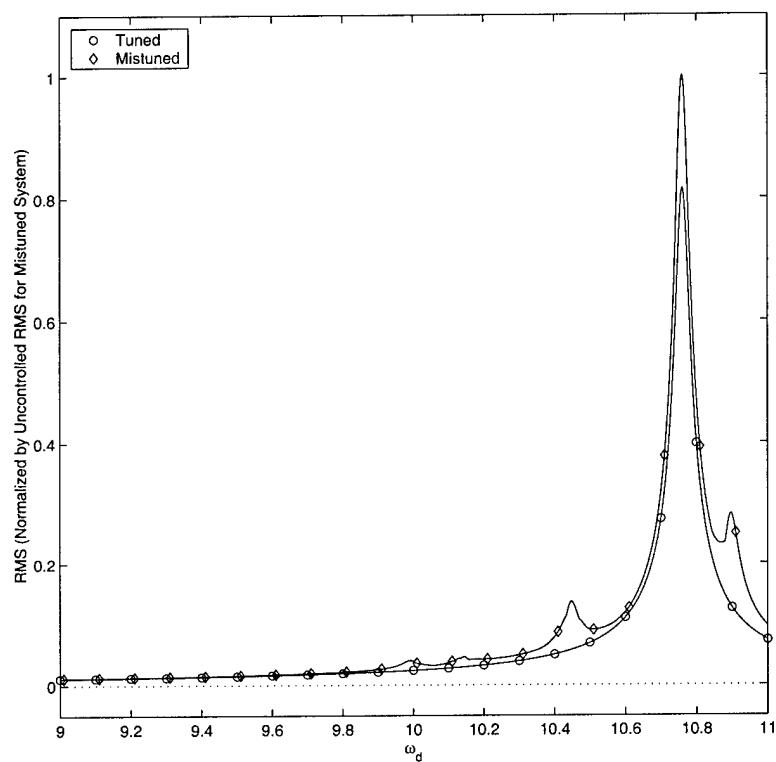
Figure 4.36   Comparison of Maximum RMS of Displacements for the Tuned & Mistuned
Cyclic Systems: Uncontrolled, Cyclic Disturbance, $E_o = 3$
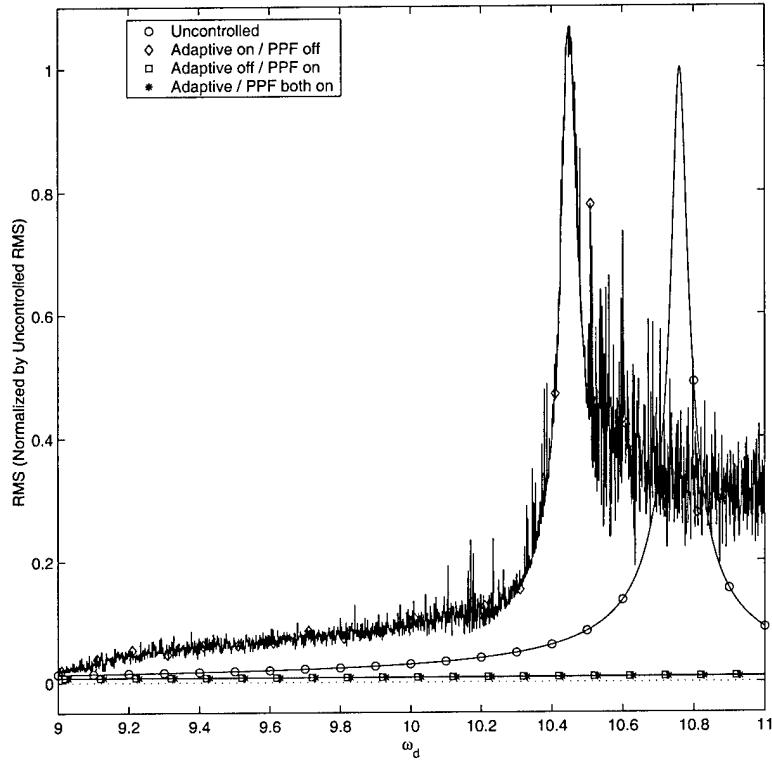
Figure 4.37   Maximum RMS of Displacements for the Tuned 8 Blade System: Cyclic
Disturbance, $E_o = 3$

equally well, resulting in a near zero response. Therefore, even though the uncontrolled response of the mistuned system is substantially greater than the tuned system, it performs as well as the tuned system when PPF control is used.

4.2.5.1 Summary.
The 8 blade system behaved much like the 4 DOF system. For $E_o = 3$, the controller still looses tracking, causing the displacement amplitudes to pulse at regular intervals. These pulses coincide with the parameter estimates converging and then immediately loosing convergence. As before, the two estimators for each parameter are finding equal and opposite solutions.

It was demonstrated that the uncontrolled mistuned system is everywhere greater than the tuned system, peaking at nearly 20%. The results presented in Figure 4.36, are dynamically similar to those found by Duffield in his numerical simulations for $E_o = 3$ [5].
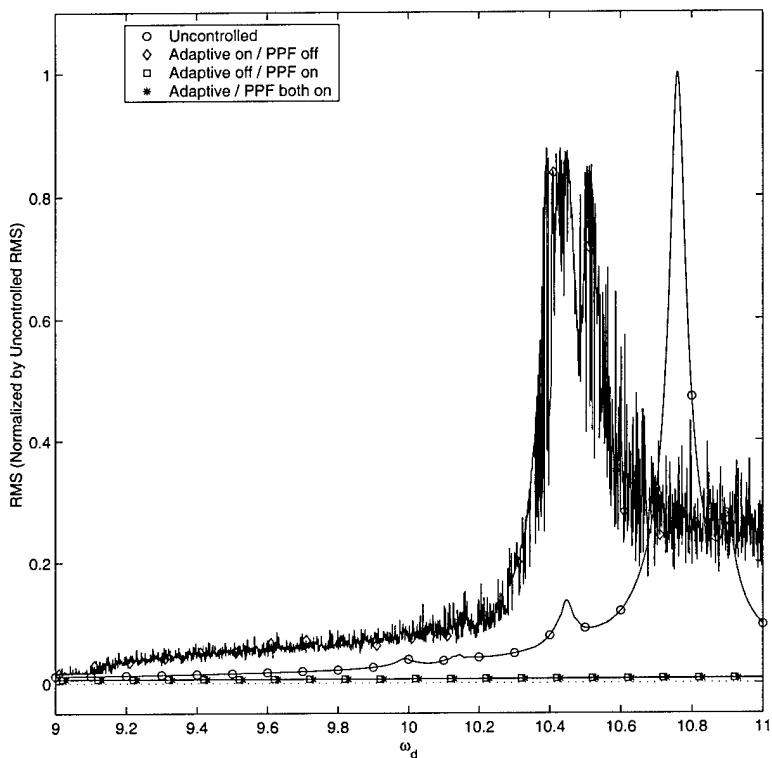
Figure 4.38   Maximum RMS of Displacements for the Mistuned 8 Blade System: Cyclic Disturbance, $E_o = 3$

He went on to demonstrate similar mistuning effects experimentally. Thus, it is reasonable to expect that the theoretical controls used here, may be as effective on experimental hardware.

Finally, using maximum RMS plots, it was shown that Adaptive/PPF and PPF-Only controls perform equally well, resulting in a near zero response.

4.3   Synopsis

In this chapter, the Adaptive/PPF control developed in Chapter 3 was expanded to controlling all of the DOFs of an RPS. The Adaptive/PPF control and parameter estimation law were rederived in generic terms. It was then inductively proven that this new system is stable. Finally, simulations were run with the 4 DOF cart model used previously, and a model of an 8 blade compressor disk. These systems were subjected to a cyclic disturbance with various engine orders. The systems were also mistuned to study the effects. Response plots were presented and discussed.

In the next and final chapter, the results of all the previous chapters are summarized. Overall conclusions and recommendations for future areas of research are also presented

V. Conclusions and Recommendations

5.1 Summary

The research goal was to suppress vibrations in a rotationally periodic structure (RPS) analogous to a compressor bladed disk. To that end, this thesis dealt with three primary theories. First, the hybrid active/passive piezoelectric shunt network developed by Wang and Tang [18] for an RPS was studied. While providing excellent performance, it requires prior knowledge of the inter-blade coupling strength, a quantity not well defined. It was also shown that the passive part of the system must be actively synthesized for practical applications. Next, the active control theory of positive position feedback (PPF) was discussed [8]. It was proven that this method is guaranteed stable under certain restrictions. The "optimal" PPF tuning parameters were found through numerical simulation. Finally, an adaptive parameter estimation and control technique suggested by Ertur, et al, was explored [6]. Their method cancels unknown bounded disturbances while compensating for uncertainties.

The main objective of this thesis was to use Ertur's adaptive control technique to eliminate the inter-blade coupling forces. In addition, PPF was shown to be a purely active replacement for the passive piezoelectric shunt. In Chapter 3, the adaptive control and PPF techniques were combined into a single control law. This was used to suppress the vibrations of a single DOF in a 4 DOF system. Then, in Chapter 4, the Adaptive/PPF control theory was expanded to suppress vibrations in all of the substructures of an RPS. Finally, this new control was used with a simulated 8 blade compressor disk subjected to a cyclic disturbance. The effects of changing the engine order of the disturbance and mistuning the stiffness of the structure were studied.

5.2 Conclusions

5.2.1 Adaptive Control for a Single DOF.
Adaptive control by itself was first used to control a single DOF. The controller was applied to cart 2 of a 4 cart chain system, with a sinusoidal disturbance on cart 3. For this set-up, adaptive control

completely suppressed the response of cart 2. It was shown that the parameter estimator requires a minimum level of input in the uncontrolled coordinates to work properly. Since cart 1 is isolated from the disturbance, its response was negligible. The estimator was unable to determine the parameters between carts 1 & 2 in this case. However, when the system was changed to a cyclic system, and cart 1 was no longer isolated from the disturbance, all of the parameters converged quickly.

When the other inputs to the estimation law are at acceptable levels, the individual estimator gains ($\gamma_1, \ldots, \gamma_4$) allow for some adjustments in the convergence of the stiffness and damping parameter estimates. That is, of course, if you are in the neighborhood of a feasible solution. There are some combinations of the gains which will cause the estimates to diverge from the correct values. This is unacceptable in a real system, because it will eventually saturate some component or computer registry. It is important to note that even if the parameters converge to the wrong values, the response of the system may be substantially reduced.

Finally, it should be pointed out, that the actual values of the estimated parameters are unknown in a real system. That is in fact why they are estimated. This raises the question, should the gains be set to drive the estimates to uncertain parameter values, or should the deciding factor merely be system performance.

5.2.2 Adaptive/PPF Control for a Single DOF.

Next, Adaptive/PPF control was used on cart 2 of the 4 cart cyclic system. The response was completely suppressed and all parameters converged quickly to their correct values. The response was also completely suppressed when the system was subjected to a harmonic disturbance that cycled between all carts. However, the parameter estimates did not converge to the correct values; in fact, one of them even converged to a negative value. There are two possible causes for these problems. First, recall that in the development of the adaptive estimator, there is no guarantee that the parameter estimates will converge. In fact, there is no guarantee that there is a unique solution to the estimation law. The estimator may find a solution where the estimates do not converge to the correct values, but still produce a control force that results in good performance. The second possible cause is

that there is a disturbance applied to cart 2. Even though all of the stability requirements were met, Ertur's adaptive control technique was not developed with a disturbance applied directly to the controlled coordinate. Once again, excellent performance was achieved with poor parameter estimates.

There are three possible control configurations for this system: Adaptive/PPF, Adaptive-Only, and PPF-Only. The average RMS response of cart 2 was calculated for each configuration over a range of disturbance frequencies. When compared, it was shown that Adaptive-Only and Adaptive/PPF control performed the best. However, PPF-Only control performed satisfactorily as well.

5.2.3 Adaptive/PPF Control for all DOFs.

Finally, Adaptive/PPF control was used on all DOFs of the four cart cyclic system and an 8 blade compressor model. When the system is subjected to the cyclic disturbance with $E_o = 1$ or 3, the responses of all substructures were substantially reduced, but not completely suppressed like they were for the single control system. There are also regular periods when the controller seems to loose tracking, and the response pulses to a higher amplitude, which is still lower than the uncontrolled system.

The parameter estimates nearly converge, immediately loose convergence, and then attempt to reacquire. This creates a distinctive sawtooth pattern in the estimate plots. The pulses noted in the response plots correspond to when the parameter estimates loose convergence. Of greater concern, however, is that the two estimators for each parameter are finding equal and opposite solutions. The only difference between $E_o = 1$ & 3, was that the equal and opposite parameter estimates were reversed. Once again, recall that the adaptive technique does not guarantee that the estimates will converge, or that there is even a unique solution. While the solutions for the parameter estimates may not always be correct, they can still provide acceptable response reduction in some cases.

The simulation was run again with $E_o = 4$ & 12, which produced identical responses to each other. However, the steady state response was slightly greater than for $E_o = 1$ or 3, and there was no pulsing, or loss of convergence. This is most likely because the two estimators for each parameter find the same solution in this case. Unfortunately, the

parameters diverge. It is not surprising that identical responses occur when $E_o = 4 \& 12$; engine orders with similar forcing phase angles should produce similar responses. This is also most likely the reason that $E_o = 1 \& 3$ are producing equivalent responses, but the parameter estimates are reversed. The nominal phase angles for these two cases are equivalent, but opposite in phase.

Mistuning effects on the system were also studied. The simulation demonstrated the occurrence of mode localization; some of the substructures had higher steady state amplitudes than the others. When Adaptive/PPF control was turned on, the effects of mode localization were nullified, and all substructures had identical responses. For the 8 blade model, it was shown that the maximum RMS response for the mistuned system had several distinct peaks, due to mode localization, and was everywhere greater than the tuned response. This is an important finding since it is similar to results reported by Duffield [5]. He went on to demonstrate equivalent mistuning effects experimentally. Thus, it is reasonable to expect that the theoretical controls used here, may be as effective on experimental hardware.

Finally, the three control configurations (Adaptive/PPF, Adaptive-Only, and PPF-Only) were again compared using the average RMS plots. For both the tuned and mistuned systems, it was obvious that the Adaptive/PPF and PPF-Only controls performed equally well, resulting in a near zero response. When Adaptive-Only control was used, it produced very poor results, and at best was no better than the uncontrolled system. This is quite different from the single control case. Recall for the single control system, Adaptive/PPF control and Adaptive-Only control provided nearly identical reduction in the response. When adaptive control was used on a single cart, it was able to isolate it from the others, and completely suppressed the response. It appears now, however, that the adaptive estimators on each cart work against each other.

5.2.4 Overall.

Adaptive control appears to work well when it is only controlling a single DOF, and there is no direct disturbance. However, there are several problems with the theory when you attempt to control all the substructures of an RPS subjected to a cyclic disturbance. First, it was shown that adaptive control used by itself actually

causes a poorer response than the uncontrolled system, most likely because the adjacent estimators are working against each other. Second, Adaptive/PPF and PPF-Only controls performed equally well. It is therefore surmised that the PPF is just overpowering the adaptive part. Finally, the estimator solution is not unique; excellent performance is achieved, even when the parameter estimates do not converge to the correct values. In the end, adaptive control is not worth the extra effort required to determine the estimator gains to achieve convergence to uncertain values.

PPF, on the other hand, works well when controlling a single substructure of an RPS or all of them. It is guaranteed stable, and it was shown to provide broadband vibration suppression. In contrast to Wang and Tang's piezoelectric shunt network, PPF does not require any prior knowledge of the coupling strength, and excellent performance was achieved with suboptimal PPF tuning parameters. For these reasons, it is therefore concluded that PPF is the best option for vibration suppression in a compressor bladed disk.

5.3 Recommendations for Future Research

First and foremost, the theoretical results presented here should be verified experimentally. Duffield describes an 8 bladed experimental test article that he used for modal testing [5]. A cyclic disturbance, similar to the one used here, was created by placing opposing magnets on the blade tips, and on a rotating flywheel in front of the bladed disk. With piezoelectric patches attached to each blade, this set-up could be used to test the Adaptive/PPF control law experimentally.

Second, in this research, PPF provided excellent performance with suboptimal tuning parameters. However, this might not be the case for all systems. Ideally, an analytical solution for the optimal PPF tuning parameters would be best. However, if this is not possible, the problem should be studied with numerical optimization techniques. Preliminary work suggests that the PPF problem can be set up as an H_2 or H_∞ control problem. This would allow for easier application of the control actuator.

Third, the numerical simulations in this research used a single coupling strength and mistuning pattern. Further characterization of the system should be accomplished by studying the effects of varying these parameters.

Finally, while adaptive control proved ineffective for this system, the theory is not completely without merit. However, further study is required in several areas. The estimator solution is not unique. This may be why acceptable performance is sometimes achieved even though the parameter estimates diverge from the correct values, or become negative. A procedure for selecting the estimator gains should be developed, so that the parameter estimates are driven to the desired solution. Also, the interaction of multiple estimators should be investigated, to ensure that they are not working against each other.

Appendix A. $SIMULINK^{TM}$ Models and $MATLAB^{TM}$ Code

A.1 PPF Parameter Determination for 1 DOF System

PPF for One Cart
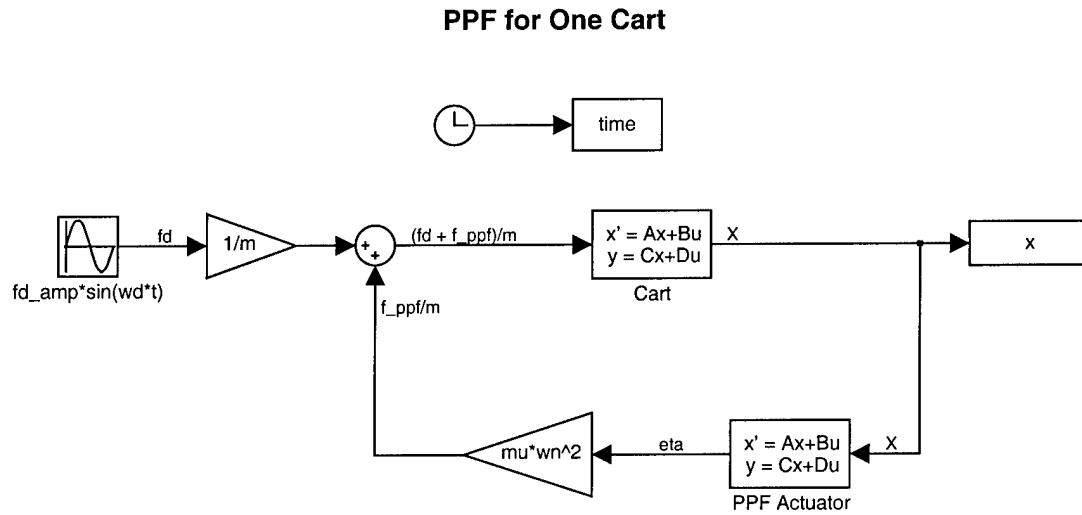
Figure A.1   Simulink Model for 1 DOF PPF Parameter Determination

A.1.1 Matlab Code for PPF Gain Determination.

```
% ppf1_mu_rms.m
%
%  This m-file runs PPF on a single cart.  The value of the PPF gain, mu,
%  is varied from 0 to 1.  For each mu, the disturbance freq is swept over
%  a range of values and the RMS of the signal is found.


clear all; close all;

tfinal = 60;


% System parameters

m = 1; ko = 100; kc = 5;   zeta_n = 0.01;     % units:  [m] = Kg, [k] = N/m


% Determine natural freq of cart (wn)

wn = sqrt((ko + 2*kc)/m);  % units:  [wn] = rad/sec


% Set disturbance parameters
```

```
fd_amp = 10;


% Set PPF parameters

wf = wn;   zeta_f = 0.4;


% Set-up cart state-space

A = [0  1;  -wn^2  -2*zeta_n*wn];


% Set-up PPF state-space

Af = [0  1;  -wf^2  -2*zeta_f*wf];  Bf = [0; wf^2];


% Vary PPF gain to find optimal value

j = 0;

for mu = 0.0:0.1:1,

    j = j + 1;

    if mu == 0.0,  mu_text(j,:) = ['\mu = 0.0'];
        else mu_text(j,:) = ['\mu = ' num2str(mu)];
    end;

    % Iteratively run simulation and determine RMS values

    i = 0;
    for wd = 0:0.02:20
        i = i + 1;  omega(i) = wd;  disp([mu wd]); disp(' ');
        sim('ppf1_sim');
        ibegin  = min(find(time>=tfinal-30));
        x_rms(i,j) = rms(x,ibegin);
        clear x;
    end;

end;


% Save & Plot results

save rms1_mu;

figure;
plot(omega,x_rms);  frame(omega,x_rms,'y',wn);
h = title(['\bf RMS of Displacement for Single Cart System as \mu varies  (\omega_f = \omega_n, \zeta_f = '...
        num2str(zeta_f) ')']);
xlabel('\omega_d  (rad/sec)');  ylabel('RMS'); legend(mu_text);
z = axis;  text(wn, 0.95*z(4), ' \leftarrow \omega_d = \omega_n');
```

A.1.2   Matlab Code for PPF Damping Ratio Determination.

```
% ppf1_zeta_rms.m
%
%  This m-file runs PPF on a single cart.  The value of the PPF damping,
%  zeta_f, is varied from 0 to 1.  For each mu, the disturbance freq is
%  swept over a range of values and the RMS of the signal is found.
```

```
clear all; close all;

tfinal = 60;


% System parameters

m = 1; ko = 100; kc = 5;   zeta_n = 0.01;      % units:  [m] = Kg, [k] = N/m


% Determine natural freq of cart (wn)

wn = sqrt((ko + 2*kc)/m);  % units:  [wn] = rad/sec


% Set disturbance parameters

fd_amp = 10;


% Set PPF parameters

wf = wn;   mu = 0.4;


% Set-up cart state-space

A = [0  1;  -wn^2  -2*zeta_n*wn];


% Vary PPF damping to find optimal value

j = 0;

for zeta_f = 0.0:0.1:0.9,

    j = j + 1;

    zeta_f_test = round(100*zeta_f)
    if zeta_f == 0,   zeta_text(j,:) = ['\zeta_f = 0.00'];
        elseif zeta_f_test == 10,   zeta_text(j,:) = ['\zeta_f = 0.10'];
        elseif zeta_f_test == 20,   zeta_text(j,:) = ['\zeta_f = 0.20'];
        elseif zeta_f_test == 30,   zeta_text(j,:) = ['\zeta_f = 0.30'];
        elseif zeta_f_test == 40,   zeta_text(j,:) = ['\zeta_f = 0.40'];
        elseif zeta_f_test == 50,   zeta_text(j,:) = ['\zeta_f = 0.50'];
        elseif zeta_f_test == 60,   zeta_text(j,:) = ['\zeta_f = 0.60'];
        elseif zeta_f_test == 70,   zeta_text(j,:) = ['\zeta_f = 0.70'];
        elseif zeta_f_test == 80,   zeta_text(j,:) = ['\zeta_f = 0.80'];
        elseif zeta_f_test == 90,   zeta_text(j,:) = ['\zeta_f = 0.90'];
        else zeta_text(j,:) = ['\zeta_f = ' num2str(zeta_f)];
    end;


    % Set-up PPF state-space

    Af = [0  1;  -wf^2  -2*zeta_f*wf];  Bf = [0; wf^2];


    % Iteratively run simulation and determine RMS values

    i = 0;
    for wd = 0:0.02:20
        i = i + 1;  omega(i) = wd;  disp([zeta_f wd]); disp(' ');
```

```
       sim('ppf1_sim');
       ibegin  = min(find(time>=tfinal-30));
       x_rms(i,j) = rms(x,ibegin);
       clear x;
    end;

end;


% Save & Plot results

save rms1_zeta;

figure;
plot(omega,x_rms);  frame(omega,x_rms,'y',wn);
h = title(['\bf RMS of Displacement for Single Cart System as \zeta_f varies  (\omega_f = \omega_n, \mu = '...
     num2str(mu) ')']);
xlabel('\omega_d  (rad/sec)');  ylabel('RMS'); legend(zeta_text);
z = axis;  text(wn, 0.5*z(4), ' \leftarrow \omega_d = \omega_n');
```

A.1.3   Matlab Code for PPF Frequency Determination.

```
% ppf1_wf_rms.m
%
%  This m-file runs PPF on a single cart.  The value of the PPF damping,
%  wf, is varied from 0 to 20.  For each wf, the disturbance freq is
%  swept over a range of values and the RMS of the signal is found.


clear all; close all;

tfinal = 60;


% System parameters

m = 1; ko = 100; kc = 5;  zeta_n = 0.01;     % units:  [m] = Kg, [k] = N/m


% Determine natural freq of cart (wn)

wn = sqrt((ko + 2*kc)/m); % units:  [wn] = rad/sec


% Set disturbance parameters

fd_amp = 10;


% Set PPF parameters

mu = 0.4;  zeta_f = 0.4;


% Set-up cart state-space

A = [0  1;  -wn^2  -2*zeta_n*wn];


% Vary PPF freq to find optimal value

j = 0;
```

```
for wf = 0:20,

    j = j + 1;

    if wf < 10, wf_text(j,:) = ['\omega_f =  ' num2str(wf)];
        else    wf_text(j,:) = ['\omega_f = ' num2str(wf)];
    end;

    % Set-up PPF state-space

    Af = [0  1;  -wf^2  -2*zeta_f*wf];  Bf = [0; wf^2];


    % Iteratively run simulation and determine RMS values

    i = 0;
    for wd = 0:0.02:20
        i = i + 1;  omega(i) = wd;  disp([wf wd]); disp(' ');
        sim('ppf1_sim');
        ibegin  = min(find(time>=tfinal-30));
        x_rms(i,j) = rms(x,ibegin);
        clear x;
    end;

end;


% Save & Plot results

save rms1_wf;

figure;
plot(omega,x_rms);  frame(omega,x_rms,'y',wn);
h = title(['\bf RMS of Displacement for Single Cart System as \omega_f varies  (\zeta_f = '...
      num2str(zeta_f) ', \mu = ' num2str(mu) ')']);
xlabel('\omega_d  (rad/sec)');  ylabel('RMS'); legend(wf_text);
z = axis;  text(wn, 0.5*z(4), ' \leftarrow \omega_d = \omega_n');
```

A.2   Simulation of the Adaptive 4/1 DOF System

This section contains Matlab and Simulink files for the Adaptive 4 DOF system, with only 1 DOF controlled.

Adaptive System: 4 carts, controling only 1
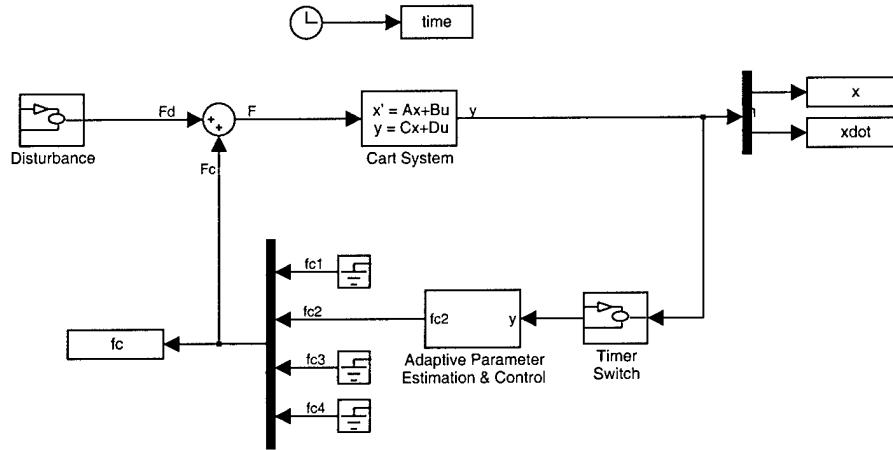
Figure A.2   Simulink Model for Adaptive 4 DOF System, with 1 DOF Controlled

Adaptive Parameter Estimation & Control Law Sub-system
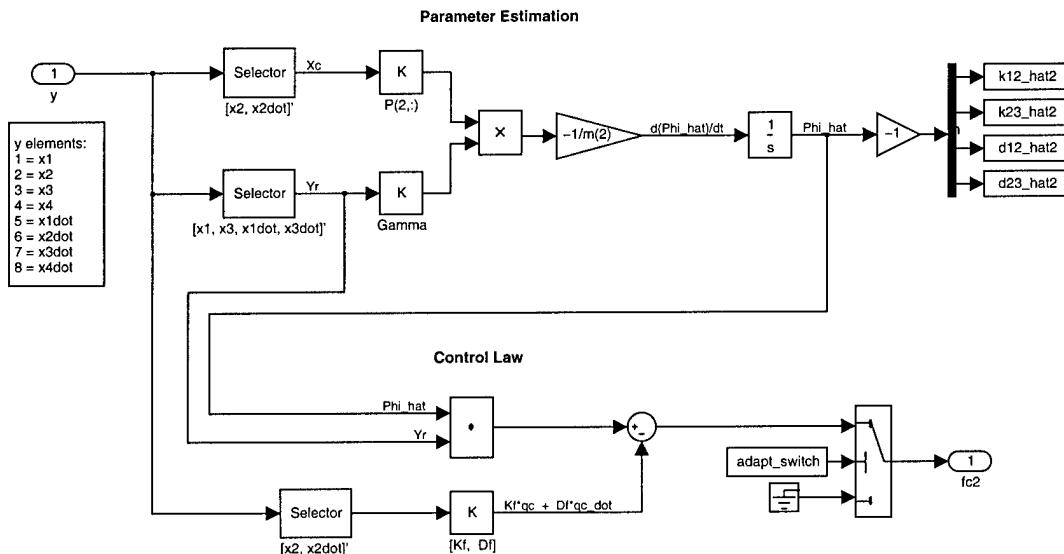
Figure A.3   Adaptive Parameter Estimation and Control Sub-system from Model in Figure A.2

A.2.1   Matlab Code for Adaptive 4/1 DOF Chain System.

```
% adaptive41t_chain.m
%
%  This m-file runs a 4 cart chain system with adaptive parameter estimation
%  and control on cart #2 only.


clear all; close all;

print_switch = 0;       % Sends plots to printer if = 1
eps_switch   = 0;       % Saves plots to eps file if = 1


% Simulation parameters

tfinal = 60;

adapt_switch   = 1;  % turn adaptive control on (1) / off(0)
disturb_switch = 2;  % disturbance on cart #3:  1 = random, 2 = sine

timer_switch = 10;   % adaptive control is off at the beginning of the sim
                     % and turned on after this many seconds


% System parameters

N = 4;               % number of carts
zeta_n = 0.01;       % damping ratio
ko = 100; kc = 5;    % ground & coupling stiffness, [k] = N/m

m(1) = 1;   m(2) = 1;   m(3) = 1;   m(4) = 1;   % [m] = Kg
k0(1)= ko;  k0(2)= ko;  k0(3)= ko;  k0(4)= ko;  % [k] = N/m
k12  = kc;  k23  = kc;  k34  = kc;  k41  = 0;   % k41 = 0 b/c it's a chain system

M = diag([m(1) m(2) m(3) m(4)]); M_inv = diag(1./[m(1) m(2) m(3) m(4)]);

K = [ k0(1)+k12+k41    -k12            0               -k41;
      -k12             k0(2)+k12+k23   -k23            0;
      0                -k23            k0(3)+k23+k34   -k34;
      -k41             0               -k34            k0(4)+k34+k41];


% Determine lowest natural freq of the undamped cart system (wn)

[evalues,evectors] = eign(K,M);
wn  = sqrt(min(evalues));       % lowest natural freq, [wn] = rad/sec


% Form the damping matrix (D) from K, zeta_n, & the evectors

D = real(evectors*(2*zeta_n*sqrt(evectors'*K*evectors))*evectors');
for i = 1:N,  for j = 1:N,  if K(i,j) == 0,  D(i,j) = 0;  end;  end;  end;
d12 = -D(1,2);  d23 = -D(2,3);  d34 = -D(3,4);  d41 = -D(4,1);

% Partition out controlled part of system matrices

Mc = M(2,2);  Kc = K(2,2);  Dc = D(2,2);

Mu = diag([M(1,1)  M(3,3)  M(4,4)]);   Mu_inv = diag([1/M(1,1)  1/M(3,3)  1/M(4,4)]);
Ku = diag([K(1,1)  K(3,3)  K(4,4)]);
Du = diag([D(1,1)  D(3,3)  D(4,4)]);


% Set adaptation parameters and find P
```

```
Gain = 1e4;  Gamma = Gain*diag([6 1 0.00045 1]);
%Gain = 1e4;  Gamma = Gain*diag([1 1 1 1]);

wf = wn;  zeta_f = 0.7;           % freq & damping ratio of adaptive controller
Kf = wf^2*Mc;  Df = 2*zeta_f*wf*Mc; % stiffness & damping for controller

Ac = [0  1;  -(Kc+Kf)/Mc  -(Dc+Df)/Mc];
Q = diag([1  m(2)/K(2,2)]);
P = lyap(Ac',Q);


% Check stability requirments

Au = [zeros(3)  eye(3);  -Mu_inv*Ku  -Mu_inv*Du];

if -abs(real(eig(Ac))) ~= real(eig(Ac)), disp(' '); disp('Ac is not negative definite'); end;
if -abs(real(eig(Au))) ~= real(eig(Au)), disp(' '); disp('Au is not negative definite'); end;
if abs(real(eig(P))) ~= real(eig(P)), disp(' '); disp('P is not positive definite'); end;
if P ~= P', disp(' '); disp('P is not symmetric'); end;


% Set disturbance parameters

fd_amp = 10;    % amplitude of disturbance
amp1 = 0;       % allows for direct forcing on cart #1, fd1 = amp1*fd3
amp2 = 0;       % allows for direct forcing on cart #2, fd2 = amp2*fd3
wd = wn;        % set disturbance freq = natural freq of system
eo = 1;         % engine order for rotary disturbance (not used for this system)



% Set-up the cart state-space system

A = [zeros(N)  eye(N);  -M_inv*K  -M_inv*D];
B = [zeros(N);  M_inv];
C = eye(2*N);


% Run simulation

sim('adaptive41t_sim');


% Generate text for output

ttext = 'Chain System';
if adapt_switch == 1,  ttext = [ttext ' Adaptation on Cart #2 turned on after ' num2str(timer_switch) ' sec.'];
   else  ttext = [ttext ' Adaptation Off'];
end;

if disturb_switch == 1,
     fdtext = ['f_{d3} = Random (mag \leq ' num2str(fd_amp) ')'];
   elseif disturb_switch == 2,
     fdtext = ['f_{d3} = ' num2str(fd_amp) ' sin(' num2str(wd) 't)'];
   elseif disturb_switch == 3,
     fdtext = ['\{f_d\}_i = ' num2str(fd_amp) ' cos(' num2str(wd) 't + \phi_i)'];
end;

fdstr = '_fd3';
if amp2 ~= 0,
   if amp2 == 1, fdtext = [fdtext ', f_{d2} = f_{d3}'];
   else fdtext = [fdtext ', f_{d2} = ' num2str(amp2) '*f_{d3}']; end;
   fdstr = [fdstr '3'];
end;
```

```
if amp1 ~= 0,
   if amp1 == 1, fdtext = [fdtext ', f_{d1} = f_{d3}'];
   else fdtext = [fdtext ', f_{d1} = ' num2str(amp1) '*f_{d3}']; end;
   fdstr = [fdstr '1'];
end;

gtext = [',  \Gamma = 10^{' num2str(log10(Gain)) '} * ' mat2str(diag(Gamma/Gain))];
line2  = ['\rm \fontsize{10}' fdtext  gtext];

dname = ['i:\thesis\figures\appf41\'];

fname = ['adpt41t_chn_d' num2str(disturb_switch) fdstr '_a' num2str(adapt_switch) '_t' num2str(timer_switch)];


% Plot/Save Results

if eps_switch  == 1,
   diary([dname 'appf41_captions.txt']);
   disp([' ';' ']); disp(ttext); disp(' ');
end;

plot41_displacements;
plot41_forces_a;
plot41_parameters;
diary off
```

A.2.2 Matlab Code for Adaptive 4/1 DOF Cyclic System.

```
% adaptive41t_cyclic.m
%
%  This m-file runs a 4 cart cyclic system with adaptive parameter estimation
%  and control on cart #2 only.


clear all; close all;

print_switch = 1;       % Sends plots to printer if = 1
eps_switch   = 1;       % Saves plots to eps file if = 1


% Simulation parameters

tfinal = 60;

adapt_switch = 1;    % turn adaptive control on (1) / off(0)
disturb_switch = 2;  % disturbance on cart #3:  1 = random, 2 = sine

timer_switch = 10;   % adaptive control is off at the beginning of the sim
                     % and turned on after this many seconds


% System parameters

N = 4;               % number of carts
zeta_n = 0.01;       % damping ratio
ko = 100; kc = 5;    % ground & coupling stiffness, [k] = N/m

m(1) = 1;   m(2) = 1;   m(3) = 1;   m(4) = 1;   % [m] = Kg
k0(1)= ko;  k0(2)= ko;  k0(3)= ko;  k0(4)= ko;  % [k] = N/m
k12  = kc;  k23  = kc;  k34  = kc;  k41  = 5;    % k41 = 0 b/c it's a chain system

M = diag([m(1) m(2) m(3) m(4)]); M_inv = diag(1./[m(1) m(2) m(3) m(4)]);
```

```
K = [ k0(1)+k12+k41      -k12                0                   -k41;
        -k12             k0(2)+k12+k23       -k23                0;
        0                -k23                k0(3)+k23+k34       -k34;
        -k41             0                   -k34                k0(4)+k34+k41];


% Determine lowest natural freq of the undamped cart system (wn)

[evalues,evectors] = eign(K,M);
wn  = sqrt(min(evalues));            % lowest natural freq, [wn] = rad/sec


% Form the damping matrix (D) from K, zeta_n, & the evectors

D = real(evectors*(2*zeta_n*sqrt(evectors'*K*evectors))*evectors');
for i = 1:N,  for j = 1:N,  if K(i,j) == 0,  D(i,j) = 0;  end;  end;  end;
d12 = -D(1,2);  d23 = -D(2,3);  d34 = -D(3,4);  d41 = -D(4,1);

% Partition out controlled part of system matrices

Mc = M(2,2);  Kc = K(2,2);  Dc = D(2,2);

Mu = diag([M(1,1)  M(3,3)  M(4,4)]);   Mu_inv = diag([1/M(1,1)  1/M(3,3)  1/M(4,4)]);
Ku = diag([K(1,1)  K(3,3)  K(4,4)]);
Du = diag([D(1,1)  D(3,3)  D(4,4)]);


% Set adaptation parameters and find P

Gain = 1e3;   Gamma = Gain*diag([100 100 1 1]);

wf = wn;  zeta_f = 0.7;              % freq & damping ratio of adaptive controller
Kf = wf^2*Mc;  Df = 2*zeta_f*wf*Mc; % stiffness & damping for controller

Ac = [0  1;  -(Kc+Kf)/Mc  -(Dc+Df)/Mc];
Q = diag([1  m(2)/K(2,2)]);
P = lyap(Ac',Q);


% Check stability requirments

Au = [zeros(3)  eye(3);  -Mu_inv*Ku  -Mu_inv*Du];

if -abs(real(eig(Ac)))  ~= real(eig(Ac)), disp(' '); disp('Ac is not negative definite'); end;
if -abs(real(eig(Au)))  ~= real(eig(Au)), disp(' '); disp('Au is not negative definite'); end;
if abs(real(eig(P)))  ~= real(eig(P)), disp(' '); disp('P is not positive definite'); end;
if P ~= P', disp(' '); disp('P is not symmetric'); end;


% Set disturbance parameters

fd_amp = 10;    % amplitude of disturbance
amp1 = 0;       % allows for direct forcing on cart #1, fd1 = amp1*fd3
amp2 = 0;       % allows for direct forcing on cart #2, fd2 = amp2*fd3
wd = wn;        % set disturbance freq = natural freq of system
eo = 1;         % engine order for rotary disturbance (not used for this system)


% Set-up the cart state-space system

A = [zeros(N)  eye(N);  -M_inv*K  -M_inv*D];
B = [zeros(N);  M_inv];
C = eye(2*N);
```

```
% Run simulation

sim('adaptive41t_sim');


% Generate text for output

ttext = 'Cyclic System';
if adapt_switch == 1,  ttext = [ttext ' Adaptation on Cart #2 turned on after ' num2str(timer_switch) ' sec.'];
   else  ttext = [ttext ' Adaptation Off'];
end;

if disturb_switch == 1,
      fdtext = ['f_{d3} = Random (mag \leq ' num2str(fd_amp) ')'];
   elseif disturb_switch == 2,
      fdtext = ['f_{d3} = ' num2str(fd_amp) ' sin(' num2str(wd) 't)'];
   elseif disturb_switch == 3,
      fdtext = ['\{f_d\}_i = ' num2str(fd_amp) ' cos(' num2str(wd) 't + \phi_i)'];
end;

fdstr = '_fd3';
if amp2 ~= 0,
   if amp2 == 1, fdtext = [fdtext ', f_{d2} = f_{d3}'];
   else fdtext = [fdtext ', f_{d2} = ' num2str(amp2) '*f_{d3}']; end;
   fdstr = [fdstr '3'];
end;
if amp1 ~= 0,
   if amp1 == 1, fdtext = [fdtext ', f_{d1} = f_{d3}'];
   else fdtext = [fdtext ', f_{d1} = ' num2str(amp1) '*f_{d3}']; end;
   fdstr = [fdstr '1'];
end;

gtext = [',  \Gamma = 10^{' num2str(log10(Gain)) '} * ' mat2str(diag(Gamma/Gain))];
line2  = ['\rm \fontsize{10}' fdtext  gtext];

dname = ['i:\thesis\figures\appf41\'];

fname = ['adpt41t_cyc_d' num2str(disturb_switch) fdstr '_a' num2str(adapt_switch) '_t' num2str(timer_switch)];


% Plot/Save Results

if eps_switch   == 1,
   diary([dname 'appf41_captions.txt']);
   disp([' ';' ']); disp(ttext); disp(' ');
end;

plot41_displacements;
plot41_forces_a;
plot41_parameters;
diary off
```

A.3 Simulation of the Adaptive/PPF 4/1 DOF System

This section contains Matlab and Simulink files for the Adaptive/PPF 4 DOF system, with only 1 DOF controlled.

Adaptive/PPF System: 4 carts, controling only 1
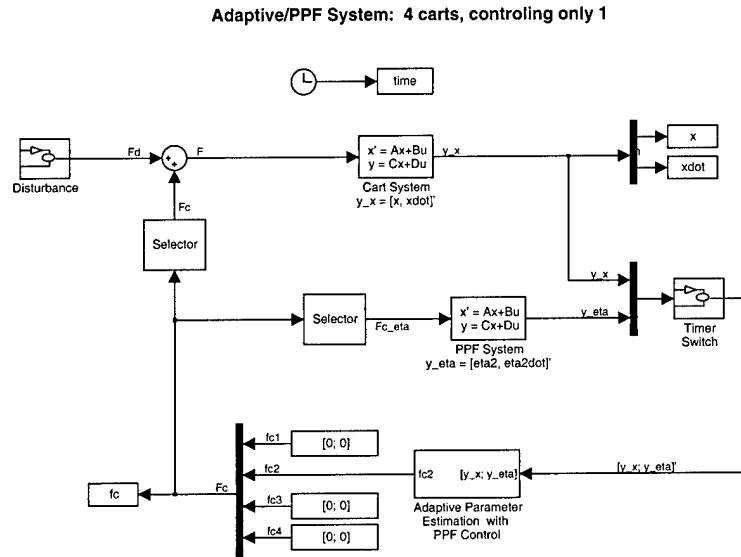
Figure A.4   Simulink Model for Adaptive/PPF 4 DOF System, with 1 DOF Controlled

Adaptive Parameter Estimation & Control Law Sub-system
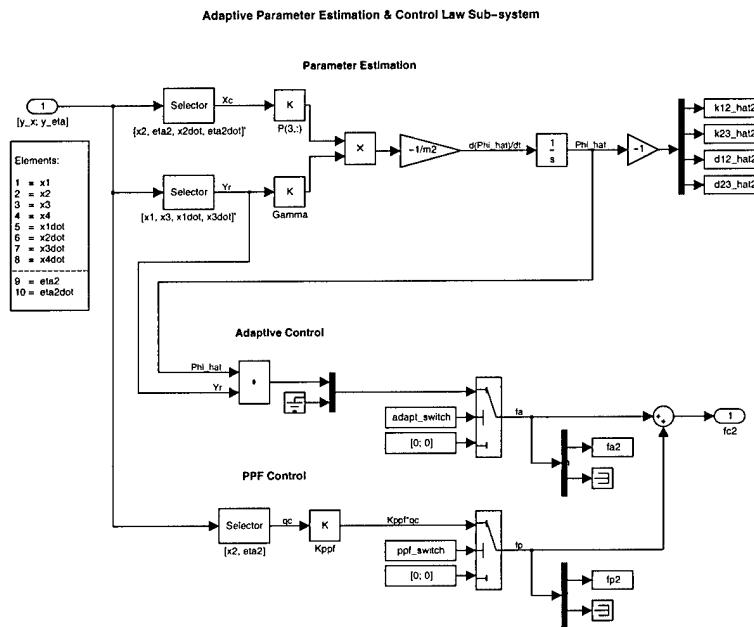
Figure A.5   Adaptive Parameter Estimation and PPF Control Sub-system from Model in Figure A.4

A.3.1 Matlab Code for Adaptive/PPF 4/1 DOF Cyclic System.

```
% ppf41_cyclic.m
%
%  This m-file runs a 4 cart cyclic system with adaptive parameter estimation
%  and PPF control on cart #2 only.


clear all; close all;

print_switch = 1;      % Sends plots to printer if = 1
eps_switch   = 1;      % Saves plots to eps file if = 1


% Simulation parameters

tfinal = 60;

ppf_switch    = 1;    % turns ppf control on (1) / off (0)
adapt_switch = 1;     % turns adaptive control on (1) / off(0)
timer_switch  = 10;   % turn on estimator/control at t = timer_switch
disturb_switch = 3;   % disturbance:  1 = random, 2 = sine, 3 = rotary


% System parameters

N = 4;                 % number of carts
zeta_n = 0.01;         % damping ratio
ko = 100; kc = 5;      % ground & coupling stiffness, [k] = N/m

m1  = 1;   m2  = 1;   m3  = 1;   m4  = 1;    % [m] = Kg
k01 = ko;  k02 = ko;  k03 = ko;  k04 = ko;   % [k] = N/m
k12 = kc;  k23 = kc;  k34 = kc;  k41 = kc;

M = diag([m1 m2 m3 m4]); M_inv = diag(1./[m1 m2 m3 m4]);

K = [ k01+k12+k41   -k12          0             -k41;
        -k12         k02+k12+k23  -k23           0;
         0          -k23          k03+k23+k34   -k34;
        -k41          0          -k34           k04+k34+k41];


% Determine lowest natural freq of the undamped cart system (wn)

[evalues,evectors] = eign(K,M);
wn  = sqrt(min(evalues));         % lowest natural freq, [wn] = rad/sec


% Form the damping matrix (D) from K, zeta_n, & the evectors

D = real(evectors*(2*zeta_n*sqrt(evectors'*K*evectors))*evectors');
for i = 1:N,  for j = 1:N,  if K(i,j) == 0,  D(i,j) = 0;  end;  end;  end;
d12 = -D(1,2);  d23 = -D(2,3);  d34 = -D(3,4);  d41 = -D(4,1);


% Set ppf and adaptation parameters

%Gain = 1e1;  Gamma = Gain*diag([100 20 0.01 1]);  % adaptive gain matrix for d = 2
Gain = 1e1;  Gamma = Gain*diag([1 100 1 1]);        % adaptive gain matrix for d = 3
mu = 0.4; zeta_f = 0.4; wf = wn;                     % ppf gain, freq & damping ratio
if ppf_switch ~= 0,  Kppf = [0  mu*K(2,2);  wf^2  0];  else,  Kppf = zeros(2);  end;


% Partition out controlled  & uncontrolled parts of the system matrices
```

```
Mc = diag([M(2,2)  1]);                 Mc_inv = diag([1/M(2,2)  1]);
Kc = diag([K(2,2)  wf^2]);
Dc = diag([D(2,2)  2*zeta_f*wf]);

Mu = diag([M(1,1)  M(3,3)  M(4,4)]);    Mu_inv = diag([1/M(1,1)  1/M(3,3)  1/M(4,4)]);
Ku = diag([K(1,1)  K(3,3)  K(4,4)]);
Du = diag([D(1,1)  D(3,3)  D(4,4)]);


% Find P

Ac = [zeros(2)  eye(2);  -Mc_inv*(Kc-Kppf)  -Mc_inv*Dc];
Q = diag([1  wf^2/K(2,2)  M(2,2)/K(2,2)  1/K(2,2)]);
P = lyap(Ac',Q);


% Check stability requirments

Au = [zeros(3)  eye(3);  -Mu_inv*Ku  -Mu_inv*Du];

if -abs(real(eig(Ac))) ~= real(eig(Ac)), disp(' '); disp('Ac is not negative definite'); end;
if -abs(real(eig(Au))) ~= real(eig(Au)), disp(' '); disp('Au is not negative definite'); end;
if abs(real(eig(P))) ~= real(eig(P)), disp(' '); disp('P is not positive definite'); end;
if P ~= P', disp(' '); disp('P is not symmetric'); end;


% Set disturbance parameters

fd_amp = 10;    % amplitude of disturbance
amp1 = 0;       % allows for direct forcing on cart #1, fd1 = amp1*fd3
amp2 = 0;       % allows for direct forcing on cart #2, fd2 = amp2*fd3
wd = wn;        % set disturbance freq = natural freq of system
eo = 1;         % engine order for rotary disturbance (not used for this system)


% Set-up the cart & ppf state-space systems

A = [zeros(N)  eye(N);  -M_inv*K  -M_inv*D];
B = [zeros(N);  M_inv];
C = eye(2*N);

Af = [0  1;  -wf^2  -2*zeta_f*wf];
Bf = [zeros(1,N);  0  1  0  0];
Cf = eye(2);


% Run simulation

sim('ppf41_sim');


% Generate text for output

ttext = 'Cyclic System, Cart #2:';
if adapt_switch == 1 & ppf_switch == 1,         ttext = [ttext 'Adaptive / PPF Both On '];
   elseif adapt_switch == 1 & ppf_switch == 0, ttext = [ttext 'Adaptive on / PPF off '];
   elseif adapt_switch == 0 & ppf_switch == 1, ttext = [ttext 'Adaptive off / PPF on '];
   elseif adapt_switch == 0 & ppf_switch == 0, ttext = [ttext 'Adaptive / PPF Both Off'];
end;

if disturb_switch == 1,
     fdtext = ['f_{d3} = Random (mag \leq ' num2str(fd_amp) ')'];
   elseif disturb_switch == 2,
     fdtext = ['f_{d3} = ' num2str(fd_amp) ' sin(' num2str(wd) 't)'];
   elseif disturb_switch == 3,
```

```
        fdtext = ['\{f_d\}_i = ' num2str(fd_amp) ' cos(' num2str(wd) 't + \phi_i)'];
end;

gtext = [',  \Gamma = 10^{' num2str(log10(Gain)) '} * ' mat2str(diag(Gamma/Gain))];
line2 = ['\rm \fontsize{10}' fdtext  gtext];

dname = ['i:\thesis\figures\appf41\'];

fname = ['ppf41_cyc_d' num2str(disturb_switch) '_a' num2str(adapt_switch)...
         '_p' num2str(ppf_switch) '_t' num2str(timer_switch)];


% Plot/Save Results

plot41_displacements;
plot41_forces_ap;
plot41_parameters;
```

A.3.2 Matlab Code for RMS Response of Adaptive/PPF 4/1 DOF Cyclic System.

```
% ppf41_cyclic_rms.m
%
%  This m-file runs a 4 cart cyclic system with adaptive parameter estimation
%  and PPF control on cart #2 only.  The RMS values for the displacements and
%  parameter estimates are calculated over a range of disturbance frequencies.
%  It is currently set-up to be called by script file so that several different
%  cases can be run at once.


tfinal = 120;
timer_switch    = 0;    % turn on estimator/control at t = timer_switch
%ppf_switch     = 0;    % turns ppf control on (1) / off (0)
%adapt_switch   = 0;    % turns adaptive control on (1) / off(0)
%disturb_switch = 2;    % disturbance:  1 = random, 2 = sine, 3 = rotary


% System parameters

N = 4;                  % number of carts
zeta_n = 0.01;          % damping ratio
ko = 100; kc = 5;       % ground & coupling stiffness, [k] = N/m

m1  = 1;   m2  = 1;   m3  = 1;   m4  = 1;     % [m] = Kg
k01 = ko;  k02 = ko;  k03 = ko;  k04 = ko;    % [k] = N/m
k12 = kc;  k23 = kc;  k34 = kc;  k41 = kc;

M = diag([m1 m2 m3 m4]); M_inv = diag(1./[m1 m2 m3 m4]);

K = [ k01+k12+k41    -k12          0             -k41;
      -k12           k02+k12+k23   -k23          0;
      0              -k23          k03+k23+k34   -k34;
      -k41           0             -k34          k04+k34+k41];


% Determine lowest natural freq of the undamped cart system (wn)

[evalues,evectors] = eign(K,M);
wn  = sqrt(min(evalues));       % lowest natural freq, [wn] = rad/sec


% Form the damping matrix (D) from K, zeta_n, & the evectors
```

A-15

```
D = real(evectors*(2*zeta_n*sqrt(evectors'*K*evectors))*evectors'));
for i = 1:N,  for j = 1:N,  if K(i,j) == 0,  D(i,j) = 0;  end;  end;  end;
d12 = -D(1,2);  d23 = -D(2,3);  d34 = -D(3,4);  d41 = -D(4,1);


% Set ppf and adaptation parameters

Gain = 1e1;  Gamma = Gain*diag([1 100 1 1]);       % adaptive gain matrix for d = 3
mu = 0.4; zeta_f = 0.4; wf = wn;                    % ppf gain, freq & damping ratio
if ppf_switch ~= 0,  Kppf = [0  mu*K(2,2); wf^2  0];  else,  Kppf = zeros(2);  end;


% Partition out controlled  & uncontrolled parts of the system matrices

Mc = diag([M(2,2)  1]);              Mc_inv = diag([1/M(2,2)  1]);
Kc = diag([K(2,2)  wf^2]);
Dc = diag([D(2,2)  2*zeta_f*wf]);

Mu = diag([M(1,1)  M(3,3)  M(4,4)]);
Ku = diag([K(1,1)  K(3,3)  K(4,4)]);
Du = diag([D(1,1)  D(3,3)  D(4,4)]);


% Find P

Ac = [zeros(2)  eye(2);  -Mc_inv*(Kc-Kppf)  -Mc_inv*Dc];
Q = diag([1  wf^2/K(2,2)  M(2,2)/K(2,2)  1/K(2,2)]);
P = lyap(Ac',Q);


% Set disturbance parameters

fd_amp = 10;     % amplitude of disturbance
amp1 = 0;        % allows for direct forcing on cart #1, fd1 = amp1*fd3
amp2 = 0;        % allows for direct forcing on cart #2, fd2 = amp2*fd3
wd = wn;         % set disturbance freq = natural freq of system
eo = 1;          % engine order for rotary disturbance (not used for this system)


% Set-up the cart & ppf state-space systems

A = [zeros(N)  eye(N);  -M_inv*K  -M_inv*D];
B = [zeros(N);  M_inv];
C = eye(2*N);

Af = [0  1;  -wf^2  -2*zeta_f*wf];
Bf = [zeros(1,N);  0  1  0  0];
Cf = eye(2);


% Iteratively run simulation and determine RMS values

i = 0;  wd_step = 0.001;

for wd = 0:wd_step:20.0,
    i = i + 1;  omega(i) = wd;     disp(' '); disp([case_name num2str(wd)]);
    sim('ppf41_rms_sim');
    ibegin  = min(find(time>=tfinal/2));
    x_rms(i) = rms(x(:,2),ibegin);
end;
```

A.4 Simulation of the Adaptive/PPF 4/4 DOF System

This section contains Matlab and Simulink files for the Adaptive/PPF 4 DOF system, with all 4 DOF controlled.

Adaptive/PPF System: Controlling All 4 Carts
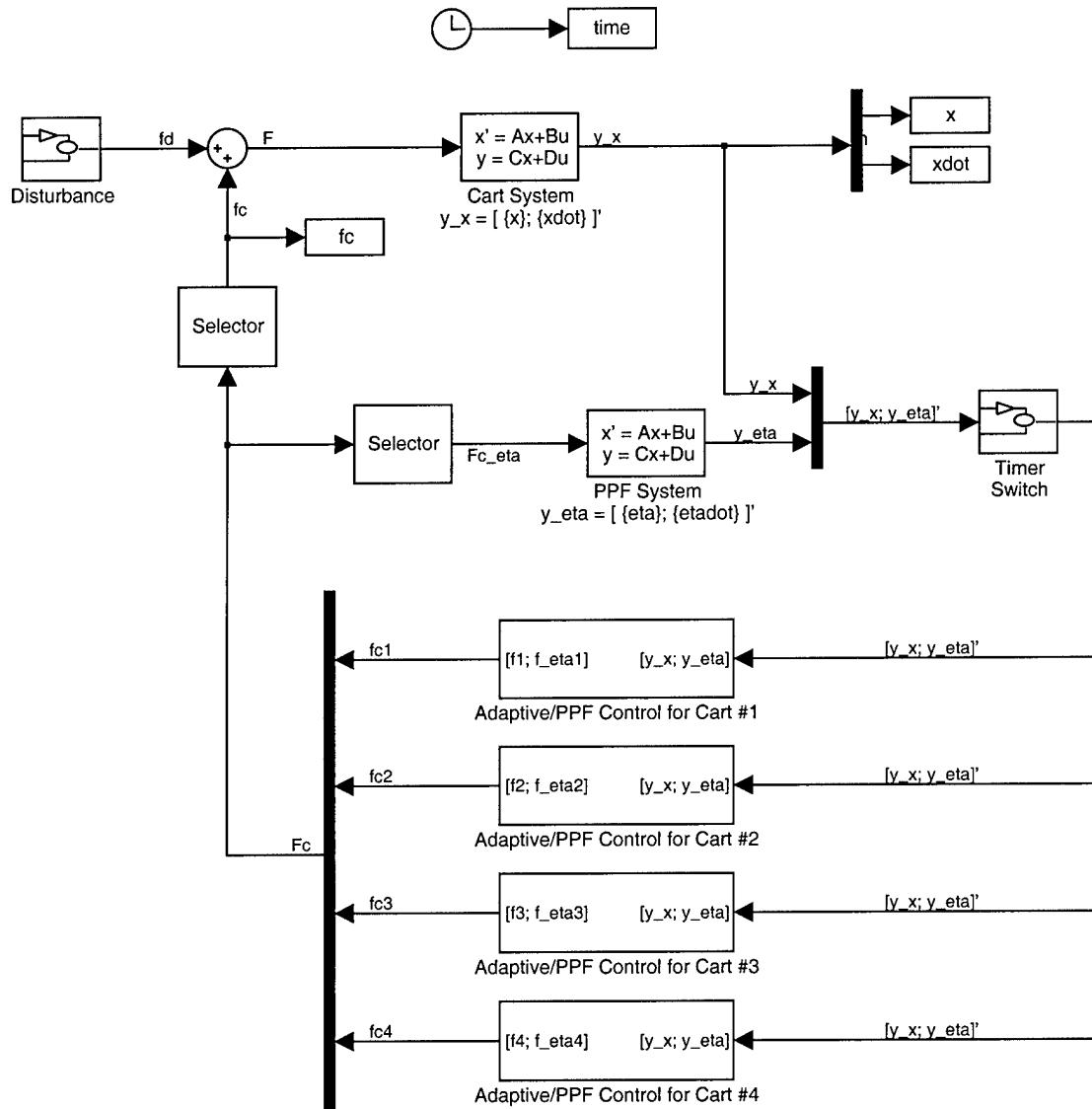
Figure A.6   Simulink Model for Adaptive/PPF 4 DOF System, with all 4 DOF Controlled
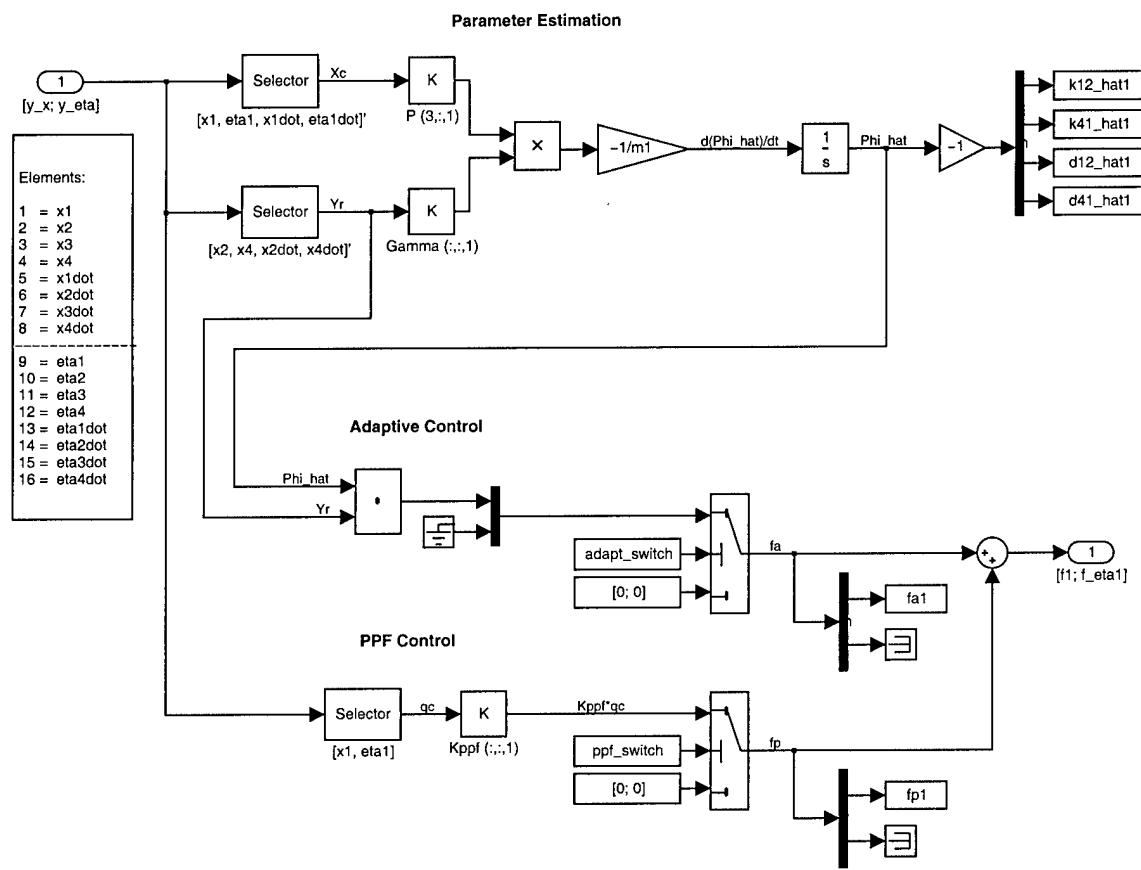
Figure A.7   Adaptive Parameter Estimation and PPF Control Sub-system for Cart 1, from Model in Figure A.6

A.4.1 Matlab Code for Adaptive/PPF 4/4 DOF System.

```
% ppf4.m
%
%  This m-file runs a 4 cart ring system with adaptive parameter estimation
%  and PPF control on all carts.  The are three settings for the disturbance.
%  The first and second have a random or sine input, respectively, always on
%  cart #3, with the option to put a multiple of that on cart #1.  The third
%  is a disturbance rotating between all four, fd_i = cos(wd*t + phi_i).


clear all; close all;

print_switch = 0;       % Sends plots to printer if = 1
eps_switch   = 0;       % Saves plots to eps file if = 1


% Simulation parameters

tfinal = 1750;

sim_switch      = 1;    % 1 = standard, 2 = exact parameters, 3 = odd only
disturb_switch = 3;     % disturbance:  1 = random, 2 = sine, 3 = rotary
eo              = 1;    % engine order for rotary disturbance

mistuned        = 0;    % grounding springs are mistuned if = 1

ppf_switch      = 1;    % turns ppf control on (1) / off (0)
adapt_switch    = 1;    % turns adaptive control on (1) / off(0)

timer_switch    = 0;    % turn on estimator/control at t = timer_switch


% System parameters

N = 4;                  % number of carts
zeta_n = 0.002;         % damping ratio
ko = 100; kc = 5;       % nominal ground & coupling stiffness, [k] = N/m

m1  = 1;   m2  = 1;   m3  = 1;   m4  = 1;   % [m] = Kg
k12 = kc;  k23 = kc;  k34 = kc;  k41 = kc;  % [k] = N/m

if mistuned == 0,
      k01 = ko;  k02 = ko;  k03 = ko;  k04 = ko;
      ttext = 'Cyclic System';
   else,
      k01 = ko+4.7787; k02 = ko+5.996; k03 = ko+7.2268; k04 = ko+5.9069;
      ttext = 'Mistuned Cyclic System';
end;

M = diag([m1 m2 m3 m4]); M_inv = diag(1./[m1 m2 m3 m4]);

K = [ k01+k12+k41    -k12            0             -k41;
      -k12           k02+k12+k23    -k23           0;
      0              -k23           k03+k23+k34    -k34;
      -k41           0              -k34           k04+k34+k41];


% Find lowest natural freq (wn) of the undamped system; [wn] = rad/sec

[evalues,evectors] = eign(K,M);  wn  = sqrt(min(evalues));


% Form the damping matrix (D) from K, zeta_n, & the evectors
```

```
D = real(evectors*(2*zeta_n*sqrt(evectors'*K*evectors))*evectors');
for i = 1:N,  for j = 1:N,  if K(i,j) == 0,  D(i,j) = 0;  end;  end;  end;
d12 = -D(1,2);  d23 = -D(2,3);  d34 = -D(3,4);  d41 = -D(4,1);


% Set adaptation and ppf parameters

Gain = 1e2;
Gamma(:,:,1) = Gain*diag([1 1 1 1]);   % adaptive gain matrix for cart #1
Gamma(:,:,2) = Gamma(:,:,1);           % adaptive gain matrix for cart #2
Gamma(:,:,3) = Gamma(:,:,1);           % adaptive gain matrix for cart #3
Gamma(:,:,4) = Gamma(:,:,1);           % adaptive gain matrix for cart #4

mu = 0.4; wf = wn; zeta_f = 0.4;       % ppf gain, freq & damping ratio


% Begin looping through each cart

for i = 1:N,

    % Set-up Kppf

    if ppf_switch ~= 0,  Kppf(:,:,i) = [0  mu*K(i,i); wf^2 0];
        else, Kppf(:,:,i) = zeros(2);
    end;


    % Partition out controlled & uncontrolled parts of the system matrices

    Mc = diag([M(i,i)  1]);            Mc_inv = diag([1/M(i,i)  1]);
    Kc = diag([K(i,i)  wf^2]);
    Dc = diag([D(i,i)  2*zeta_f*wf]);


    % Calculate P

    Ac = [zeros(2)  eye(2);  -Mc_inv*(Kc-Kppf(:,:,i))  -Mc_inv*Dc];
    Q = diag([1  wf^2/K(i,i)  M(i,i)/K(i,i)  1/K(i,i)]);
    P(:,:,i) = lyap(Ac',Q);


    % Check stability requirments

    if abs(real(eig(P(:,:,i)))) ~= real(eig(P(:,:,i))),
        disp(' '); disp(['P' num2str(i) ' is not positive definite']); end;
    if P(:,:,i) ~= P(:,:,i)', disp(' '); disp(['P' num2str(i) ' is not symmetric']); end;


    % Set-up vectors for selecting Xc_i and Yr_i

    select_Xc(i,:) = [i,  i+2*N,  i+N,  i+3*N];
    if i == 1,        select_Yr(i,:) = [2,  N,  2+N,  N+N];
        elseif i == N, select_Yr(i,:) = [1,  N-1,  1+N,  N-1+N];
        else,         select_Yr(i,:) = [i-1,  i+1,  i-1+N,  i+1+N];
    end;

end;  % End looping through each cart


% Set disturbance parameters

fd_amp = 10;   % amplitude of disturbance
wd = wn;       % set disturbance freq = natural freq of system
if disturb_switch == 3, amp1 = 0; else, amp1 = 0; end;  % fd1 = amp1*fd3
```

A-20

```
% Set-up the cart & ppf state-space systems

A = [zeros(N)  eye(N);  -M_inv*K  -M_inv*D];
B = [zeros(N);  M_inv];
C = eye(2*N);


Af = [zeros(N)  eye(N);  -wf^2*eye(N)  -2*zeta_f*wf*eye(N)];
Bf = [zeros(N); eye(N)];
Cf = eye(2*N);


% Run simulation

if        sim_switch == 1, sim('ppf4_sim');    ttext = [ttext ':  '];
   elseif  sim_switch == 2, sim('ppf4ep_sim'); ttext = [ttext ' (w/ exact parameters):  '];
   elseif  sim_switch == 3, sim('ppf4odd_sim'); ttext = [ttext ':  Carts #2&4 - Uncontrolled; Carts#1&3 - '];
end;


% Generate text for output

timer_txt = ['@ t = ' num2str(timer_switch)];
if adapt_switch == 1 & ppf_switch == 1,           ttext = [ttext 'Adaptive / PPF Both on ' timer_txt];
   elseif adapt_switch == 1 & ppf_switch == 0, ttext = [ttext 'PPF off / Adaptive on ' timer_txt];
   elseif adapt_switch == 0 & ppf_switch == 1, ttext = [ttext 'Adaptive off / PPF on ' timer_txt];
   elseif adapt_switch == 0 & ppf_switch == 0, ttext = [ttext 'Adaptive / PPF Both off'];
end;

if disturb_switch == 1,
      fdtext = ['f_{d3} = Random (mag \leq ' num2str(fd_amp) ')'];
   elseif disturb_switch == 2,
      fdtext = ['f_{d3} = ' num2str(fd_amp) ' sin(' num2str(wd) 't)'];
   elseif disturb_switch == 3,
      fdtext = ['f_{d_i} = ' num2str(fd_amp) ' cos(' num2str(wd) 't + \phi_i)'];
end;

if amp1 ~= 0,
   if amp1 == 1, fdtext = [fdtext ', f_{d1} = f_{d3}'];
      else fdtext = [fdtext ', f_{d1} = ' num2str(amp1) '*f_{d3}'];
   end;
end;

fdtext  = [fdtext ',  EO = ' num2str(eo)];
gtext   = [',  \Gamma = 10^{' num2str(log10(Gain)) '} * \{' mat2str(diag(Gamma(:,:,1)/Gain)) ', ... \}'];
line2   = ['\rm \fontsize{10}' fdtext  gtext];

if timer_switch ~= 0, timer_str = '_t1'; else timer_str = '_t0'; end;
if eo < 10, eo_str = ['0' num2str(eo)]; else eo_str = num2str(eo);   end

dname = ['i:\thesis\figures\ppf4\'];

fname = ['ppf4_d' num2str(disturb_switch) '_e' eo_str  '_m' num2str(mistuned)...
         '_p' num2str(ppf_switch) '_a' num2str(adapt_switch)];

if        sim_switch == 1,  fname = [fname timer_str];
   elseif  sim_switch == 2,  fname = [fname 'ep' timer_str];  adapt_switch = 0;  % no parameter estimation plots
   elseif  sim_switch == 3,  fname = [fname 'odd' timer_str];
end;


% Plot Results

if eps_switch   == 625,
   diary([dname 'ppf4_captions.txt']);
```

A-21

```
    disp([' ';' ']); disp(ttext); disp(' ');
end;


plot4_displacements;
plot4_forces;
plot4_parameters;
diary off
```

A.4.2   Matlab Code for RMS Response of Adaptive/PPF 4/4 DOF System.

```
% ppf4_rms.m
%
%  This m-file runs a 4 cart cyclic system with adaptive parameter estimation
%  and PPF control on all carts.  The disturbance is fd_i = cos(wd*t + phi_i).
%  The RMS values for the displacements and parameter estimates are calculated
%  over a range of disturbance frequencies.  It is currently set-up to be called
%  by script file so that several different cases can be run at once.


%clear all; close all;


% Simulation parameters

tfinal = 500;
sim_switch    = 1;      % 1 = standard, 2 = exact parameters, 3 = odd only
timer_switch  = 0;      % turn on estimator/control at t = timer_switch


%eo            = 1;      % engine order for rotary disturbance
%mistuned      = 1;      % grounding springs are mistuned if = 1
%ppf_switch    = 1;      % turns ppf control on (1) / off (0)
%adapt_switch = 1;       % turns adaptive control on (1) / off(0)

% System parameters

N = 4;                  % number of carts
zeta_n = 0.002;         % damping ratio
ko = 100; kc = 5;       % ground & coupling stiffness, [k] = N/m

m1  = 1;   m2  = 1;   m3  = 1;   m4  = 1;    % [m] = Kg
k12 = kc;  k23 = kc;  k34 = kc;  k41 = kc;   % [k] = N/m

if mistuned == 0,
      k01 = ko;  k02 = ko;  k03 = ko;  k04 = ko;
      ttext = 'Cyclic System';
   else,
      k01 = ko+4.7787; k02 = ko+5.996; k03 = ko+7.2268; k04 = ko+5.9069;
      ttext = 'Mistuned Cyclic System';
end;

M = diag([m1 m2 m3 m4]); M_inv = diag(1./[m1 m2 m3 m4]);

K = [ k01+k12+k41    -k12            0               -k41;
      -k12           k02+k12+k23    -k23             0;
      0              -k23            k03+k23+k34     -k34;
      -k41           0              -k34             k04+k34+k41];


% Find lowest natural freq (wn) of the undamped system; [wn] = rad/sec

[evalues,evectors] = eign(K,M);  wn  = sqrt(min(evalues));
```

```
% Form the damping matrix (D) from K, zeta_n, & the evectors

D = real(evectors*(2*zeta_n*sqrt(evectors'*K*evectors))*evectors');
for i = 1:N, for j = 1:N, if K(i,j) == 0, D(i,j) = 0; end; end; end;
d12 = -D(1,2); d23 = -D(2,3); d34 = -D(3,4); d41 = -D(4,1);


% Set adaptation and ppf parameters

Gain = 1e2;
Gamma(:,:,1) = Gain*diag([1 1 1 1]);   % adaptive gain matrix for cart #1
Gamma(:,:,2) = Gamma(:,:,1);           % adaptive gain matrix for cart #2
Gamma(:,:,3) = Gamma(:,:,1);           % adaptive gain matrix for cart #3
Gamma(:,:,4) = Gamma(:,:,1);           % adaptive gain matrix for cart #4

mu = 0.4; wf = wn; zeta_f = 0.4;       % ppf gain, freq & damping ratio


% Begin looping through each cart

for i = 1:N,

   % Set-up Kppf

   if ppf_switch ~= 0, Kppf(:,:,i) = [0  mu*K(i,i);  wf^2 0];
      else, Kppf(:,:,i) = zeros(2);
   end;


   % Partition out controlled & uncontrolled parts of the system matrices

   Mc = diag([M(i,i)  1]);              Mc_inv = diag([1/M(i,i)  1]);
   Kc = diag([K(i,i)  wf^2]);
   Dc = diag([D(i,i)  2*zeta_f*wf]);


   % Calculate P

   Ac = [zeros(2)  eye(2);  -Mc_inv*(Kc-Kppf(:,:,i))  -Mc_inv*Dc];
   Q = diag([1  wf^2/K(i,i)  M(i,i)/K(i,i)  1/K(i,i)]);
   P(:,:,i) = lyap(Ac',Q);


   % Set-up vectors for selecting Xc_i and Yr_i

   select_Xc(i,:) = [i,  i+2*N,  i+N,  i+3*N];
   if i == 1,        select_Yr(i,:) = [2,  N,  2+N,  N+N];
      elseif i == N, select_Yr(i,:) = [1,  N-1,  1+N,  N-1+N];
      else,          select_Yr(i,:) = [i-1,  i+1,  i-1+N,  i+1+N];
   end;

end;  % End looping through each cart


% Set disturbance parameters

fd_amp = 10;   % amplitude of disturbance


% Set-up the cart & ppf state-space systems

A = [zeros(N)  eye(N);  -M_inv*K  -M_inv*D];
B = [zeros(N);  M_inv];
C = eye(2*N);
```

```
Af = [zeros(N)  eye(N);  -wf^2*eye(N)  -2*zeta_f*wf*eye(N)];
Bf = [zeros(N); eye(N)];
Cf = eye(2*N);


% Iteratively run simulation and determine RMS values

i = 0;  wd_step = 0.001;

for wd = 9:wd_step:11,

    i = i + 1;  omega(i) = wd;  disp(' '); disp([case_name num2str(wd)]);
    sim('ppf4_rms_sim');
    ibegin  = min(find(time>=(tfinal-100)));

    for j = 1:N,  x_rms(i,j) = rms(x(:,j),ibegin); end;
    avg_x_rms(i,1) = sum(x_rms(i,:),2)/N;
    max_x_rms(i,1) = max(x_rms(i,:));

end;

if eo < 10, eo_str = ['0' num2str(eo)]; else eo_str = num2str(eo);  end

fname = ['rms4_e' eo_str  '_m' num2str(mistuned) '_p' num2str(ppf_switch) '_a' num2str(adapt_switch)];
```

A.5 Simulation of the Adaptive/PPF 8 Blade System

This section contains Matlab and Simulink files for the 8 Blade Compressor Disk Model with Adaptive/PPF control on all 8 blades. Note that the Adaptive Parameter Estimation and PPF Control Sub-system is similar in form to Figure A.7

Adaptive/PPF System: Controlling All 8 Blades
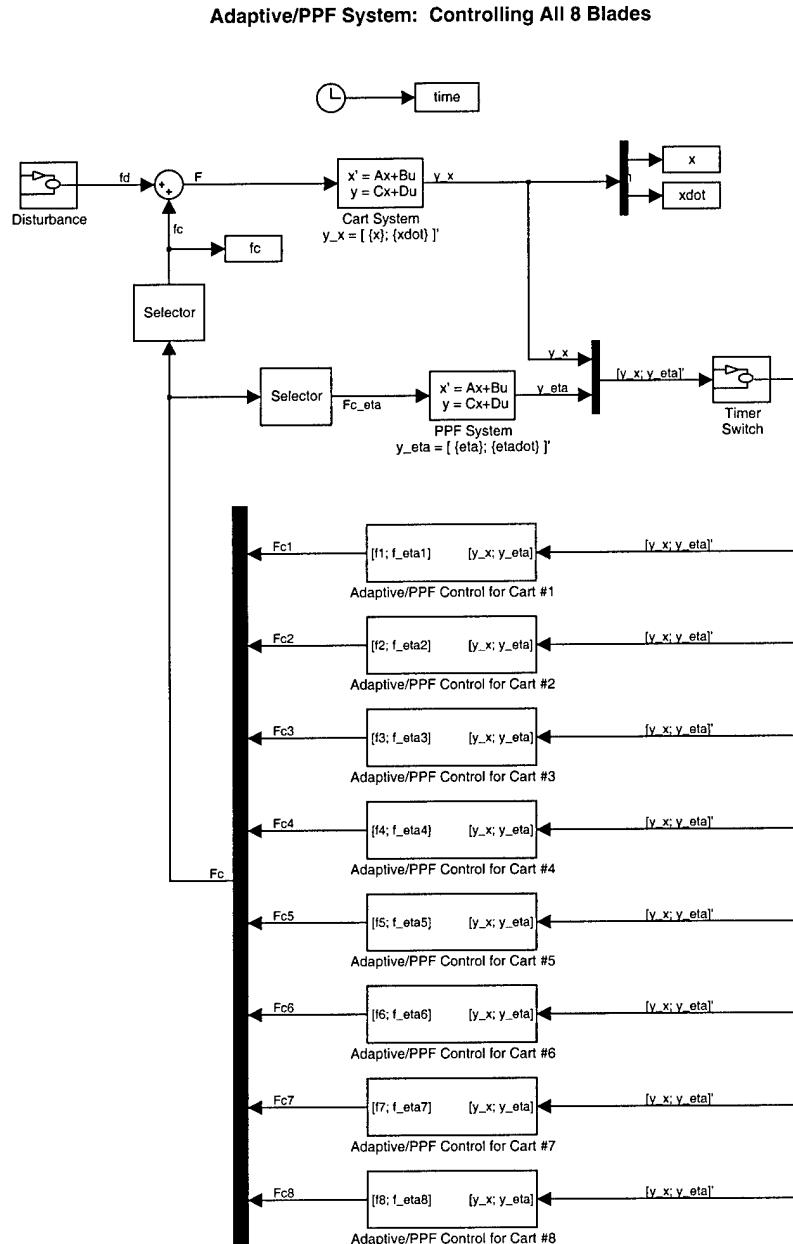
Figure A.8   Simulink Model for an 8 Blade System with Adaptive/PPF control on all 8 blades

A.5.1 Matlab Code for the Adaptive/PPF 8 Blade System.

```
% ppf8.m
%
%  This m-file runs a 8 blade cyclic system with adaptive parameter estimation
%  and PPF control on all carts.  The are three settings for the disturbance.
%  The first and second have a random or sine input, respectively, always on
%  cart #3, with the option to put a multiple of that on cart #1.  The third
%  is a disturbance rotating between all eight, fd_i = cos(wd*t + phi_i).


clear all; close all;

print_switch = 0;       % Sends plots to printer if = 1
eps_switch   = 0;       % Saves plots to eps file if = 1


% Simulation parameters

tfinal = 1000;

sim_switch      = 1;    % 1 = standard, 2 = exact parameters, 3 = odd only
disturb_switch = 3;     % disturbance:  1 = random, 2 = sine, 3 = cyclic
eo              = 1;    % engine order for cyclic disturbance

mistuned        = 0;    % grounding springs are mistuned if = 1 or 2

ppf_switch      = 1;    % turns ppf control on (1) / off (0)
adapt_switch    = 1;    % turns adaptive control on (1) / off(0)

timer_switch    = 0;    % turn on estimator/control at t = timer_switch


% System parameters

N  = 8;               % number of blades
L  = 1;               % length of blade
zeta_n = 0.05;        % damping ratio
ko = 100; kc = 5;     % nominal ground & coupling stiffness, [k] = N/m

m1 = 1; m2 = 1; m3 = 1; m4 = 1; m5 = 1; m6 = 1; m7 = 1; m8 = 1;  % [m] = Kg

k12 = kc;  k23 = kc;  k34 = kc;  k45 = kc;   % [k] = N/m
k56 = kc;  k67 = kc;  k78 = kc;  k81 = kc;   % [k] = N/m

if mistuned == 0,
      k01 = ko;  k02 = ko;  k03 = ko;  k04 = ko;
      k05 = ko;  k06 = ko;  k07 = ko;  k08 = ko;
      ttext = 'Cyclic System';
   elseif mistuned == 1,
      k01 = ko*(1 + 0.0122);  k02 = ko*(1 + 0.0003);  k03 = ko*(1 - 0.0003);  k04 = ko*(1 - 0.0038);
      k05 = ko*(1 - 0.0117);  k06 = ko*(1 - 0.0012);  k07 = ko*(1 - 0.0074);  k08 = ko*(1 + 0.0126);
      ttext = 'Mistuned Cyclic System';
end;

M = diag([m1 m2 m3 m4 m5 m6 m7 m8]); M_inv = diag(1./[m1 m2 m3 m4 m5 m6 m7 m8]);

cp8 = cos(pi/8);  L2cp8 = L^2*cp8;
K(1,1) = k81 + k12 + k01/(L2cp8);  K(1,8) = -k81;  K(1,2) = -k12;
K(2,2) = k12 + k23 + k02/(L2cp8);  K(2,1) = -k12;  K(2,3) = -k23;
K(3,3) = k23 + k34 + k03/(L2cp8);  K(3,2) = -k23;  K(3,4) = -k34;
K(4,4) = k34 + k45 + k04/(L2cp8);  K(4,3) = -k34;  K(4,5) = -k45;
K(5,5) = k45 + k56 + k05/(L2cp8);  K(5,4) = -k45;  K(5,6) = -k56;
K(6,6) = k56 + k67 + k06/(L2cp8);  K(6,5) = -k56;  K(6,7) = -k67;
K(7,7) = k67 + k78 + k07/(L2cp8);  K(7,6) = -k67;  K(7,8) = -k78;
```

```
K(8,8) = k78 + k81 + k08/(L2cp8);  K(8,7) = -k78;  K(8,1) = -k81;
K = cp8*K;

% Find lowest natural freq (wn) of the undamped system; [wn] = rad/sec

[evalues,evectors] = eign(K,M);  wn  = sqrt(min(evalues));


% Form the damping matrix (D) from K, zeta_n, & the evectors

D = real(evectors*(2*zeta_n*sqrt(evectors'*K*evectors))*evectors');
for i = 1:N, for j = 1:N, if K(i,j) == 0, D(i,j) = 0; end; end; end;
d12 = -D(1,2);  d23 = -D(2,3);  d34 = -D(3,4);  d45 = -D(4,5);
d56 = -D(5,6);  d67 = -D(6,7);  d78 = -D(7,8);  d81 = -D(8,1);


% Set adaptation and ppf parameters

Gain = 1e2;
Gamma(:,:,1) = Gain*diag([1 1 1 1]);   % adaptive gain matrix for cart #1
Gamma(:,:,2) = Gamma(:,:,1);           % adaptive gain matrix for cart #2
Gamma(:,:,3) = Gamma(:,:,1);           % adaptive gain matrix for cart #3
Gamma(:,:,4) = Gamma(:,:,1);           % adaptive gain matrix for cart #4
Gamma(:,:,5) = Gamma(:,:,1);           % adaptive gain matrix for cart #5
Gamma(:,:,6) = Gamma(:,:,1);           % adaptive gain matrix for cart #6
Gamma(:,:,7) = Gamma(:,:,1);           % adaptive gain matrix for cart #7
Gamma(:,:,8) = Gamma(:,:,1);           % adaptive gain matrix for cart #8

mu = 0.4; wf = wn; zeta_f = 0.4;       % ppf gain, freq & damping ratio


% Begin looping through each cart

for i = 1:N,

    % Set-up Kppf

    if ppf_switch ~= 0,  Kppf(:,:,i) = [0  mu*K(i,i);  wf^2 0];
        else, Kppf(:,:,i) = zeros(2);
    end;


    % Partition out controlled & uncontrolled parts of the system matrices

    Mc = diag([M(i,i)  1]);            Mc_inv = diag([1/M(i,i)  1]);
    Kc = diag([K(i,i)  wf^2]);
    Dc = diag([D(i,i)  2*zeta_f*wf]);


    % Calculate P

    Ac = [zeros(2)  eye(2);  -Mc_inv*(Kc-Kppf(:,:,i))  -Mc_inv*Dc];
    Q = diag([1  wf^2/K(i,i)  M(i,i)/K(i,i)  1/K(i,i)]);
    P(:,:,i) = lyap(Ac',Q);


    % Check stability requirments

    if -abs(real(eig(Ac))) ~= real(eig(Ac)), disp(' '); disp('Ac is not negative definite'); end;
    if abs(real(eig(P(:,:,i)))) ~= real(eig(P(:,:,i))), disp(['P' num2str(i) ' is not positive definite']); end;
    if P(:,:,i) ~= P(:,:,i)', disp(' '); disp(['P' num2str(i) ' is not symmetric']); end;


    % Set-up vectors for selecting Xc_i and Yr_i
```

```
        select_Xc(i,:) = [i,   i+2*N,  i+N,   i+3*N];
        if i == 1,          select_Yr(i,:) = [2,  N,   2+N,   N+N];
            elseif i == N, select_Yr(i,:) = [1,  N-1,  1+N,   N-1+N];
            else,           select_Yr(i,:) = [i-1, i+1,  i-1+N,  i+1+N];
        end;

end;  % End looping through each cart


% Set disturbance parameters

fd_amp = 10;    % amplitude of disturbance
wd = wn;        % set disturbance freq = natural freq of system


% Set-up the cart & ppf state-space systems

A = [zeros(N)  eye(N);  -M_inv*K  -M_inv*D];
B = [zeros(N);  M_inv];
C = eye(2*N);

Af = [zeros(N)  eye(N);  -wf^2*eye(N)  -2*zeta_f*wf*eye(N)];
Bf = [zeros(N); eye(N)];
Cf = eye(2*N);


% Run simulation

if        sim_switch == 1, sim('ppf8_sim');    ttext = [ttext ':   '];
   elseif  sim_switch == 2, sim('ppf8ep_sim');  ttext = [ttext ' (w/ exact parameters):  '];
   elseif  sim_switch == 3, sim('ppf8odd_sim'); ttext = [ttext ':  Even Blades - PPF only; Odd Blades - '];
end;


% Generate text for output

timer_txt = ['@ t = ' num2str(timer_switch)];
if adapt_switch == 1 & ppf_switch == 1,         ttext = [ttext 'Adaptive / PPF Both on ' timer_txt];
   elseif adapt_switch == 1 & ppf_switch == 0, ttext = [ttext 'PPF off / Adaptive on ' timer_txt];
   elseif adapt_switch == 0 & ppf_switch == 1, ttext = [ttext 'Adaptive off / PPF on ' timer_txt];
   elseif adapt_switch == 0 & ppf_switch == 0, ttext = [ttext 'Adaptive / PPF Both off'];
end;

if disturb_switch == 1,
        fdtext = ['f_{d3} = Random (mag \leq ' num2str(fd_amp) ')'];
   elseif disturb_switch == 2,
        fdtext = ['f_{d3} = ' num2str(fd_amp) ' sin(' num2str(wd) 't)'];
   elseif disturb_switch == 3,
        fdtext = ['f_{d_i} = ' num2str(fd_amp) ' cos(' num2str(wd) 't + \phi_i)'];
end;

fdtext  = [fdtext ', E0 = ' num2str(eo)];
gtext   = [', \Gamma = 10^{' num2str(log10(Gain)) '} * \{' mat2str(diag(Gamma(:,:,1)/Gain)) ', ... \}'];
line2   = ['\rm \fontsize{10}' fdtext gtext];

if timer_switch ~= 0, timer_str = '_t1'; else timer_str = '_t0'; end;
if eo < 10, eo_str = ['0' num2str(eo)]; else eo_str = num2str(eo);  end;

dname = ['i:\thesis\figures\ppf8\'];

fname = ['ppf8_d' num2str(disturb_switch) '_e' eo_str  '_m' num2str(mistuned)...
          '_p' num2str(ppf_switch) '_a' num2str(adapt_switch)];

if        sim_switch == 1, fname = [fname timer_str];
   elseif  sim_switch == 2, fname = [fname 'ep' timer_str];  adapt_switch = 0;  % no parameter estimation plots
```

```
      elseif  sim_switch == 3,  fname = [fname 'odd' timer_str];
end;


% Plot Results

if eps_switch   == 625,
   diary([dname 'ppf8_captions.txt']);
   disp([' ';' ']); disp(ttext); disp(' ');
end;

plot8_displacements;
plot8_forces;
plot8_parameters;
diary off
```

A.5.2   Matlab Code for RMS Response of the Adaptive/PPF 8 Blade System.

```
% ppf8_rms.m
%
%  This m-file runs a 8 blade cyclic system with adaptive parameter estimation
%  and PPF control on all carts.  The disturbance is fd_i = cos(wd*t + phi_i).
%  The RMS values for the displacements and parameter estimates are calculated
%  over a range of disturbance frequencies.  It is currently set-up to be called
%  by a script file so that several different cases can be run at once.


%clear all; close all;

%print_switch = 0;        % Sends plots to printer if = 1
%eps_switch   = 0;        % Saves plots to eps file if = 1


% Simulation parameters

tfinal = 500;
eo             = 3;     % engine order for cyclic disturbance
disturb_switch = 3;     % disturbance:  3 = cyclic only
timer_switch   = 0;     % turn on estimator/control at t = timer_switch

%mistuned      = 1;     % grounding springs are mistuned if = 1
%ppf_switch    = 0;     % turns ppf control on (1) / off (0)
%adapt_switch  = 0;     % turns adaptive control on (1) / off(0)



% System parameters

N  = 8;                 % number of blades
L  = 1;                 % length of blade
zeta_n = 0.002;         % damping ratio
ko = 100; kc = 5;       % nominal ground & coupling stiffness, [k] = N/m

m1 = 1; m2 = 1; m3 = 1; m4 = 1; m5 = 1; m6 = 1; m7 = 1; m8 = 1;  % [m] = Kg

k12 = kc;  k23 = kc;  k34 = kc;  k45 = kc;   % [k] = N/m
k56 = kc;  k67 = kc;  k78 = kc;  k81 = kc;   % [k] = N/m

if mistuned == 0,
     k01 = ko;  k02 = ko;  k03 = ko;  k04 = ko;
     k05 = ko;  k06 = ko;  k07 = ko;  k08 = ko;
     ttext = 'Cyclic System';
   elseif mistuned == 1,
```

```
        k01 = ko*(1 + 0.0122);  k02 = ko*(1 + 0.0003);  k03 = ko*(1 - 0.0003);  k04 = ko*(1 - 0.0038);
        k05 = ko*(1 - 0.0117);  k06 = ko*(1 - 0.0012);  k07 = ko*(1 - 0.0074);  k08 = ko*(1 + 0.0126);
        ttext = 'Mistuned Cyclic System';
end;

M = diag([m1 m2 m3 m4 m5 m6 m7 m8]); M_inv = diag(1./[m1 m2 m3 m4 m5 m6 m7 m8]);

cp8 = cos(pi/8);  L2cp8 = L^2*cp8;
K(1,1) = k81 + k12 + k01/(L2cp8);  K(1,8) = -k81;  K(1,2) = -k12;
K(2,2) = k12 + k23 + k02/(L2cp8);  K(2,1) = -k12;  K(2,3) = -k23;
K(3,3) = k23 + k34 + k03/(L2cp8);  K(3,2) = -k23;  K(3,4) = -k34;
K(4,4) = k34 + k45 + k04/(L2cp8);  K(4,3) = -k34;  K(4,5) = -k45;
K(5,5) = k45 + k56 + k05/(L2cp8);  K(5,4) = -k45;  K(5,6) = -k56;
K(6,6) = k56 + k67 + k06/(L2cp8);  K(6,5) = -k56;  K(6,7) = -k67;
K(7,7) = k67 + k78 + k07/(L2cp8);  K(7,6) = -k67;  K(7,8) = -k78;
K(8,8) = k78 + k81 + k08/(L2cp8);  K(8,7) = -k78;  K(8,1) = -k81;
K = cp8*K;

% Find lowest natural freq (wn) of the undamped system; [wn] = rad/sec

[evalues,evectors] = eign(K,M);  wn  = sqrt(min(evalues));


% Form the damping matrix (D) from K, zeta_n, & the evectors

D = real(evectors*(2*zeta_n*sqrt(evectors'*K*evectors))*evectors');
for i = 1:N,  for j = 1:N,  if K(i,j) == 0,  D(i,j) = 0;  end;  end;  end;
d12 = -D(1,2);  d23 = -D(2,3);  d34 = -D(3,4);  d45 = -D(4,5);
d56 = -D(5,6);  d67 = -D(6,7);  d78 = -D(7,8);  d81 = -D(8,1);


% Set adaptation and ppf parameters

Gain = 0.1;
Gamma(:,:,1) = Gain*diag([1 1 1 1]);   % adaptive gain matrix for cart #1
Gamma(:,:,2) = Gamma(:,:,1);           % adaptive gain matrix for cart #2
Gamma(:,:,3) = Gamma(:,:,1);           % adaptive gain matrix for cart #3
Gamma(:,:,4) = Gamma(:,:,1);           % adaptive gain matrix for cart #4
Gamma(:,:,5) = Gamma(:,:,1);           % adaptive gain matrix for cart #5
Gamma(:,:,6) = Gamma(:,:,1);           % adaptive gain matrix for cart #6
Gamma(:,:,7) = Gamma(:,:,1);           % adaptive gain matrix for cart #7
Gamma(:,:,8) = Gamma(:,:,1);           % adaptive gain matrix for cart #8

mu = 0.4; wf = wn; zeta_f = 0.4;       % ppf gain, freq & damping ratio


% Begin looping through each cart

for i = 1:N,

   % Set-up Kppf

   if ppf_switch ~= 0,  Kppf(:,:,i) = [0  mu*K(i,i);  wf^2 0];
      else, Kppf(:,:,i) = zeros(2);
   end;


   % Partition out controlled & uncontrolled parts of the system matrices

   Mc = diag([M(i,i)  1]);                Mc_inv = diag([1/M(i,i)  1]);
   Kc = diag([K(i,i)  wf^2]);
   Dc = diag([D(i,i)  2*zeta_f*wf]);


   % Calculate P
```

```
    Ac = [zeros(2)  eye(2);  -Mc_inv*(Kc-Kppf(:,:,i))  -Mc_inv*Dc];
    Q = diag([1  wf^2/K(i,i)  M(i,i)/K(i,i)  1/K(i,i)]);
    P(:,:,i) = lyap(Ac',Q);


    % Check stability requirments

    if -abs(real(eig(Ac))) ~= real(eig(Ac)), disp(' '); disp('Ac is not negative definite'); end;
    if abs(real(eig(P(:,:,i)))) ~= real(eig(P(:,:,i))), disp(['P' num2str(i) ' is not positive definite']); end;
    if P(:,:,i) ~= P(:,:,i)', disp(' '); disp(['P' num2str(i) ' is not symmetric']); end;


    % Set-up vectors for selecting Xc_i and Yr_i

    select_Xc(i,:) = [i,  i+2*N,  i+N,  i+3*N];
    if i == 1,        select_Yr(i,:) = [2,  N,  2+N,  N+N];
       elseif i == N, select_Yr(i,:) = [1,  N-1,  1+N,  N-1+N];
       else,          select_Yr(i,:) = [i-1,  i+1,  i-1+N,  i+1+N];
    end;

end;  % End looping through each cart


% Set disturbance parameters

fd_amp = 10;   % amplitude of disturbance


% Set-up the cart & ppf state-space systems

A = [zeros(N)  eye(N);  -M_inv*K  -M_inv*D];
B = [zeros(N);  M_inv];
C = eye(2*N);

Af = [zeros(N)  eye(N);  -wf^2*eye(N)  -2*zeta_f*wf*eye(N)];
Bf = [zeros(N); eye(N)];
Cf = eye(2*N);


% Iteratively run simulation and determine RMS values

i = 0;  wd_step = 0.001;

for wd = 9:wd_step:11,

    i = i + 1;  omega(i) = wd;  disp(' '); disp([case_name num2str(wd)]);
    sim('ppf8_rms_sim');
    ibegin  = min(find(time>=(tfinal-100)));

    for j = 1:N,  x_rms(i,j) = rms(x(:,j),ibegin); end;
    avg_x_rms(i,1) = sum(x_rms(i,:),2)/N;
    max_x_rms(i,1) = max(x_rms(i,:));

end;
```

Bibliography

1.   Agnes, Gregory, "Informal correspondence between G. Agnes and M. Keller."

2.   Agnes, Gregory S. "Active/Passive Piezoelectric Vibration Suppression." 1995.

3.   Agnes, Gregory S. and Daniel J. Inman. "Nonlinear Piezoelectric Vibration Absorbers," *Smart Material Structures*, *5*:704–714 (1996).

4.   Castanier, M. and C. Pierre. "Investigation of the Combined Effects of Intentional and Random Mistuning on the Forced Response of Bladed Disk." *34th AIAA/ASME/SAE/ASEE Joint Propulsion Conference and Exhibit*. Washington DC: AIAA, July 1998.

5.   Duffield, Colin J. *An Experimental Investigation on Periodic Forced Vibrations of a Bladed Disk*. MS thesis, AFIT/GAE/ENY/00M-05, Air Force Institute of Technology, Wright-Patterson AFB, OH, March 2000.

6.   Ertur, David, et al. "Adaptive Vibration Isolation for Flexible Structures," *Journal of Vibration and Acoustics*, *121*:440–445 (October 1999).

7.   Ewins, D. J. "Vibration Characteristics of Bladed Disc Assemblies," *Journal of Mechanical Engineering Science*, *15*(3):165–186 (March 1973).

8.   Fanson, J. L. and T. K. Caughey. "Positive Position Feedback Control for Large Space Structures," *AIAA Journal*, *28*(4) (April 1990).

9.   Forward, Robert L. "Electronic Damping of Vibrations in Optical Structures," *Applied Optics*, *18*(5):690–697 (1 March 1979).

10. Goh, C. J. and T. K. Caughey. "On the Stability Problem Caused by Finite Actuator Dynamics in the Collocated Control of Large Space Structures," *International Journal of Control*, *41*(3):787–802 (2 August 1983).

11. Hagood, N. W. and A von Flotow. "Damping of Structural Vibrations with Piezoelectric Materials and Passive Electrical Networks," *Journal of Sound and Vibration*, *146*(2):243–268 (1991).

12. Hollkamp, Joseph J. and Jr. Thomas F. Starchville. "The Piezoelectric Vibration Absorber.".

13. Jarosh, Julian R. *Active and Adaptive Control for Payload Launch Vibration Isolation*. MS thesis, AFIT/GA/ENY/00M-03, Air Force Institute of Technology, Wright-Patterson AFB, OH, March 2000.

14. Lesieutre, George A. "Vibration Damping and Control Using Shunted Piezoelectric Materials," *The Shock and Vibration Digest*, *30*(3):187–195 (May 1998).

15. Lin, C.-C. and M. P. Mignolet. "Effects on Damping and Damping Mistuning on the Forced Vibration Response of Bladed Disks," *Journal of Sound and Vibration*, *193*(2):525–540 (1996).

16. Pierre, C. and D. V. Murthy. "Aeroelastic Modal Characteristics of Mistuned Blade Assemblies: Mode Localization and Loss of Eigenstructure," *AIAA Journal*, *30*(10):2483–2496 (October 1992).

17. Slater, Joseph C. and Andrew J. Blair. *A Design Strategy for Preventing High Cycle Fatigue by Minimizing Sensitivity of Bladed Disks to Mistuning*. Technical Report, Bolling AFB, Washington DC: USAF Office of Scientific Research, 1996.

18. Tang, J. and K. W. Wang. "Vibration Control of Rotationally Periodic Structures Using Passive Piezoelectric Shunt Networks and Active Compensation," *Journal of Vibration and Acoustics*, *121*:379–390 (July 1999).

19. USAF Scientific Advisory Board. *Structural Failure Modes of Titanium Components in Fans and Compressors of Air Force Gas Turbine Engines*. Technical Report P25; No. 108. Washington DC: Government Printing Office, 1994.

20. Wei, S. T. and C. Pierre. "Localization Phenomena in Mistuned Assemblies with Cyclic Symmetry Part II: Forced Vibrations," *Journal of Vibration, Acoustics, Stress, and Reliability in Design*, *110*(10):439–449 (October 1988).

Vita

Captain Mark J. Keller was born in Williamsport, PA. He graduated from Williamsport Area High School. Captain Keller received a Bachelor of Science degree in Aerospace Engineering from Penn State University, State College, PA. He was selected for membership in Tau Beta Pi, the National Engineering Honor Society, and Scabbard and Blade Military Honor Society. Upon graduation, he was commissioned a Second Lieutenant in the United States Air Force through the AFROTC program, of which he was a distinguished graduate.

Captain Keller began his active duty Air Force career at the Sacramento Air Logistics Center, McClellan AFB, CA. His first assignment was as a systems engineer for the A-10/F-111 Systems Program Office. Later, he was selected to be the Executive Officer for the Aircraft Management Directorate. Captain Keller then transferred to Detachment 9 of the Space and Missile Systems Center, Test and Evaluation Directorate, Vandenberg AFB, CA. He served as a test manager for the Space Maneuver Vehicle program, the Milstar satellite program, and several other research satellite programs.

In August of 1999, Captain Keller entered the Graduate School of Engineering and Management at the Air Force Institute of Technology. Upon completion of his degree of Master of Science degree in Aeronautical Engineering, he will be assigned to the Air Vehicles Directorate of the Air Force Research Laboratory, Wright-Patterson AFB, OH.

REPORT DOCUMENTATION PAGE

The public reporting burden for this collection of information is estimated to average 1 hour per response, including the time for reviewing instructions, searching existing data sources, gathering and maintaining the data needed, and completing and reviewing the collection of information. Send comments regarding this burden estimate or any other aspect of this collection of information, including suggestions for reducing the burden, to Department of Defense, Washington Headquarters Services, Directorate for Information Operations and Reports (0704-0188), 1215 Jefferson Davis Highway, Suite 1204, Arlington, VA 22202-4302. Respondents should be aware that notwithstanding any other provision of law, no person shall be subject to any penalty for failing to comply with a collection of information if it does not display a currently valid OMB control number.
PLEASE DO NOT RETURN YOUR FORM TO THE ABOVE ADDRESS.

1. REPORT DATE *(DD-MM-YYYY)*	2. REPORT TYPE	3. DATES COVERED *(From - To)*
20-03-2001	Master's Thesis	March 2000 - March 2001

4. TITLE AND SUBTITLE	5a. CONTRACT NUMBER
VIBRATION SUPPRESSION OF A ROTATIONALLY PERIODIC STRUCTURE USING AN ADAPTIVE/PPF CONTROL LAW	5b. GRANT NUMBER
	5c. PROGRAM ELEMENT NUMBER

6. AUTHOR(S)	5d. PROJECT NUMBER
MARK J. KELLER, Captain, USAF	5e. TASK NUMBER
	5f. WORK UNIT NUMBER

7. PERFORMING ORGANIZATION NAME(S) AND ADDRESS(ES)	8. PERFORMING ORGANIZATION REPORT NUMBER
Air Force Institute of Technology Graduate School of Engineering and Management (AFIT/EN) 2950 P Street, Bldg 640 WPAFB, OH 45433-7765	AFIT/GAE/ENY/01M-05

9. SPONSORING/MONITORING AGENCY NAME(S) AND ADDRESS(ES)	10. SPONSOR/MONITOR'S ACRONYM(S)
AFOSR/NA (Dr. Daniel Segalman) 801 North Randdolph St / Mailroom 732 Arlington, VA 22203-1977 (703)696-7259	11. SPONSOR/MONITOR'S REPORT NUMBER(S)

12. DISTRIBUTION/AVAILABILITY STATEMENT

13. SUPPLEMENTARY NOTES

14. ABSTRACT

For a compressor disk, effective vibration suppression requires broadband control, and the elimination of inter-blade coupling forces. Previous researchers achieved this using an active/passive piezoelectric shunt network. Unfortunately, optimal tuning of the shunt requires prior knowledge of the coupling strength, which is not well defined. This thesis uses an adaptive parameter estimator to eliminate the inter-blade coupling forces. In addition, the passive shunt is replaced with an analogous positive position feedback method. The resulting control law was used on a simulated four and eight bladed system. While substantial reductions in system response were achieved for the Adaptive/PPF control technique, the parameter estimates did not always converge to the correct solution. Similar reductions in the response were achieved using PPF control by itself.

15. SUBJECT TERMS

Bladed Disk, Cyclic Structures, Rotationally Periodic Structures, Compressor Blades, Active Control, Positive Position Feedback, Adaptive Control, Parameter Estimation

16. SECURITY CLASSIFICATION OF:			17. LIMITATION OF ABSTRACT	18. NUMBER OF PAGES	19a. NAME OF RESPONSIBLE PERSON
a. REPORT	b. ABSTRACT	c. THIS PAGE			Major Gregory S. Agnes, ENY
U	U	U	UU	187	19b. TELEPHONE NUMBER *(Include area code)* (937)255-6565, ext. 4317, gregory.agnes@afit.edu